1998

THE FATIGUE PROPERTIES OF SPRING STEEL

HATTINGH, DANIEL GERHARDUS

THE FATIGUE PROPERTIES OF SPRING STEEL

by

DANIËL GERHARDUS HATTINGH

A thesis submitted to the University of Plymouth
in partial fulfilment for the degree of

DOCTOR OF PHILOSOPHY

School of Manufacturing, Material and Mechanical Engineering
Faculty of Technology

March 1998

Abstract

Author: **DANIËL GERHARDUS HATTINGH**

Title: **THE FATIGUE PROPERTIES OF SPRING STEEL**

The nature and scope of this thesis can be divided into three categories, namely stress distribution modelling in coil springs; fatigue and failure analysis, an investigation into measurement of residual stresses and the relation to fatigue life.

The operation of springs is directly concerned with the theories of torsion and bending which makes the better understanding of these theories essential. The first part of the thesis is involved with a mathematical evaluation of these theories and a case study of an isolated loop of a coil spring. The mathematical modelling is verified by measuring the strain levels in a coil spring with the aid of strain gauges located at different positions in the coil spring. This evaluation gave a better understanding of the operational stress distribution for input into the two methods currently used by industry for the fatigue testing, namely isolated loop and complete coil spring samples.

The remaining part of the thesis revolves around the understanding of the relationship between fatigue life, process effects and residual stresses. The relationship between fatigue failures and process effects was investigated to reveal the mechanism responsible for component fatigue failure in a 55Cr3 automotive suspension spring steel. This was done by subjecting coil springs, withdrawn from different stages of the manufacturing process, to fatigue tests, ensuring that all possible sources of fatigue initiation in this material batch have been identified, including those not dominant in the finished component. Failures prior to shot peen process was mainly surface relate as where those withdrawn after this process were subsurface (inclusions) related. Fractographic analysis, using an XL30 scanning electron microscope, has revealed a number of sources of initiation, which are largely related to mechanical damage and inherent material defects.

The results indicate that decreasing defect levels in the material would represent a valid method for enhancing the fatigue response, specifically levels of nonmetallic inclusions and surface mechanical damage, but also that certain manufacturing process stages (cold scragg) are responsible for drop in fatigue life.

With a model of spring life from process effects and fatigue failures of spring steel, the influence of residual stresses had to be revealed. This measurement was done by means of centre hole drilling using an air abrasive powder system and residual strain rosettes as sensors.

The results reveal the nature and magnitude of the stresses induced into the manufactured component by each manufacturing process individually and the relation these induced stresses have to the fatigue properties of the component. In the final analysis this research reveals a model showing the relation and impact of manufacturing processes of 55Cr3 spring steel on the residual stresses present and fatigue properties of the material.

Contents

			Page
CHAPTER	1	INTRODUCTION	1
	1.1	GENERAL OBJECTIVES	1
	1.2	PROBLEM STATEMENTS	2
		1.2.1 The first subproblem	2
		1.2.2 The second subproblem	2
		1.2.3 The third subproblem	3
	1.3	HYPOTHESIS	3
	1.4	DELIMITATIONS	3
	1.5	ASSUMPTION	3
	1.6	THE SIGNIFICANCE OF THE RESEARCH	3
	1.7	INDUSTRIAL SUPPORT	4
	1.8	REVIEW OF RELATED LITERATURE	4
		1.8.1 The applications of strain gauges	4
		1.8.2 Forces in a helical coiled spring	6
		1.8.3 Fatigue testing of process springs	6
		1.8.4 Residual stresses	7
	1.9	SUMMARY	8
CHAPTER	2	FORCES IN A HELICAL COILED SPRING	9
	2.1	FORCES IN A AUTOMOTIVE COIL SPRING UNDER AXIAL LOADING	9
		2.1.3 Forces in an open coiled helical spring	10
	2.2	MEASUREMENT OF STRESSES IN COIL SPRINGS	14
		2.2.1 Mathematical analysis of isolated coil	14

Page

2.2.2 Stress determination by means of strain gauges 18

2.2.2.1 Test sample 18

2.2.2.2 Test method 19

2.2.2.3 Results 22

2.2.2.4 Calculations 25

2.2.2.5 Possible errors 25

2.3 DISCUSSION OF FINDINGS 26

2.3.1 Principal stress and deflection 28

2.3.2 Load *versus* deflection 29

2.4 SUMMARY 30

CHAPTER 3 THE INFLUENCE OF MANUFACTURING PROCESS ON FATIGUE PROPERTIES OF 55Cr3 SPRING STEEL 31

3.1 MANUFACTURING SPECIFICATIONS OF 55Cr3 COIL SPRING MATERIAL 31

3.1.1 Material specifications 31

3.1.2 Chemical analysis 31

3.1.3 Mechanical properties 32

3.2 MANUFACTURING PROCESS (summary) 32

3.3 PRINCIPLES OF HEAT AND SURFACE TREATMENTS OF 55Cr3 SPRING STEEL 34

3.3.1 Heat treatments 34

3.3.1.1 Austenitise and quench 34

3.3.1.2 Tempering 35

3.3.1.3 Hot scragging 36

Page

3.3.1.4 Shot peening 39

3.3.1.5 Painting process 41

3.3.1.6 Cold scragg/Load test 41

3.4 FATIGUE TESTS 43

3.4.1 Manufacture of fatigue samples 43

3.4.2 Fatigue test method 44

3.5 ANALYSIS OF FATIGUE FAILURES AND FRACTURE SURFACES 46

3.5.1 Quench 46

3.5.1.1 Position of fracture 46

3.5.1.2 Macroscopic observations 47

3.5.1.3 Microscopic observations 48

3.5.1.4 Fatigue life 49

3.5.2 Quenched tempered samples 50

3.5.2.1 Position of fracture 50

3.5.2.2 Macroscopic observation in fracture quenched tempered samples 50

3.5.2.3 Microscopic observation in quenched tempered samples 51

3.5.2.4 Fatigue life 53

3.5.3 Hot scragged samples 53

3.5.3.1 Position of fracture 53

3.5.3.2 Macroscopic observations 54

3.5.3.3 Microscopic observations 55

Page

3.5.3.4 Fatigue life 57

3.5.4 Shot peening samples 57

3.5.4.1 Position of fracture 57

3.5.4.2 Macroscopic observations 58

3.5.4.3 Microscopic observations 59

3.5.4.4 Fatigue life 61

3.5.5 Painted Samples 61

3.5.5.1 Position of fracture 61

3.5.5.2 Macroscopic observations 62

3.5.5.3 Microscopic observations 63

3.5.5.4 Fatigue life 64

3.5.6 Load tested samples (final component) 64

3.5.6.1 Position of fracture 64

3.5.6.2 Macroscopic observations 65

3.5.6.3 Microscopic analysis 67

3.5.6.4 Fatigue life 69

3.6 SUMMARY 70

3.6.1 General 70

3.6.2 Effect of process upon fatigue response 72

CHAPTER 4 RESIDUAL STRESSES 76

4.1 RESIDUAL STRESSES 77

4.1.1 Definition of residual stresses 77

Page

4.1.2 Calculation of residual stresses 78

4.2 MEASUREMENT OF RESIDUAL STRESSES 84

4.2.1 The need for measurement of residual stresses 84

4.2.2 Different methods for the measurement of residual stresses 85

4.2.3 Measurement of residual stresses by centre hole drilling 86

4.2.3.1 High-speed drilling or milling 87

4.2.3.2 Air-abrasive machining 88

4.2.3.3 Measurement procedures 88

4.2.3.4 Theory of hole drilling strain gauge rosette 89

4.3 SUMMARY 103

CHAPTER 5 PROCESS EFFECTS OF 55Cr3 SPRING STEEL ON RESIDUAL STRESSES 106

5.1 DESCRIPTION OF EQUIPMENT AND DRILLING PROCEDURE 107

5.1.1 Air-abrasive centre hole drilling 107

5.1.2 Measurement procedure 108

5.1.2.1 Alignment of sapphire nozzle 108

5.1.2.2 Selection and application of residual strain rosette gauges 109

5.1.2.3 Alignment of drilling guide and drilling device 110

5.1.2.4 Drilling procedure 112

5.2 MEASURED STRAIN DATA 114

5.2.1 Results 114

Page

5.2.2 Sources of error in hole drilling 115

5.3 CALCULATION OF RESIDUAL STRESSES MEASURED FROM STRAIN DATA 116

5.4 RELATION BETWEEN PROCESS EFFECTS AND RESIDUAL STRESSES 118

5.4.1 Quench 118

5.4.2 Tempering 120

5.4.3 Hot scragging 121

5.4.4 Shot peening 123

5.4.5 Painted 125

5.4.6 Load tested 126

5.5 FADING OF RESIDUAL STRESSES IN 55Cr3 SPRING STEEL 127

5.6 INFLUENCE OF RESIDUAL STRESSES ON FRACTURE PLANE OF 55Cr3 128

5.7 SUMMARY 130

CHAPTER 6 PROCESS EFFECTS ON 55Cr3 SPRING STEEL TRANSFORMATIONS 133

6.1 INVESTIGATION INTO MICRO STRUCTURAL TRANSFORMATION OF 55Cr3 SPRING STEEL 133

6.1.1 Equipment 133

6.1.2 Sample preparation 134

6.1.2.1 Removal of specimen from bulk material 134

6.1.2.2 Final thinning 136

6.1.3 Image formation 138

			Page
		6.1.4 Transformations in 55Cr3 spring steel	139
	6.2	SUMMARY	144
CHAPTER	**7**	**THE FATIGUE ANALYSIS OF SPRING STEEL (Discussion)**	145
	7.1	POSITION AND REASON FOR FAILURE	146
	7.2	THE RELATION BETWEEN MECHANICAL AND FATIGUE PROPERTIES OF SPRING STEEL	148
	7.3	EFFECTS OF PROCESS ON RESIDUAL STRESS AND FATIGUE RESPONSE	149
	7.4	SUMMARY	152
CONCLUSION			154
FUTURE RESEARCH			156
REFERENCES			157
APPENDIX - A		Calculation of forces in a closed coil spring	167
APPENDIX - B		Results from strain gauge readings from isolated loop and complete coil spring	175
APPENDIX - C		Calculation of residual stresses in a rectangular beam	182
APPENDIX - D		Case study in the application of ASTM method for calculating residual stresses	186
APPENDIX - E		Principles of Photo-elastic and X-ray diffraction techniques for the measurement of residual stresses	197
APPENDIX - F		The analysis of process effects of 55Cr3 spring steel on residual stresses and the relation to fatigue properties	220
APPENDIX - G		Observation of fatigue failures in 55Cr3 automotive coil suspension springs	231

LIST OF FIGURES

		Page
2.1	Open coiled helical spring	10
2.2	Schematic representation of forces in a coil spring	10
2.3	Illustration of test set-up for isolated loop	15
2.4	Position of maximum stress on a isolated loop of a coil spring	18
2.5	Orientation of strain gauge rosettes	19
2.6	Placements of strain gauges with respect to top view of coil spring	19
2.7	Set up of a full spring in test jig	20
2.8	Locating pin assembly use for fatigue testing of isolated coils	21
2.9	Final installation of isolated loop in test equipment	22
2.10	FEA plot indicating the area of high stress in a coil spring	27
2.11	Load *versus* deflection graph	29
2.12	Overall comparison of result	30
3.1	Hysteresis loop	38
3.2	Effect of austenite grain size on hysteresis loop area	38
3.3	Effects of shot peening on fatigue life of 0.9%C steel when done before and after preset (12mm diameter)	39
3.4	Relation between scatter in fatigue data and the manufacturing processes	40
3.5	Improvement of fatigue properties by reduction in scatter through shot peening	40
3.6	Coil spring fatigue tester	44
3.7	The fatigue test stress deflection relation for 55Cr3 coil springs samples	45

		Page
3.8	Scatter in fatigue results of quenched samples	49
3.9	Position of fracture of different processed samples	70
3.10	Dominant macroscopic features of 55Cr3 fatigue samples withdrawn at different manufacturing stages	71
4.1	Effect of residual stresses on surface layer of component	76
4.2	Tensile test curve	79
4.3	Stress distribution in a fully plastic shaft	80
4.4	Stress distribution of partially plastic shaft	83
4.5	Hole shapes as produced by air abrasive drilling	88
4.6	Flat plate subjected to a uniform stress	90
4.7	Thin flat plate with hole drilled in the centre subjected to a uniform stress	90
4.8	Variation of relieved radial and tangential strains with distance (along principal axes) from the centre of the drilled hole - uniaxial residual stress	94
4.9	Strain gauge rosette arrangement	96
4.10	Relieved strain versus Z/D	99
5.1	Set-up of the air abrasive drilling apparatus	108
5.2	Alignment of nozzle for drilling operation	109
5.3	Set-up drilling guide for drilling with the aid of the optical instrument.	109
5.4	Damage to gauge due to slight misalignment of drilling jig	111
5.5	Set up of the drilling apparatus over sample to be drilled	111
5.6	Cross section of drilled hole	113

		Page
5.7	Damaged gauge due to improper protection against air abrasive powder	113
5.8	Top view of drilled hole	113
5.9	Graphical representation of measured strain values for 55Cr3 processed samples	115
5.10	Process effects on principal residual stresses at different hole depth as indicated in Table 5.3	118
5.11	Magnitude and nature of the residual stress distribution in a quenched sample of 55Cr3 steel	118
5.12	Schematic of ideal residual stress distribution of a heat treated sample	120
5.13	Magnitude and nature of the residual stress distribution in a tempered sample of 55Cr3 steel	121
5.14	Magnitude and nature of the residual stress distribution in a hot scragged sample of 55Cr3 steel	122
5.15	Schematic representation of residual stresses induced during scragging and the effect on re-loading after scragging	122
5.16	Magnitude and nature of the residual stress distribution in a shot peened sample of 55Cr3 steel	124
5.17	Magnitude and nature of the residual stress distribution in a painted sample of 55Cr3 steel	125
5.18	Magnitude and nature of the residual stress distribution in a load tested sample of 55Cr3 steel	126
5.19	Fading of residual strains at full depth (1mm) in 55Cr3 processed samples due to fatigue cycling	128
5.20	Relation between micro hardness values and process effects on 55Cr3 spring steel	130
5.21	The relation between residual stress and strain magnitudes for 55Cr3 spring steel samples withdrawn at different process stages	131
6.1	Removal of sample from bulk material	135

		Page
6.2	Diffraction pattern of a perfect crystal	141
6.3	Diffraction pattern of a damage crystal	141
7.1	Influence of manufacturing processes of 55Cr3 spring steel on fracture position and initiation area	147
7.2	Relation between manufacturing processes and mechanical properties and fatigue	148
7.3	Fatigue life of processed samples	149
7.4	The relation between residual stresses and fatigue life	150
7.5	Model for the relation and process effects to 55Cr3 spring steel properties	153

List of Tables

		Page
2.1	Results of strain measurement	22
3.1	Process conditions of fatigue samples	33
3.2	Fatigue data of processed samples (55Cr3)	42
3.3	Cross sectional hardness values of fatigue samples (Hv10)	42
3.4	Mechanical properties of processed fatigue samples	42
3.5	Fatigue test installation specifications	46
5.1	EA-06-03-031 RE - 120 residual stress gauge specifications	110
5.2	Measured strain data for processed samples at various depths	114
5.3	Strain and stress results for 55Cr3 processed samples	117
7.1	Effects of manufacturing processes on position and cause of failure	146

List of Plates

			Page
3.1	Reduction of decarburised zone due to grinding process.		32
3.2	Untempered martensite in oil quenched 55Cr3 spring steel (870°C)		35
3.3	Tempered martensite of tempered coil at 375°C for 90 min		35
3.4	Dislocations in hot scragged 55Cr3 spring steel (X25 000 - TEM micrograph)		37
3.5	Martensite structure of a coil withdrawn after hot scragging at 200°C		37
3.6	Processed fatigue samples		43
3.7	Position and type of fracture common to quenched fatigue samples		47
3.8	Typical fracture surfaces present in the quenched fatigue samples		47
3.9	a)	Shows a fracture initiated from a stamp mark	48
	b)	Magnification of (a)	
	c)	Initiation from mechanical damage	
	d)	Enlargement of (c)	
3.10	a)	Transition stage	49
	b)	Slow fracture surface	
	c)	Fast fracture surface	
3.11	a)	Shows the position and type of fracture in tempered samples	50
	b)	Tempered fatigue sample failed due to buckling after 2 450 cycles	
3.12	Helical type fracture from different tempered fatigue samples		51
3.13	a)	Area of initiation	52
	b)	Inclusion present in initiation are	
	c)	Cause of fracture (mechanical damage)	
	d)	Sem image of secondary cracks	
	e)	Back scatter image of (d)	

			Page
3.14	a)	Fatigue area	52
	b)	Fast fracture surface	
3.15	a)	Mechanical damage due to coil interference (clash)	53
	b)	Initiation area of failure	
3.16		Position and type of fracture in fatigue sample withdrawn after hot scragging.	54
3.17	a)	Dominant fracture type of hot scragged fatigue samples	54
	b)	Reveals some axial growth at edges of slow fracture surface	
3.18	a)	Axial type fracture of a hot scragged fatigue sample	55
	b)	"Fish eye" appearance on fracture surface of hot scragged sample	
3.19	a)	Failure origin in a hot scragged fatigue sample	56
	b)	Micro structure of fracture surface at origin	
	c)	Micro structure of fast fracture surface	
3.20	a)	"Fish eye" in hot scragged 55Cr3 fatigue sample	56
	b)	Enlargement of (a)	
3.21		Typical fracture position for shot peened samples	57
3.22	a)	Helical type fracture of a shot peened fatigue sample	58
	b)	Shear type failure of a shot peened fatigue sample	
3.23	a)	Origin of fatigue failure of shot peen sample in 3.22 (a)	58
	b)	Origin of failure of shot peen sample shown in 3.22 (b)	
	(c)	Surface damage inside responsible for failure in (b)	
3.24	a)	Fracture origin of shot peen sample shown in Plate 3.22 (a)	59
	b)	Sem image of inclusion in (a)	
	c)	Back scatter SEM image of (b)	
3.25	a)	Slow fracture surface of shot peen sample close to the initiation area	60
	b)	Fast fracture surface of same sample	

			Page
3.26	a) b) c) d)	Origin of a failure close to the surface of a shot peened component Indentation caused by a shot close to origin Indication of failure Enlargement of (b) reveals possible remains of an inclusion	60
3.27		Position of fracture of painted fatigue samples	62
3.28	a) b) c)	Helical failure of a painted fatigue sample Origin of failure in (a) Mechanical damage on surface close to origin of failure	62
3.29	a) b)	SEM picture of the area of origin Back scatter image of (a)	63
3.30	a) b)	Fracture surface close to origin of a painted fatigue sample Fast fracture surface of same failure	64
3.31		Fracture positions as it appeared in load tested samples	65
3.32		The fracture appearances of load tested samples	65
3.33		Initiation of failure in first load tested fatigue sample	66
3.34		"Fish eye" type initiation in a load tested sample	66
3.35		SEM micrographs of a load tested fatigue sample	67
3.36	a) b) c)	Sulfide strainer marks in a load test sample Fracture surface close to origin Fast fracture surface	68
3.37	a) b) c)	SEM picture of fatigue origin Back scatter image of fatigue origin Back scatter image of inclusion itself	69
3.38		Mechanical damage due to coil clash - sample withdrawn after painting	72
6.1		Transmission electron micro graphs illustrating crystalline features and the diffraction pattern of a quenched sample of 55Cr3 spring steel	142
6.2		Transmission electron micro graphs illustrating	143

crystalline features and the diffraction patterns
of a quenched tempered sample of 55Cr3 spring steel

6.3 Transmission electron micro graphs illustrating crystalline features and the diffraction pattern of a hot scragged sample of 55Cr3 spring steel 143

6.4 Transmission electron micro graphs illustrating crystalline features and the diffraction pattern of a shot peened sample of 55Cr3 spring steel 144

Glossary of terms

A

age hardening. Hardening by ageing, usually after rapid cooling or cold working.

alignment. A mechanical or electrical adjustment of the components of an optical device so that the path of the radiating beam coincides with the optical axis or other predetermined path in the system.

alloying element. An element added to and remaining in a metal that changes structure and properties.

analyser. An optical device capable of producing plane-polarised light. It is used for detecting the effect of the object on plane-polarised light produced by the polariser.

angstrom unit (Å). A unit of linear measure equal to 10^{-10} m, or 0.1 nm. Although not an accepted unit, it is occasionally used for small distances, such as interatomic distances and some wavelengths.

annealing. Heating to and holding at a suitable temperature followed by cooling at a suitable rate.

anneal to temper. A final partial anneal that softens a cold-worked nonferrous alloy to a specified level of hardness or tensile strength.

austempering. Cooling (quenching) an austenitised steel at a rate high enough to suppress formation of high-temperature transformation products, then holding the steel at a temperature below that for pearlite formation and above that for martensite formation until transformation to an essentially bainitic structure is complete. Generally, a solid solution of one or more alloying elements in a face-centred cubic polymorph of iron.

austenitic grain size. The size attained by the grains in steel when heated to the austenitic region.

austenitising. Forming austenite by heating a ferrous alloy into the transformation range or

above the transformation range.

B

back scatter reflection. The diffraction of x-rays at a Bragg angle approaching 90°C.

bainite. A eutectoid transformation product of ferrite and a fine dispersion of carbide generally formed below 450 to 500°C.

bending stress. If a beam is subjected to a bending moment the fibres in the upper part are extended and these in the lower part are compressed. Tensile and compressive stresses are thereby induced which vary from zero at the neutral axis of the beam to a maximum at the outer fibres. These stresses are called bending stresses.

Bragg angle. The angle between the incident beam and the lattice planes considered.

brittle fracture. Rapid fracture preceded by little or no plastic deformation.

brittleness. The tendency of a material to fracture without first undergoing significant plastic deformation.

C

carbide. A compound of carbon with one or more metallic elements.

carburising. A case-hardening process in which an austenitised ferrous material contacts a carbonaceous atmosphere having sufficient carbon potential to cause absorption of carbon at the surface and, by diffusion, to create a concentration gradient.

chemical polishing. A process that produces a polished surface by the action of a chemical etching solution.

cleavage. Fracture of a crystal by crack propagation across a crystallographic plane of low index.

cleavage fracture. A fracture, usually of a polycrystalline metal, in which most of the grains have failed by cleavage, resulting in bright reflecting facets.

cleavage plane. A characteristic crystallographic plane or set of planes in a crystal on

which cleavage fracture occurs easily.

coil spring. A compression or tension spring made of bar stock or wire coiled into a helical form on which the load is applied along the helix axis.

cold scragging. See scragging.

D

decarburisation. Loss of carbon from the surface of a ferrous alloy as a result of heating in a medium that reacts with carbon.

deflection. In coil springs deflection refers to change in axial length due to axial loading. If at any section of an unloaded beam the neutral surface is displaced by the application of lateral loads then this displacement is called the deflection of the beam at that section.

depth of field. The depth in the subject over which features can be seen to be acceptably in focus in the final image produced by a microscope.

dislocation. A linear imperfection in a crystalline array of atoms.

E

electrolytic polishing. An electrochemical polishing process in which the metal to be polished is made the anode in an electrolytic cell where preferential dissolution at high points in the surface topography produces a specularly reflective surface.

electron beam. A stream of electrons in an electron-optical system.

electron diffraction. The phenomenon, or the technique of producing diffraction patterns through the incidence of electrons upon matter.

electron microscopy. The study of materials by means of an electron microscope.

etchant. A chemical solution used to etch a metal to reveal structural details.

etching. Subjecting the surface of a metal to preferential chemical or electrolytic attack to reveal structural details for metallographic examination.

F

ferrite. Generally, a solid solution of one or more elements in body-centred cubic iron. In plain carbon steels, the interstitial solid solution of carbon in α-iron.

final polishing. A polishing process in which the primary objective is to produce a final surface suitable for microscopic examination.

G

grain. An individual crystal in a polycrystalline metal or alloy, including twinned regions or subgrains if present.

grain boundary. An interface separating two grains at which the orientation of the lattice changes from that of one grain to that of the other. When the orientation change is very small the boundary is sometimes referred to as a sub-boundary structure.

grain growth. An increase in the grain size of a metal usually as a result of heating at an elevated temperature.

grain size. A measure of the areas or volumes of grains in a polycrystalline metal or alloy, usually expressed as an average when the individual sizes are fairly uniform. Grain size is reported in terms of number of grains per unit area or volume, average diameter, or as a number derived from area measurements.

granular fracture. An irregular surface produced when metal fractures. This fracture is characterised by a rough, grain like appearance. It can be sub-classified into trans-granular and intergranular forms.

graphite. The polymorph of carbon with a hexagonal crystal structure.

grinding. Removing material from a workpiece using a grinding wheel or abrasive belt.

H

hardenability. The relative ability of a ferrous alloy to form martensite when quenched from a temperature above the upper critical temperature.

hardening. Increasing hardness by suitable treatment, usually involving heating and cooling.

hot quenching. An imprecise term for various quenching procedures in which a quenching medium is maintained at a prescribed temperature above 70°C.

hot scragging. See scragging.

hot working. Deformation under conditions that result in re-crystallisation.

I

impurities. Undesirable elements or compounds in a material.

inclusion count. Determination of the number, kind, size and distribution of nonmetallic inclusions.

inclusions. Particles of foreign material in a metallic matrix.

interference. The effect of a combination of wave trains of various phases and amplitudes.

intergranular. Within or across crystals or grains. Same as transcrystalline and trans-granular.

Isolated loop. Any one complete helical coil of 360° which has been removed from a whole helical spring.

L

lamination. An abnormal structure resulting in a separation or weakness aligned generally parallel to the worked surface of the metal.

longitudinal direction. That direction parallel to the direction of maximum elongation in a worked material. See also *normal direction* and *transverse direction.*

M

macrograph. A graphic reproduction of a prepared surface of a specimen at a magnification not exceeding 25x.

macrostructure. The structure of metals as revealed by macroscopic examination of the etched surface of a polished specimen.

magnification. The ratio of the length of a line in the image plane.

martensite. A generic term for microstructures formed by diffusion less phase transformation in which the parent and product phases have a specific crystallographic relationship.

martensitic. A platelike constituent having an appearance and a mechanism of formation similar to that of martensite.

maximum shear strain. A stress of this nature is said to exist on a section of a body if on opposite faces of the section equal and opposite parallel forces exist.

maximum bending Strain. A cylindrical shaft is said to be subject to pure torsion when the torsion is caused by a couple, applied so that the axis of the couple coincides with the axis of the shaft. The state of stress, at any point in the cross-section of the rod, is one of pure shear, and the strain is such that one cross-section of the shaft moves relative to another.

microcrack. A crack of microscopic proportions.

micrograph. A graphic reproduction of the prepared surface of a specimen at a magnification greater than 25x.

Micro structure. The structure of a prepared surface of a metal as revealed by a microscope at a magnification exceeding 25x.

N

nitriding. A case-hardening process that introduces nitrogen into the surface layer of a ferrous material by holding it at a suitable temperature in a nitrogenous atmosphere.

nodular graphite. Rounded clusters of tempered carbon.

nodular pearlite. Pearlite that has grown as a colony with an approximately spherical morphology.

O

orientation (crystal). Arrangements in space of the axes of the lattice of a crystal with respect to a chosen reference or coordinate system.

P

pearlite. A metastable eutectoid-transformation product consisting of alternating lamellae of ferrite and cementite resulting from the transformation of austenite at temperatures above the bainite range.

pearlitic structure. A Micro structure resembling that of the pearlite constituent in steel.

phase. A physically homogeneous and distinct portion of a material system.

plastic deformation. Deformation that remains or will remain permanent after release of the stress that caused it.

plasticity. The capacity of a metal to deform nonelastically without rupturing.

polished surface. A surface that reflects a large proportion of the incident light in a specular manner.

principal strains. The maximum and minimum direct strains in a material, subjected to complex stress are called Principal Strains. These strains act in the directions of the principal stresses.

principal stresses. At any point within a stressed material it will be found that there exist three mutually perpendicular planes on each of which the resultant stress is a normal stress (i.e. no shear stresses occur on these planes). These mutually perpendicular planes are called principal planes, and the resultant normal stresses are called Principal Stresses.

Q

quench hardening. In ferrous alloys, hardening by austenitising, then cooling at a rate so that a substantial amount of austenite transforms to martensite.

quenching crack. Cracks formed as a result of thermal stresses produced by rapid cooling from a high temperature.

R

re-crystallisation. A change from one crystal structure to another, such as that occurring upon heating or cooling through a critical temperature.

S

sagging. Loss of height or ability to resist given level of stress after a number of stress reversals or cycling.

scanning electron microscope. An electron microscope in which the image is formed by a beam operating in synchronism with an electron probe scanning the object.

scragging. A operation used to obtain higher elastic limits and hence greater load capacity without set for helical compression springs. It consist of compressing the spring beyond the elastic limit either at an elevated temperature (hot scragging) or at room temperature (cold scragging).

shear bands. Bands in which deformation has been concentrated in homogeneously in sheets that extend across regional groups of grains.

single coil. Any one complete helical coil of 360° which has been removed from a whole helical spring.

slip. Plastic deformation by the irreversible shear displacement of one part of a crystal relative to another in a definite crystallographic direction and usually on a specific crystallographic plane.

slip band. A group of parallel slip lines so closely spaced as to appear as a single line when observed under an optical microscope.

strain. Strain is a measure of the deformation of a body acted upon by external forces and can be expressed as a change in dimension per unit of original dimension or in the case of shear as a change in angle between two initially perpendicular planes.

strain amplifier. The ratio of the voltage supplied to the voltage delivered by the Wheatstone Bridge as a result of the unbalance caused by a change of strain gauge resistance is equivalent to the strain and is amplified into a suitable voltage or current which can be fed into an analogue or digital indicator or graphic recorder.

strain rosettes. A combination of three strain gauges set with there axis at 45° (or 60°)

with each other - used to determine strain at a point on a surface when the strain directions are unknown.

stress. Load applied to a piece of material tends to cause deformation which is resisted by internal forces set up within the material which are referred to as stresses. The intensity of the stress is estimated as the force acting on unit area of the cross-section, namely as Newtons per square metre or Pascals.

stress relieving. Heating to a suitable temperature, holding long enough to reduce residual stresses, then cooling slowly enough to minimise the development of new residual stresses.

stringer. A microstructural configuration of alloy constituents or foreign nonmetallic material lined up in the direction of working.

sulfide-type inclusions. In steels, nonmetallic inclusions composed essentially of manganese iron sulfide solid solutions.

T

tempered martensite. The decomposition products that result from heating martensite below the ferrite-austenite transformation temperature.

tempering. In heat treatment, reheating hardened steel to some temperature below the eutectoid temperature to decrease hardness and/or increase toughness.

transmission electron microscope. A microscope in which the image-forming rays pass through the specimen being observed.

twin bands. Bands across a crystal grain, observed on a polished and etched section, where crystallographic orientations have a mirror-image relationship to the orientation of the matrix grain across a composition plane that is usually parallel to the sides of the band.

Z

zone. Any group of crystal planes that are all parallel to one line, which is called the zone axis.

(Note: For other definitions and nomenclature see text.)

Acknowledgements

The work presented in this thesis would never have materialised without the support from industry, academic institutions, colleagues and friends. This research work originated in the automotive coil spring manufacturing industry which was looking at the development of an enhanced coil spring.

Firstly, I would like to acknowledge the management teams of the University of Plymouth and Port Elizabeth Technikon in overcoming all stumbling blocks to make this joint venture an enriching experience. Special mention must be made of Dr David Grieve from Plymouth University and Professor Hugh Jeffery from the Port Elizabeth Technikon who were the major role players in getting the ball rolling.

The completion of this thesis would not have been possible without the support of many individuals. I would like to express my gratitude to the following people and organisations for their invaluable assistance, time and encouragement.

- Dr David Grieve, Chief Supervisor for his encouragement, involvement and professional guidance.
- The staff of the SMMME at the University of Plymouth for positive criticism and guidance, and in particular to Dr David Plane, Mr David Short and Terry for their patience.
- Alan Holman and other fellow researchers for their support and encouragement.
- The Foundation for Research Development and the Port Elizabeth Technikon's Research Committee for their financial support of this project.
- The staff of the Faculty of Mechanical Engineering at Port Elizabeth Technikon, and

in particular Professor Jeffery, Professor Twigg, Mr Pat McGrath and Mr Colin du Preez.

- The industrial support received from the following companies and individuals:

  Eskom Technology Group, Mr Mark Newby, who assisted with the residual stress measurements.

  Volkswagen of South Africa, Quality Assurance, Mr N. Rafferty, who assisted with the fatigue testing of coil springs.

  National Springs SA, Mr L Dockray for supplying research material.
- Louise Taylor and Angie Henning for assisting in turning my 'difficult to read' work into a typed script.

Finally I would like to thank my family for their support, patience and prayers, especially my wife Marinda and children, Marelise and Chris, for their understanding and patience.

All honour to my Heavenly Father for giving me the insight and health to complete this work.

Author's declaration

At no time during registration for the degree of Doctor of Philosophy has the author been registered for any other university degree.

This study was financed with the aid of the Foundation for Research Development of South Africa, Port Elizabeth Technikon, National Springs and Volkswagen of South Africa.
A programme of advanced study was undertaken, which included attendance of a course at the University of Port Elizabeth, Physics Department; Department of Materials and Metallurgical Engineering at Port Elizabeth Technikon and Centre for Technology and Research at Eskom, Johannesburg.

Relevant scientific seminars and conferences were regularly attended at which work was presented. Many external institutions were visited for consultation purposes and several papers prepared for publication.

Publications:

* Observations of fatigue failures in 55Cr3 automotive coil suspension spring.
  Hattingh, D G & Holman, A E L (In press).
* The analysis of process effects of 55Cr3 spring steel on residual stresses and the relation to fatigue properties.
  Hattingh, D G & Du Preez, K H
  Surface Treatments 97, Oxford, United Kingdom.

Presentations and Conferences Attended:

Measurement of residual stresses using the air abrasive centre hole drilling method.

Eskom, Cleveland, 17-19 January 1995.

Strain measurement.

Rivonia, Johannesburg, 22-25 October 1996.

Measurement of residual stresses using an automatic hole drilling (milling) device.

HBM Darmstadt, Germany, 17-20 February 1997.

Fracture design and fatigue analysis.

Rosebank, Johannesburg, 9-11 April 1997.

Surface treatments 97.

Oxford, United Kingdom, 15-17 July 1997.

External Contacts:

Mr L Dockray, National Spring, Germiston

Mr N Rafferty, Volkswagen of South Africa, Uitenhage

Mr Klaus Gehrke, HBM, Germany

Prof. J J Neethling, University of Port Elizabeth, Port Elizabeth

Mr Mark Newby, TRI - Eskom, Cleveland

Mr M Chetty, Mercedes Benz SA, East London

Signed.....

Date.....05/05/98.....

CHAPTER 1

INTRODUCTION

INTRODUCTION

The aim of this thesis is to contribute to the development of an enhanced automotive coil spring by evaluating existing manufacturing processes and relating this to fatigue properties and residual stresses in the components.

The development of a coil spring that is 15% lighter and which can operate at 20% higher stresses, will bring about a major revolution in the manufacturing of automotive suspensions. This could result not only in a lighter vehicle but also a reduction in space required by suspensions, which could open the way for new, less drag resistant front body panels.

1.1 GENERAL OBJECTIVES

The author of this thesis aimed at satisfying the following objectives.

- In-depth study into the uses of strain gauges to evaluate stress levels in coil springs and isolated loops of coil springs with the aim of understanding their relation to forces present in coil spring fatigue samples subjected to axial loading.
- Investigation into the influence each manufacturing process has on the fatigue life of spring steel to enable ideal optimization of manufacturing processes and development of a model for better understanding of the fatigue mechanism by evaluating fracture surfaces.
- To identify a feasible method for measuring residual stress in components withdrawn from different stages of manufacture and to physically apply this method to reveal the magnitude and nature of residual stress in the component after each stage of manufacture.

- To determine the residual stress induced into the component by each manufacturing process.
- To relate residual stress induced to microstructural and fatigue properties of spring steel.
- To investigate the distribution of dislocations and the form of electron diffraction patterns by means of transmission electron microscopy in an attempt to produce a better understanding for relation of residual stresses to manufacturing process..

The work done in this thesis is a contribution towards a better understanding of fatigue properties of spring steel and the relation to manufacturing processes. The hypothesis of the author is that eventually all research done by different researchers will lead to the development of coil springs with increased performance and a reduction in weight, although not all of it was done on the same material.

1.2 PROBLEM STATEMENTS

The aim of the researcher will be to contribute to the development of an automotive coil spring with an increase in performance and a reduction in weight by evaluating the influences of manufacturing processes on 55Cr3 spring steel.

1.2.1 The first subproblem

Investigate the behaviour of a coil spring subjected to an axial load by means of mathematical modelling and strain gauges. This would resolve the nature of forces and stresses set up in the material and reveal the relation between strain and stress, strain and deflection and strain and load to assist with the interpretation of fatigue information.

1.2.2 The second subproblem

Investigate the fatigue properties of spring steel to establish the influence of the different manufacturing processes on the properties of spring steel.

1.2.3 The third subproblem

Measuring of residual stresses in spring steel to reveal the influence of the different stages of the manufacturing process on the magnitude and nature of these stresses. To set up a model for the relation between residual stresses and fatigue properties of 55Cr3 spring steel.

1.3 HYPOTHESIS

That the research done by all different parties will lead to the development of a coil spring with an increased performance and decrease in weight.

1.4 DELIMITATIONS

That the study be based on a specific part number of coil spring as manufactured by National Springs SA of the material 55Cr3 (SiMn+V) spring steel for the Volkswagen Golf range for Volkswagen South Africa.

1.5 ASSUMPTION

That a new coil spring can be developed with increased performance from 55Cr3 spring steel by refinement of manufacturing parameters. That the above will be possible with no or very little increase in manufacturing cost.

1.6 THE SIGNIFICANCE OF THE RESEARCH

The development of high strength steel coil springs is receiving a great deal of attention and research by spring makers world-wide, particularly by Japanese spring makers. The aim is to

raise working stresses by 20% with a weight reduction of 15%. This weight-saving is very attractive to car designers as part of a development programme to reduce vehicle weight stemming from environmental pressures.

1.7 INDUSTRIAL SUPPORT

A number of motor manufacturers were approached for support and involvement. Two companies responded, namely Volkswagen SA, based in Uitenhage, ± 60 km from Port Elizabeth, and the other one was Mercedes Benz SA, ± 300 km from Port Elizabeth. Both these companies were supplied with coil springs from the same company in Johannesburg. Their main support was in the form of technical assistance, material and free utilisation of laboratories and testing equipment. Both companies also gave letters of strong support for the project and research to be done.

Once this vital link was set up with the motor manufacturing companies, the spring manufacturers, who supplied these companies with the components, were approached. The research project was met with an overwhelming response from National Spring who immediately agreed to supply and process all research materials. The Foundation of Research and Development and Port Elizabeth Technikon agreed to assist with financing the project.

1.8 REVIEW OF RELATED LITERATURE

A number of fields had to be reviewed in preparation for researching the above problems. This will be reviewed very briefly in this section as it will appear in more detail in the appropriate sections of the thesis.

1.8.1 The applications of strain gauges

The field of strain measurement is a very complex and diverse field. It requires a working knowledge of the following engineering subjects Mechanics of Machines, Metrology, Engineering Design, Materials and Electronic Circuits. By studying strain gauges and their application, each user develops his own unique perspective and application expertise. The most important measuring method in the experimental stress analysis is the strain gauge technique. This technique makes it possible to assess the stressing of a structural part within wide limits, without damaging or destroying the part. Here follows some of the topics, which were investigated relating to strain measuring:

- Selection of adhesives
  - Function
  - Characteristics
  - Types
- Fixing of strain gauges
  - Preparation of specimen and gauge
  - Method of application
  - Bonding process
  - Connection of cables
  - Protection
- Wheatstone bridge
  - Application of circuit
  - Measurement of tensile, bending, torque
  - Stress compensation
  - Temperature compensation
- Consideration for Accuracy

The researcher's aim with this study was to expand his knowledge on the application and use of strain gauges as the application of strain gauges formed an integral part of the research.

1.8.2 Forces in a helical coiled spring

Springs design inherently involves the theories of torsion, bending and strain energy. This study was done to enable the researcher to understand the effects of torsion and other forces set up in a coiled spring by investigating the forces set up in a coil spring under axial loading. Both cases of a closed and open coil spring were considered. Detailed mathematical modelling for both cases was performed to determine equations for bending stresses, shear stresses and the behaviour of internal energy. The relation between stress and strain was also carefully investigated to assist the researcher to form a better picture of the behaviour of all the variables in a coiled spring. This was followed by a study into the prediction of the stress variation in coil springs.

1.8.3 Fatigue testing of process springs

The researcher visited the spring manufacturer, National Springs, and familiarised himself with the different processes needed for the manufacture of springs. The objective was to see at which stage processed material could be withdrawn for fatigue and mechanical testing. Production schedules were also looked at before selecting a specific spring, to ensure that the specific spring would still be in production for a few months to come. Incoming material is drawn to an area reduction after which it is cut to length and then centre-less ground to reduce the decarburised zone. The ground bar is then austinitised and hot coiled before being quenched in oil. The quenched components are tempered and hot sgragged before being shot peened. After this the component is coated by means of phosphate and black paint before being cold scragged and load rated. Processed springs were withdrawn at the following stages:

After hot coil and quenching, tempering, hot scrag, shot peening, painting and after load testing. Review of related literature was done on all the above processes. This was followed by an in-depth study into the field of fracture analysis.

1.8.4 Residual stresses

One of the major challenges for the researcher was understanding of the role played by residual stresses in high tensile spring material. Residual stress is a phenomenon that still raises many questions in the mind of the materials specialist, as well as in that of the engineer. Residual stresses are locked into a component due to manufacturing processes and it is independent of any external loading[1]. Increased attention has been given to residual stresses lately for the purpose of reducing material cost, extended lifetime of existing structures and to satisfy demands for increased reliability of components. A comprehensive literature study was done on this subject, and a number of months were spent studying the effects of residual stresses in general. The literature currently available on residual stresses is limited and scattered over a large number of references. Specific attention was given primarily to investigate the reasons and effects for the presence of residual stresses, and to evaluate different methods available for measuring residual stresses. The following topics were addressed:

- Introduction into the significance of residual stresses.
- Calculation of residual stresses in an elastic-perfectly plastic material. Bending, as well as the effect of torsion is considered.
- Influence of residual stresses on bending and torsional strengths.
- Reasons for residual stresses. The first part of this section looks at the effect of mechanical processes e.g. shot peening, cold rolling, etc. Secondly, the effects of chemical treatments are also considered e.g. carburising, nitriding, etc. The last part

of this section looks at the effects of heat treatments on residual stresses.

- The part on residual stresses and failure explains the role that these stresses play in structural failures. It firstly looks at the concept of fading of residual stresses and secondly at the influence of residual stresses on the fracture plane.
- Measurement of residual stresses.

  A large part of the review is devoted to describing measuring techniques. Residual stresses are difficult to measure since they are independent from external loading and are imposed by manufacturing processes and treatments. A wide range of measuring techniques have been used with limited success in the past. The methods are discussed in detail later in the thesis.
- An investigation into preparation of transmission electron microscopy samples for evaluating the relation of diffraction patterns and dislocations to the presence of residual stresses.

1.9 SUMMARY

This study and compiling of a short information document, gave the researcher the insight and background to enter the field with a lot more confidence. It allowed him to consider all available methods for measuring residual stresses and fatigue tests, and to select the most appropriate method for his application, after the evaluation of all available methods.

The study enabled the researcher to make a well-defined conclusion on the effect which the manufacturing process of coil springs had on residual stresses and the relation to fatigue.

CHAPTER 2

FORCES IN A HELICAL COILED SPRING

INTRODUCTION

Springs are directly concerned with the theories of torsion, bending and strain energy. Many machines and not only automotive suspensions, incorporate springs to assist in their operation. The principal function of a spring can be summarised by saying that it is to absorb energy, store it for a long period or a short period, and then return the energy to the surrounding material. To explain the above in a practical sense, one can consider the example of two extremes of operations found in the operations of a watch and an internal combustion engine's valve spring. In the watch, energy is stored for a long period and in the valve spring the process is very rapid.

The objective of this chapter is to study the effects of torsion and the forces set up in a coiled spring under axial-loading. This will give the researcher a clearer picture of the operating conditions of a coil spring under axial loading. The last part of this chapter will involve a mathematical analysis to determine the stress distribution inside an isolated loop of a coil spring followed by studying the stresses in a coil spring and isolated loop with the aid of strain gauges.

2.1 FORCES IN A AUTOMOTIVE COIL SPRING UNDER AXIAL LOADING [1,2]

A helical spring is usually loaded by an axial force. For this study we will assume a circular cross section for the spring wire and we will ignore small end effects, as when ends are unbent, or ground flat to provide a bearing plane. We will assume throughout this section that the wire diameter is considerably smaller than the helix radius (R) so that curved-beam considerations may be neglected.

2.1.1 Forces in an open coiled helical spring[2,3]

Standard spring design theory suggest the following:

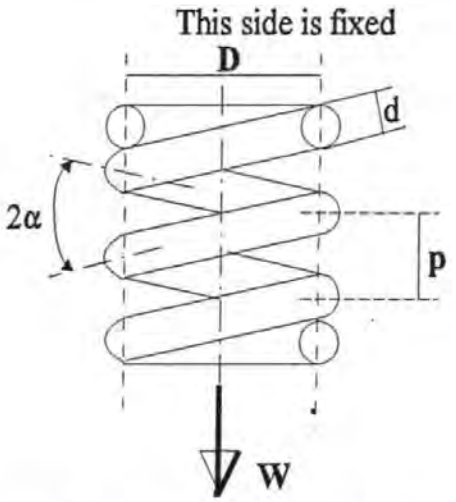

Figure 2.1: Open coiled helical spring.

Length of wire $l = \frac{\pi Dn}{\cos\alpha}$ (Where n = number of coils)

Consider the following:

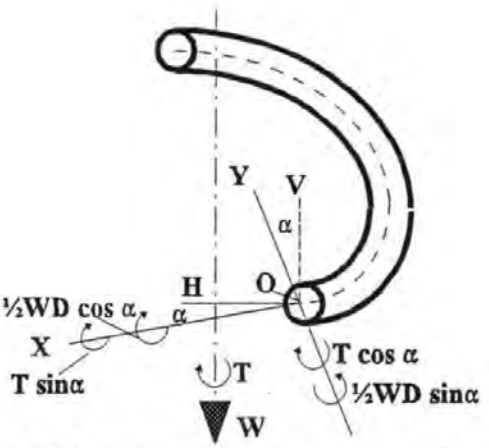

Figure 2.2: Schematic representation of forces in a coil spring.

OX = Polar axis (axis of twisting at any normal cross section). It is inclined at $\angle\alpha$ to the

horizontal OH.

OY = Bending axis and is inclined at $\angle\alpha$ to the vertical OV. All the axes OX; OY; OV and OH are in the vertical plane which is tangential to the helix at O.

If an axial load W is applied to the spring, it can be solved as follows:

Resolving the effect of W about OX & OY.

$\therefore$ Twisting couple about $OX = \frac{WD}{2}\cos\alpha$

Bending couple about $OY = \frac{WD}{2}\sin\alpha$

$\therefore$ Combine bending and twisting couple $= \frac{WD}{2}\cos\alpha + \frac{WD}{2}\sin\alpha$

Strain energy U = ½ Wx or U = ½ TΘ where x = Total deflection and Θ axial angle of rotation.

$\therefore$ External work = resilience in torsion and bending.

$\therefore \quad \frac{1}{2}Wx = \frac{1}{2}[\frac{WD}{2}\cos\alpha]\Theta + \frac{1}{2}[\frac{WD}{2}\sin\alpha]\phi$

Where Θ = Angle of rotation on cross-section (OX)

ϕ = Angle of rotation about longitudinal axis (OY)

Therefor $x = \frac{D}{2}[(\cos\alpha)\Theta + (\sin\alpha)\phi]$

But from equation 4 Appendix A:

$$\Theta = \frac{TL}{JG}$$

Adapting this formula for open coil springs we have to consider the helix angle:

$\therefore \quad T = W\frac{D}{2}\cos\alpha$

and $\Theta = \frac{W(D/2)L}{JG}\cos\alpha$

To determine the angle of rotation ϕ about longitudinal axis let us first consider the strain energy in pure bending for a beam.

The total strain energy = External work done in straining a bar.

$$U = \frac{(stress)^2}{2E}$$ per unit volume (E = modulus of rigidity)

$\therefore$ Strain energy in a small piece of length dx under area dA $= \frac{\delta^2}{2E} .dx.dA$

but $\delta = \frac{MY}{I}$ (direct stress)

$$\therefore \quad U = \frac{M^2Y^2}{2I^2E} dx.dA$$

where Y = distance from neutral axis

M = load × distance

$$\therefore \quad U\ total = \sum \frac{M^2Y^2}{2I^2E} dx.dA$$

$$= \frac{M^2dx}{2I^2E} .\sum dAY^2$$

But $\Sigma dAY^2 = I$

$$\therefore \quad U = \int_0^L \frac{M^2}{2EI} dx$$ where L = span of beam

$$\therefore \quad U = \frac{M^2 L}{2IE} \quad = \text{Resilience}$$

Now if ϕ is the angle of rotation about the longitudinal axis of one end relative to the other, the work done is $\frac{1}{2}M\phi$

$$\therefore \quad \tfrac{1}{2}M\phi = \frac{M^2 L}{2EI} \qquad \left(M = W\frac{D}{2}\right)$$

$$\therefore \quad \phi = \frac{ML}{IE}$$

But for a spring $\qquad M = W\frac{D}{2}\sin\alpha$

$$\phi = \frac{W(\frac{D}{2})L}{IE}\sin\alpha$$

From $x = \frac{1}{2}D[(\cos\alpha)\theta + (\sin\alpha)\phi]$

$$\theta = \frac{W(\frac{D}{2})L\cos\alpha}{JG}$$

$$\phi = \frac{W(\frac{D}{2})L\sin\alpha}{IE}$$

$$x = \frac{D}{2}[(\cos\alpha)^2\frac{W(\frac{D}{2})L}{JG} + (\sin\alpha)^2\frac{W(\frac{D}{2})L}{IE}]$$

$$now \quad L = \frac{\Pi Dn}{\cos\alpha}$$

$$x = W(\frac{D}{2})^2 L[\frac{\cos^2\alpha}{JG} + \frac{\sin^2\alpha}{IE}]$$

$$x = \frac{\Pi Dn}{\cos\alpha} W\frac{D^2}{4}[\frac{\cos^2\alpha}{JG} + \frac{\sin^2\alpha}{IE}]$$

now for a circular rod: $I = \frac{\Pi d^4}{64}$ $J = \frac{\Pi d^4}{32}$

$$\therefore x = \tfrac{1}{4}W \frac{\Pi D^3 n}{\cos\alpha} \left[\frac{\cos^2\alpha}{(\frac{\Pi d^4}{32})G} + \frac{\sin^2\alpha}{(\frac{\Pi d^4}{64})E}\right]$$

$$x = \frac{W\Pi D^3 n}{4\cos\alpha} \cdot \frac{1}{\Pi d^4} \cdot \left[\frac{32\cos^2\alpha}{G} + \frac{64\sin^2\alpha}{E}\right]$$

$$x = \frac{8WD^3 n}{d^4\cos\alpha} \left[\frac{\cos^2\alpha}{G} + \frac{\sin^2\alpha}{E}\right]$$

2.2 MEASUREMENT OF STRESSES IN COIL SPRINGS

Currently two methods are used for the fatigue testing of coil springs. The first and more acceptable method is the cycling of a complete coil spring through predetermined stress levels. The second method is to remove a single loop from a coil spring and subject it to cycling by applying point loads at the free ends (see method for testing isolated loop). Currently this is done at half the load capacity of a complete coil spring.

This case study will involve a mathematical analysis of the stresses in an isolated loop, followed by evaluating actual strain levels in both a complete coil spring and isolated loop by applying strain gauges to predetermined points. From the above a comparison can be made of stresses induced in an isolated loop versus a complete spring when the isolated loop is loaded at the end points with half the load of that of the complete spring.

2.2.1 Mathematical analysis of isolated coil

The aim of this study is to investigate and locate the points of maximum shear stress and bending stress mathematically on an isolated loop of a coil spring.

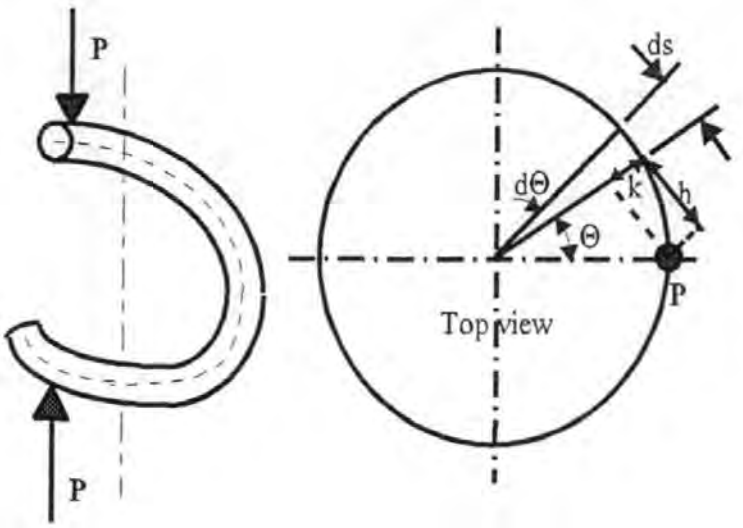

Figure 2.3: Illustration of test set-up for isolated loop.

For the purpose of this study we will investigate an isolated loop of a coil spring subjected to a vertical point load at the free ends. For the following study the effect of the helix angle will be neglected.

Where: Θ = angular displacement

M_B = bending moment

M_T = moment due to torsion

δ_B = bending stress

τ = shear stress

P = point load

R = radius of coil

d = coil wire diameter

D = coil diameter

At position Θ

$$M_B = Ph \qquad [h = R \sin\Theta]$$

$$M_T = Pk \qquad [k = R(1 - \cos\Theta)]$$

Therefore:

$$M_B = PR \sin\Theta$$

$$M_T = PR (1 - \cos\Theta)$$

$$\delta_B = PR\sin\theta\frac{32}{\Pi d^3} = \frac{16PD}{\Pi d^3}\sin\theta \quad \ldots\ldots(1)$$

and

$$\tau = PR(1-\cos\theta)\frac{16}{\Pi d^3} = \frac{8PD}{\Pi d^3}(1-\cos\theta) \quad \ldots\ldots(2)$$

From (1) δ_B is maximum at $\Theta = 90°$

From (2) τ is maximum at $\Theta = 180°$

For $\tau_{max} = \frac{1}{2}\sqrt{[(\delta_x - \delta_y)^2 + 4\tau_{xy}^2]}$

$$= \frac{1}{2}\sqrt{(\frac{16PD}{\Pi d^3}\sin\theta)^2 + 4(\frac{8PD}{PId^3}[1-\cos\theta])^2}$$

$$= \frac{1}{2}\sqrt{(\frac{16PD}{\Pi d^3})^2\sin^2\theta + (\frac{16PD}{\Pi d^3}[1-\cos\theta])^2}$$

$$= \frac{1}{2}\sqrt{(\frac{16PD^2}{\Pi d^3})^2[\sin^2\theta + (1-\cos\theta)^2]}$$

$$= \frac{16PD}{2\Pi d^3}\sqrt{\sin^2\theta + (1-\cos\theta)^2}$$

$$= \frac{8PD}{\Pi d^3}\sqrt{\sin^2\theta + 1 - 2\cos\theta + \cos^2\theta}$$

$$= \frac{8\sqrt{2}PD}{\Pi d^3}\sqrt{[1-\cos\theta]}$$

Therefore at θ=180°

$$\tau_{MAX} = \frac{16PD}{\Pi d^3}$$

$$\delta_{max} = \frac{\delta_x+\delta_y}{2} \pm \tfrac{1}{2}\sqrt{[(\delta_x-\delta_y)^2+4\tau_{xy}^2]}$$

where $\delta_x+\delta_y = \delta_b$

For this consideration of the isolated loop $\delta_y = 0$ and $\delta_B=\delta_x$

$$\delta_x + \delta_y = \delta_B = PR\sin\theta \frac{32}{\Pi d^3} = \frac{16PD}{\Pi d^3}(\sin\theta) \quad \text{.....(1)}$$

$$\tau_{xy} = PR(1-\cos\theta)\frac{16}{\Pi d^3} = \frac{8PD}{\Pi d^3}(1-\cos\theta) \quad \text{.....(2)}$$

$$\delta_{max} = \frac{16PD}{2\Pi d^3}\sin\theta \pm \frac{8\sqrt{2}PD}{\Pi d^3}\sqrt{(1-\cos\theta)}$$

$$\delta_{max} = \frac{8PD}{\Pi d^3}[\sin\theta \pm \sqrt{2}\sqrt{(1-\cos\theta)}]$$

Position of the max of δ_{max} : where $\frac{d\delta_{max}}{d\theta} = 0$

$$0 = +\cos\theta \pm \frac{\sqrt{2}\sin\theta}{2\sqrt{(1-\cos}$$

(Solve for θ to find position for δ_{max})

Let us find the angle on the isolated loop where δ_{max} will occur by plotting a graph of angle of rotation θ versus X1 and X2. (Where X1 and X2 will indicate points of maximum bending)

Where: X1 = sinθ + √2√(1- cosθ) [θ is in radians]

X2 = sinθ - √2√(1- cosθ) [θ is in radians]

From the graph in Figure 2.4 it can be concluded that the maximum bending stress will occur at 120° for equation X1 and at 240° for equation X2.

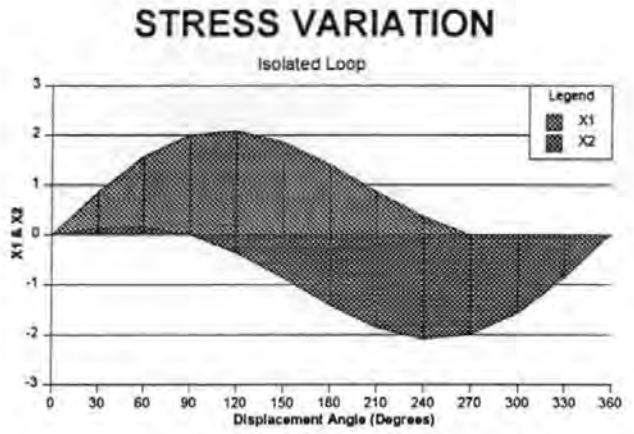

Figure 2.4: Position of maximum stress on a isolated loop of a coil spring.

2.2.2 Stress determination by means of strain gauges

To compare the strains/stresses imposed on a coil of a spring by means of strain gauges when it is loaded as follows:

- When a single coil is part of a complete spring which is loaded until the specific coil has a certain deflection
- When the single coil is removed from complete spring and loaded at the free ends until the isolated coil has a deflection that is the same as that of the complete spring.

This will reveal important data about stress comparisons between a full spring and isolated loop for the validation of a single coil fatigue specimen as substitute for full coil spring in mechanical testing.

2.2.2.1 Test sample

Automotive coil spring material: 55Cr3

Number of coils between end contacts: 5

Diameter of coil: 140 mm

Wire diameter: 12.5 mm

2.2.2.2 Test method

The first step was to apply strain rosettes at specific points on the complete coil spring. The gauges used were type FRA-2-11 45° rosettes, with a gauge length of 2 mm and 120 Ω resistance. These gauges were applied with the centre gauge along the axis of the coil wire, as illustrated in Figure 2.5.

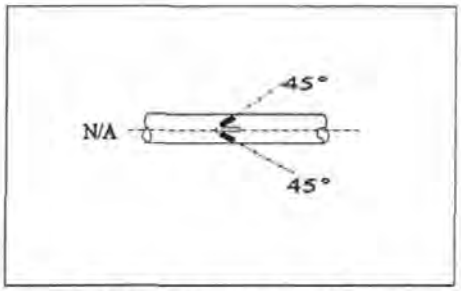

Figure 2.5: Orientation of strain gauge rosettes.

The selection of placement of gauges was based on the mathematical modelling done, which

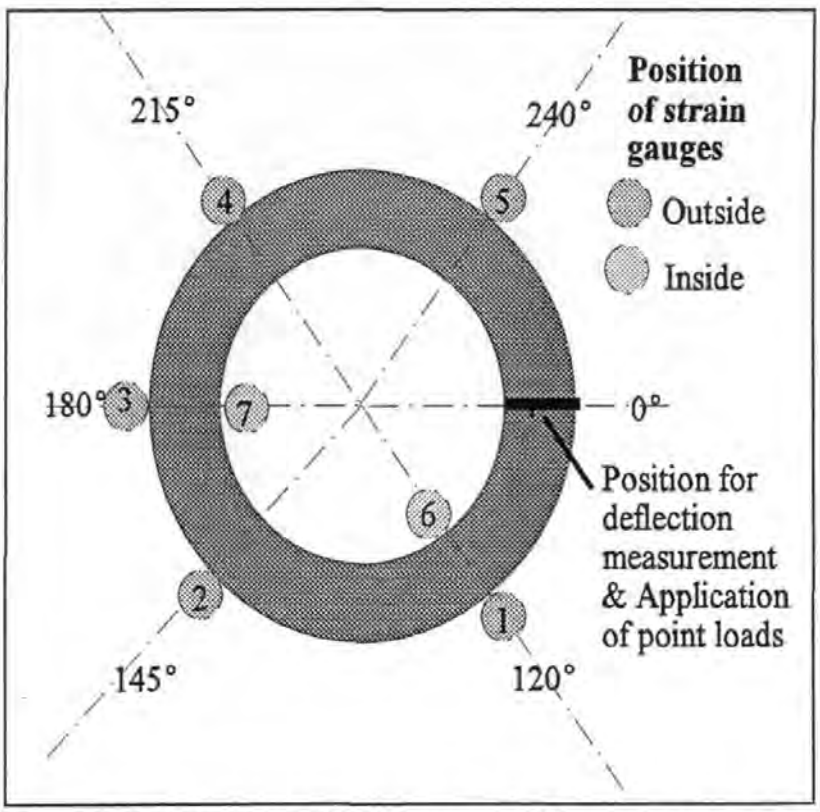

Figure 2.6: Placements of strain gauges with respect to top view of coil spring.

reveals that in the case of an isolated loop maximum shear would occur at 180°, and maximum

bending at 120° and 240°. In total seven gauges were applied. Figure 2.6 illustrates the position of gauges with respect to the top view of the coil.

The gauges were used in a quarter bridge configuration with temperature compensation. This resulted in each grid having three leads and, therefore, nine leads per gauge. Considering the small size of the gauges, this became a major task. Figure 2.7 illustrates the strain gauged coil spring as installed in the compression test machine, ready for testing. The extent of the wiring is quite clear and in the bottom left hand corner, the temperature compensation gauge assembly is visible. All strain measurements were done by means of an HBM-UBM40 strain amplifier with 20 channels.

Before carrying out the test, the spring was pre-loaded to 500 N, all gauges were zeroed and the system was balanced. The measurement procedure was as follows:

Figure 2.7: Set up of a full spring in test jig.

Data Recorded: 1. Deflection

2. Load

3. Strain values for all gauges (e_1, e_2, e_3)

This was done for deflection increments of 2 mm up and to a total deflection of 20 mm. The deflection was recorded at the rear side of the spring, directly opposite gauge (3)as illustrated by Figure 2.6. The whole process was then reversed from the total deflection of 20 mm to 0 mm to confirm that all strain readings are still the same.

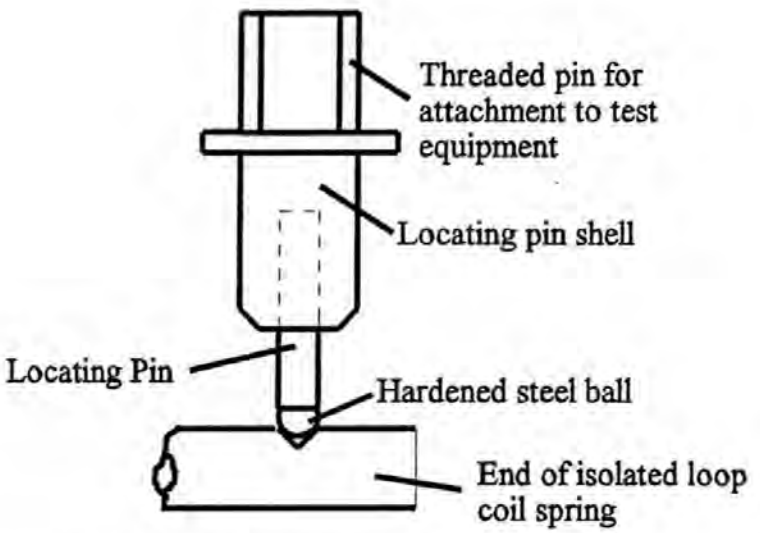

Figure 2.8: Locating pin assembly use for fatigue testing of isolated coils.

On completion of the complete spring test, the loop on which the strain gauges were installed, was carefully sectioned from the full spring for testing. The section removed was then prepared for loading. Indentations were made into the free ends of the coil at 0° position to accommodate purpose-made pins for the load application. Figure 2.8 illustrates the detail of the locating pins and the seating into the isolated loop, whereas Figure 2.9 shows the final installation.

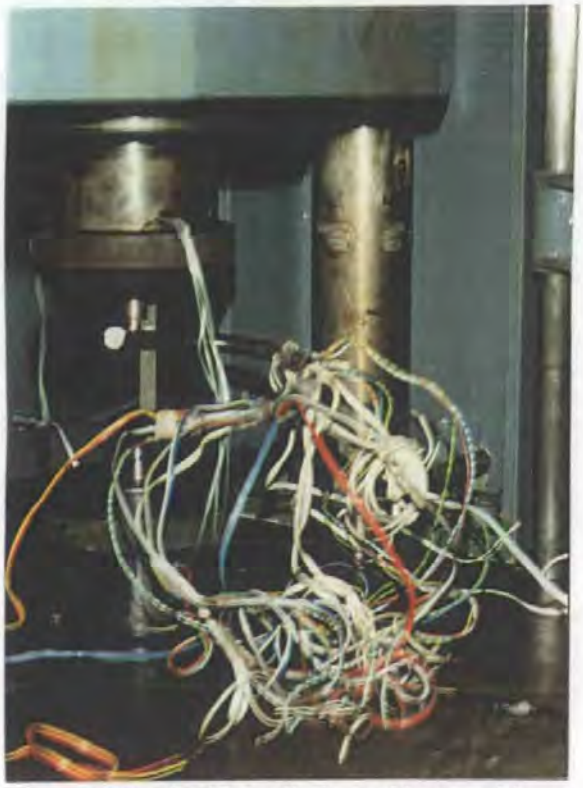

Figure 2.9: Final installation of isolated loop in test equipment.

The same loading procedures as for the full spring were followed in this case, except that the pre-load was adjusted to 250 N to produce the same moment as for the complete spring.

2.2.2.3 Results

	FULL SPRING Gauge 1				*ISOLATED COIL Gauge 1*			
Def mm	**Load N**	**Strain e1**	**Strain e2**	**Strain e3**	**Load N**	**Strain e1**	**Strain e2**	**Strain e3**
2	750	264.041	76.000	-222.581	350	135.625	44.000	-121.000
4	1000	510.101	146.000	-384.186	480	293.486	89.000	-260.571
6	1260	776.753	227.000	-465.448	620	454.667	139.000	-396.800
8	1525	941.403	304.000	-514.332	750	613.462	181.000	-536.897
10	1780	1150.000	385.000	-689.75	870	768.262	223.000	-678.802
12	2050	1523.000	475.000	-803.405	990	915.750	265.000	-809.262
14	2315	1797.000	559.000	-986.818	1125	1090.000	305.000	-960.811
16	2600	1997.000	645.000	-1214	1250	1252.000	346.000	-1100.000
18	2925	1877.000	740.000	-1407	1380	1405.000	385.000	-1246.000
20	3230	2267.000	830.000	-1553	1520	1590.000	422.000	-1398.000

	FULL SPRING Gauge 2				*ISOLATED COIL Gauge 2*			
Def mm	**Load** N	**Strain** e1	**Strain** e2	**Strain** e3	**Load** N	**Strain** e1	**Strain** e2	**Strain** e3
2	**780**	258.008	98.000	-200.296	**375**	194.377	69.000	-168.314
4	**1060**	499.714	191.000	-399.349	**510**	398.710	143.000	-345.873
6	**1375**	759.082	283.000	-604.000	**650**	608.447	214.000	-534.338
8	**1625**	985.490	364.000	-790.701	**775**	814.000	285.000	-720.353
10	**1920**	1241.000	461.000	-996.405	**900**	1015.000	350.000	-898.000
12	**2150**	1482.000	561.00	-1187.000	**1040**	1227.000	419.000	-1091.000
14	**2375**	1710.000	661.000	-1384.000	**1160**	1451.000	484.000	-1282.000
16	**2625**	1957.000	774.000	-1592.000	**1280**	1643.000	542.000	-1436.000
18	**2880**	2183.000	874.000	-1758.000	**1410**	1844.000	608.000	-1625.000
20	**3225**	2393.000	995.000	-1957.000	**1540**	2056.000	673.000	-1814.000

	FULL SPRING Gauge 3				*ISOLATED COIL Gauge 3*			
Def mm	**Load** N	**Strain** e1	**Strain** e2	**Strain** e3	**Load** N	**Strain** e1	**Strain** e2	**Strain** e3
2	**780**	251.613	87.000	-193.239	**410**	289.412	81.000	-250.835
4	**1010**	486.449	178.000	-385.000	**530**	511.000	144.000	-435.822
6	**1250**	716.000	251.000	-574.000	**660**	746.000	210.000	-631.700
8	**1525**	957.417	333.000	-771.000	**775**	989.000	270.000	-828.344
10	**1800**	1201.000	414.000	-952.418	**920**	1258.000	336.000	-1058.000
12	**2125**	1458.000	492.000	-1173.000	**1050**	1480.000	401.000	-1270.000
14	**2340**	1700.000	573.000	-1371.000	**1175**	1761.000	465.000	-1496.000
16	**2560**	1934.000	652.000	-1572.000	**1280**	1982.000	518.000	-1660.000
18	**2835**	2162.000	720.000	-1756.000	**1400**	2202.000	575.000	-1862.000
20	**3175**	2422	810.000	-1964.000	**1540**	2476	636.000	-2064.000

	FULL SPRING Gauge 4				*ISOLATED COIL Gauge 4*			
Def mm	**Load** N	**Strain** e1	**Strain** e2	**Strain** e3	**Load** N	**Strain** e1	**Strain** e2	**Strain** e3
2	**825**	266.538	90.000	-233.750	**400**	217.000	72.000	-230.000
4	**1060**	468.167	169.000	-389.676	**525**	431.000	138.000	-398.208
6	**1375**	700.000	233.000	-586.397	**650**	653.000	203.000	-572.197
8	**1660**	942.025	298.000	-773.317	**775**	875.000	262.000	-756.000
10	**1925**	1161.000	354.000	-959.000	**900**	1097.000	327.000	-950.000
12	**2160**	1372.000	417.000	-1160.000	**1040**	1317.000	384.000	-1145.000
14	**2380**	1583.000	479.000	-1349.000	**1150**	1554.000	444.000	-1340.000
16	**2590**	1819.000	535.000	-1533.000	**1275**	1760.000	502.000	-1530.000
18	**2875**	2043.000	579.000	-1742.000	**1390**	1975.000	552.000	-1701.000
20	**3180**	2247.000	636.000	-1940.000	**1525**	2202.000	613.000	-1898.000

	FULL SPRING Gauge 5				*ISOLATED COIL Gauge 5*			
Def mm	**Load** N	**Strain** e1	**Strain** e2	**Strain** e3	**Load** N	**Strain** e1	**Strain** e2	**Strain** e3
2	**750**	238.291	40.000	-142.683	**410**	189.000	46.000	-153.75
4	**1040**	453.283	105.000	-317.778	**540**	379.019	87.000	-289.029
6	**1325**	678.204	145.000	-487.411	**660**	540.000	124.000	-451.000
8	**1575**	880.062	184.000	-659.591	**780**	710.000	165.000	-628.000
10	**1860**	1110.000	208.000	-865.024	**925**	903.417	205.000	-872.432
12	**2135**	1352.000	234.000	-1105.000	**1040**	1060.000	236.000	-1102.000
14	**2375**	1567.000	260.000	-1321.000	**1150**	1234.000	271.000	-1318.000
16	**2590**	1801.000	279.000	-1561.000	**1280**	1414.000	305.000	-1518.000
18	**2875**	2028.000	287.000	-1791.000	**1410**	1587.000	334.000	-1689.000
20	**3225**	2291.000	305.000	-2031.000	**1540**	1766.000	367.000	-1834.000

	FULL SPRING Gauge 6				*ISOLATED COIL Gauge 6*			
Def mm	**Load** N	**Strain** e1	**Strain** e2	**Strain** e3	**Load** N	**Strain** e1	**Strain** e2	**Strain** e3
2	**800**	324.000	81.000	-344.774	**400**	154.000	59.000	-221.463
4	**1080**	585.000	147.000	-672.000	**540**	345.176	115.000	-442.000
6	**1380**	840.814	218.000	-1012.000	**660**	513.785	166.000	-665.000
8	**1625**	1097.000	305.000	-1330.000	**775**	693.421	214.000	-880.321
10	**1850**	1342.000	399.000	-1675.000	**900**	860.114	261.000	-1091.000
12	**2140**	1618.000	494.000	-2041.000	**1040**	1051.000	304.000	-1315.000
14	**2400**	1865.000	588.000	-2374.000	**1150**	1223.000	345.000	-1529.000
16	**2640**	2123.000	685.000	-2686.000	**1280**	1404.000	386.000	-1751.000
18	**2900**	2362.000	779.000	-3017.000	**1400**	1571.000	420.000	-1947.000
20	**3225**	2627.000	866.000	-3422.000	**1540**	1753.000	459.000	-2188.000

	FULL SPRING Gauge 7				*ISOLATED COIL Gauge 7*			
Def mm	**Load** N	**Strain** e1	**Strain** e2	**Strain** e3	**Load** N	**Strain** e1	**Strain** e2	**Strain** e3
2	**825**	218.000	110.000	-319.196	**410**	251.857	79.000	-367.000
4	**1100**	463.784	219.000	-652.870	**530**	501.537	154.000	-648.759
6	**1400**	696.912	309.000	-956.667	**660**	761.000	234.000	-943.000
8	**1640**	970.675	408.000	-1245.000	**780**	993.000	309.000	-1248.000
10	**1875**	1205.000	490.000	-1552.000	**900**	1232.000	373.000	-1505.000
12	**2150**	1462.000	584.000	-1866.000	**1040**	1506.000	455.000	-1844.000
14	**2400**	1717.000	674.000	-2166.000	**1160**	1775.000	529.000	-2141.000
16	**2660**	1984.000	758.000	-2469.000	**1280**	2013.000	594.000	-2436.000
18	**2940**	2242.000	843.000	-2786.000	**1400**	2254.000	648.000	-2706.000
20	**3275**	2496.000	939.000	-3090.000	**1530**	2493.000	710.000	-2983.000

Table 2.1: Results of strain measurements.

Table 2.1 contains the results of both the complete spring and the isolated loop. This first set

of tables reveals the recorded data for both the full coil spring and the isolated loop for each strain gauge rosette separately

2.2.2.4 Calculations

From the data in Table 2.1, the principal strain, stresses and maximum shear stress and strain were calculated by using the following equations:

$$\epsilon_1,\epsilon_2=[\frac{1}{2}(\epsilon_x+\epsilon_y)\pm\frac{1}{\sqrt{2}}\sqrt{(\epsilon_x-\epsilon_y)^2+\phi^2}]$$

Where:

$$\epsilon_x=e_1 \qquad \epsilon_y=e_3 \qquad \phi=e_1+e_3-2e_2$$

Principal stresses:

$$\sigma_{min}=\frac{E(\epsilon_2+\upsilon\epsilon_1)}{1-\upsilon^2} \qquad \sigma_{max}=\frac{E(\epsilon_1+\upsilon\epsilon_2)}{1-\upsilon^2}$$

Maximum shear stress:

$$\tau_{max}=\frac{\sigma_1-\sigma_2}{2}$$

2.2.2.5 Possible errors

The accuracy of strain readings could have been influenced by a number of possible sourses. The influence of some factors can be quantified where again other are more difficult to quantify. Although errors and uncertainties are always present to varying degree in all measurements of physical variables great care was taken to limit their influence to a minimum.

The following area of concern for errors had been identified.

- Behaviour of coil spring during compression. Great care had to be taken to ensure that movement at the ends of the coil spring was eliminated as far as possible as any movement during the experiment could influence strain readings.
- It was important not to restrict the free end of the isolated loop.
- Drilling of the locating holes for the hardened steel balls for the isolated loop required a large degree of accuracy. Any mis-alignment of these holes would cause a extra twist couple which could influence strain readings.
- The measurement of the deflection had to be done to a high degree of accuracy as this was the only variable that was kept constant between the isolated loop and the full spring.
- Another possible error and most likely one to influence results was the misalignment of the strain rosettes. Considering the size of the grid length (2 mm) it is all most impossible to align these gauges 100%. Making use of the Mohr's strain or stress circle these errors were calculated and the average mis-alignment error was found to be $\pm 4°$.

Although every effort was made to limit the effects and influence of errors on results it must be realised that these phenomena will always have an influence on the results. However it is important to note that in this study the comparison of characteristics play a more important role than the actual magnitude of values.

2.3 DISCUSSION OF FINDINGS

Comparison between full coil springs and isolated loop stress results are shown in the set of graphs attached as Appendix B. The first set of graphs shows the relation between the load and strain measured on each individual grid of the rosettes. The second set shows the relation between principal stresses and the deflection for each gauge position of the full spring and the

isolated loop. The graph in Figure 2.11 gives an indication of the relationship between load and deflection.

From the first set of curves, that of strain versus load, the following can be concluded:

In general it can be observed that for both the isolated loop and full spring, the strain values for e_1 and e_3 compared favourably, while those of e_2 were considerably lower for both test

Figure 2.10: FEA plot indicating the area of high stress in a coil spring.

conditions and gauge position. Considering the gauge orientations with the grid measuring e_1 and e_3 at 45° to the neutral axis of the coil and the grid measuring e_2 along the neutral axis, it becomes clear that the most prominent player is torsion, with bending effect considerably smaller as the strain recorded by the gauges at 45° to the neutral axis measuring torsional strain were considerable higher than the gauge on the neutral axis measuring bending(See Appendix B). The difference in magnitude of e_1 and e_3 on the graph is due to slight misalignment of strain gauges. Theoretically these values should be the same, but of opposite sign as the strain grids are both orientated with 45° to the neutral axis.

The highest strain value in the full spring was recorded by gauge 6 which was located on the inside of the coil at 180° away from the position where the deflection was measured. Second highest strain was recorded by gauge 7, also situated on the inside but only 120° away from the position where the deflection was measured. In the isolated loop, the highest strain was

again recorded by gauges 6 and 7, but their difference was of a smaller magnitude. This underlines the fact that the high stress in coil springs always occurs on the inside of the spring. Figure 2.10 shows the results from a finite element analysis, which clearly shows that the highest stress occurs on the inside as indicated by the red area.

The strain induced at gauge 3 was ± the same in both the isolated loop and full spring, but at all other gauge positions, the strain measurement on the full spring was slightly higher than those measured on the isolated loop. If the load induced is considered, it can be seen that the same strain levels in the isolated coil and the full spring were not induced by exactly doubling or halving the load as revealed by the graph in Figure 2.11. It must always be borne in mind that during these tests the only variable kept constant in both set-ups was the deflection, which was measured between the strain gauged coils at a position 180° opposite to that of gauges 3 and 6 as shown in Figure 2.6.

2.3.1 Principal stress and deflection (For graphs see Appendix B figure 2)

In comparing the results of the full spring and the isolated loop, the principal stresses compared with in 10% to each other except for positions 1 and 6 where this was 40%. At both these positions the principal stresses present in the isolated loop were lower than that in the full spring at 20mmdeflection. The magnitude of the principal stress varied between gauge positions with the maximum value (-620 MPa)calculated at gauge 6 and the second highest (-580 MPa) at gauge 7. The minimum principal stresses were calculated at gauge 1(-210 MPa). The magnitude of the principal stresses at position 6 and 7 (which is on the inside of the coil) at any given deflection, indicates a considerable increase of the principal stresses at the same position just on the outside, e.g. at 20 mm deflection maximum stresses at 6 and 7 are 620 MPa and 580 MPa, and 420 MPa at gauge 3 and 1 respectively. These are for the full spring. For more comparisons consult Table 2.1. Again it is important to read these results in conjunction with the load deflecting ratios from the graph in Figure 2.11. The load deflection ratio can be

better expressed by means of a "k-factor". This k-factor reflects the relation between the load applied to the complete spring to that applied to the isolated loop for obtaining the same deflection. This is clearly illustrated in section 2.3.2.

2.3.2 Load versus deflection

Deflection was the common variable to both the isolated loop and the full spring test. If the

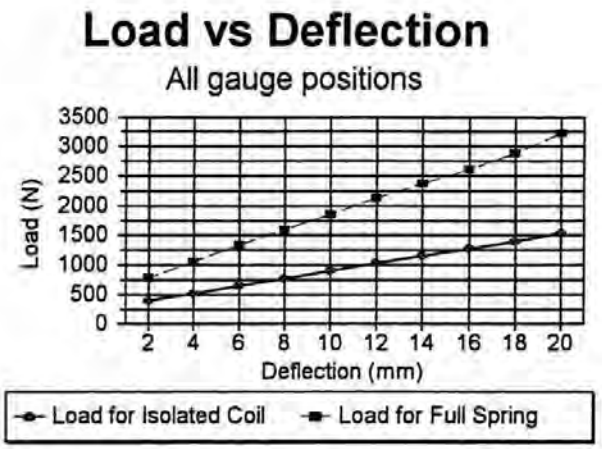

Figure 2.11: Load versus deflection graph.

average loads are used for the full spring and the isolated loop and plotted against deflection, it reveals a few interesting factors. Both the load deflection graphs display linear characteristics. On closer examination of the results a comparison between the load applied to the isolated loop and to the full spring for achieving the same deflection yielded the following.

Deflection	2	4	6	8	10	12	14	16	18	20
k-factor	2.0	2.011	2.054	2.066	2.06	2.059	2.055	2.046	2.066	2.1

Where: k-factor is calculated from load ratio for producing same deflection:

$$k\text{-}factor = \frac{Load\ complete\ spring}{Load\ isolated\ loop}$$

The percentage variation that exists between the load used for the full spring and twice the load on the isolated loops is illustrated in the graph in Figure 2.12. This relation is not linear but varies, as the deflection was increased the percentage error increased as well. This could

have resulted as the ends of the isolated loop were unrestricted and pin loaded.

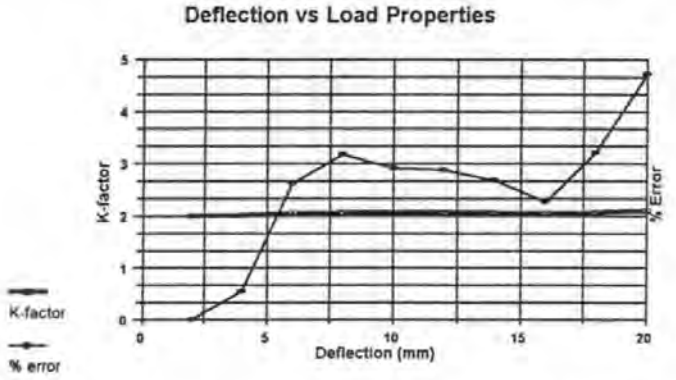

Figure 2.12: Overall comparison of result.(Full spring vs Loop)

2.4 SUMMARY

This study yielded some interesting results around stresses and their distribution in a full spring and an isolated coil. It confirmed that the maximum stress occurs on the top inside of the coil, but that the stress is not uniform throughout. The bending component in the spring material was 70% smaller than the torsional effect, but should never be disregarded. The higher stresses on the inside can be attributed to the short fibre length at the inside of the coil[2]. One can conclude from this that the fatigue failure should usually originate from the inside of the coil. As far as load ratio goes, it appears that the loads used on an isolated loop of a coil, applied at the free ends, should be about half of the axially applied load on a complete spring to induce the same stress levels keeping in mind that this is only applicable to a limited deflecting range. Also interesting was the fact that the same deflection range as was applied to both the isolated loop and full spring induced the same stress levels. This implies that for the above cases the same deflection is achieved by halving the load. From all data presented, it is clear that there exists some correlation within limits of the stress conditions between the isolated loop and the complete spring. It, however, should be realised that percentage error in load versus deflection increases as the deflection gets larger as the isolated loop have more freedom for movement than the complete coil spring during testing. The isolated loop can be used as a replacement fatigue test method and should yield reasonable results within acceptable limits.

CHAPTER 3

THE INFLUENCE OF MANUFACTURING PROCESS ON FATIGUE PROPERTIES OF 55Cr3 SPRING STEEL

INTRODUCTION

This chapter is to reveal the relationships between fatigue failures and process effects in 55Cr3 spring steel. This mechanism was investigated by fatigue testing coil springs withdrawn from different stages of manufacture and then determining the causes of failure by fracture analysis. The main objective is to identify and highlight failures that occur due to process parameters and to identify any possible change to the manufacturing process that could lead to an increase in the fatigue life of the material. All fatigue samples were manufactured from 55Cr3 spring material by National Spring, Johannesburg, South Africa.

3.1 MANUFACTURING SPECIFICATIONS OF 55Cr3 COIL SPRING MATERIAL

3.1.1 Material specifications

Type: 55Cr3 Comparison: SAE 5160

DIN 55Cr3	- Germany
NBN 55Cr3	- Belgium
BS 525 H 60	- Great Britain
AFNOR 55Cr3	- France
UNI 55Cr3	- Italy
JIS SUP9(A)	- Japan
SS 2253	- Sweden

3.1.2 Chemical analysis

C	:	0,52 - 0,59
Si	:	0,25 - 0,50

Mn	:	0,70 - 1,00	
Cr	:	0,7 - 1.00	
P	:	0,03	TRACE ELEMENT
S	:	0,03	TRACE ELEMENT

3.1.3 Mechanical properties

Tensile Strength	:	1520 MPa
Yield Strength	:	1175 MPa
% Elongation	:	6%
Hardness (Normalised)	:	310 HB
(Soft annealed)	:	248 HB
Young's Modulus (E)	:	206 GPa
Poison's Ratio (ν)	:	0.28 - 0.3

3.2 MANUFACTURING PROCESS (Summary)

Incoming material is drawn to an area reduction of 10 to 20% . The drawn steel is cut to length and then goes through a process of centre-less grinding to reduce the diameter by 3%. This is done to reduce the decarburised zone as shown in Plate 3.1.

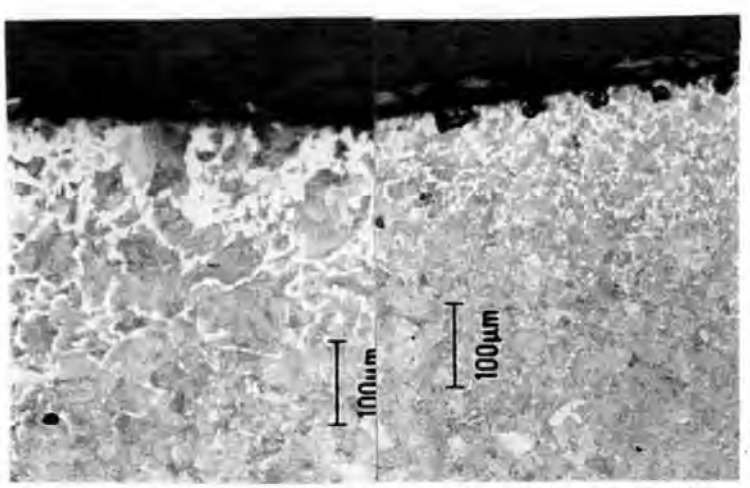

Plate 3.1: Reduction of decarburised zone due to grinding process. Ground material is shown on right.

The ground bar is austinitised at 868°C to 880°C and hot coiled. After coiling it is quenched in oil of which the temperature can vary between 35°C and 70°C but under normal production runs at 60°C. After quenching the components are tempered at 375°C for 90 minutes to assure a grain size of 5 x 8 ASTM.

After tempering the components are allowed to cool down to between 180°C and 200°C and are then hot scragged three times to solid length at this temperature. This process will induce a torsional stress which will resist sagging. The hot scragging is done at 200°C as the material yield point is lower at this increased temperature and thus the applied stress exceeds this during scragging which will result in a hysteresis effect inducing increased torsional residual stresses into the steel.

The component is now checked for any surface defects and cracks using a dye penetrant test. After this quality assurance procedure the component will be shot peened to induce compressive residual stresses in the surface to offset any applied tensile stress effectively and increase the fatigue life. This mechanism of shot peening will later be explained in detail. The shot peened component is now coated by means of phosphate and black paint and then oven dried. Before the component is despatched to the motor manufacturer it is cold scragged and rated according to its load rate. Consult Table 3.1 for identification of where samples for fatigue test have been withdrawn.

Batch no	Drawn Grind	Hot-Coil	Quench	Tempered	Hot-Scrag	Shot-Peened	Painted	Load Tested
1	✔	✔	✔					
2	✔	✔	✔	✔				
3	✔	✔	✔	✔	✔			
4	✔	✔	✔	✔	✔	✔		
5	✔	✔	✔	✔	✔	✔	✔	
6	✔	✔	✔	✔	✔	✔	✔	✔

Table 3.1: Process conditions of fatigue samples.

3.3 PRINCIPLES OF HEAT AND SURFACE TREATMENTS OF 55Cr3 SPRING STEEL

3.3.1 Heat treatments

It is the purpose of this section to explain in detail the material changes due to the heat treatment of 55Cr3 steel bar. This will be done with reference to microstructural changes and other properties.

3.3.1.1 Austenitise and quench

The first heat treatment of the spring manufacturing process is austenising of the drawn and ground steel bars. This is done at a temperature range of 868°C to 880°C which is well into the austenitic temperature range for the steel. In the austenitic state the crystal structure will be a face centred cubic iron with carbon in a solid solution[4,5,6]. The coiling is performed at this elevated temperature as it will allow coiling to take place with limited distortion of grains which could influence the hardness. If structural steel is air cooled from the austenitic range it will produce ferrite-pearlite microstructures, but for the development of high tensile strengths steel it requires the generation of lower temperature transformation products such as martensite. This is achieved by quenching the austenitic coil into oil which is maintained at a temperature of 35°C to 70°C. It must be clearly understood that fast cooling rates such as in oil quenching, promote the formation of martensite but are not the only role player in this effect as the presence of alloying elements will assist in resisting the formation of ferrite and pearlite, allowing martensite to be formed at the relatively slow cooling rate[4]. The austenitised coil which is quenched will then produce an untempered martensite structure as shown in Plate 3.2 (This picture was taken on a Phillips XL30 SEM x 3 000 magnification). The above heat treatment will increase the hardness and strength levels of the material, but the hardenability of the material is to a large extent determined by the alloying elements[7]. For influence on mechanical properties and fatigue life see Table 3.2. If compared to the hardness of the drawn

material the heat treatment results in 40% increase in hardness at full depth. (See Table 3.3 for hardness values).

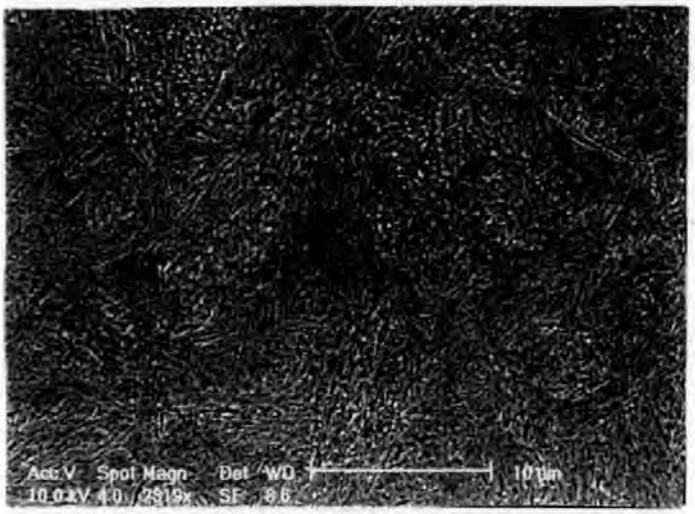

Plate 3.2: Untempered martensite in oil quenched 55Cr3 spring steel (870°C).

3.3.1.2 Tempering

The second heat treatment involves the tempering of the quenched coils and this involves heating the coils to 375°C and keeping it at this elevated temperature for 90 minutes. In the manufacturing of spring steel the tempering process is critical and must be accurately controlled. The mechanism of tempering of 55Cr3 spring steel produces a physical size change of the coil that was quenched hardened. The structural change causes a contraction[4]. Compare

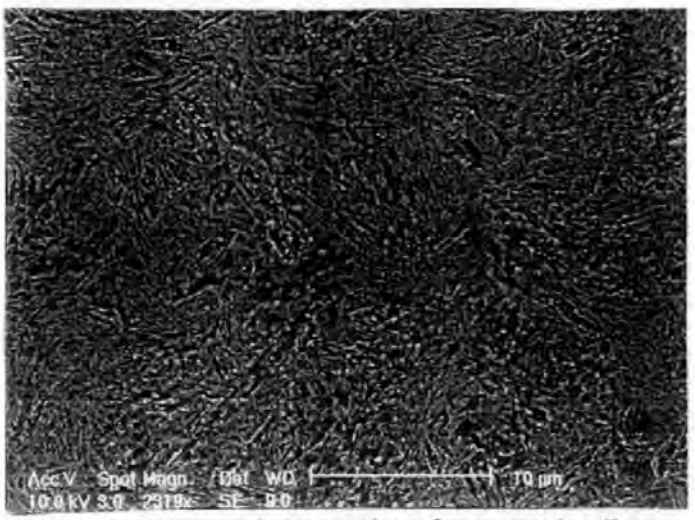

Plate 3.3: Tempered martensite of tempered coil at 375°C for 90 min.

the two microstructures in Plate 3.2 and 3.3, where the one is untempered martensite from a quenched coil and on the other that of tempered martensite of a tempered coil. The effect of the tempering operation on the strength of the spring is very slight (see Table 3.4.) but it will result in a grain size of 5 x 8 ASTM. The full depth hardness of the tempered coil will be reduced by 33% (see Table 3.3) in comparison to that of the quenched coil.

The mechanism of tempering observed in 55Cr3 spring steel involves the diffusion of carbon atoms from the martensite to form carbide precipitates. Very little austenite was retained and no evidence of the presence of ferrite was found. The influence of the heat treatments on the fatigue life of the coil springs will be explained later in this chapter.

3.3.1.3 Hot scragging

The main purpose of the hot-scragging process in the manufacture of 55Cr3 spring steel is to improve the sag resistance of the spring[2,7]. The mechanism of sag resistance correlates well with the Bauschinger effect. During the hot scragging of 55Cr3 spring steel micro-residual back stresses are introduced that will reduce the effect of applied stresses. This is done by controlling the cooling of the coils after the tempering process. When the coil reaches a temperature of 200°C it is scragged (x3) to its solid length. At this higher temperature the yield stress of the material is lowered allowing it to be exceeded by the stress induced by scragging. The spring steel is subjected to plastic strain which will cause some dislocations to pile up at the grain boundaries[7,8,9]. This will allow some dislocations to tangle with each other which produces micro-residual back stresses. Plate 3.4 shows the dislocations present in a hot scragged component of 55Cr3 spring steel at 1.5 mm below the surface.

When the spring is settled, the residual stresses reduce the actual magnitude of the applied stresses as they are in an opposing direction. It was also noted that the hot scragging process

contributed to a reduction in the overall length of the spring compared to the coils withdrawn after quenching and tempering, this overall length reduction is in the order of 12,6%.

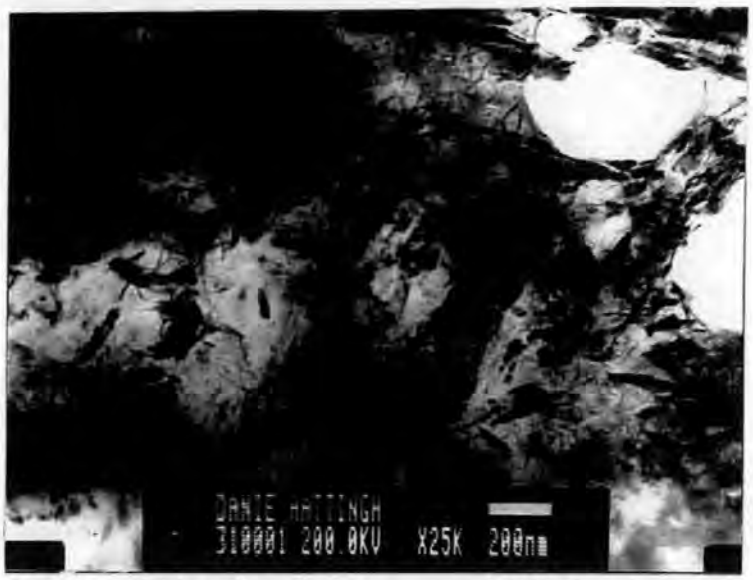

Plate 3.4: Dislocations in hot scragged 55Cr3 spring steel (x25000 - TEM Micrograph).

The hot scragging process has little effect on the microstructure of the material as illustrated by Plate 3.5. The micrograph reveals a compact tempered martensite structure which is similar to that of the tempered sample.

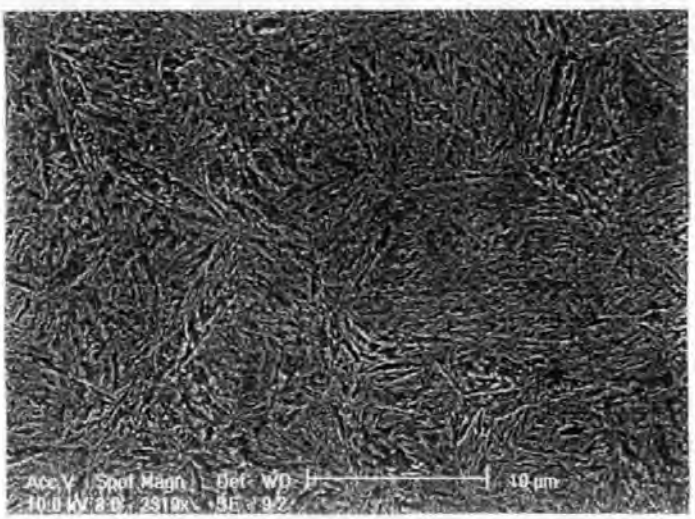

Plate 3.5: Martensite structure of a coil withdrawn after hot scragging at 200°C.

The effect of manufacturing process on other properties of the steel can be seen in Table 3.4.

There are a number of other factors that play a role in sag resistance of 55Cr3 spring steel. The presence of silicon[7] is known to increase sag resistance of spring steel as well as reducing the grain size[8]. The relative sag resistance can be evaluated by the magnitude of the hysteresis

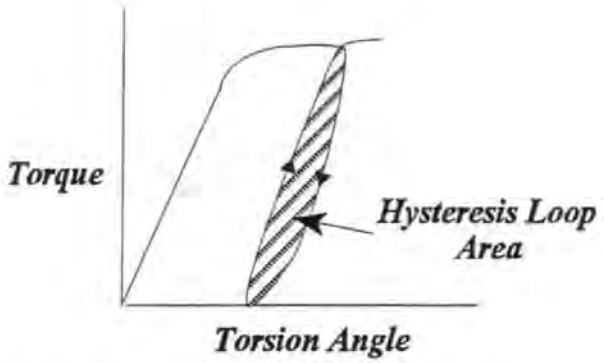

Figure 3.1: Hysteresis loop.

loop area, shown in Figure 3.1. The larger the loop area the better the sag resistance as this implies an improvement in work hardening which will result in a increase in the ultimate tensile stress of the material because of this increase in hardness. Figure 3.2, shows that the finer the grain size the larger the hysteresis loop will be, resulting in better sag resistance of the material[7].

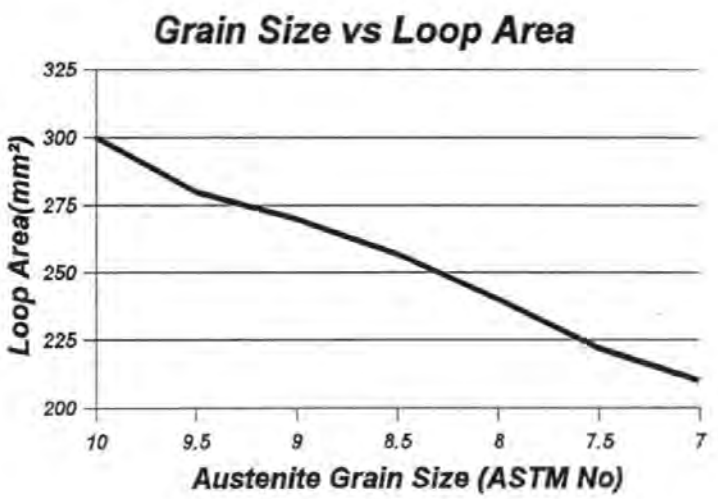

Figure 3.2: Effect of austenite grain size on hysteresis loop area.

3.3.1.4 Shot peening

It is a well known fact that shot peening can greatly improve the fatigue strength of spring steel but it is not always done at the correct stage of manufacture. A large number of spring manufacturers still apply the shot peening before the preset (scrag) process which is not the most effective. In the manufacture of 55Cr3 spring steel it is done after the presetting process.

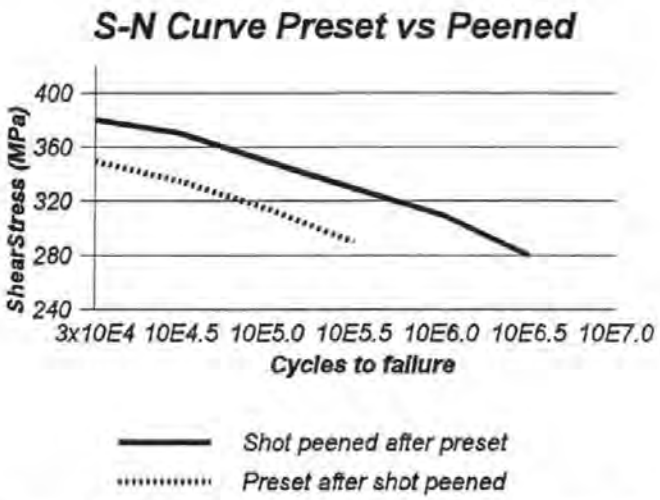

Figure 3.3: Effects of shot peening on fatigue life of 0.9% C steel when done before and after preset. (12 mm diameter)

The effect of this can be seen in the graph of Figure 3.3. Shot peening after presetting definitely produces better fatigue properties[6]. The mechanism of fatigue improvement by the shot peening process in 55Cr3 spring steel will be discussed in detail in the chapter relating to process effects and residual stresses.

The shot peen process will induce compressive residual stresses at the surface which improves the fatigue life considerably, this can be seen in Table 3.2. These compressive surface stresses will improve the ability of the material to resist the propagation of fatigue cracks in the surface[4].

Another important observation is that the shot peen process will notably reduce the scatter of

fatigue data as illustrated in Figure 3.4. From the fatigue tests done on 55Cr3 spring steel during this research the variation in fatigue data after the quench process was 86% and after shot peening only 25% as this process reduced the notch sensitivity of the material.

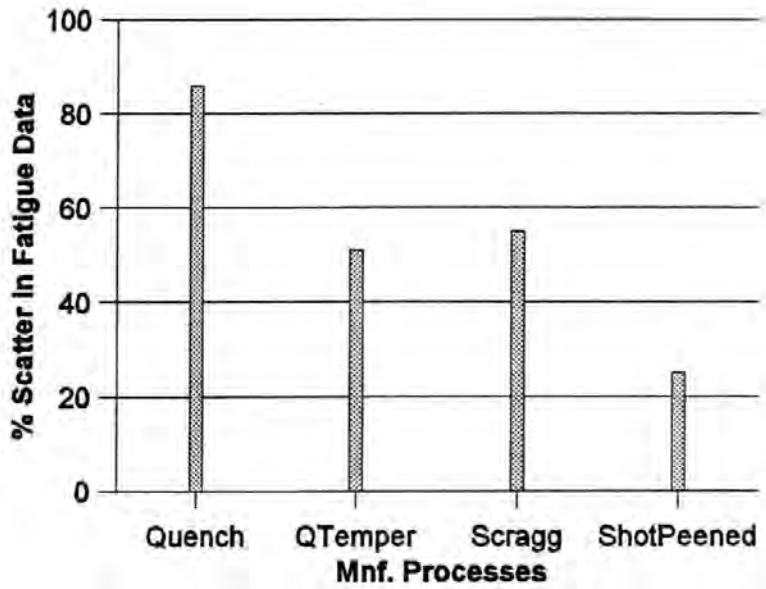

Figure 3.4: Relation between scatter in fatigue data and the manufacturing processes.

On the statistical side shot peening will contribute by significantly decreasing the standard

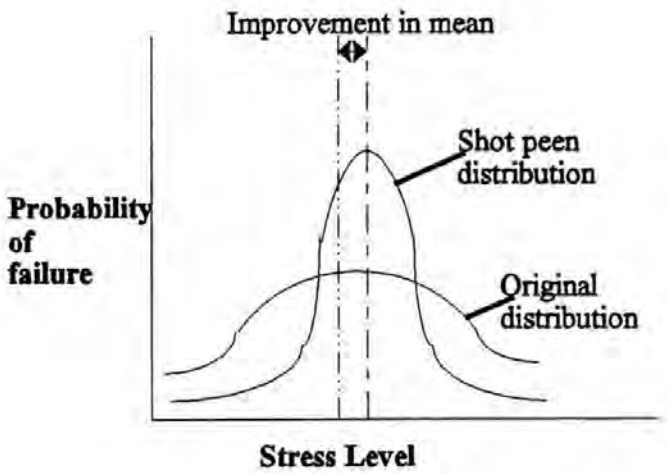

Figure 3.5: Improvement of fatigue properties by reduction in scatter through shot-peening.

deviation of data distribution by the induction of a compressive layer in the surface of the spring[6]. Figure 3.5 shows that the minimum fatigue strength may be greatly improved even if

the mean improvement is small as the reduction of not sensitivity of the material allows for more reliable fatigue data. The practical importance of this observation underlines the necessity for shot peening in critical regions of highly stressed fatigue sensitive components. Shot peening is a surface treatment and has no influence on the overall microstructure or full depth hardness of the material.

3.3.1.5 Painting process

The painting process involves two stages. The first is the application of a phosphate and E coat black paint to the shot peened component. It is then hooked onto a conveyer line which moves through a drying oven at 180°C, after which it is allowed to cool naturally.

It would seem that the only objectives of this process is to protect the material from corrosion and to improve the appearance of the product. An important observation made after this process was that it had a minor influence on the fatigue properties. This process had no effect on microstructure or hardness of the material.

3.3.1.6 Cold scrag /Load test

This is the final manufacturing process of the coil spring and is done to verify the load rate of the final component. Again some important observations were made, although the microstructure, hardness and other mechanical properties stayed mostly unchanged, the fatigue life of the coil was influenced considerably (see Table 3.2 for comparison of results). The principle of cold scragging is very closely related to that of the hot scragging process whereby a dislocation pile-up is created[2] and residual stresses are induced to improve sag resistance of the coil. The influence of this process on the fatigue life of the coil spring will be elaborated on later in this chapter.

Process stage	Cycles of failure (Avg)
Quench	737
Quench tempered	1 792
Hot scragged	2 315
Shot peen	2912710
Painted (Before LT)	3034650
Load tested	725480

Table 3.2: Fatigue data of processed samples (55Cr3).
(For test conditions - see section 3.4.2)

Process / Position	Quench	Quench Tempered	Hot Scragged	Shot peened	Painted	Load tested (Cold scrag)
Left edge	782	525	530	548	560	554
Off centre	782	525	525	530	560	554
Centre	792	530	536	530	542	566
Off centre	782	525	519	530	554	548
Right edge	782	530	525	542	554	554

Table 3.3: Cross sectional hardness values of fatigue samples.(Hv10)

	Raw	Drawn	Quench	Quench Tempered	Hot Scrag	Shot peened	Painted	Load tested Cold scrag
Tensile (UTS)Mpa	756.0	962.9	2847	1633	1633 *	1760*	1820*	1760*
% Elongation	17.2 %	6.6%	0%	4.8%	-	-	-	-
Torsional Shear MPa	591.6	772.6	932.5	982.5	-	-	-	-
% Increase Impact**	Ref. 0%	0%	15%	36%	47%	56%	42%	37%

NOTE: * Tensile values as converted from Hv30 hardness values.
****% Increase of impact strength are reflected w.r.t raw material as non standard specimens were used. Impact specimens where machined from complete coil spring.**

Table 3.4: Mechanical properties of processed fatigue samples.

3.4 FATIGUE TESTS

3.4.1 Manufacture of fatigue samples

A number of methods exist for preparing fatigue samples of which the most popular is the rotating bending type test specimen[5]. This method was considered but it was felt that a test specimen, more representative of the final production component, should be used. The first step was to study the manufacturing process to identify stages at which coils could be withdrawn successfully. After a number of attempts, it was decided to withdraw samples after the following stages of manufacture:

1. After hot coil and quenching
2. After tempering
3. After hot scrag
4. After shot peening
5. After painting (before load test)
6. After load test (cold scrag)

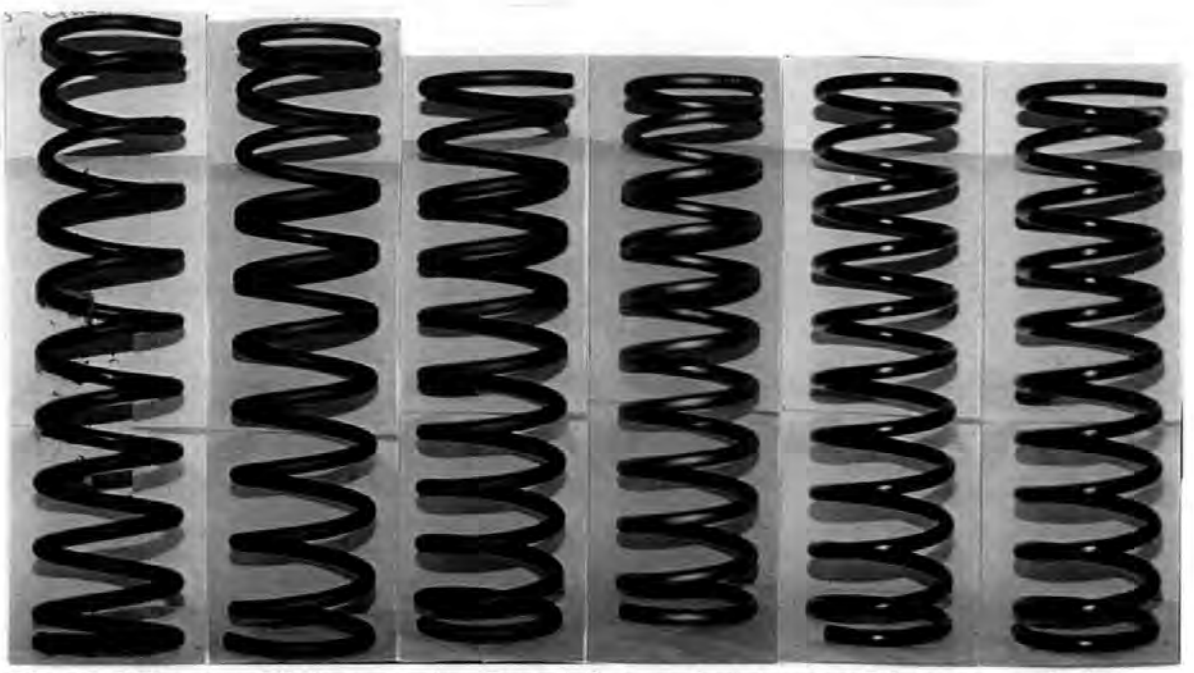

Plate 3.6: Processed fatigue samples: From left, quenched, tempered, hot scragged, shot peened, painted, load tested.

Plate 3.6 shows the processed sample ready for fatigue testing. The samples were withdrawn

on a random basis from the production line of one specific part number. These were coil springs manufactured for the suspension of the Volkswagen Golf motor car. A total of 30 samples were withdrawn, twenty four for fatigue test purposes(four samples per manufacturing process) and six for the measurement of residual stresses (one samples per manufacturing process).

3.4.2 Fatigue test method

The fatigue tests were performed on a "Coil Spring Fatigue Tester" type P137/1340/1-29 supplied by Rohloff Germany as illustrated in Figure 3.6. The machine stands ± 4 m high and is approximately 2 m in diameter.

The equipment makes use of an eccentric principle to cycle the coil spring and must be loaded with four coil springs at all times. The coil spring is installed and then compressed by tightening it to achieve the desired minimum stress levels before tests commence. The operating speed is 4 Hz. The line of operation of the equipment is vertical and fixtures are designed in such a way that minimum interference occurs and very little stresses are induced. It is very important to ensure that no failures are equipment related. End fixtures are manufactured to a high degree

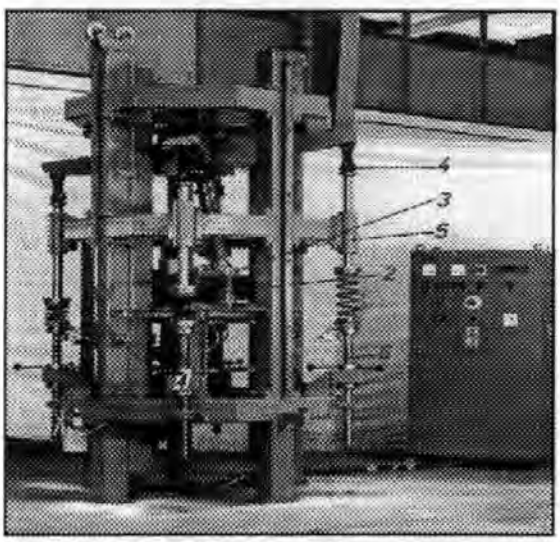

Figure 3.6: Coil spring fatigue tester- type P137/1340/1-29 (Quality Assurance Laboratory, Volkswagen SA)

of accuracy with minimum interference of specimen under test. Loading through end fixtures is perfectly axial. Once a failure occurs the machine automatically stops and a replacement sample must be installed to continue the test. Table 3.5 shows the installation test specifications for samples withdrawn from different stages of the manufacturing process, while Figure 3.7 reveals the relation for the stresses induced at different deflections. The overall lengths of the coil springs withdrawn after quenching and tempering were 50 mm longer than samples withdrawn after the hot scrag stage. It was therefore necessary to adjust the test set-up for these samples in order to ensure that the induced stresses were the same for all samples.

The samples were subjected to a comprehensive stress range from 85,7 MPa (minimum) to 951 MPa (maximum), calculated using standard theory[2] as follows:

$$K = \frac{4c-1}{4c-K} + \frac{0.615}{C}$$

$$C = \frac{D}{d}$$

$$\tau = \frac{8PC}{Kd}$$

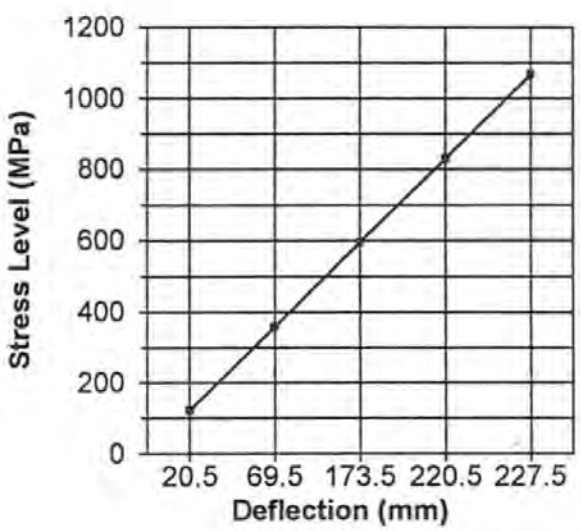

Figure 3.7: The fatigue test stress deflection relation for 55Cr3 coil springs samples.

All tests were performed at the Quality Assurance Laboratory of Volkswagen of SA, at their

Uitenhage assembly plant.

Process Stage	*Overall Length (mm)	**Installed Length (mm)	***Compressed Length (mm)
Quench	396,5	376	176
Temper	396,5	376	176
Hot Scrag	346,5	326	126
Shot Peen	346,5	326	126
Before load test (painted)	346,5	326	126
Load test	346,5	326	126

*** Overall length = Total length of cool spring as withdrawn from manufacturing process**
**** Installed length = Length to which spring is compressed before fatigue test is commenced**
***** Compressed length = Length to which spring is compressed during each fatigue cycle**

Table 3.5: Fatigue test installation specifications.

3.5 ANALYSIS OF FATIGUE FAILURES AND FRACTURE SURFACES

The objective of this section can be summarised by K J Miller's question posed in his paper, Metal Fatigue - A New Perspective:[10]

> *"Under what condition will a metal, component or structure survive indefinitely when subjected to cyclic forces, and what changes occur that introduce the possibility of failure?"*

The failure analysis was done by considering what the influence of the different processes was on the mechanism of failure. During the analysis the following topics were considered: Position of failure, Macroscopic observations, Microscopic analysis and Fatigue life.

3.5.1 Quench

3.5.1.1 Position of fracture

All the quenched fatigue samples failed within the first turn of the coil spring as illustrated in Plate 3.7. The fracture initiating from the inside of the coil wire and from the photo it can clearly be seen that initial fracture results in a series of secondary fracture surfaces as the coil

shattered into a number of pieces.

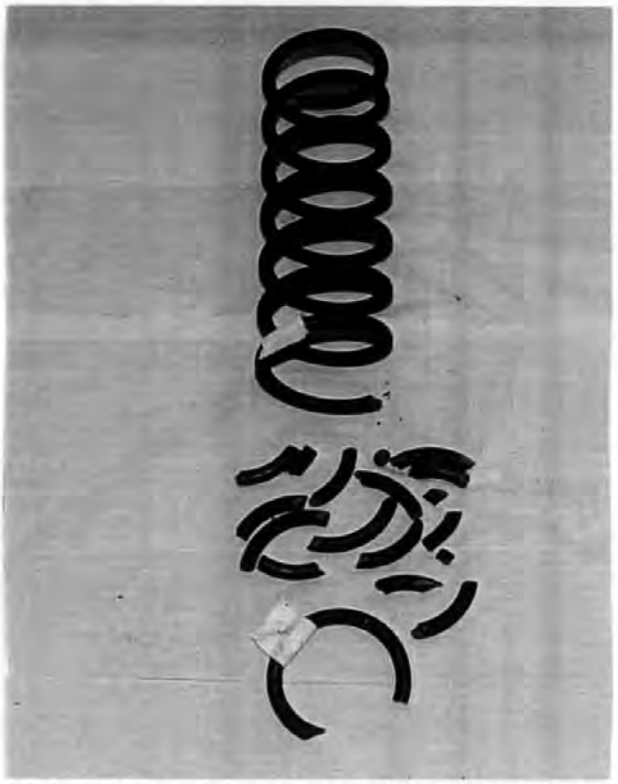

Plate 3.7: Position and type of fracture common to quenched fatigue samples.

3.5.1.2 Macroscopic observations

The characteristic macroscopic fracture observed in the quenched components is as illustrated by the following macrographs of fracture surfaces of the quenched fatigue samples.

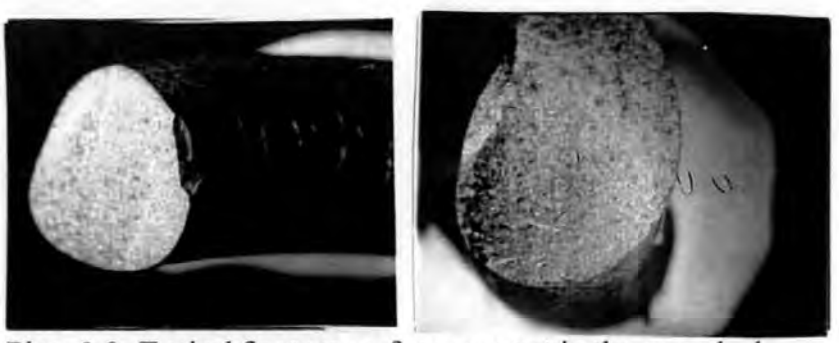

Plate 3.8: Typical fracture surfaces present in the quenched fatigue samples.

In this state the material is relatively hard and notch sensitive, resulting in a very brittle fracture. There appears to be very little evidence of torsional and more a resemblance to bending type fractures.

3.5.1.3 Microscopic observations

Mechanical damage/surface indentation was the dominant cause of failure in the quenched samples. As illustrated in Plate 3.9 it can be observed that all fractures initiated from the surface of the material.

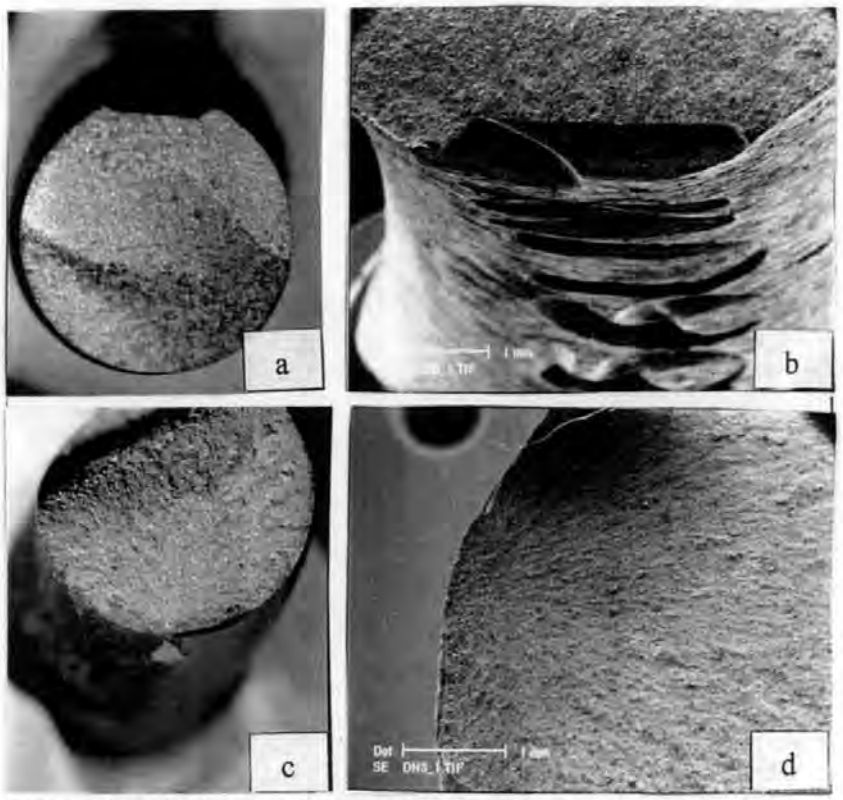

Plate 3.9: (a) Shows a fracture initiated from a stamp mark
(b) Magnification of (a)
(c) Initiation from mechanical damage
(d) Enlargement of (c).

There was a definite transition in the appearance of the microstructure from point of fracture initiation (slow fracture surface) to the fast fracture surface. This is clearly illustrated by the microstructures shown in Plate 3.10. Plate 3.10 (a) shows the transition phase from the slow fracture surface to the fast fracture surface. From (b) which represents a high magnification of the propagation area it is clearly illustrated that the fracture propagation is mainly along grain boundary, whereas in (c) it is clear that the fast fracture surface now mainly includes fractured grain surfaces (inter granular).

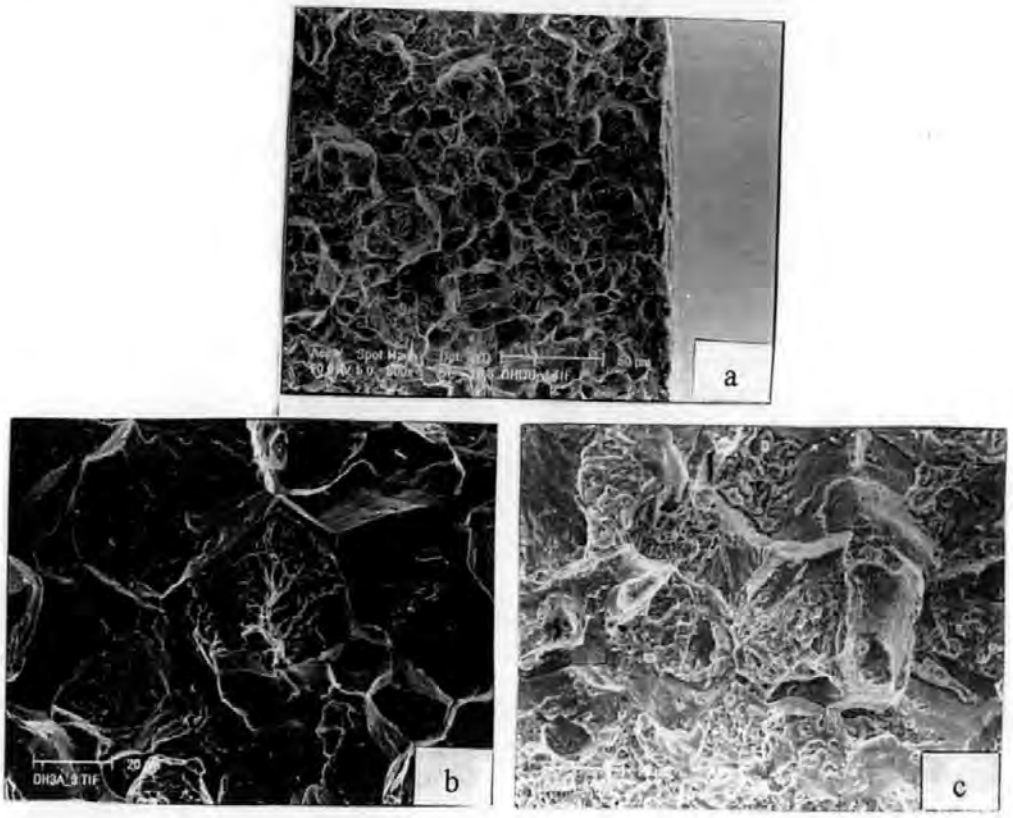

Plate 3.10: (a) Transition stage
(b) Slow fracture surface (close to point of initiation)
(c) Fast fracture surface.

3.5.1.4 Fatigue life

Due to the fact that the quenched samples are relatively notch sensitive, it has resulted in a large scatter band of fatigue results as shown in Figure 3.8.

The sample that failed at 160 cycles, failed at the stamp mark as illustrated in Plate 3.10(a).

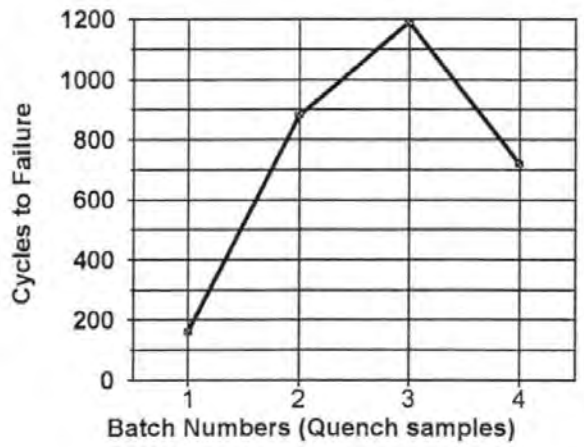

Figure 3.8: Scatter in fatigue results of quenched samples.

3.5.2 Quenched tempered samples

3.5.2.1 Position of fracture

As illustrated in Plate 3.11 all the fractures in the Quenched Tempered samples have occurred within the first turn as was the phenomenon present in the quenched samples. One noticeable difference is that the degree of shattering of the material has been reduced to a large extent. Coil number 6, as illustrated in Plate 3.11(b) has actually not fractured but failed due to buckling.

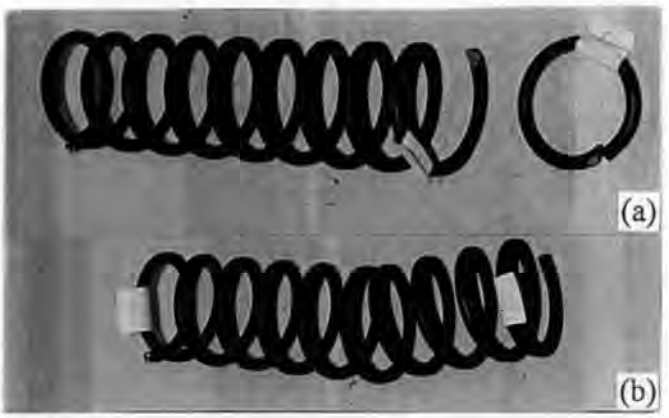

Plate 3.11:
(a) Shows the position and type of fracture in tempered samples.
(b) Tempered fatigue sample failed due to buckling after 2450 cycles.

3.5.2.2 Macroscopic observation in fracture quenched tempered samples

Most of the initiations of fractures occurred or started at either the top or bottom of the coil wire. The fracture surfaces reveal a helical brittle appearance as illustrated in the macro graphs in Plate 3.12. If compared to the quenched sample it can be observed that the type of fracture has more resemblance of a bending type failure (Plate 3.8) in the case of the quenched samples to a more torsional type failure (Plate 3.12) in the quenched tempered samples.

Plate 3.12: Helical type fracture from different tempered fatigue samples.

3.5.2.3 Microscopic observation in quenched tempered samples

The microscopic analysis of quenched tempered fracture surfaces revealed a number of possible causes of failure which varied from inclusions, surface damage due to manufacturing process and surface damage incurred during fatigue testing.

The first sample investigated showed initiation close to the outside surface as illustrated in Plate 3.13 (a). Once the area of initiation was analysed with an SEM, it revealed the presence of an inclusion as shown by (b), ± 2 mm in from the surface of the material. Although this inclusion was present in the initiation area, it was obviously not the primary cause of initiation. On further investigation of the other side of the fracture it became clear that the fracture initiated from damage on the surface as shown in (c).

Another interesting observation was the presence of secondary cracks and intergranular failure in the edge of fast fracture surface as illustrated by (d) and (e).

Plate 3.14 (a) and (b) illustrated the difference in appearance of slow and fast fracture surface. Note the presence of micro cracks in the fast fracture surface compared to that of the slow fracture surface. Again as in the case of the quenched sample, there is evidence of trans

granular and inter granular appearance of the fracture surface structure.

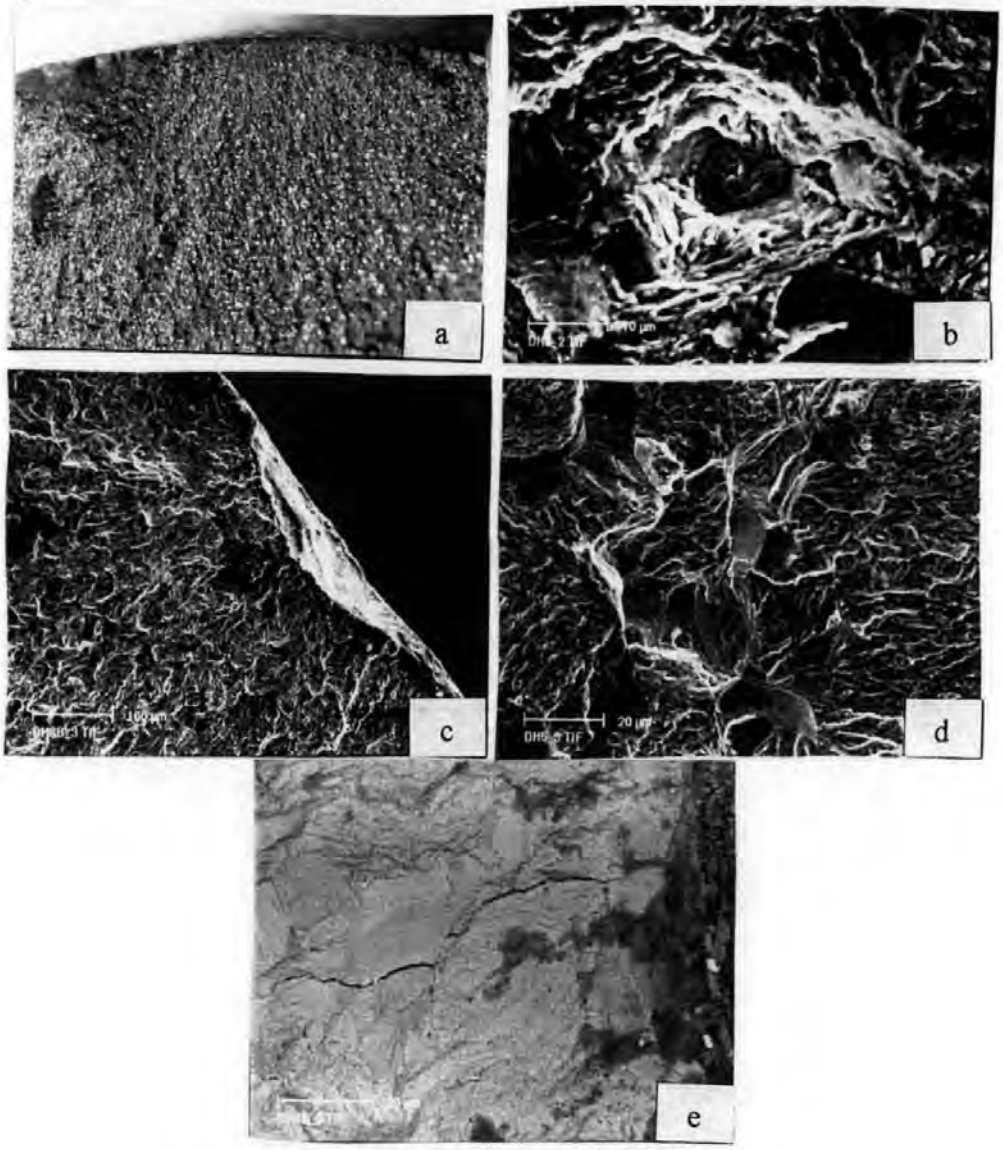

Plate 3.13: (a) Area of initiation (b) Inclusion present in initiation area
(c) Cause of fracture (mechanical damage)
(d) SEM image of secondary cracks (e) Back scatter image of (d)

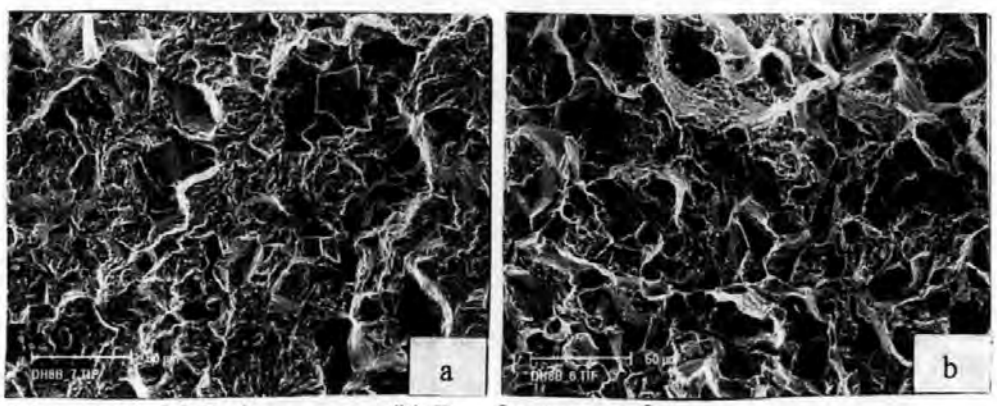

Plate 3.14: (a) Fatigue area. (b) Fast fracture surface.

Plate 3.15 (a) and (b) show detail of another quenched tempered fatigue sample fracture. From

(a) it is clear that some external damage to the surface was responsible for the fracture. This damage runs along the top of the coil wire and can be attributed to coil clashing during the fatigue test. Interesting to note in (b) is that the initiation was to the right hand side of the clash mark at a stress raiser.

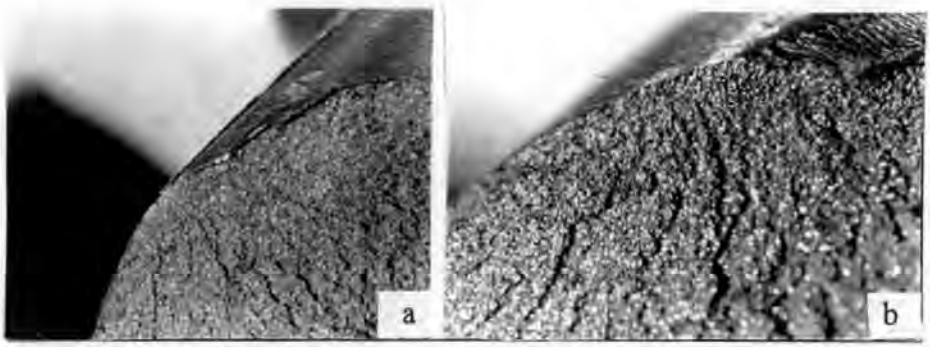

Plate 3.15: (a) Mechanical damage due to coil interference. (clash)
(b) Initiation area of failure.

3.5.2.4 Fatigue life

Compared to the quenched samples, the quenched tempered sample showed a slight increase in fatigue life, as well as considerable reduction in scatter of fatigue results. With the quenched sample a scatter of 86% was recorded, whereas in the quenched tempered sample it was reduced to 51%.

The temper process is partially responsible for reducing the notch sensitivity of the material and for creating a more repeatable component[4]. The increase in fatigue life due to the temper process was 58% on the comparison of the average fatigue life of the two types of samples.

3.5.3 Hot scragged samples

3.5.3.1 Position of fracture

With no exception, all hot scragged samples failed in the first turn of the coil spring as illustrated in Plate 3.16. The fracture shows one fracture plane with no shattering.

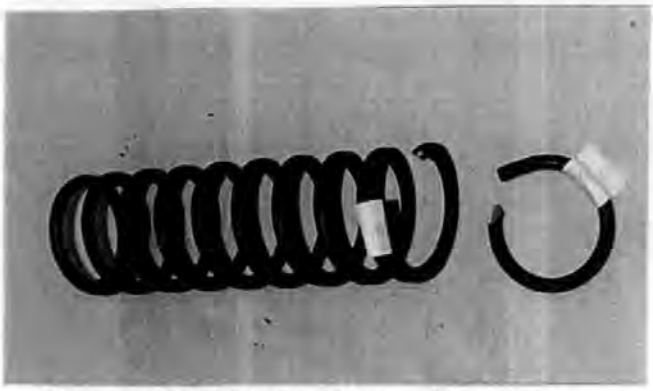

Plate 3.16: Position and type of fracture in fatigue sample withdrawn after hot scragging.

3.5.3.2 Macroscopic observations

Three out of four failure analyses showed a helical initiation with some axial growth but with the fast fracture mainly of a helical nature. Plate 3.17 (a) shows the helical type fracture while (b) illustrates clearly a small amount of axial growth at the edges of the slow fracture surface before it followed a helical path for the fast fracture part.

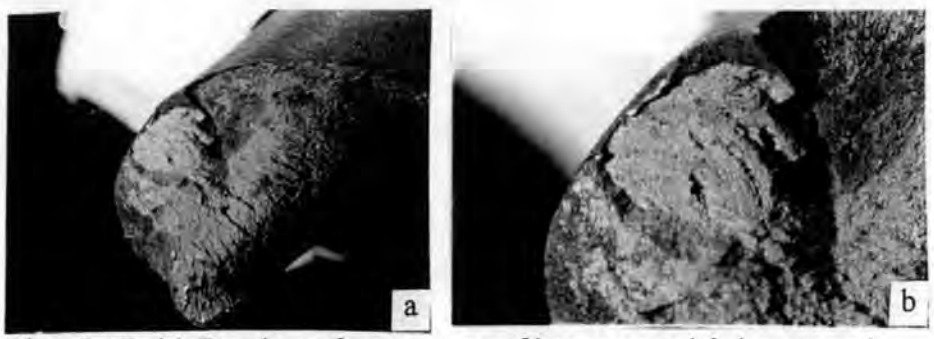

Plate 3.17: (a) Dominant fracture type of hot scragged fatigue samples.
(b) Reveals some axial growth at edges of slow fracture surface.

One failure of hot scragged samples revealed a torsional axial type failure as illustrated by Plate 3.18 (a). The appearance of the fracture is that of a torsional overload, perpendicular to the wire axis of the coil spring while (b) reveals a "fish eye" type appearance on the fracture surface,

also visible in (a). This will be discussed in detail under microscopic observations.

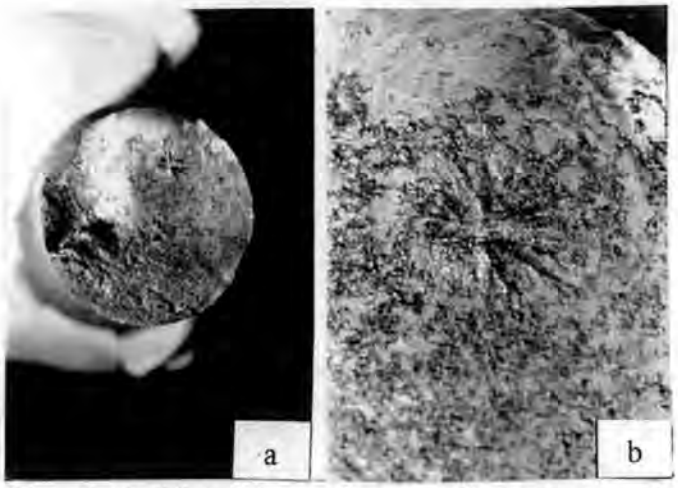

Plate 3.18: (a) Axial type fracture of a hot scragged fatigue sample.
(b) "Fish eye" appearance on fracture surface of hot scragged sample.

3.5.3.3 Microscopic observations

Two scragged samples were analysed microscopically as the other failure showed the same type of failure as the first sample. The first sample revealed a transverse failure origin, as shown in Plate 3.19(a). The origin is close to the outside surface of the wire but due to mechanical damage caused by the violent way in which the sample broke, it is difficult to pinpoint the exact cause. A similar failure as in (a) is also shown in the Metals Handbook, vol. 10, page 554, and the cause of that failure was attributed to the presence of transverse marks remnant of a grinding operation[11]. If considering that these fatigue samples were also subjected to a grinding process during manufacture, it could be concluded that this failure originated from surface damage induced by the manufacturing process. The micrographs (b) and (c) illustrates the difference between the appearance of the structure of the initiation area (a) and the fast helical fracture surface (b) at the same magnification.

The second failure analysed microscopically was the one that revealed evidence of a "fish eye" type failure. These types of failures are an indication of hydrogen embrittlement[12]. On closer

examination, no evidence of an inclusion could be found in the "fish eye" area as illustrated by the micrographs of Plate 3.20 (a) and (b).

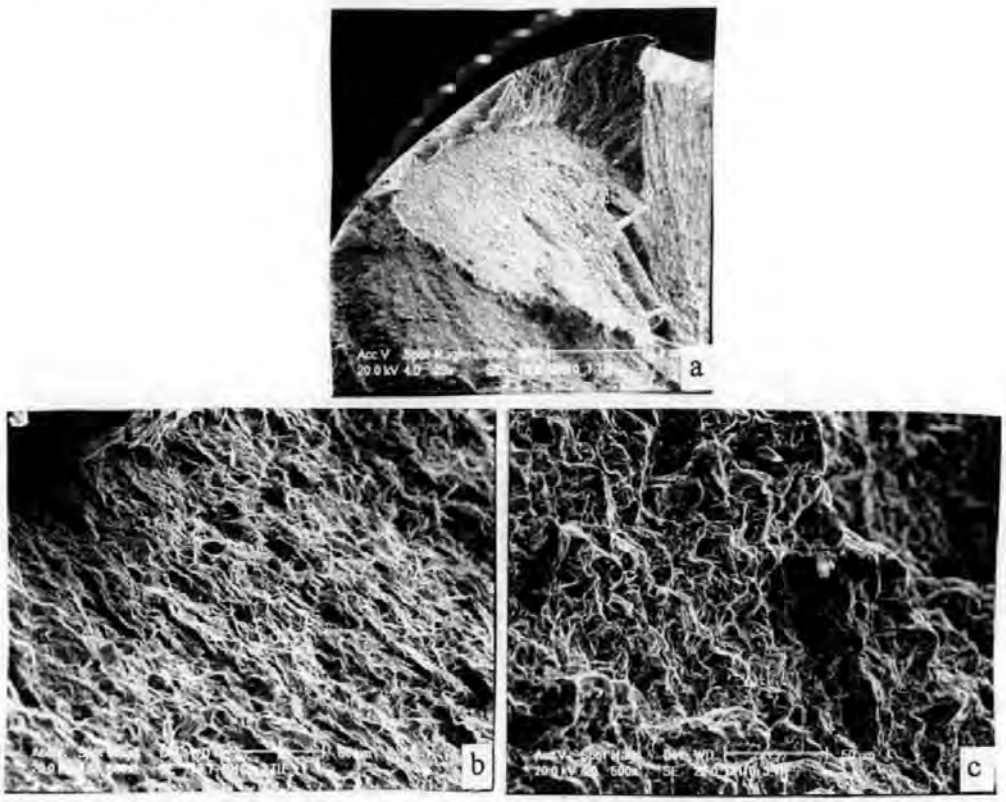

Plate 3.19: (a) Failure origin in a hot scragged fatigue sample.
(b) Microstructure of fracture surface at origin.
(c) Microstructure of fast fracture surface.

The hydrogen embrittlement is the result of hydrogen absorbed throughout the metal at the molten stage, which would then be released around inclusions, precipitates and other

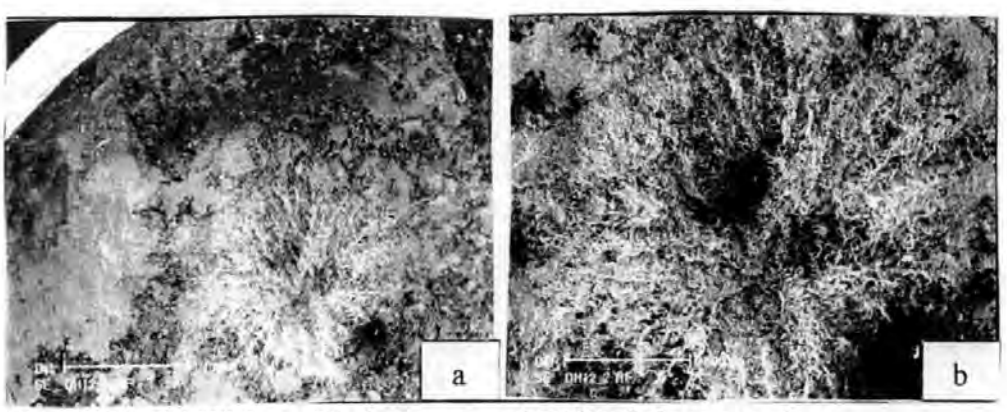

Plate 3.20: (a)"Fish eye" in hot scragged 55Cr3 fatigue sample.
(b) Enlargement of (a).

discontinuities. In this failure no evidence of an inclusion could be found, although the opposite fracture surface was not in a suitable condition for analysis.

3.5.3.4 Fatigue life

Again there was a marginal improvement of the fatigue life due to the hot scrag process, compared to the quenched tempered samples. The scatter in the fatigue data was very similar to that of the quenched tempered samples. From this it can be concluded that the hot scragging process has very little influence on the fatigue life of the components, although the process is responsible for inducing a certain amount of residual stresses and plastic deformation into the sample to improve it's sag properties. The predominant cause of failure was surface defects or damage, which indicates that there is still a certain amount of notch sensitivity in the component.

3.5.4 Shot peening samples

3.5.4.1 Position of fracture

An interesting observation is that in all the previous processes the sample fracture occurred within the first turn of the coil springs, but as illustrated in Plate 3.21 the position of the fracture occurred more to the centre of the spring. This was the case in all of the shot peened fatigue samples.

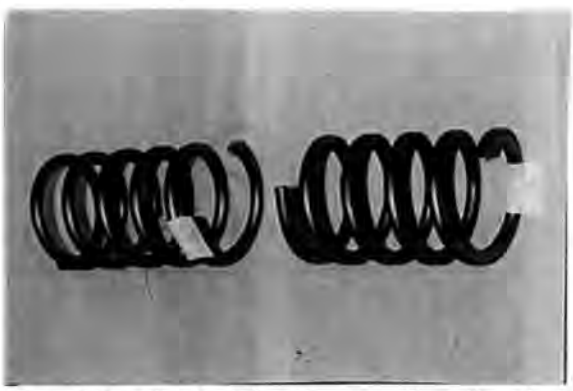

Plate 3.21: Typical fracture position for shot peened samples.

3.5.4.2 Macroscopic observations

Two different types of fractures have been observed as illustrated by Plate 3.22 (a) and (b). The helical fracture illustrated in (a) was the dominant type of fracture with only one fracture failing with a shear type failure perpendicular to the wire axis, as illustrated in (b).

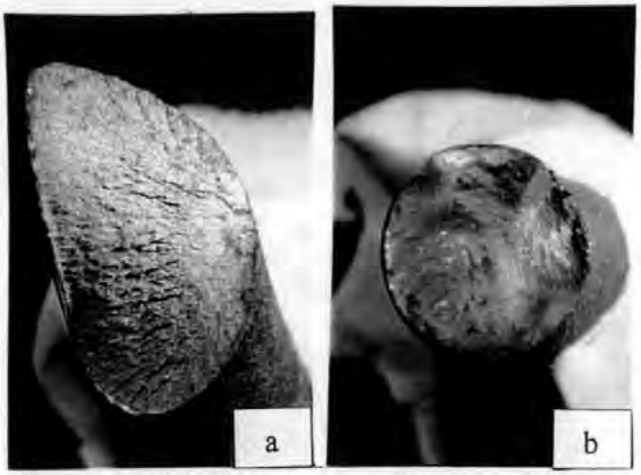

Plate 3.22: (a) Helical type fracture of a shot peened fatigue sample.
(b) Shear type failure of a shot peened fatigue sample.

The failure origin in the fracture illustrated in (a) was below the surface as clearly illustrated by the macro graph in Plate 3.23 (a), whilst that of (b) was again close to the surface as illustrated by Plate 3.23 (b). Plate 3.23 (c) illustrates the damage on the side of the shot peened sample, close to the origin of the sample illustrated in (b). The nature of this damage would imply that

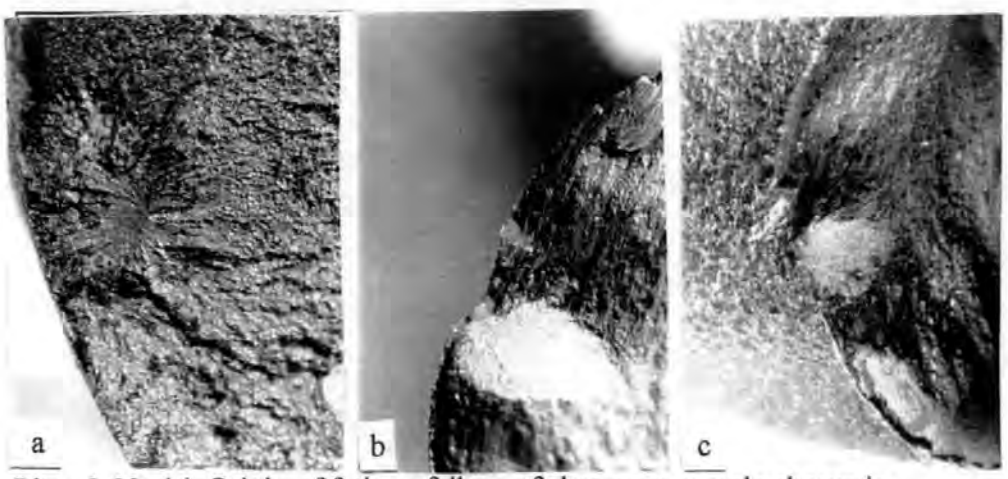

Plate 3.23: (a) Origin of fatigue failure of shot peen sample shown in 3.22 (a).
(b) Origin of failure of shot peen sample shown in 3.22 (b).
(c) Surface damage in side responsible for failure in (b).

it was caused by the shot peening process itself. A possible scenario is that a "shot" actually penetrated the surface of the material or dislodged an inclusion in the surface of the material. The diameter of the indentation is ± 1.5 mm.

3.5.4.3 Microscopic observations

Let us first consider the fracture of the shot peened sample originating below or sub surface, as was illustrated by Plate 3.22 (a). On closer examination, using SEM, it almost appeared to be another "fish eye" type failure, but by enlarging the centre portion, it became evident that the cause of failure was an inclusion of 60 μm just below the surface of the material as illustrated by Plate 3.24 (b) and (c). On performing an EDAX x-ray analysis, the following elements were identified: Al, Mg, Ca and O, ie a standard alumina-type inclusion in steel.

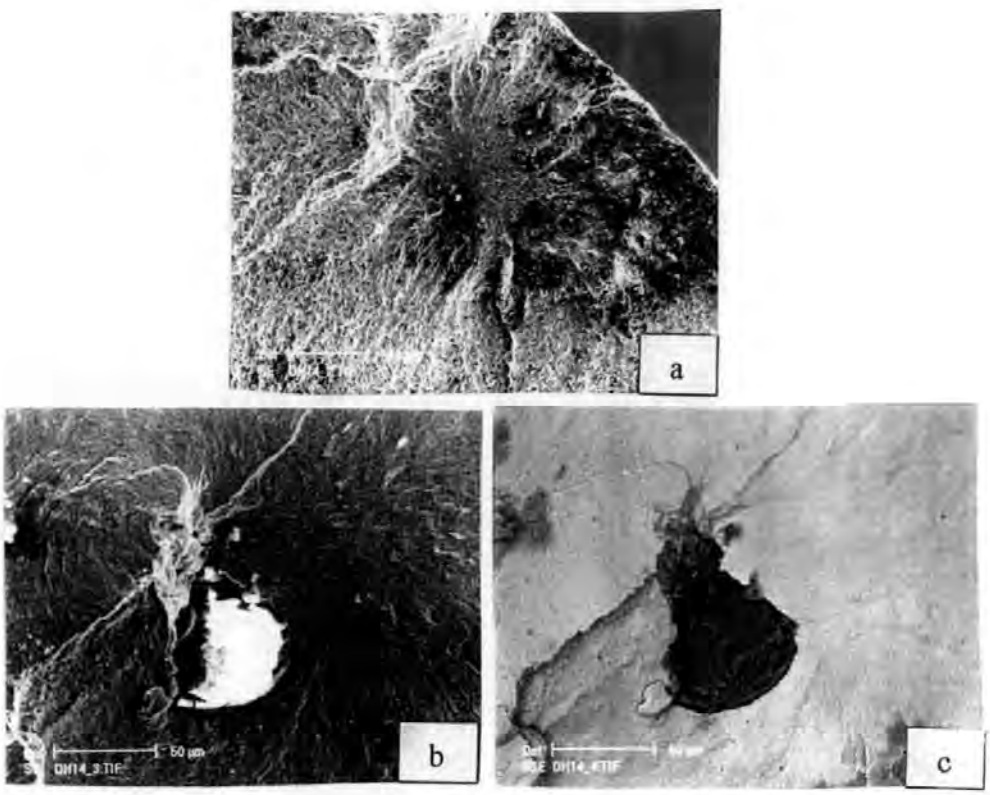

Plate 3.24: (a) Fracture origin of shot peen sample shown in Plate 3.22(a).
(b) SEM image of inclusion in (a).
(c) Back scatter SEM image of (b).

Another interesting observation of this fracture surface was the appearance of the microstructure of the surface close to the origin and that of the fast fracture surface. This is

illustrated by Plate 3.25 (a) and (b), where (a) is the surface close to the origin with very little topography, and (b) the fast fracture surface revealing a large amount of trans granular fracture structure.

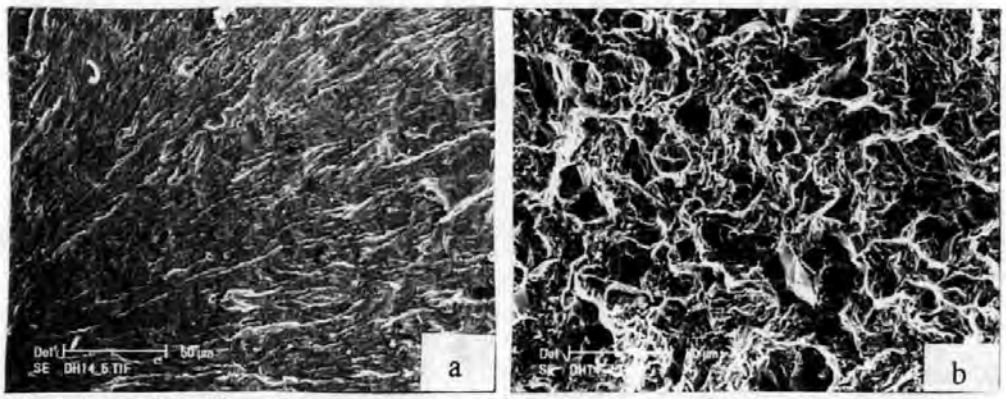

Plate 3.25:(a) Slow fracture surface of shot peen sample close to the initiation area.
(b) Fast fracture surface of same sample.

The second failure analysed showed an interesting phenomena and that is a shot peened sample,

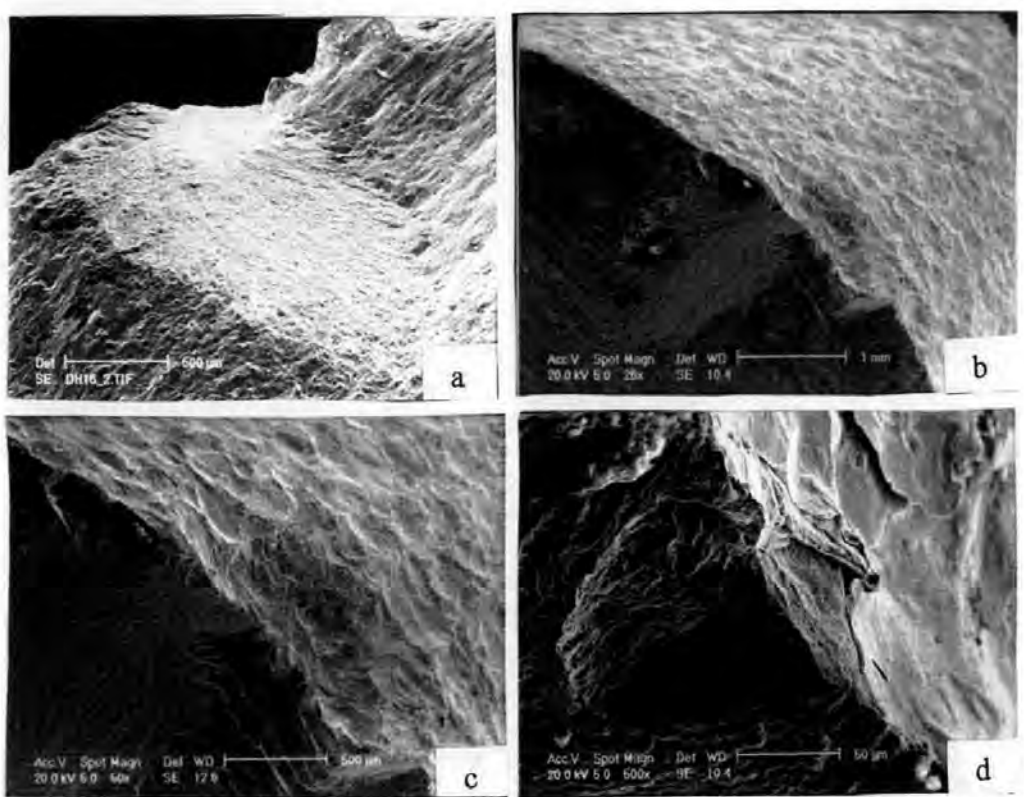

Plate 3.26:(a) Origin of a failure close to the surface of a shot peened component.
(b) Indentation caused by a shot close to origin.
(c) Indication of failure.
(d) Enlargement of (b) reveals possible remains of an inclusion.

failing due to a surface defect. It must be stressed that only one of the shot peened samples failed in this manner. Plate 3.26 (a) shows an SEM picture of the origin area of the failure, while (b) shows the position of the indent on the side with respect to the origin area. If (b) is enlarged, an interesting feature appears close to the centre of the origin as illustrated by (c). If this is enlarged further as illustrated by (d), it strengthens the theory that a shot was responsible for dislocating a part of an inclusion in the surface, leaving a stress raiser from where the fatigue failure originates.

3.5.4.4 Fatigue life

The shot peened fatigue samples showed a major increase in fatigue cycles resisted. Where the fatigue results for all the previously processed samples were expressed in a couple of hundreds of cycles, the shot peened sample were resisting more than 2 700 000 cycles on average. This represents an increase of 100 000 fold in fatigue life of the component compared to that of the previous samples. The reasons for this will be explained in detail in the chapter concerned with residual stresses. The scatter in fatigue data was high and more samples will have to be tested for a clearer picture of this. The scatter showed a 25% improvement compared to that in the previous processes.

3.5.5 Painted samples

3.5.5.1 Position of fracture

The painted samples showed a bit of variation as far as the position of the fracture was concerned. One sample fractured in the middle, as illustrated by Plate 3.27 (a). Another two failed in the second/third turn from the bottom as illustrated in (b). In the last samples tested the test was discontinued after more than 6 000 000 cycles were completed without failure.

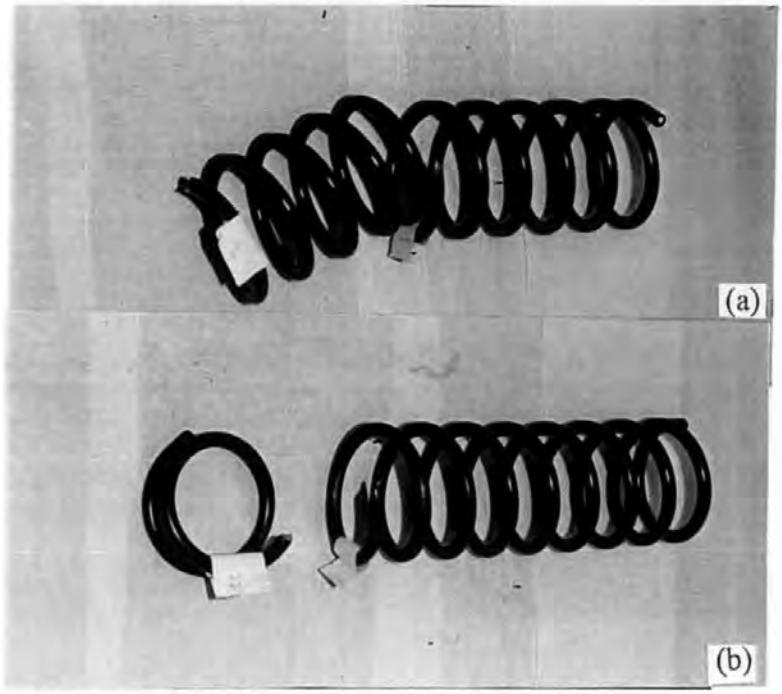

Plate 3.27: Position of fracture of painted fatigue samples.

3.5.5.2 Macroscopic observations

All the fracture surfaces reveal the same type of helical brittle appearance as illustrated by Plate 3.28 (a), while (b) illustrates the origin of the fracture surface which appeared to be close to the

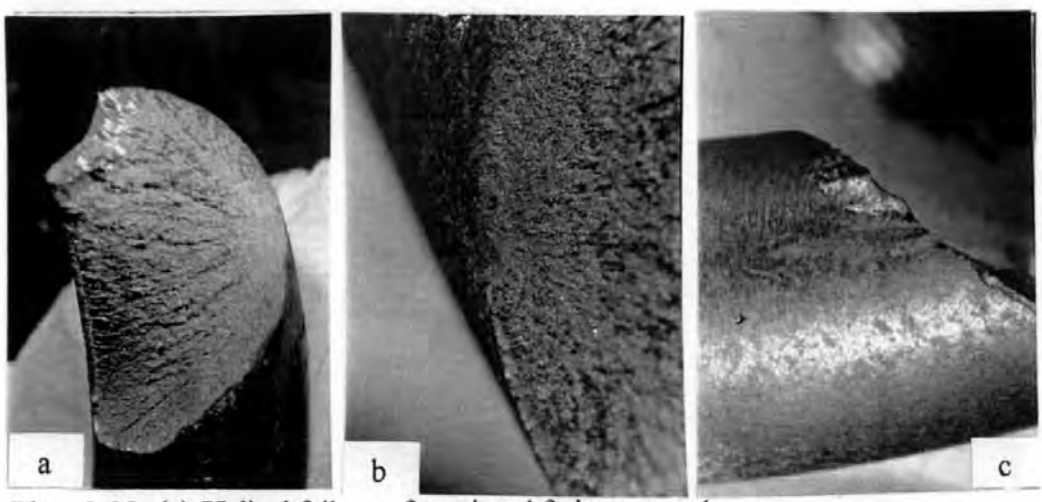

Plate 3.28: (a) Helical failure of a painted fatigue sample.
(b) Origin of failure in (a).
(c) Mechanical damage on surface close to origin of failure.

outside surface and on the inside of the coil which is a high stress area[2] as was illustrated by the FEA model in (chapter 2 (Red = High Stress)). It would appear that the failure was due to surface damage as shown in (c).

3.5.5.3 Microscopic observations

During the microscopic observation of the failure, it was very difficult to pinpoint the exact cause of failure. There are two possible causes namely, that the surface damage occurred post-fracture, therefore inclusions present in the fatigue origin area were responsible for initiating the fracture and secondly that the surface damage occurred before testing. As illustrated by Plate 3.29 (a) and (b), it is clear that inclusions are present in the area of origin but also if the edge of the sample is considered, it is clear that the surface damage has resulted in high spots close to the fatigue initiation.

If (a) is studied carefully, the origin appears to be at the arrow as indicated and was most likely initiated by an inclusion located on the surface of the material. The irregularity of the surface at this spot can largely be attributed to the shot peening process and not to mechanical or surface damage.

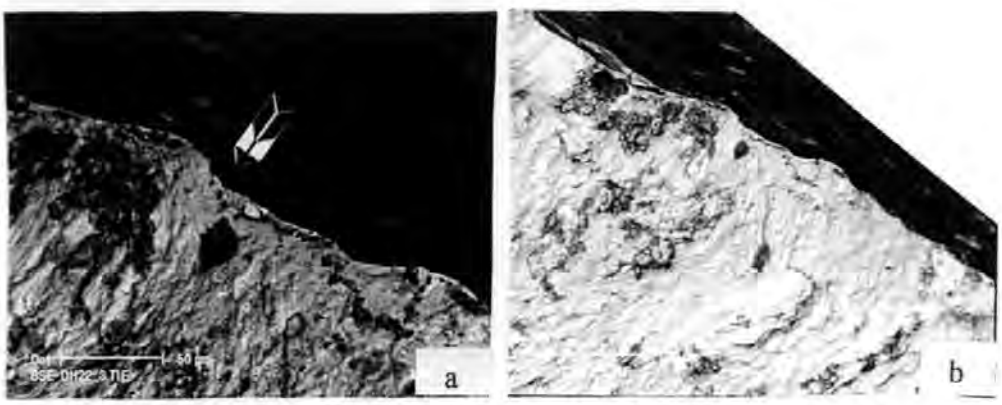

Plate 3.29: (a) SEM picture of the area of origin.
(b) Back scatter image of (a).

Plate 3.30 (a) and (b) illustrate the difference between the fracture surface close to the origin and the fast fracture surface. The slow fracture surface appears a lot smoother than that of the

fast fracture surface.

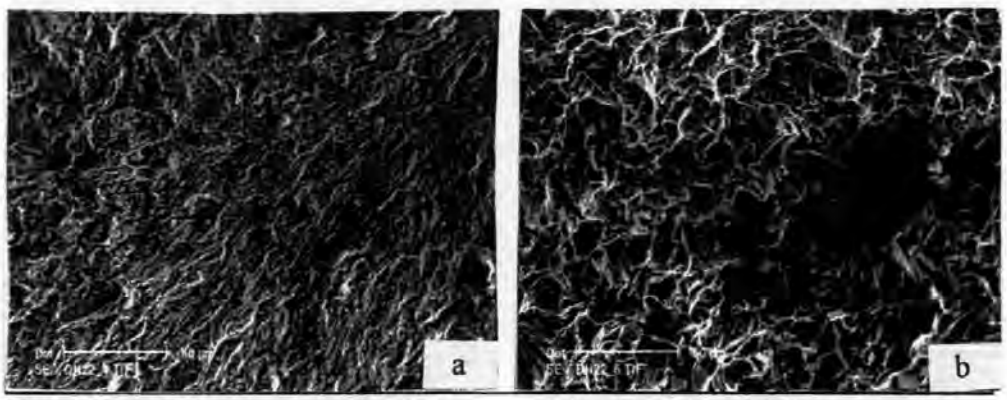

Plate 3.30: (a) Fracture surface close to origin of a painted fatigue sample.
(b) Fast fracture surface of same failure.

3.5.5.4 Fatigue life

There was a marginal increase in the fatigue life of the painted samples compared to the shot peened samples. The increase in the fatigue life will have to be investigated further to establish the exact reasons. The influence of residual stress on the fatigue life will be discussed later in this thesis and might shed more light on this phenomena. The painted fatigue samples showed very little scatter in fatigue data, the scatter was in the order of 30%, a major improvement but will have to be confirmed by testing a larger number of samples.

3.5.6 Load tested samples (Final Component)

3.5.6.1 Position of fracture

As was the case with the painted samples, the load tested samples also showed some variation in position of fracture. Two of the samples fractured towards the middle, while another fractured three turns up from the bottom and the last one failed in the first turn of the sample.

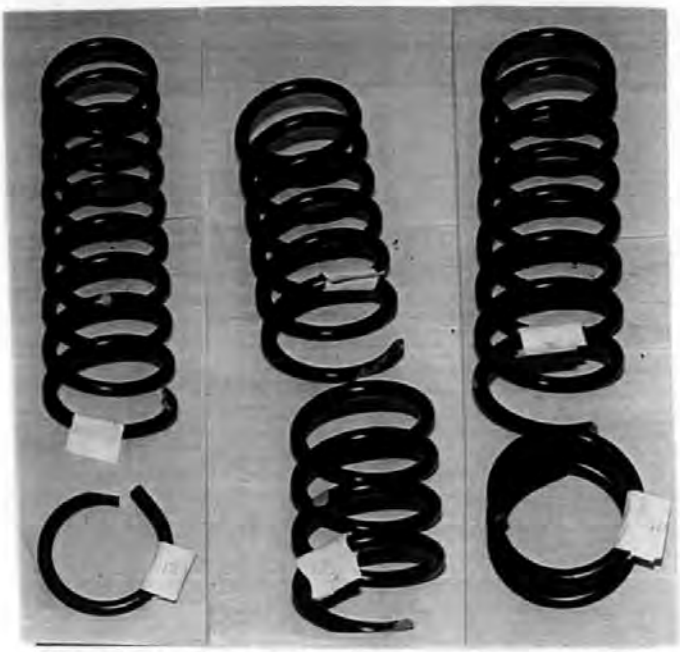

Plate 3.31: Fracture positions as it appeared in load tested samples.

3.5.6.2 Macroscopic observations

For the macroscopic observations three fracture surface were analysed as illustrated in Plate 3.32 (a), (b) and Plate 3.34.

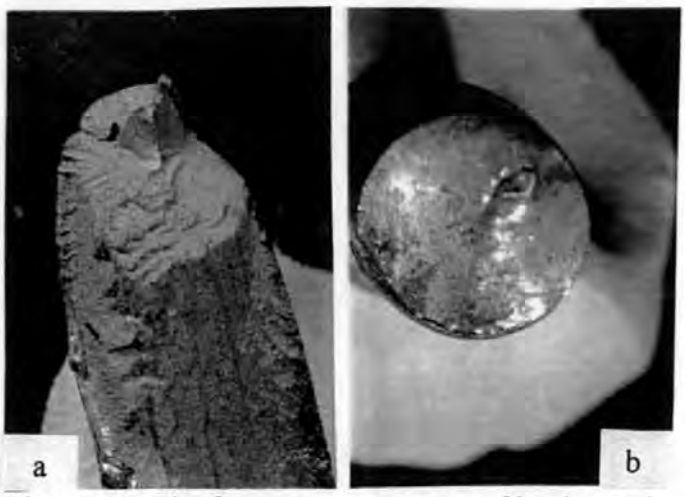

Plate 3.32: The fracture appearances of load tested samples where in (a) a large amount of axial growth is visible and (b) reveals a torsional shear type failure.

From (a) it is visible that there was a helical initiation of the fracture which started close to the surface as is illustrated by Plate 3.33. This was followed by a large amount of axial growth and

finally the fast fracture surface was in a helical format again.

Plate 3.33: Initiation of failure in first load tested fatigue sample.

The optical microscopy showed no definite cause of the failure in the first sample. The second sample as shown in (b) revealed a torsional type failure. It appears very plastic and the indication of an off-centre torsional pivot indicates failure due to combined bending and torsion. A third failure revealed a helical initiation with "fish eye" appearance in the centre, it grew some way axially and some perpendicular to the wire axis. The fast fracture surface was mainly helical. Plate 3.34 shows a clear picture of the "fish eye" type initiation a few millimetre away from the surface of the sample.

Plate 3.34:
"Fisheye"type initiation in a load tested sample.

There is a clear indication of the presence of an inclusion (see microscopic analysis of sample).

3.5.6.3 Microscopic analysis

Let us consider the sample shown in Plate 3.32 (a). Plate 3.35 (a), (b) and (c) illustrate SEM micrographs of this sample where (a) clearly shows the origin of the fracture close to the surface of the material whilst (b) is at a higher magnification and reveals some indication of the presence of a small seam to the bottom side of the origin. No surface damage could be observed and the failure most likely was caused by a small inclusion close to the surface of the material. If the surface is analysed by using the back scatter image the presence of an inclusion can be seen close to the origin as illustrated by (c).

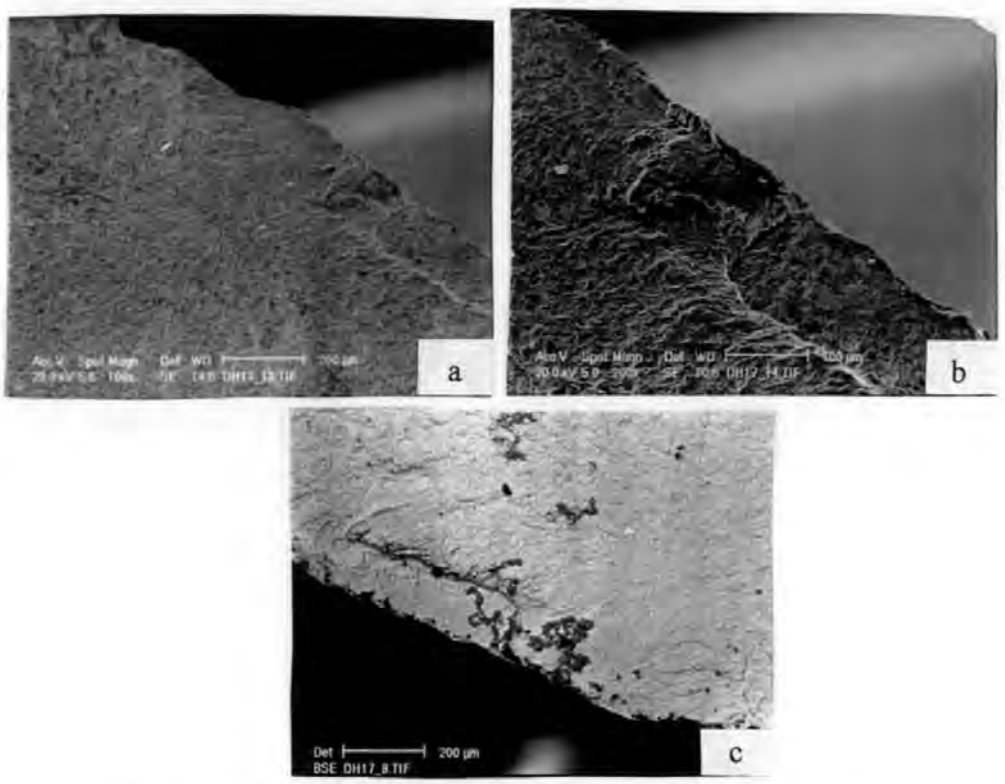

Plate 3.35: SEM micrographs of a load tested fatigue sample
(a) Fatigue origin.
(b) Higher magnification of (a).
(c) Back scatter image revealing a inclusion.

Other interesting observations in the fracture surface are illustrated by SEM micrographs illustrated in plate 3.36 (a), (b) and (c). The first reveals the presence of sulfide stringer on the axial fracture surface as shown in (a). The length of these stringers varied with some as long as 50 µm. The micrographs in (b) are the structure close to the origin of the fracture, whilst (c)

shows the structure of the fast fracture surface of this failure. As was the case with the painted sample, the structure close to the origin appears very smooth, while that at the fast fracture appears relatively topographical and cross granular. Note the sulfide stringer on the fast fracture surface.

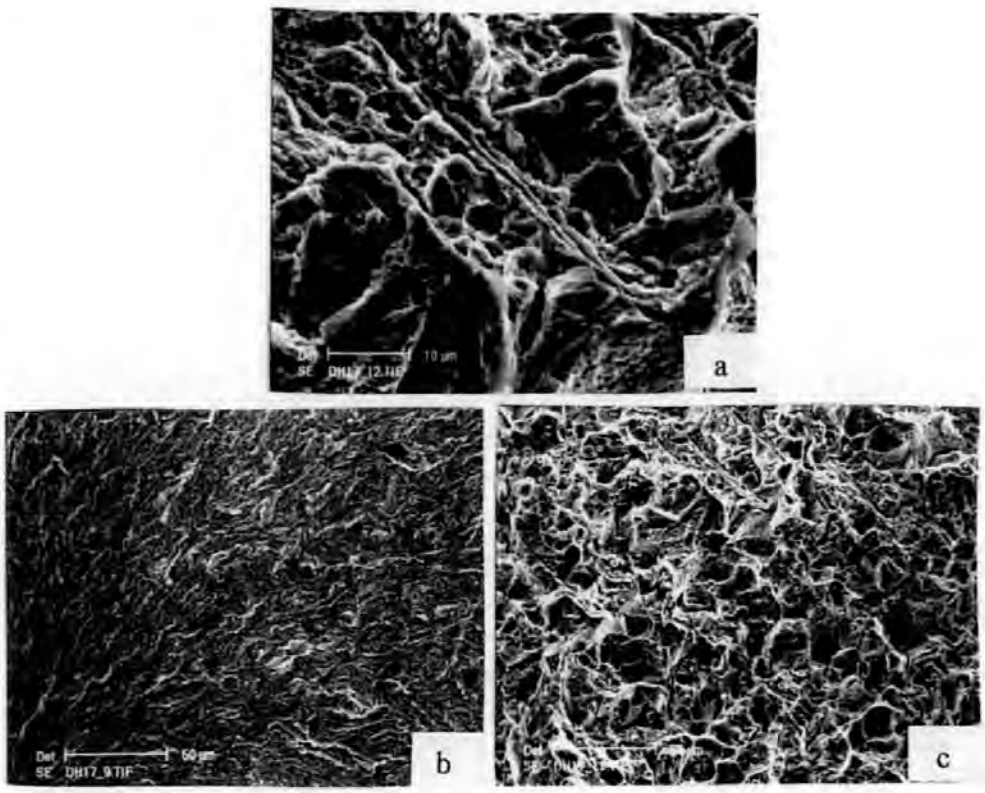

Plate 3.36: (a) Sulfide stringer marks in a load test sample.
(b) Fracture surface close to origin.
(c) Fast fracture surface.

The second fracture analysed was the fracture with the "fish eye" appearance. It revealed the presence of a large inclusion. Plate 3.37 (a) and (b) illustrate photo's taken with a SEM of the fracture surface. Although the sample was in a bad state with some corrosion on the surface, it was not beyond analysis. The micrograph in (a) shows the origin with the inclusion visible, while (b) and (c) show the inclusion at different magnifications. The inclusion had a cross section of ± 50 μm and showed signs of breaking up as illustrated by (c). There can be no doubt that this failure was inclusion related. On (c) the origin can clearly be traced back to the inclusion.

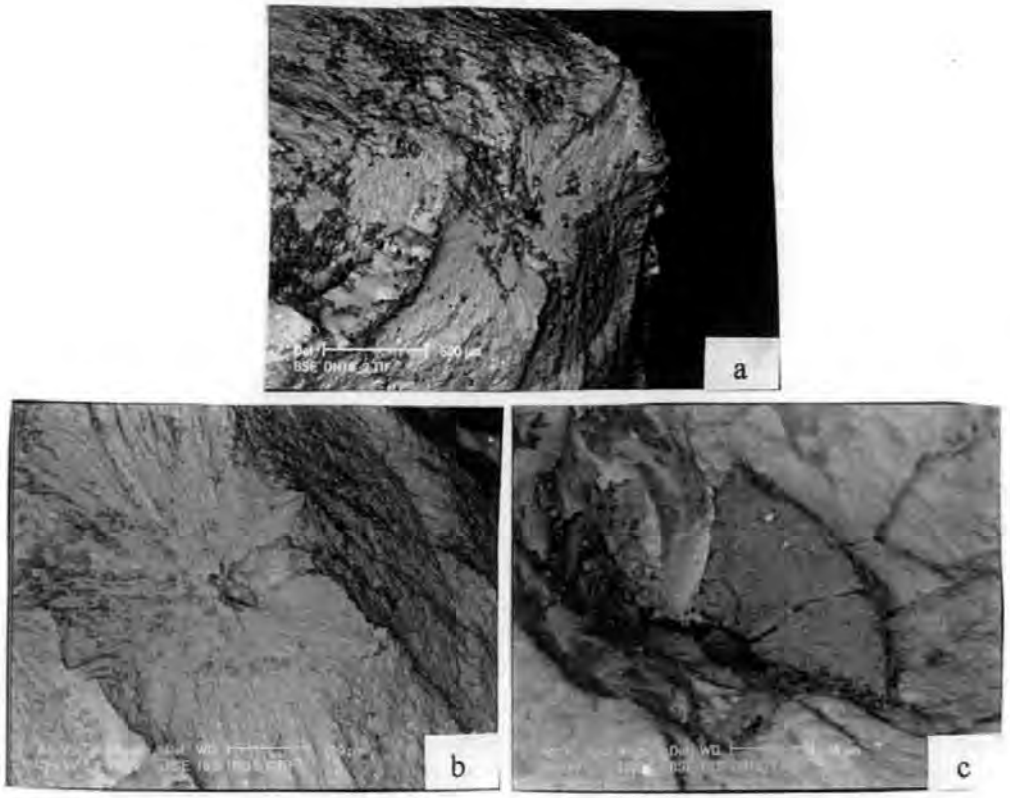

Plate 3.37:(a) SEM picture of fatigue origin.
(b) Back scatter image of fatigue origin.
(c)) Back scatter image of inclusion itself.

The last fatigue fracture as was illustrated in Plate 3.32 (c) was damaged to such an extent that SEM analysis was impossible. A large amount of rubbing occurred on the surface before fracture.

3.5.6.4 Fatigue life

A very interesting feature of the fatigue cycle life was a substantial drop in the fatigue resistance of the load tested samples, compared to the shot peened and painted samples. On average this represented a 75% drop in the number of cycles resisted. In the final analysis the cycles resisted by these samples, were still well above the specified limit. The change caused by this process will be investigated further by looking at the residual stress later in this thesis, but definitely holds a key to improve spring material performance and should be researched further. It would seem that a large amount of plastic deformation is set into the material during load testing[2].

3.6 SUMMARY

3.6.1 General

All samples were analysed visually, optically and using a Phillips XL 30 SEM. Some elemental analysis of particles was performed using a energy dispersive x-ray (EDAX) technique. Some samples were damaged post-fracture and beyond analysis. This can be attributed to the violent way in which the fatigue sample will leave the machine after fracture.

The location of the fatigue fractures was very process specific. This is illustrated by the following schematic diagram (Figure 3.9).

From the graph it is clear that the majority of the sample broke within the first three turns of the coil. There is a definite move towards the centre of the sample after the shot peened process

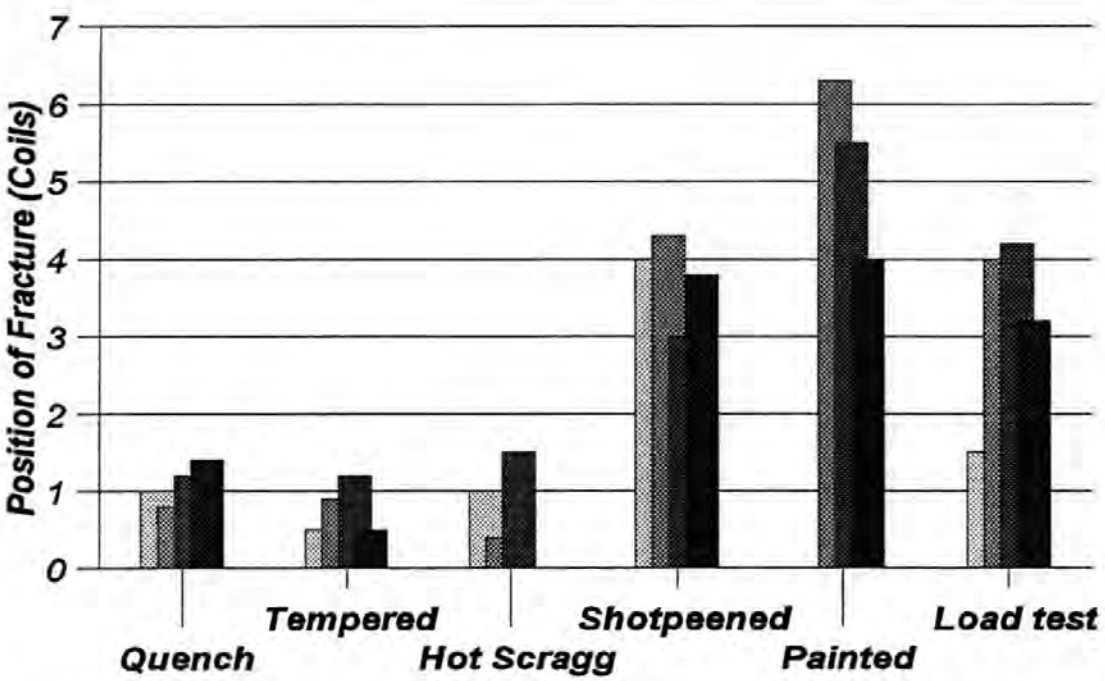

Figure 3.9: Position of fracture of different processed samples. The y-axis indicate the coil number. (1= Bottom; 3.5=Centre & 7= Top)

and the processes after this follows the same trend. The stress state in the first turn of the samples is complicated as the design of the coil is such that a reduction in pitch has to be incorporated to give the component parallel ends. This could also be an indication that some

interference occurs with the fatigue test equipment end fixing fixtures. After a thorough investigation into this possibility no evidence could be found to support this theory. The end fixtures on the test jig are well designed and the spring is only restricted in one direction by them. The load application is also perfectly axial introducing no external stress factors.

Three characteristic macroscopic fracture types were observed in all samples tested. The most common type was the helical type which occurred in samples withdrawn from all the processes. The next type was an axial/helical type fracture mainly present in samples withdrawn after the shot peened process, while the torsional slow type fracture occurred in only three samples but was not process specific. The three types of macroscopic fractures are illustrated in Figure 3.10.

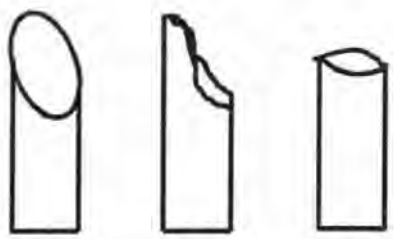

Figure.3.10: Dominant macroscopic features of 55Cr3 fatigue samples withdrawn at different manufacturing stages.(a) Helical fracture (b) Axial/helical fracture (c) Torsional shear.

As far as buckling is concerned, only one sample failed in this manner, no sample after the hot scragging process failed by buckling. The microscopic analysis revealed three general causes of fatigue initiations, namely surface damage, non-metallic inclusions and an isolated case of hydrogen embrittlement.

Several coils failed from damage due to coil clash between the first coil and the coil end. This was a dominant failure of samples withdrawn before the shot peening process. The influence of coil clash on failure initiation seems to disappear after the shot peened process. As illustrated

by Plate 3.38, this confirms that the clashing still takes place but is not responsible for fatigue initiations. It can be observed that the damage is severe but it seems that the shot peened process is effective in neutralising surface damage to a large extent.

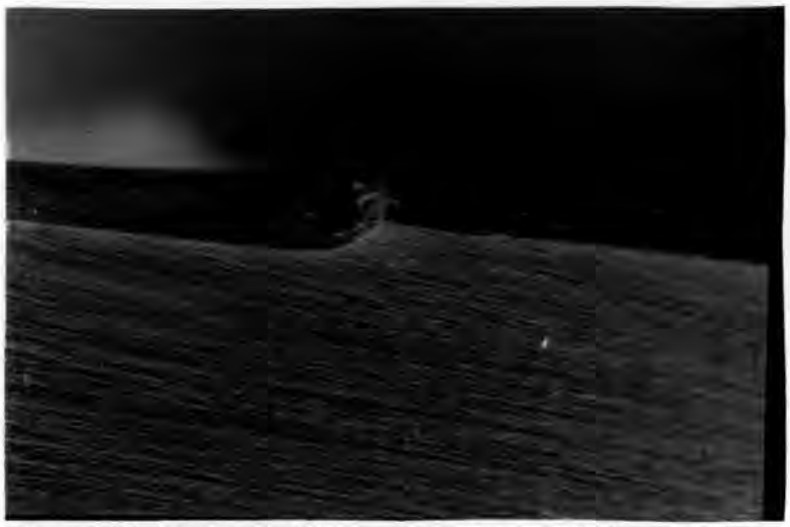

Plate 3.38: Mechanical damage due to coil clash - sample withdrawn after painting.

3.6.2 Effect of process upon fatigue response

Several sources of fatigue crack initiation have been identified in this experiment and, although not all are dominant in the finished component, some interesting trends have emerged. The sample size for each stage was four and this should therefore be considered before analysing the average fatigue performance figures presented in Table 3.2.

In as quenched and quenched tempered coils, the cause of failure was found solely to be mechanical damage to the material surface. Despite a reduction in hardness during the tempering process, average fatigue life of tempered coils was slightly increased as expected. After subsequent processes the variation in measured hardness values proved insignificant.

The hot scrag operation is applied at the tempering temperature to coil springs manufactured from chromium steels in order to impart a degree of relaxation resistance to the finished component[2]. However, it is evident that the operation also has an effect in terms of fatigue

performance, resulting in an average increase in fatigue life of approximately 28% over the quenched tempered coils. In addition it was observed that subsurface fatigue initiation begins to occur only after this process.

The most significant process in terms of promotion of high fatigue life was that of shot peening, producing a massive increase in excess of hundred thousand-fold. Coils withdrawn from after shot peening, or later stages, were found to fail predominantly from defects other than surface or mechanical damage. A further increase in the fatigue performance was noted from the painted spring samples, although the increase was so small that it can be regarded as insignificant.

The most surprising change in fatigue performance was observed for the final product, after load testing, resulting in a four-fold reduction in fatigue life. This stage consists of compressing each spring to solid height three times at room temperature and is essential in order to ensure constant length of the finished components and for grading of final components in bands of equal stiffness. It is evident that a serious detrimental mechanism is introduced during this stage.

As discussed the stresses in a helical coil spring can be calculated using standard theory. For design purposes spring characteristics can be determined via standard formulae[3]. These formulae include a correction factor to accommodate the complex nature of stress in the helix which results in a higher stress on the inside of the coil, reducing towards the outside surface. There are two reasons for this.

1. The torque moment results in a steeper twist angle for the short fibres at the inside of the coil than for the long ones at the outside and thus produces a higher shear stress at

the inside.

2. The axial load causes a direct shear stress which adds to the shear stress at the inside of the coil but is subtracted from the outside.

Considering this, it would be expected that most coil failures should occur at the inside of the coil, whereas it was found that approximately 70% of failures occurred at the top or bottom of the wire. Three reasons are suggested for this:

1. The bending element in this spring design is more significant than the design formulae suggest, thus creating a peak combined stress at the top/bottom of the wire.

2. The standard design theory assumes that no bending element are present. Although springs were loaded axially it would seem that bending was not completely eliminated.

3. Some damage to these (top and bottom) wire areas occurs during the scragging processes or cycling when fatigue tested.

In addition it was noted that of the five failures from inside the coil, four occurred in shot peened coils. This would indicate that the shot peened coverage is reduced in the inward surfaces of the component due to shielding of these areas.

The current work has highlighted some interesting relationships between fatigue failure and critical defect presence in automotive coil spring components. In addition it has been illustrated how the surface condition of the material, specifically with regard to the process effects, alters the source of fatigue failure and the order of importance of defects with respect of fatigue

performance. It has been shown that for components manufactured from the current material, the critical defects in finished components are subsurface non-metallic inclusions and hydrogen damage.

Finally, it has become evident that the last stage in the manufacturing process, the cold scrag operation, actually leads to a reduction in the fatigue performance of the finished product. It is, therefore, clear that further work is required in this area in order to determine that nature of the process by which this detrimental effect occurs.

CHAPTER 4

RESIDUAL STRESSES

INTRODUCTION

Residual stresses, also referred to as internal, bulk, forming, fabrication, building or *in situ* stresses, have only been considered seriously in engineering design recently[1]. The preferred term of those mentioned above is residual stresses. All engineering components produced by processes like welding, forging, heat treating, rolling, grinding, machining, etc. will contain residual stresses. It is probably true to state that all engineering components contain residual stresses of variable magnitude (unless specifically stress relieved) and sign (tensile or compressive) before being used in service conditions owing to the manufacturing history of such a component. It is very important to realise that residual stresses are "locked into" the component because of the manufacturing process and that in the absence of external loading

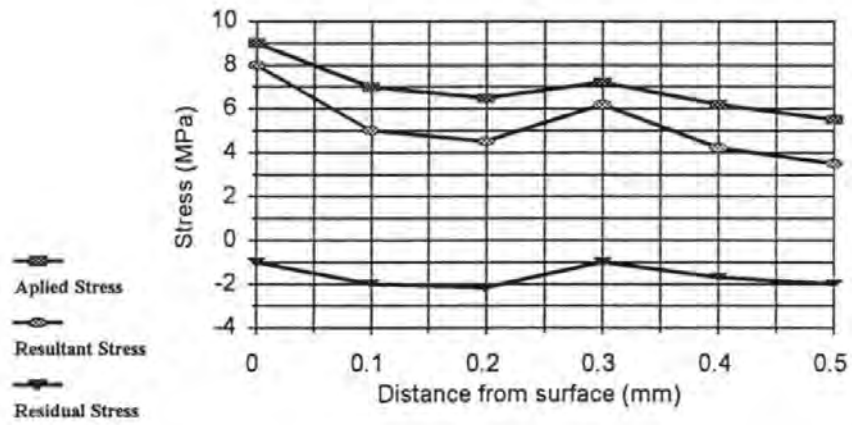

Figure 4.1: Effects of residual stresses on surface layer of a component.

this will represent a datum stress. When the component is put into service, the applied stress is subsequently superimposed over the residual stresses as illustrated by Figure 4.1. Although most residual stresses are caused by plastic deformation of the metal through severe temperature gradients or mechanical forces, they can also be induced to a lesser extent by

permanent expansion or contraction of the metallic lattice in processes such as carburising, nitriding, or heat treatment, which cause phase transformation. There are a number of reasons why residual stresses are receiving increased attention from design engineers. Primarily their presence may reduce the cost of material used, extend the useful lifetime of existing structures, and satisfy the demand for greater reliability of components if of opposite nature to the applied load..

Residual stress is nothing new to the engineering world of today, and substantial efforts have been made to investigate their magnitudes and distributions with depth in components and their influences on service life. The problem of residual stresses has largely been overcome in the past by incorporating sufficiently larger safety factors to mask their effect. However, with the current pressure on the manufacturing world to produce cheaper, more reliable and environmental friendly products, design procedures have become far more stringent and residual stresses can no longer be ignored.

In this chapter the reasons for and effects of the presence of residual stresses in coil springs, manufactured from 55Cr3 spring steel by National Springs in Johannesburg for Volkswagen South Africa are investigated. The second objective is to find a suitable method for the measuring of residual stresses in 55Cr3 spring steel and relating it to the manufacturing processes and fatigue life of the different samples tested.

4.1 RESIDUAL STRESSES

4.1.1 Definition of residual stresses

Residual stresses are those stresses which exist in the component, without, and prior to the application of any service or other external loads.

4.1.2 Calculation of residual stresses

From information given in the introduction, it can be seen that residual stresses can be compressive or tensile: If by fortune or design, the stress caused by the applied load is of opposite sign (positive or negative) to that of the residual stress, then part of the applied load goes to counter or to reduce the residual stress as is illustrated in Figure 4.1. This brings about that part of the load is overcome by the residual stresses before the combined stress can rise again. Such residual stresses are thus extremely beneficial to the strength of the component and significantly higher fatigue strength can result. If, however, both service and residual stresses are of the same sign, e.g. both compressive or tensile, then a smaller service load is required to produce failure than in the case where the stresses are of opposite signs. Thus, one can conclude by saying that both sign and magnitudes of the residual stresses are important to fatigue life considerations. It is very risky if a designer assumes that stresses are zero at zero load, since it is not the case in most instances in practice. The designer must always fully estimate the levels of residual stresses present, as well as their influence or effect on the strength of the design, or the manufacturing processes must be changed to reduce residual stresses to a minimum. If fatigue life of a component is critical, compressive residual stresses will be preferred and are often deliberately introduced into the surface of components (e.g. shot peening) to enhance the fatigue life. However, in buckling, compressive residual stresses on the surface can lead to premature buckling failure if service loads are also compressive[13,14].

Let us consider the residual stress in a beam of an elastic, perfectly plastic material subject to bending after yielding. If a material is loaded past the yield point, permanent deformation appears. This means that part of the beam section will stay elastic while the remaining fibres yield. The permanent deformation associated with the yielded areas prevents the parts of the material which are elastically stressed from returning to their original state, when the load is removed. This will produce residual stresses in the beam. For us to determine the magnitude

of the residual stresses, we have to work from the assumption that the unloading is completely elastic from either a partially plastic or fully plastic state. Consider the tensile test graph in Figure 4.2.

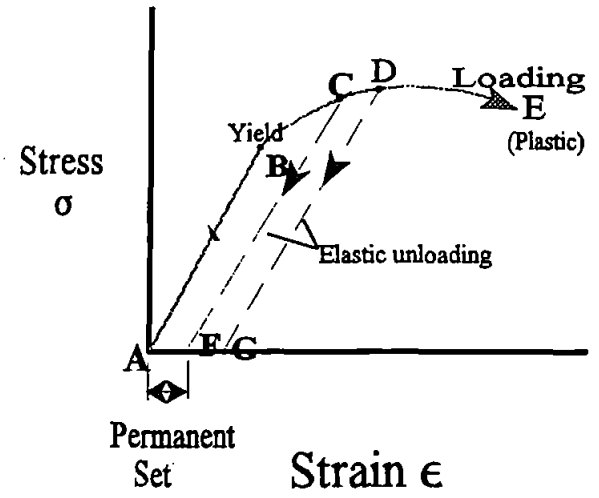

Figure 4.2: Tensile test curve.

From A to B the loading is elastic (NO permanent deformation). At point B the material starts to yield which will cause permanent deformation. So, if the load is removed at C, it will not return to A, but to F, because of the deformation (permanent set) that has taken place[1]. The unloading is still considered to be an elastic unloading. The same applies if the specimen is reloaded to point C and then unloaded to return to G. If the specimen is now removed from the tensile machine, it will look the same as what was originally the case, but now it possesses a certain amount of extra built-in stresses which will definitely influence the material's service performance.

From the graph it is clear that the unloading stress distribution is linear and can be subtracted graphically from the stress distribution in the plastic or partially plastic state to obtain the residual stresses. To explain this consider calculation shown in Appendix C for a beam loaded to a fully plastic state.

Considering the operating condition of a helical coil spring in a car, one will find that it is mainly subjected to torsion. Let us now consider a shaft subjected to torsion beyond the elastic limit (plastic torsion). We can assume that for shaft material the stress/strain curve is very similar to that shown in Figure 4.2, and that the stress is proportional to the strain up to the elastic limit and constant after that. Consider the shear stress distribution in the cross-section of the shaft shown in Figure 4.3, keeping in mind that the assumption is that the plane cross-section remains plane and that any radial line across the section remains straight.

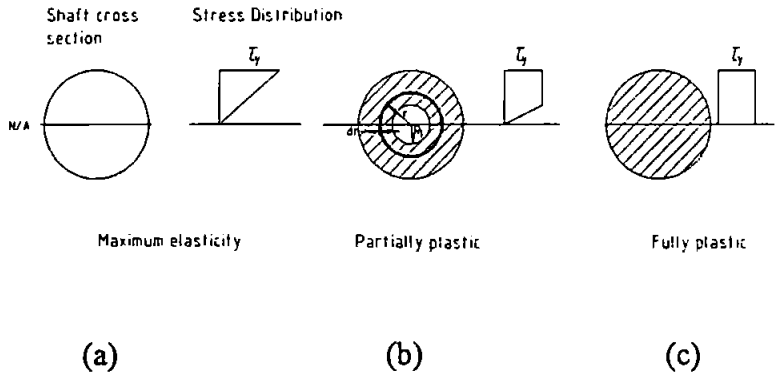

Figure 4.3: Stress distribution of a fully plastic shaft.

From (a) it can be seen that if the shaft stays elastic, the stress distribution remains linear and as the torque increases, the shear stress in the outer fibres increases and will eventually reach the yield stress τ_y. This is the maximum torque the shaft can withstand without permanent deformation.

From torsion theory[1]: $$\frac{T}{J} = \frac{\tau}{r} \quad \text{.....(1)}$$

Therefore the maximum elastic torque(T_E):

$$T_E = \frac{\tau_y J}{R} = \frac{\tau_y}{R}\frac{\pi R^3}{2} = \frac{\pi R^3}{2}\tau_y \quad \text{.....(2)}$$

In (b) the torque has been increased past the maximum allowable elastic torque causing partially plastic deformation. As the torque is increased, more of the material will yield and take up the yield stress. Consider the case in (b) where the material has yielded to a radius R_1.

$\therefore$ The partial plastic Torque (T_{pp}) = Elastic Torque in core + Plastic Torque on outsides.

From equation 2 Elastic Torque in core = $\frac{\pi R_1^3}{2}\tau_y$ .....(3)

with R_1 replacing R in equation 2.

For the plastic torque let us consider an elementary ring of radius r and thickness dr. The stress carried by this portion is τ_y because all fibres in the plastic zone have reached the yield stress.

Force on element = $\tau_y \times 2\pi r dr$.

Torque on element = Force x radius

$= (\tau_y \times 2\pi r dr) \times r$

$= \tau_y 2\pi r^2 dr$

Total torque = $\int_{RI}^{R} \tau_y 2\pi r^2 dr$

$= \tau_y 2\pi \int_{RI}^{R} r^2 dr$

$= \tau_y 2\pi [\frac{r^3}{3}]_{RI}^{R}$

$$T_p = \frac{2\pi \tau_y}{3}[R^3 - R_1^3] \quad \text{.....(4)}$$

Therefore the partial plastic torque:

$$T_{pp} = \frac{\pi R_1^3}{2} \tau_y + \frac{2\pi}{3} \tau_y [R^3 - R_1^3]$$

$$= \frac{\pi}{6} \tau_y [4R^3 - R_1^3] \quad \text{.....(5)}$$

From equation 5 the torque for (c) can be expressed as follows:

In Figure 4.3 (c) $R_1 = 0$

$$\therefore T_{FP} = \frac{2\pi}{3} \tau_y R^3 \quad \text{.....(6)}$$

From this it can be concluded that a considerable torque capacity exists beyond that required to produce initial yield.

Ratio of fully plastic to maximum torque is:

$$\frac{T_{FP}}{T_E} = \frac{2\pi R^3}{3} \tau_y \times \frac{2}{\pi R^3} \tau_y = \frac{4}{3}$$

The fully plastic torque for a solid shaft is 33% greater than the maximum elastic torque. This larger margin can either be incorporated in design procedures to increase the allowable torque, or it can be used as an additional factor of safety. Important to remember is that as soon as a shaft is stressed beyond the yield point of the material, permanent deformation will occur.

As soon as there is permanent deformation, residual stress has been set up. This residual stress will affect the overall service performance of the component[15], so it is important for a design engineer to be able to determine their magnitude. We start off by assuming that the removal of the torque is a completely elastic process, so that the stress distribution caused by the unloading is linear.

The residual stresses are obtained from subtracting the elastic unloading stress distribution from that of the partially plastic stress distribution. From equation 5 the partially plastic torque is equal to T_{pp} and, therefore, the torque to be applied during unloading must equal T_{pp} as well.

This torque will induce a stress τ' at the outer fibres of the shaft and if assumed that it is an elastic material, this stress will be given by the torsion theory of

$$\frac{T}{J} = \frac{\tau}{R} \qquad \therefore \tau' = \frac{T_{pp}\, R}{J}$$

Let us consider the shaft in Figure 4.4 (a) loaded into partial plastic state.

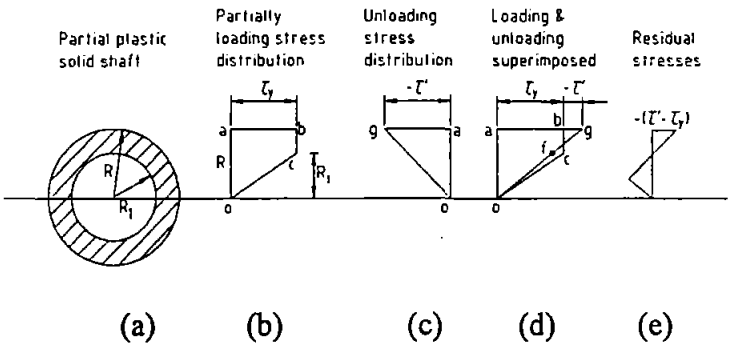

Figure 4.4: Stress distribution of partially plastic shaft.

The torque needed for stress distribution in (b) is therefore:

$$T_{pp} = \frac{\pi\, \tau_y}{6} [4R^3 - R_1^3] \qquad \text{from equation (5)}$$

To determine the residual stress after unloading, the unloading (c) is assumed completely elastic. Therefore an equivalent moment to T_{pp}, but in opposite sense must be applied for the unloading moment. The effective stress introduced at the outer fibres by this process, is thus

given by the torsion theory

$$\frac{T}{J} = \frac{\tau}{R}$$

$$\therefore \tau = \frac{TR}{J} = \tau' \text{ at point (g)}$$

The magnitude of the residual stress at the outer surface is therefore equal to $-(\tau' - \tau_y)$. Now the unloading stress distribution is linear from zero at the centre of the bar to τ' at the outside. If τ' is subtracted from the partially loading stress distribution in (b), it will produce the residual stress distribution as shown in (e).

Any manufacturing process or service application causing yielding in a material will produce residual stresses which can be favourable to future overloads if acted in the same direction, and/or unfavourable to future overloads acting in the opposite direction. If residual stresses represent a favourable stress distribution to a specific service condition, this stress distribution has first to be overcome before any adverse stress can be introduced into the component. A typical example of this is where spring manufacturers intentionally yield springs in the direction of anticipated service loads to improve service life and performance with the aid of residual stresses.

4.2 MEASUREMENT OF RESIDUAL STRESSES

4.2.1 The need for measurement of residual stresses[16]

The question is: why bother to measure residual stresses if it is such a complex uncertain procedure? Well, it can be shortly answered as follows: The safe and durable operation of structures and components depend on the relationship between stresses in the component and the limiting stress levels in the material. The existing stresses in a component is superimposed or added to the external stresses induced on the component. This could have major influence on the final design of a component. The applied external stresses can be determined accurately

with existing methods of stress analysis, but the residual component of the stresses are a bit more complicated to determine and are therefore sometimes ignored. If residual stresses can be determined accurately and in a straight forward manner it will allow for incorporating them into design calculations, assisting to produce safer and more reliable components.

Another advantage to an easy reliable method of measuring residual stresses is the optimising of manufacturing processes. It is common knowledge that minor changes to process procedures, e.g. heat treatment, machinery rates, welding profiles, etc. can introduce residual stresses in relatively stress free components.

The need for world class manufacturing which involve the production of enhanced and more reliable components while at the same time considering energy conservation principles emphasise the need to be able to measure residual stresses induced during manufacturing processes. Over-design and the waste associated with it is no longer acceptable and the engineering world will have to start considering the beneficial and detrimental effects of residual stresses in design.

4.2.2 Different methods for the measurement of residual stresses [17,18,19,20,21,22,23]

Residual stresses are difficult to measure since they are independent of the applied external load and are imposed during the manufacturing or heat treatment processes. A wide range of methods are available to measure residual stresses, with each method having its own set of advantages and disadvantages for different applications. Below are some of the methods that have been used successfully in the past:

- Chemical etch
- Hardness studies
- Hole drilling

- Layer removal
- Magnetic method
- Modified layer removal
- Neutron diffraction
- Photo-elasticity
- Progressive turning
- Stress out brittle lacquer drilling
- Ultrasonic
- X-ray

The most frequently used techniques for the measurement of residual stresses are the hole-drilling and X-ray measurement procedures. One of the biggest drawbacks of most of the methods mentioned is that they use destructive measuring techniques and mobile equipment to do on-site measurements of residual stresses is not always available.

After a study into methods used successfully in the past, three of the above list seemed to be the more common procedures for the measurement of residual stresses namely photo elasticity, X-ray analysis and the centre hole drilling technique. Taking the following factors like the material characteristics, the position of measurement, cost and availability of equipment into account, it was decided to make use of the centre hole drilling method, not using a drilling device, but rather an air abrasive system. The next part of this chapter will do a detailed analysis of the hole drilling technique to determine residual stresses. For detailed analysis of other methods see Appendix E.

4.2.3 Measurement of residual stresses by centre hole drilling[17,21,24,25,26,27,28,29,30,31,32,33]

Residual stresses are difficult to measure with strain gauges since the load is imposed on the component before the gauges can be fitted. To sense the presence of residual stresses with

strain gauges, it is necessary to relieve the residual stresses by removing material after the gauge is mounted. On small components this can mean that it is a destructive way of measuring residual stresses. On the other hand if it was done on a large structure the drilled hole can, without difficulty, be carefully ground away.

There are several methods that can be used to relieve or remove material by the hole drilling technique. They are by drilling, milling and air abrasive methods. The principle of all these methods is the same.

The measurement procedure is relatively simple and has been standardised in ASTM standard test method E837-94a. Special expertise is needed for this method and is done by using commercially available equipment and gauges. The method is very versatile and can be performed on a wide range of components in either a laboratory or in service (field) applications. The hole drilling method mainly lends itself for application in which the residual stresses are uniform throughout the drilling depth.

4.2.3.1 High-speed drilling or milling[31,32,34,35]

This method utilises a small drill 1.5 to 3 mm in diameter or an end mill of 0.8 mm to 6 mm in diameter. The drill or mill can be accurately located over the gauge centre, using a removable eye-piece. After the fixture is accurately located the eye-piece is removed and replaced by the drilling or milling head. The main difference between the drill bit and the milling cutter is that the drill bit does not produce flat bottomed holes because of its shape, while the end mill is flat. This makes the end mill more suitable since flat-bottomed holes are assumed in the derivation of the theoretical expressions.

A problem is that the drilling operation itself introduces machining stresses into the component

that cannot be separated from the original stresses present. The hole drilling process must be very carefully controlled to prevent errors in the strain values. This can be minimised by sensitive operation of all the equipment involved.

4.2.3.2 Air-abrasive machining[23]

In this process the drilling head is replaced by a device that directs a stream of air containing abrasive particles onto the surface. This bombardment of the selected surface inside the strain rosette will erode the material forming a hole. This is considered to be a stress-free machining technique. Two types of holes can be produced by this method, as illustrated by Figure 4.5 a and b. The hole produced does not have rectangular axial sections but can be trepanned to produce asymmetric, parallel-sided holes. It has been shown that square sided holes aid, as far as repeatability of results go.

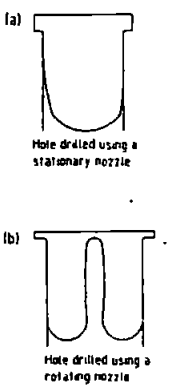

Figure 4.5: Hole shapes as produced by air abrasive drilling.

The depth of the hole must be determined and must be at least 1mm deep. This is the minimum size necessary to produce full stress relaxation in most applications[31]. The optimal hole size is believed to be between 2 and 2.2 mm.

4.2.3.3 Measurement procedures

- Determine the point where residual stress must be measured and install the strain gauge rosette on the test part.

- Connect the wires of the strain rosette to a static strain indicator through a switch-and-balance unit.
- Attach and line up the drill guide assembly to the test piece.
- Zero balance the strain gauge circuit and drill a shallow hole through the centre of the rosette.
- Record the readings of the relaxed strains.
- Calculate the principal residual stresses and their orientation.

4.2.3.4 Theory of hole drilling strain gauge rosette as per ASTM E837-94a[33]

The drilling of a hole into an area of a component with residual stresses will relax the stresses at that point. This happens because the hole surface becomes a free surface and every perpendicular line to this surface becomes a principal axis on which the shear and normal stresses are zero. Removing these stresses by drilling the hole changes the stresses in the immediate surroundings of the gauges, causing the surface strains to change correspondingly. In practice the drilled hole is mainly blind with its depth about equal to its diameter. The hole is also considered small compared to the thickness of the test component. The blind hole theory is relatively complex in that no close-form solution is available from the theory of elasticity for direct calculation of the residual stresses from the measured strips.

However, a solution can be obtained for the through drilled hole in a thin plate with relatively uniformed distributed residual stresses. This document will first look at this simpler theory for the through drilled hole and then extend it to the blind hole.

Calculations of residual stresses by through hole analysis as per ASTM E837-94a[31]

If a thin plate is subjected to an internal load which causes a uniform residual stress σ_x in the x direction the stress distribution can be determined as follows:

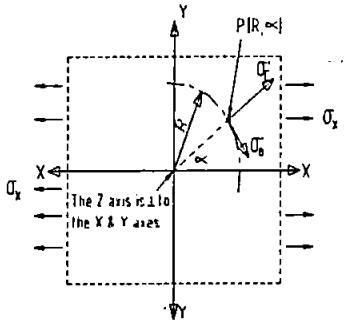

Figure 4.6: Flat plate subjected to a uniform stress.
(Illustration courtesy of the Micro Measurements division of Measurements Group Inc., Raleigh, NC USA.)

Let us consider Figure 4.6:

The initial stress state at point P at radius R and angle α can be expressed as follows:

Stress at $P(R,\alpha)$ is now $\sigma_{yy} = \tau_{xy} = 0$

$$\sigma_r = \sigma_x \sin^2\alpha \therefore \sigma_r = \frac{\sigma_x}{2}(1 + \cos 2\alpha) \quad \text{.....(1)}^{31}$$

$$\sigma_\theta = \sigma_x \cos^2\alpha \therefore \sigma_\theta = \frac{\sigma_x}{2}(1 - \cos 2\alpha) \quad \text{.....(2)}$$

$$\tau_{r\theta} = \sigma_x \sin\alpha \cos\alpha + \tau_{R\theta} = \frac{-\sigma_x}{2} \sin 2\alpha \quad \text{.....(3)}$$

If the same area is used and a small hole of diameter R_o is drilled through the plate, the stresses

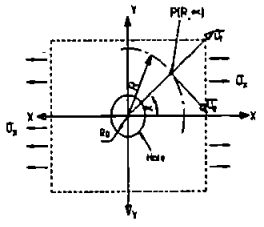

Figure 4.7: Thin flat plate with hole drilled in the centre subjected to a uniform stress.
(Illustration courtesy of the Micro Measurements division of Measurements Group Inc., Raleigh, NC USA.)

in the vicinity of the hole will be different. Consider the schematic in Figure 4.7, where a thin plate is subjected to a uniform stress with small hole drilled through centre of the plate with a radius of R_O.

$$\therefore \sigma_r = \frac{\sigma_x}{2}\left[\left(1 - \frac{R_o^2}{R^2}\right) \cdot \left(1 + \left(\frac{-3R_o^2}{R^2} + 1\right) \cos 2\alpha\right)\right] \quad \text{.....(4)}$$

$$\therefore \sigma_\theta = \frac{\sigma_x}{2}\left[\left(1 + \frac{R_o^2}{R^2}\right) - \left(1 + \frac{3R_o^4}{R^4}\right) \cos 2\alpha\right] \quad \text{.....(5)}$$

$$\tau_{r\theta} = \frac{-\sigma_x}{2}\left[\left(1 + \frac{3R_o}{R^2}\right)\left(1 - \frac{R_o^2}{R^2}\right)\left(1 - \frac{R_o^2}{R^2}\right) \sin 2\alpha\right] \quad \text{.....(6)}$$

Let $r = \frac{R}{R_o}$ for $R \geq Ro$

From equation (4):

$$\therefore \sigma_r = \frac{\sigma_x}{2}\left[\left(1 - \frac{1}{r^2}\right) \cdot \left[1 - \left(\frac{3}{r^2} - 1\right) \cos 2\alpha\right]\right.$$

Simplify:

$$\sigma_r = \frac{\sigma_x}{2}\left[\left(1 - \frac{1}{r^2}\right) + \left(-\frac{3}{r^2} + 1 + \frac{3}{r^4} - \frac{1}{r^2}\right) \cos 2\alpha\right]$$

$$= \frac{\sigma_x}{2}\left[\left(1 - \frac{1}{r^2}\right) + \left(1 + \frac{3}{r^4} - \frac{4}{r^2}\right) \cos 2\alpha\right]$$

$$\therefore \sigma_r = \frac{\sigma_x}{2}\left[\left(1 - \frac{1}{r^2}\right) + \left(1 + \frac{3}{r^4} - \frac{4}{r^2}\right) \cos 2\alpha\right] \quad \text{.....(7)}$$

From equation (5)

$$\sigma_\theta = \frac{\sigma_x}{2}\left[\left(1 + \frac{1}{r^2}\right) - \left(1 + \frac{3}{r^4}\right) \cos 2\alpha\right] \quad \text{.....(8)}$$

From equation (6)

$$\tau'_{r\theta} = -\frac{\sigma_x}{2}\left[\left(1 - \frac{1}{r^2} + \frac{3}{r^2} - \frac{3}{r^4}\right)\sin 2\alpha\right]$$

$$= \frac{-\sigma_x}{2}\left[1 + \frac{2}{r^2} - \frac{3}{r^4}\right]\sin 2\alpha \quad \text{.....(9)}$$

Subtracting the original stresses from the new stresses obtained after drilling the hole will reveal the stress relaxation at point P (R,α) due to drilling a hole.

$$\therefore \quad \Delta\sigma_r = \sigma'_r - \sigma'_r$$

$$\Delta\sigma_\theta = \sigma'_\theta - \sigma'_\theta$$

$$\Delta\tau_{r\theta} = \tau'_{r\theta} - \tau'_{r\theta}$$

From subtracting equation (1) from (7):

$$\therefore \sigma_r = \frac{\sigma_x}{2} - \frac{\sigma_x}{2r^2} + \frac{\sigma_x}{2r^2}\cos 2\alpha + \frac{3\sigma_x}{2r^4}\cos 2\alpha - \frac{4\sigma_x}{2r^2}\cos 2\alpha - \frac{\sigma_x}{2} - \frac{\sigma_2}{2}\cos 2\alpha$$

$$= -\frac{\sigma_x}{2r^2} + \frac{3\sigma_x}{2r^4}\cos 2\alpha - \frac{4\sigma_x}{2r^2}\cos 2\alpha$$

$$= \frac{\sigma_x}{2}\left(-\frac{1}{r^2} + \frac{3}{r^4}\cos 2\alpha - \frac{4}{r^2}\cos 2\alpha\right)$$

$$= -\frac{\sigma_x}{2}\left[\frac{1}{r^2} - \frac{3}{r^4}\cos 2\alpha + \frac{4}{r^2}\cos 2\alpha\right] \quad \text{.....(10)}$$

From subtracting equation: (2) from equation (8)

$$\sigma_\theta = \frac{\sigma_x}{2} + \frac{\sigma_x}{2r^2} - \frac{\sigma_x}{2}\cos 2\alpha - \frac{3\sigma_x}{2r^4}\cos 2 - \frac{\sigma_x}{2} + \frac{\sigma_x}{2}\cos 2\alpha$$

$$= \frac{\sigma_x}{2r^2} - \frac{3\sigma_x}{2r^4}\cos 2\alpha$$

$$\therefore \sigma_\theta = \frac{\sigma_x}{2}\left[\frac{1}{r^2} - \frac{3}{r^4}\cos 2\alpha\right] \quad \text{.....(11)}$$

Subtracting equation (3) from (9):

$$\tau_{r\theta} = -\frac{\sigma_x}{2}\sin 2\alpha\,\frac{2\sigma_x}{2r^2}\sin 2\alpha + \frac{3\sigma_x}{2r^4}\sin 2\alpha + \frac{\sigma_x}{2}\sin 2\alpha$$

$$= \frac{3}{2}\frac{\sigma_x}{r^2}\sin 2\alpha - \frac{2\sigma_x}{2r^2}\sin 2\alpha$$

$$= \frac{\sigma_x}{2}\left(\frac{3}{r^4} - \frac{2}{r^2}\right)\sin 2\alpha \quad \text{.....(12)}$$

Equation 10,11 and 12 yield the full expressions for the relaxed stresses due to the drilling of the hole.

If the material used was homogeneous and isotropic in its mechanical properties, and linear-elastic in its stress-strain relation, the above equations can be substituted into the biaxial Hooke's Law to solve the relieved normal strains at point "P".

The resulting expressions for strain are as follows:

$$\epsilon_r = -\frac{\sigma_x (1+\nu)}{2E}\left[\frac{1}{r^2} - \frac{3}{r^4}\cos 2\alpha + \frac{4}{r^2(1+\nu)}\cos 2\alpha\right] \quad \text{.....(13)}$$

$$\epsilon_\theta = -\frac{\sigma_x (1+\nu)}{2E}\left[-\frac{1}{r^2} + \frac{3}{r^4}\cos 2\alpha - \frac{4\nu}{r^2(1+\nu)}\cos 2\alpha\right] \quad \text{.....(14)}$$

Equation 13 and 14 can be simplified to show that the relieved tangential strains along a circle with any radius R when R ≥ Ro (Hole Radius) will vary in a sinusoidal manner.

e.g.: $\epsilon_r = \sigma_x (A + B\cos 2\alpha)$ .....(15)

$$\epsilon_\theta = \sigma_x (-A + C\cos 2\alpha) \quad \text{.....(16)}$$

Where the coefficient A, B, and C can be defined as follows:

$$A = -\frac{1+\nu}{2E}\left(\frac{1}{r^2}\right) \quad \text{.....(17)}$$

$$B = -\frac{1+\nu}{2E}\left[\left(\frac{4}{1+\nu}\right)\frac{1}{r^2} - \frac{3}{r^4}\right] \quad \text{.....(18)}$$

$$C = -\frac{1+\nu}{2E}\left[-\left(\frac{4\nu}{1+\nu}\right)\frac{1}{r^2} + \frac{3}{r^4}\right] \quad \text{.....(19)}$$

The relieved strains will vary in a complex way with distance from the hole surface as illustrated by Figure 4.8. It shows this variation where strains are plotted along the principal axes at $\alpha = 0°$ and $\alpha = 90°$. From this figure it can be observed that the strain decreases as it moves away from the hole edge. This phenomenon makes it desirable to measure the strains close to the edge of the hole. It must not be forgotten that stresses due to the drilling processes are most likely to be a maximum at the hole edges which necessitates a compromise in selecting an

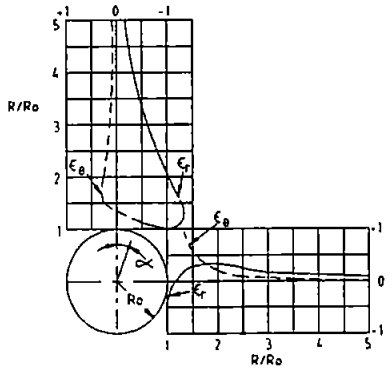

Figure 4.8: Variation of relieved radial and tangential strains with distance (along principal axes) from the centre of the drilled hole - uniaxial residual stress.
(Illustration courtesy of the Micro Measurements division of Measurements Group Inc., Raleigh, NC USA.)

optimum radius for location of the strain gauges. According to ASTM E837-94a the ratio of the R/Ro (where R = radius to longitudinal centre of gauge and Ro = hole radius) should fall in the range from 2.5 to 3.4.

Commercial strain gauge rosettes for residual stress analysis are designed with radially oriented grids to measure the relieved radial strain ϵ_r. From Figure 4.8 it is evident that the relieved radial strain along the major principal axis is opposite in sign to the initial residual stress. This occurs because the coefficient A and B in equation 15 are always negative and (for $\alpha = 0°$) $\cos 2\alpha = +1$.

The above calculation and reasoning were based on a uniaxial residual stress, but in practice residual stresses are mainly biaxial, with two non-zero principal stresses. This can be incorporated by using the superposition principle applicable to linear-elastic material behaviour. Originally in Figure 4.3 the uniaxial residual stress was along the X-axis. Had it been along the Y-axis, equation 1 and 2 would still apply except that cos 2α would be replaced by $\cos 2(\alpha + 90°)$ or by $-\cos 2\alpha$. Therefore the relieved radial strains along the Y-axis at point P (R,α) can be written as:

$$\epsilon_r^Y = \sigma_y(A - B\cos 2\alpha) \quad \text{.....(20)}$$

$$\therefore \text{ also } \quad \epsilon_r^x = \sigma_x(A + B\cos 2\alpha) \quad \text{.....(21)}$$

If the residual stress in a component includes both σ_x and σ_y, the principle of superposition permits addition of equations (20) and (21). The new equations for the relieved radial strain due to the biaxial residual stresses are:

$$\epsilon_r = \sigma_x(A + B\cos 2\alpha) + \sigma_y(A - B\cos 2\alpha) \quad \text{.....(22)}$$

or can also be written as:

$$\epsilon_r = A\ (\sigma_x + \sigma_y) + B\ (\sigma_x - \sigma_y)\ \cos 2\alpha \quad \text{.....(23)}$$

These equations underline the basic relationship of the hole drilling method for residual stress analysis.

Determining of principal stresses[31]

A three-gauge strain rosette is mounted on the component with the radially oriented strain gauge placed with the centres at a radius R from the hole site as shown in Figure 4.9. The angular spacing of the gauges can be arbitrary but must be known, in most commercial gauges these angles are in increments of 45°. The reason for using 45° increments of angular spacing of gauges is because it leads to the simplest analytical expression for solving the principal stresses.

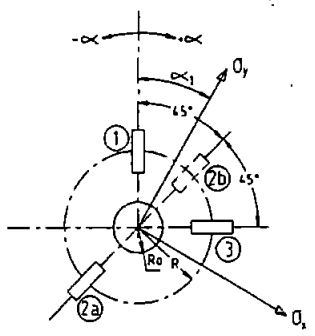

Figure 4.9: Strain gauge rosette arrangement.
(Illustration courtesy of the Micro Measurements division of Measurements Group Inc., Raleigh, NC USA.)

Angle α_1, is always the acute angle from the nearest principal axis to gauge (1), while $\alpha_2 = \alpha_1 + 45°$ and $\alpha_3 = \alpha_1 + 90°$. The angle α is measured as a positive angle in the direction of gauge numbering. In Figure 4.9 it might seem wrong at first but although gauge

2 is physically at position 2a it is effectively at position 2b for gauge numbering purposes. The reason for placing it at 2a is to assure strain sampling over as wide an area as possible around the hole. When space is very limited, the gauge can be placed at position 2b to ensure the hole is placed closest to the area of interest.

With the aid of equation 23 we can now write an equation for strain for each of the gauges in the rosette.

$$\epsilon_1 = A(\sigma_x + \sigma_y) + B(\sigma_x - \sigma_y)\cos 2\alpha \quad \text{.....(24)}$$

$$\epsilon_2 = A(\sigma_x + \sigma_y) + B(\sigma_x - \sigma_y)\cos 2(\alpha + 45°) \quad \text{.....(25)}$$

$$\epsilon_3 = A(\sigma_x + \sigma_y) + B(\sigma_x - \sigma_y)\cos 2(\alpha + 90°) \quad \text{.....(26)}$$

The principal stresses can now be calculated by substituting the above three equations successively into equation 22 or 23 and then solving them simultaneously. The result can be expressed as:

$$\sigma_{max} = \frac{\epsilon_1 + \epsilon_3}{4A} - \frac{1}{4B}\sqrt{(\epsilon_3 - \epsilon_1)^2 + (\epsilon_3 + \epsilon_1 - 2\epsilon_2)^2} \quad \text{.....(27)}$$

$$\sigma_{min} = \frac{\epsilon_1 + \epsilon_3}{4A} + \frac{1}{4B}\sqrt{(\epsilon_3 - \epsilon_1)^2 + (\epsilon_3 + \epsilon_1 - 2\epsilon_2)^2} \quad \text{.....(28)}$$

Where:

$$\tan 2\alpha = \frac{\epsilon_1 - 2\epsilon_2 + \epsilon_3}{\epsilon_1 - \epsilon_3}$$

and α is the angle between the nearest principal axis and gauge 1. To find α in a more convenient manner, we can rearrange the previous formula to define the angle from gauge 1 to the nearest principal axis by:

$$\tan 2\alpha = \frac{\epsilon_1 - 2\epsilon_2 + \epsilon_3}{\epsilon_3 - \epsilon_1} \quad \text{.....(29)}$$

The following rules can be used to determine which principal stress is referred to gauge number 1:

If $\epsilon_3 > \epsilon_1$: α refers to σ_{max}

$\epsilon_3 < \epsilon_1$: α refers to σ_{min}

$\epsilon_3 = \epsilon_1$: $\alpha = \pm 45°$

$\epsilon_2 < \epsilon_1$: σ_{max} at $+45°$

$\epsilon_2 > \epsilon_1$: σ_{max} at $-45°$

Great care must be taken in determining the values for coefficients A and B. They only apply in conditions met by Kirsch solutions. (Thin plate, through hole, stress at (r.α), uniform stress in plate). Taking into account that the strain grids have a finite element and that the grids are usually parallel to the radial lines, which make them sensitive for tangential and radial strains, more accurate values for the coefficients can be calculated by integrating equations 13 and 14 over the respective gauge grid areas. The coefficient calculated in this way are designated by $\overline{A}$ and $\overline{B}$. An alternate method of determining $\overline{A}$ and $\overline{B}$ is to measure them by experimental calibration as published in the ASTM specifications.

Most machine parts are not flat and not subjected to uniform stresses which makes the through drill method unsuitable for them. In these cases a shallow blind hole is drilled into the surface. The drilling of a blind hole into fields of plane stresses produces very complex local stress states. No exact solution is available from the theory of elasticity for this, however, the blind hole analysis reveals stress distributions closely parallel to the through hole analysis[21]. It can therefore be assumed that the relieved strains due to the drilling of the blind hole still vary sinusoidally along a circle concentric with the hole. From this it can be accepted that equation (22) and (23), as well as equations (27) and (28), are equally applicable to the blind hole

analysis as is the case with through hole analysis as long as the appropriate blind hole coefficients $\overline{A}$ and $\overline{B}$ are employed. The coefficient $\overline{A}$ and $\overline{B}$ must be determined by experimental calibration or by numerical procedures such as finite element analysis.

In the blind hole analysis an additional dimension less variable appears, namely hole depth defined by $\frac{Z}{D_o}$. (Where Z = hole depth and D_0 = hole diameter).

In general it can be said that the coefficients $\overline{A}$ and $\overline{B}$ are functions of:

$$\overline{A} = f_A\ (E,\ \nu,\ r,\ \frac{Z}{D_o}) \quad \text{.....(30)}$$

$$\overline{B} = f_B\ (E,\ \nu,\ r,\ \frac{Z}{D_o}) \quad \text{.....(31)}$$

In general it is considered that for a hole drilled the relieved strains will increase at a decreased rate as the hole depth increases up and to the point where the depth is equal to the hole diameter. For maximising strain signals ASTM E837-94a specifies that $Z/D_o = 1.2$. This

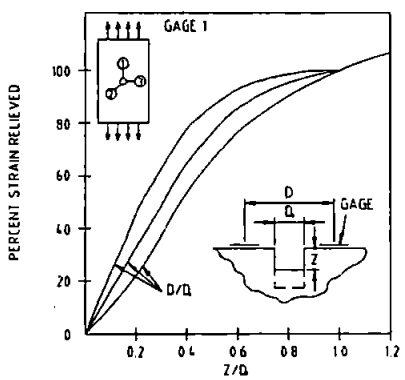

Figure 4.10: Relieved strain versus Z/D. (strains normalized to 100% at $Z/D_o = 1$)

(Measurements Group TN-503-4) (Illustration courtesy of the Micro Measurements division of Measurements Group Inc., Raleigh, NC USA.)

variation of relieved strain is illustrated in Figure 4.10. A similar plot to this is also available in the ASTM specifications as a criterion for verifying the required uniformity of stress distribution with depth in a specimen.

When strains are relieved, normalised and plotted as shown in Figure 4.10, they should fall within or close to the specified scatter band.

It is very important to realise that it has been demonstrated by Rendler and Vigness[40] that for any given set of material properties, E, ν and coefficient $\overline{A}$ and $\overline{B}$ are simple geometrical functions and then constant for all similar geometrical cases. This allows for the scaling (+ or -) of particular sizes with no change to the coefficients. The hole diameter and depth can be scaled in a similar fashion for the same material.

Schajer[50] has developed two new coefficients $\overline{a}$ and $\overline{b}$, which removed the dependence of $\overline{A}$ and $\overline{B}$ on the materials, leaving only geometric dependence.

They can be defined as follows:

$$\overline{a} = \frac{2E\,\overline{A}}{1 + \nu} \quad \text{.....(32)}$$

$$\overline{b} = 2E\,\overline{B} \quad \text{.....(33)}$$

Determining coefficients A and B[31]

The coefficients $\overline{A}$ and $\overline{B}$ must be known before any stress from the relieved strains can be calculated. The coefficients can be determined by experimental calibration which is a very popular method. It automatically accounts for mechanical properties of test material, strain rosette geometry, hole depth and diameter. This is by far the most accurate method to determine the coefficient $\overline{A}$ and $\overline{B}$ if done with the necessary sensitivity to detail. The main disadvantage of the method is that it must be repeated each time for a different set of geometric parameters.

Calibration for $\overline{A}$ and $\overline{B}$ is accomplished in the following manner:

- Install a residual strain rosette on a uniaxially stressed tensile specimen under test. The grid of number 1 gauge on the rosette must be aligned parallel to the loading direction, placing grid number 3 along the transverse axis of the specimen. Assure that bending stresses are eliminated as far as possible and that the tensile stress is uniformly distributed across the whole section of the specimen. Specimen width is to be x10 the hole diameter and the distance between machine grips, at least x5 the width. For blind hole applications the thickness must be at least x5 the hole diameter to be drilled.
- Zero balance the strain gauge rosette circuit.
- Apply a load P to the specimen that does not exceed half of the proportional limit stress for the test material. This will develop the desired calibration stress, σ in the specimen. At no instant must the applied stress plus the residual stress cause local yielding. It is suggested that the specimen be loaded incrementally and making readings of strain at each increment.
- Record the strain ϵ_1 and ϵ_3 at each increment. This permits plotting of σ_c *versus* ϵ_1' and ϵ_3' to construct best five straight lines. Only strains in grid (1) and (3) need to be recorded, since these grids are known to be aligned with the principal axes.
- Unload the specimen and remove it from tensile machine.
- The above procedure is done before drilling and is needed to eliminate the effects of strain relief that may occur due to relaxation of initial residual stresses in the specimen.
- Drill a hole in the specimen according to the specified manner. Adhere to previous specification about hole size and depth.
- Replace the specimen in tensile machine and re-zero the strain rosette circuit.
- Re-apply load "P" exactly onto specimen in same manner as described previously and measure ϵ_1'' and ϵ_3'' on drilled specimen.

The calibration strain ϵ_c corresponding to load P and stress σ_c are then:

$$\epsilon_{c1} = \epsilon_1'' - \epsilon_1' \quad \text{and} \quad \epsilon_{c3} = \epsilon_3'' - \epsilon_3'$$

Since the calibration is performed with one non-zero principal stress only, equations (15) and (16) can be used for determining the values of $\overline{A}$ and $\overline{B}$.

$$\epsilon_{c1} = \epsilon_1'' - \epsilon_1' \quad \text{and} \quad \epsilon_{c3} = \epsilon_3'' - \epsilon_3'$$

For No 1 grid $\alpha = 0°$

For No 2 grid $\alpha = 90°$

$$\epsilon_{c1} = \sigma_c [\overline{A} + \overline{B} \cos 0°] \qquad \cos 0° = 1$$

$$= \sigma_c[\overline{A} + \overline{B}]$$

and $$E_{C_3} = \sigma_c[\overline{A} + \overline{B} \cos 90°] \qquad \cos 90° = -1$$

$$= \sigma_c[\overline{A} - \overline{B}]$$

Solving for $\overline{A}$ and $\overline{B}$

$$\overline{A} = \frac{\epsilon_{c1} + \epsilon_{c3}}{2\sigma_c} \quad (Pa^{-1}) \quad \text{.....(34)}$$

$$\overline{B} = \frac{\epsilon_{c1} - \epsilon_{c3}}{2\sigma_c} \quad (Pa^{-1}) \quad \text{.....(35)}$$

(Note: ϵ can be negative and positive)

From the above information the coefficients $\overline{a}$ and $\overline{b}$ can be calculated from equations (32) and (33) if the elastic modules and Poisson's ratio is known.

It is important to note that the coefficients $\overline{A}$ and $\overline{B}$ are only applicable to conditions that match the calibration conditions.

- Material with same elastic properties
- Same rosette geometry
- Same hole size
- Same hole form (through or blind)
- Uniform stress with depth

Possible errors

Residual stress determined according to this method could exhibit a bias not exceeding ±10%[17]. This is after ensuring that no additional stresses are induced due to the hole drilling process. If a significant non-uniform stress distribution goes unrecognised, the error may be more than 10%[17] and will usually be in the direction of under estimating the maximum stress.

During a round robin test managed by ASTM on AISI 1018 carbon steel it was found that the standard deviation was 14MPa. This was calculated from 26 measurements done by eight different laboratories on eight nominally identically specimens.

For a complete case study on the application of the above calculation procedure on a steel bar, see Appendix D.

4.3 SUMMARY

Finite element analysis has shown that change in strain produced by drilling[36], is caused partially by residual stress in a specific increment of drilling and the remaining change by residual stresses in preceding increments. The reason for this is that the stress distribution changes as the hole deepens. From the study it is apparent that the stress decreases rapidly with distance from the surface. This is a clear indication that the main influence on relieving the stress lies in the layers close to the surface of the material. It is generally accepted that the greatest

influence lies in the upper half of the hole depth; up to 80% of strain relief normally occurs in this part of the hole drilling process[31].

The ideal application of the hole drilling method is for material with stresses uniform to depth. Error and uncertainty are always present, their scale just depends on sensitivity of the user towards all variables present. As was discussed earlier in this chapter the margin of error for the air abrasive hole drilling method is approximately 14 MPa.

All measurements can be made by static strain instrumentation. The strain magnitudes are, however, a great deal smaller for residual stresses than for conventional stresses. Residual stresses can be very useful in engineering applications when considered carefully, but if ignored can have disastrous effects on the performance of components.

Although the measurement of residual stresses still has a long way to go, a number of internationally accepted methods are available. The biggest drawback of most methods is the mobility of measuring equipment, destructive measuring procedures and the ability to penetrate large, thick specimens.

Neutron diffraction offers the capability for the measurement of entire residual stress field but this is at very high cost due to the safety implication when working with neutrons. Another method showing promise for the future is ultrasonic techniques. Their principle is well understood but major improvements in the gain of sensing and measuring signals are needed. Features that introduce uncertainties in interruption of residual measurements, must be identified and the processing influences clarified.

To conclude, a great need exists to increase productivity, to conserve energy and to improve reliability of materials with enhanced quality assurance in manufactured components. All of this calls for reliable and powerful methods of evaluating residual stresses. Work done on measurement of residual stresses in coil springs withdrawn from different manufacturing processes has proved that the air abrasive centre hole drilling methods is very reliable and flexible. This method of residual stress measurement and calculation was used extensively during this research as described in Chapter 5 with excellent results.

CHAPTER 5

PROCESS EFFECTS OF 55Cr3 SPRING STEEL ON RESIDUAL STRESSES

INTRODUCTION

The understanding of the relationship between fatigue life, process effects and residual stresses needs to be evaluated carefully before the manufacturing process can be optimised for enhanced quality and product characteristics. Residual stresses in manufactured components are those stresses that exist without prior application of service or external loads. Virtually all manufacturing and surface treatments will introduce residual stresses into a component which may either be beneficial or detrimental to the fatigue properties[37].

This chapter investigates the relationship that exists between fatigue properties and residual stresses and its relation to process effects in samples withdrawn from different stages of the manufacturing processes of 55Cr3 spring steel. In order to measure the residual stresses present, the locked-in stresses must be relieved by removing material to enable a sensor to register the change in strain. These measurements were done by means of centre hole drilling using an air abrasive powder system and residual strain rosettes as sensors.

Residual stresses are receiving increased attention as it is recognised that many opportunities for optimisation of design and manufacture leading to reduction of costs, are locked-up inside the correct understanding of residual stresses. There is therefore an urgent need for determining residual stresses induced into manufactured components, together with the need for reliable non-destructive techniques for determining these stresses accurately. What makes the measuring techniques so important is the fact that it is generally very difficult to determine residual stresses by analytical and computational methods.

Care should be exercised in selecting the technique to be used for measuring residual stresses for a specific application. The test samples under consideration in this chapter are 55Cr3 spring steel withdrawn at different stages of the manufacturing process. An important characteristic to consider when selecting a measuring technique is the hardness of the material. Due to this factor, most of the conventional methods for removing material were found to be unsuitable for the steel. The air abrasive centre hole drilling method (ACH) was selected to measure the residual stresses in the 55Cr3 spring steel samples specifically because of its ability to penetrate hard materials[38]. It is believed that this method will induce negligible machinery stresses during the drilling process as the inertia of the aluminium oxide powder used is very low and cooling is effective as air is used as a transport medium from the abrasive powder.

The ACH method is a proven measuring technique which yields accurate and reliable results[39]. The above concept of the hole drilling method using strain gauges, was approved by ASTM and published in 1982 ASTM Book of Standards. Specimens were withdrawn from the spring manufacturing process line for 55Cr3 coil springs after the following stages: Hot coil and quench, tempering, hot scrag, shot peen, before load test (painted) and cold scrag. These samples were of the same batch used for the fatigue testing.

5.1 DESCRIPTION OF EQUIPMENT AND DRILLING PROCEDURE

5.1.1 Air abrasive centre hole drilling

In order to measure residual stresses in 55Cr3 spring steel, the locked-in stress must be relieved by means of the destructive removal of successive layers of material. The method utilised as described in this chapter is the air abrasive centre hole drilling strain gauge method of stress relaxation, illustrated in the photograph in Figure 5.1.

Figure 5.1: Set-up of the air abrasive drilling apparatus.

On the far lefthand side of the above photograph is the drilling device, while on the right side is the aluminium oxide pressure vessel control system. The thin red line is the air supply line for the turbine, the blue line is the line through which the aluminium oxide moves and the large green pipe on the left is a vacuum line for removing excess aluminium oxide from the drilling jig.

5.1.2 Measurement procedure

5.1.2.1 Alignment of sapphire nozzle

This operation is illustrated in the photograph of Figure 5.2. The drilling device and the optical unit is strapped on to a jig. A set of small lights arranged in a circle on the front edge is switched on and by looking through the eye piece the eccentricity of the nozzle can be set by a series of grub screws on the periphery of the front part of the drilling device.

Because this is a rotating nozzle system, the eccentricity will determine the size of the hole drilled. For the purpose of these spring samples, the optimal hole was in the vicinity of 0,8 to 1 mm. This adjustment is done by trial and error and is very time-consuming especially when drilling such small holes. It is a question of re-setting and drilling pilot holes until the correct size hole is achieved.

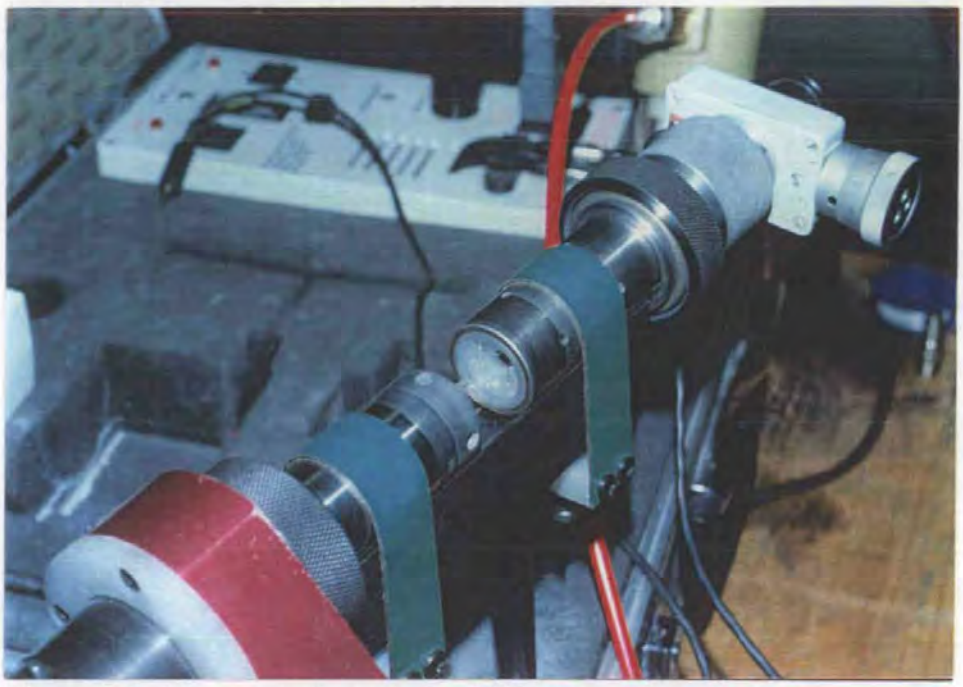

Figure 5.2: Alignment of nozzle for drilling operation.

5.1.2.2 Selection and application of residual strain rosette gauges

The selection of the strain gauge is very important as a wide variety are available for different

Figure 5.3:
Set-up drilling guide for drilling with the aid of the optical instrument. Same set-up is also used to determine hole size and depth.

applications and environment from manufactures like HBM Germany and Micro Measurements from the USA[18,40]. Taking into account that the wire diameter of the coil springs under investigation was only 11mm, immediately narrows the field down considerably. To do these

measurements as accurately as possible, a very small gauge is required. After intense research and consultation with the companies, it was decided to use EA-06-031RE-120 residual strain gauges from Micro Measurements. This is one of the smallest gauges available and although it had to be specially imported to South Africa it still was relatively affordable. The gauge dimensions are shown in Table 5.1.

Gauge Length	Grid centre line diam.	Typical hole diameter		Matrix	
		Minimum	Maximum	Length	Width
0.79	2.56	0.8	1.0	7.4	7.4

Note: All dimensions in mm.

Table 5.1: EA-06-031RE-120 residual stress gauge specifications.

The three element strain rosette is now installed at the point where stresses are to be measured. The three gauge grids are wired and connected to a static strain indicator using a full bridge six wire system. The spring with the gauge attached is now setup for drilling. It is very important that the sample is secured properly in such a manner that no external stresses are induced into it. As indicated in Figure 5.5 the spring was secured in a bench vice that was not tightened against the sample but against a plate at the bottom. The sample was then fixed to this plate by means of a soft putty to ensure it will not move during the drilling process.

5.1.2.3 Alignment of drilling guide and drilling device

A precision drilling guide is attached to the test component and accurately centred over a drilling target on the rosette by using the optical measuring equipment as illustrated by Figure 5.3. This same set-up will be used for the measurement of drilled hole size and depth. This is a critical process as the margin for error on such a small gauge is very small. It is very important not to cause any movement of the guide or the sample, as this will cause misalignment and might result in the damaging of a gauge as shown in Figure 5.4.

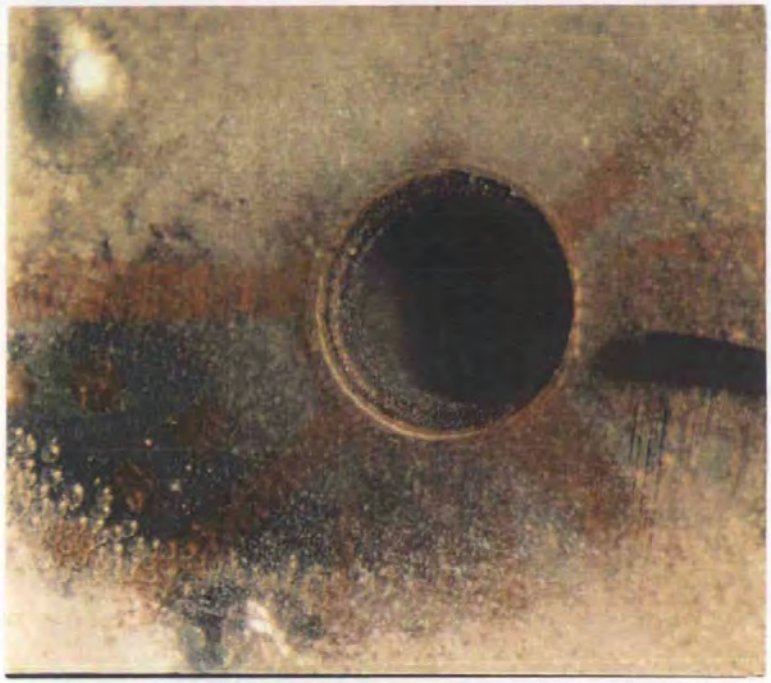

Figure 5.4: Damage to gauge due to slight miss-alignment of drilling jig.

Figure 5.5: Set-up of the drilling apparatus over sample to be drilled.

At this point the optical device is removed and replaced by the drill as illustrated in Figure 5.5, the zero balancing is performed on the gauge and a small hole is drilled through the centre of the rosette. The relieved strains are measured at different depths with the final depth being as close as possible to 1mm in this case. This is a time-consuming operation as there is no real control over depth, rate or diameter. Every now and then the process must be stopped, strain values recorded, drilling device removed and replaced by the optical device to record the depth and diameter. This is done until the required depth is reached. The foregoing procedure has more or less been standardised in the ASTM Standard Test Method E837.

5.1.2.4 Drilling procedure

Introduction of the small hole into the test specimen is one of the most critical operations in the procedure. The hole should be concentric with the drilling target on the special strain gauge rosette. It should also have the prescribed shape in terms of cylindricality, flat bottom and sharp corner at the surface[31], as illustrated in the photograph in Figure 5.6. It is clear that all the mentioned criteria was adhered to accept for the flat bottom of the hole. This characteristic is typical for small holes. An average depth was measured and used in the calculation; this could result in small variations of stress readings. As an abrasive material is used to drill the hole, it is very important to protect the measuring grids of the gauges properly. This was done by using a special high temperature tape manufactured by HBM. Any air under this tape will allow the abrasive powder to wear the tape, causing exposure of the grids which in turn is then damaged resulting in an open circuit and the loss of a gauge. An example of this scenario is illustrated by the photograph in Figure 5.7.

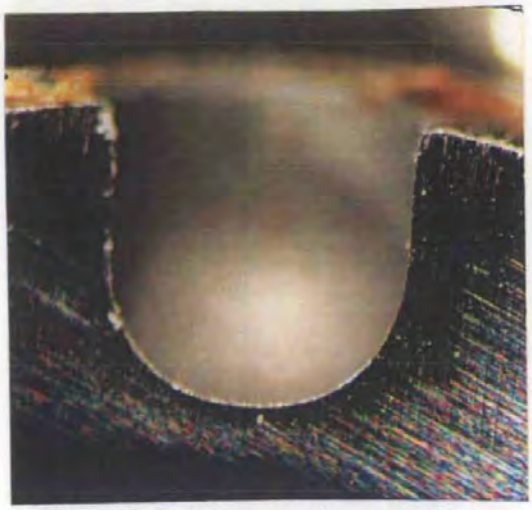

Figure 5.6: Cross section of drilled hole.

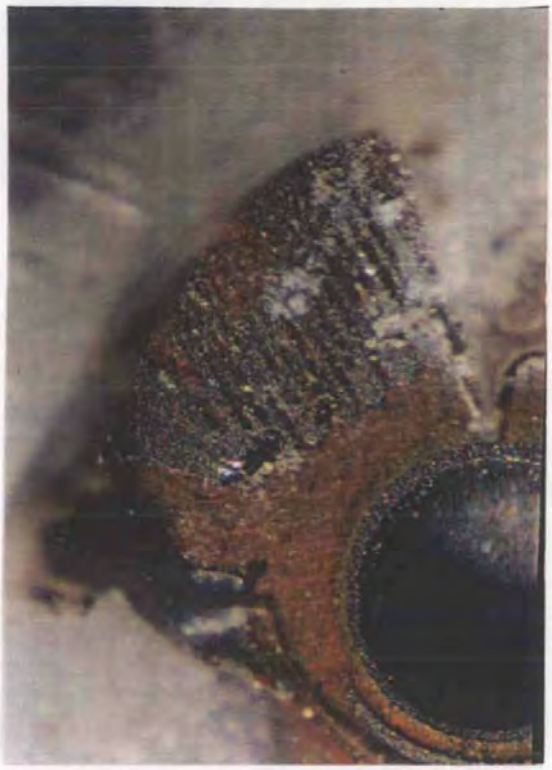

Figure 5.7:
Damaged gauge due to improper protection against air abrasive powder.

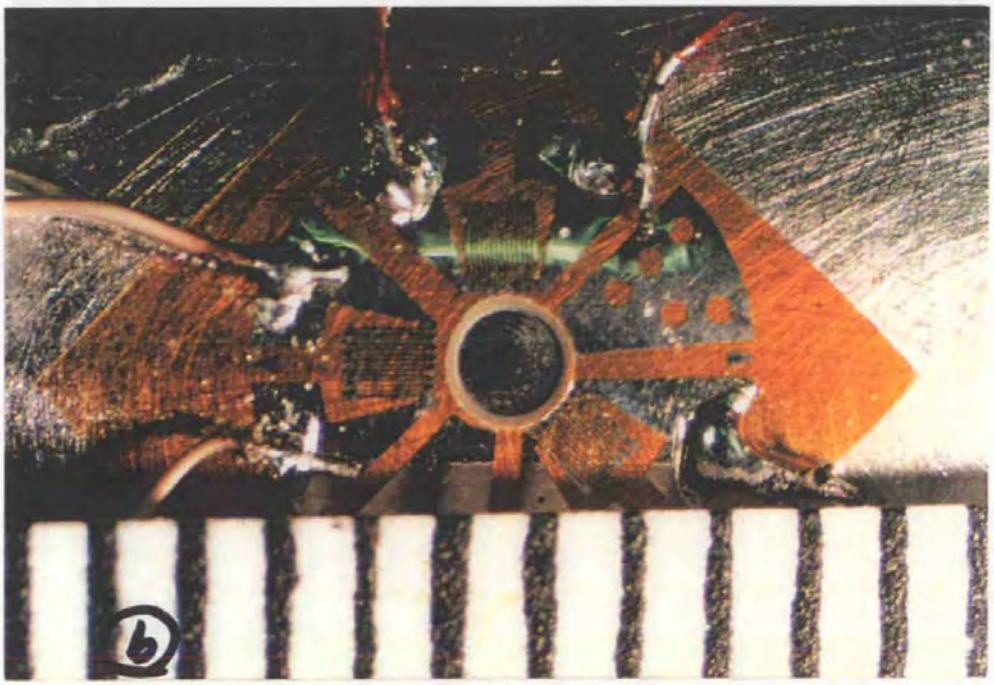

Figure 5.8: Top view of drilled hole .

5.2 MEASURED STRAIN DATA

5.2.1 Results

The table below contains all the recorded data as recorded during the drilling of the holes in the processed samples. It also reflects the hole depth and diameter at each increment.

Manufacturing Process		Quench	Tempered	HotScrag	Shot Peen	Painted	LoadTest
Sample ID		1	2	3	4	5	6
Residual Strain Data ($x10^{-6}$)	A	-331	-21.5	-25	611	549	466
	B	-360	-39.5	-13	665	570	538
	C	-344.5	-36.5	-36	647	551	493
	Depth(mm)	0.609	.495	0.533	0.533	0.546	0.508
	Diam.(mm)	1.168	1.066	1.041	1.023	1.041	1.054
	A	-286	-27	-35	580	539	684
	B	-397	-44	-16	704	507	766
	C	-346	-43	-32	507	474	940
	Depth(mm)	0.965	0.83	0.91	0.787	0.81	0.787
	Diam.(mm)	1.155	1.066	1.041	0.99	1.041	1.016
	A	-330	-42	—	679	786	565
	B	-350	-49	—	796	825	649
	C	-343	-47	—	676	851	627
	Depth(mm)	1.016	1.016	—	0.914	0.939	0.939
	Diam.(mm)	1.155	1.149		1.016	1.066	1.079
	A	—	—				755
	B	—	—				846
	C	—	—				1014
	Depth(mm)	1.016	—				1.066
	Diam.(mm)						1.079

Table 5.2: Measured strain data for processed samples at various depths.

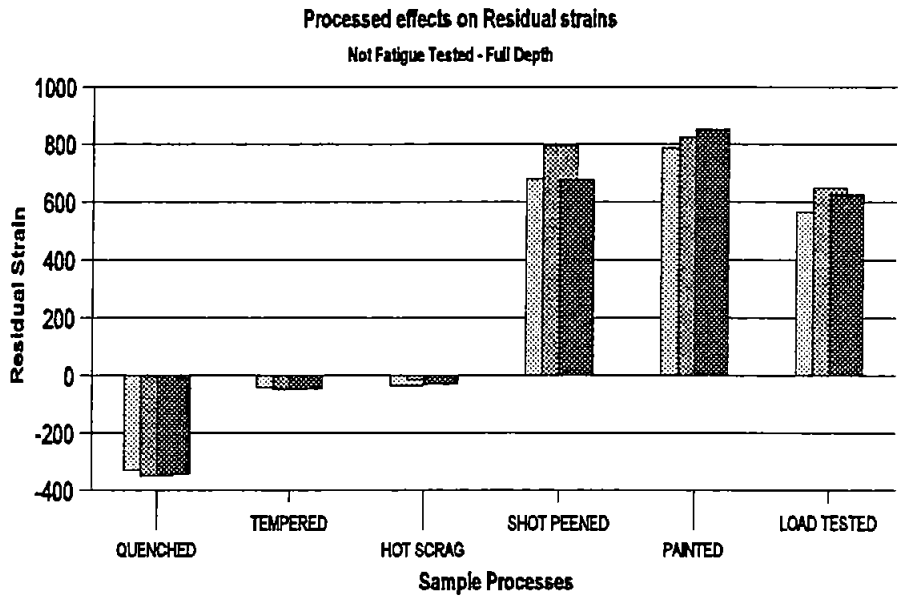

Figure 5.9: Graphical representation of measured strain values for 55Cr3 processed samples.

5.2.2 Sources of error in hole drilling

Possible sources of error when applying the hole drilling method for the determination of the depth distribution of residual stresses can be attributed to a number of sources. These possible sources can be divided into three main categories namely errors due to the drilling technique, boundary conditions and stress state.

- Drilling technique

  Introducing of residual stresses during the drilling process. Deviation from the ideal blind hole shape. Hole eccentricity and errors with hole depth and diameter measurement.

- Boundary conditions

  This is influenced by the location of the measuring grid and distance between adjacent measuring points. The shape of the components can also influence the magnitude of errors.

- Stress state

The presence of multi-axial stress states and stress gradients play a role in possible occurring errors. This also influences strain gauge orientation with regard to principal axes of stress.

Considering all of the above as possible contributions to error in measurement it become very difficult to quantify the magnitude of errors that occur during this research. Errors due to the hole drilling technique have been well researched by ASTM[17] and are documented to be in the range of ±14 MPa. Considering the stress state and boundary conditions of the spring steel sample as well as that the measurable depth range correspond to approximately half the hole diameter the accuracy of these measurements are estimated to be in the range of ±20 MPa to ±30 MPa.

5.3 CALCULATION OF RESIDUAL STRESSES MEASURED FROM STRAIN DATA

Let: Do = hole diameter

D = gauge circle diameter

Z = depth of hole

E = Youngs' modulus

ā, b = data reduction coefficients

Ā, B = geometric constants

α = angle from first principle strain from first strain gauge

$\varepsilon_1, \varepsilon_2, \varepsilon_3$ = relieved strains

$\sigma_{max}, \sigma_{min}$ = maximum/minimum principal stresses

The following formulae were used[31]:

All calculations were done according to the method set out in Chapter 4. The constants a and b were determined according to ASTM E837-94a. All measured strains are tabulated in Table 5.3 with the calculated stresses.

$$A = \frac{1+\nu}{2E} \cdot a$$

$$B = \frac{1}{2E} \cdot b$$

$$\sigma_{max/min} = \frac{\varepsilon_1 + \varepsilon_3}{4A} \pm \frac{\sqrt{(\varepsilon_3 - \varepsilon_1)^2 + (\varepsilon_3 + \varepsilon_1 - 2\varepsilon_2)^2}}{4B}$$

$$\tan 2\alpha = \frac{\varepsilon_1 - 2\varepsilon_2 + \varepsilon_3}{\varepsilon_3 - \varepsilon_1}$$

Manufacturing process : Quench									
Dia (mm)		Depth		Measured Strain με			α	Uniform Stress (x10e6)	
D_o	D_o/D	Z	Z/D	ε1	ε2	ε3		σ_1	σ_2
1.168	0.456	0.609	0.238	-331	-360	-344.5	-36.6	228	211
1.155	0.451	0.965	0.377	-286	-397	-346	-34.84	246	182
1.155	0.451	1.016	0.397	-330	-350	-343	-32.14	233	222
Manufacturing process : Before hot scrag (tempered)									
1.066	0.416	0.495	0.193	-21.5	-39.5	-36.5	-27.23	27.5	17.0
1.066	0.416	0.83	0.324	-27	-44	-43	-24.18	31.8	21.9
1.149	0.449	1.016	0.397	-42	-49	-47	-30.47	32.0	28.2
Manufacturing process : After hot scrag									
1.041	0.407	0.533	0.208	-25	-13	-36	-36.27	32.3	16.7
1.041	0.407	0.91	0.356	-35	-16	-32	-42.55	34.4	19.4
Manufacturing process : Shot peen									
1.023	0.340	0.533	0.208	611	665	647	-31.71	-511	-546
0.99	0.387	0.787	0.307	580	704	507	-38.59	-401	-553
1.02	0.397	0.914	0.357	679	796	676	-44.63	-517	-622
Manufacturing process : Before load test									
1.04	0.407	0.546	0.213	549	570	551	-43.56	-433	-450
1.04	0.407	0.81	0.316	539	507	474	-44.07	-393	-420
1.07	0.416	0.939	0.367	786	825	851	-5 .07	-615	-642
Manufacturing process : After load test									
1.054	0.412	0.508	0.198	466	538	493	-38.50	-359	-410
1.016	0.397	0.787	0.307	684	766	940	9.88	-622	-743
1.079	0.422	0.939	0.367	565	649	627	-29.84	-432	-483
1.079	0.422	1.066	0.416	660	747	820	-2.50	-535	-601
(1+v) / (2E)			E (GPa)				ν	D (mm)	
3.13e-12			206				0.29	2.56	

Table 5.3: Strain and stress results for 55Cr 3 processed samples.

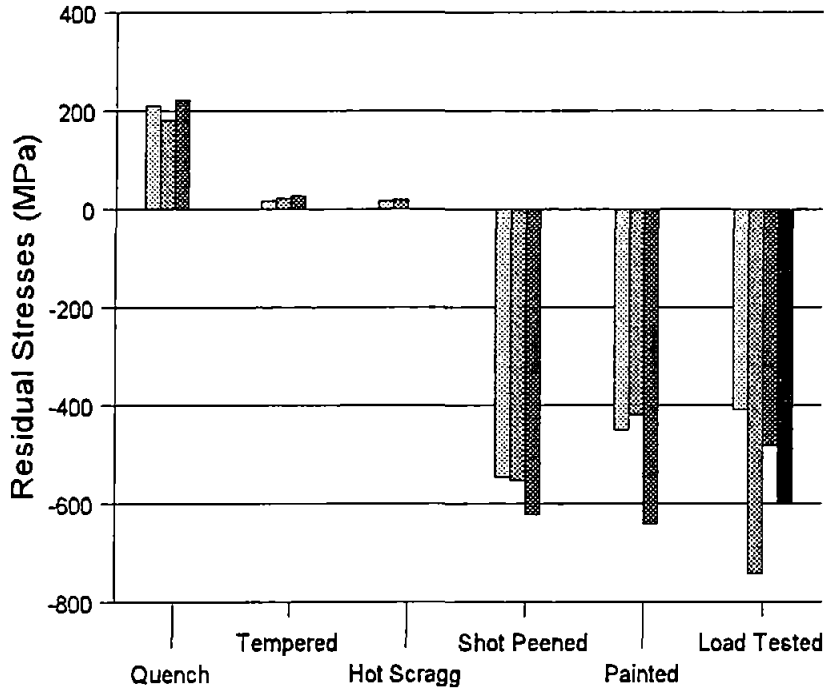

Figure 5.10: Process effects on principal residual stresses at different hole depth as indicated in Table 5.3.

5.4 RELATION BETWEEN PROCESS EFFECTS AND RESIDUAL STRESSES

5.4.1 Quench

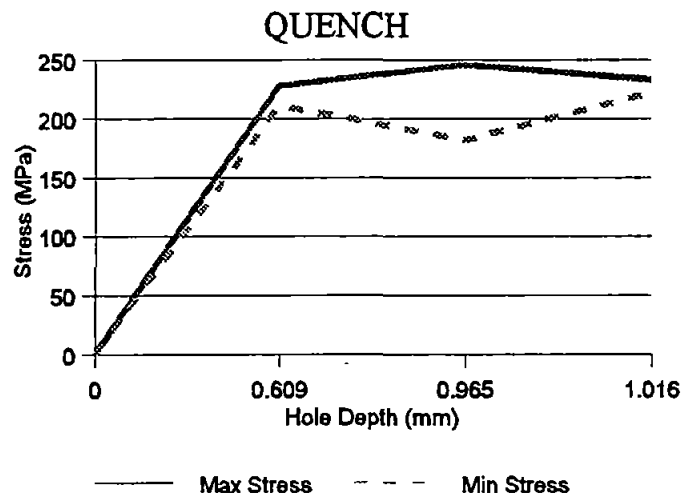

Figure 5.11:
Magnitude and nature of the residual stress distribution in a quenched sample of 55Cr3 steel.

Consider the residual stress measurement shown graphically in Figure 5.11 of a quenched sample. From the graph it is clear that the surface residual stress in the quenched samples are of a tensile nature. The hot coiled sample is quenched in an oil bath with a temperature of approximately 60° C; this will result in a temperature gradient as the surface is cooled more rapidly then the inside as well as a phase transformation due to the austenite changing to martensite.

The process by which tensile surface residual stresses are produced in the quenched sample can be explained as follows: The two major factors inducing tensile residual stresses are, the temperature gradient that exist during cooling and the transformation from austenite (f.c.c.), a more dense structure to martensite (b.c.c.), a less dense structure. It is well known that the expansion occurring during martensite formation could cause a volume increase of ± 4,6% [4] in steels. The cooling of the quenched spring can be divided into three stages namely, first the surface cools rapidly to the martensite start temperature, while the centre cools very little. During the second stage the surface will cool from the martensite start temperature through to the martensite finish temperature to reach the cooling medium temperature. At the same time the centre will now start entering the martensite start temperature. The last stage of the cooling primarily takes place in the core material as this will now cool down past the martensite finish temperature to reach cooling medium temperature.

Since the core cooling rate exceeds the critical cooling rate of the material, the part will be fully martensite. The first mechanism of inducing residual stress occurs due to the rapid cooling of the surface which will cause a temperature gradient to exist between surface and core. The surface wanting to cool faster than the inside but because the surface and inside are attached to each other the core will prevent the surface from contracting as much as it should, placing the surface in tension and the core in compression. This is clearly illustrated in Figure 5.12 as well as the sharp drop in stress at the junction of inside and outside layers. The second

mechanism for introducing residual stress occurs when the surface reaches the martensite start temperature. The austenite now transfers to martensite which causes an expansion in the surface. However, the core material is still undergoing normal contraction due to the cooling. The contraction of the core will prevent the surface from expanding as much as it should under martensite transformation, causing the surface now to be in compression, while the centre is in tension. The last mechanism that will have an influence on the nature of the residual stress takes place during the third stage of cooling. The surface will reach a hard, brittle martensite structure at room temperature, while the core starts undergoing martensite transformation. This expansion will transfer to the hard surface placing it in tension while the surface again will restrict the expansion of the core placing it in compression.

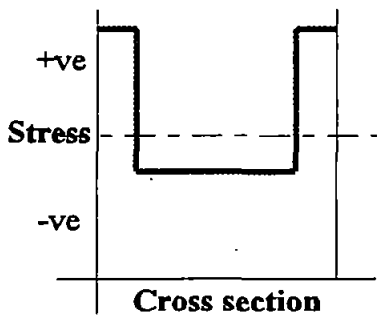

Figure 5.12:
Schematic of ideal residual stress distribution due to temperature gradient.

The presence of high residual stresses close to the surface can therefore be attributed to, firstly the temperature gradient where the surface is prevented from contracting as much as it should and secondly to the fact that the outer surface has reached a hard brittle state while the core is still expanding[4] under martensite transformation. It will be shown later in Figure 5.20 how the hardness for each manufacturing process varies with depth.

5.4.2 Tempering

From Figure 5.13 it is evident that the surface residual stresses have been reduced considerably by the tempering process. This is in line with the heat treatment rule that parts should be

tempered immediately after hardening to minimize stresses which could lead to crack formations[4,6]. The tempering process will give the surface martensite a degree of ductility before the centre transforms, reducing the stress gradient, therefore reducing the surface residual stresses.

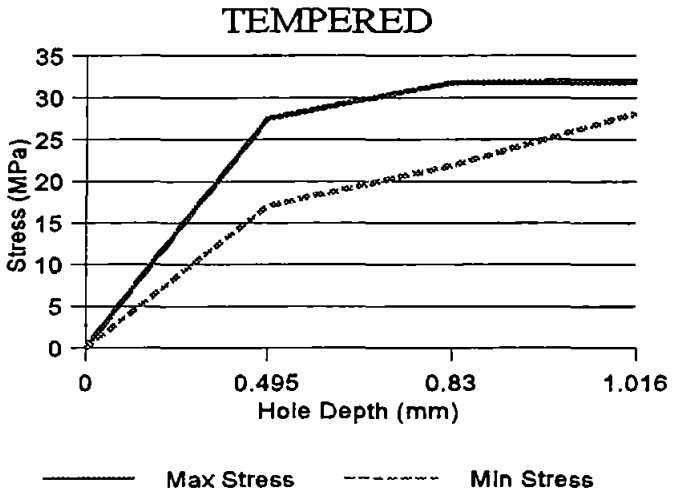

Figure 5.13:
Magnitude and nature of the residual stress distribution in a tempered sample of 55Cr3 steel.

If the residual stresses of the tempered sample in Figure 5.13 are compared to that of the quenched sample, it is clear that this was the result. This drop in residual stresses or increase in ductility is also highlighted in Figure 5.20 as a decrease in the micro hardness values. The tempering process will produce a tempered martensite structure; this martensite will be formed at nearly the same time throughout the piece. Tempering minimizes surface residual stresses and greatly reduces the danger of distortion and cracking[4]. The heat treatment is completed by tempering of the martensite to the desired grain size and hardness which will leave a very uniformed and stable material structure.

5.4.3 Hot scragging

Figure 5.14 shows the results of residual stresses after the hot scragging process. There is a slight reduction of the surface residual stresses compared to that of the tempered sample. When the residual stresses of the load tested operation, which could be considered as a cold

scragging.

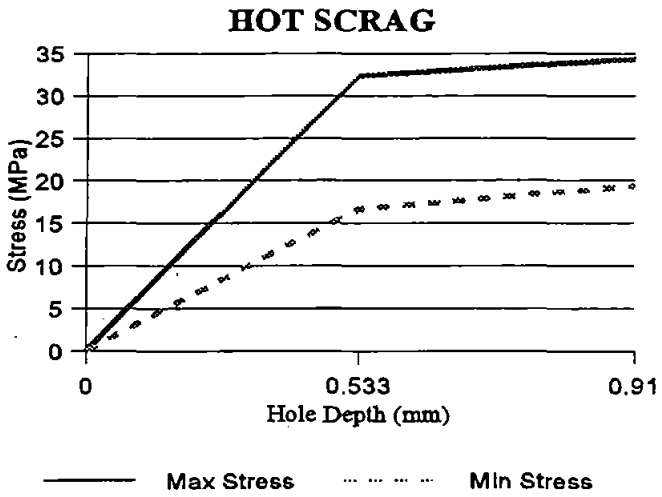

Figure 5.14:
Magnitude and nature of the residual stress distribution in a hot scragged sample of 55Cr3 steel.

process, are compared to the shot peen process, it can be seen that the change in surface residual stresses, due to that procedure, is also very low; almost of negligible change. The scragging process is used to obtain a higher elastic limit and hence a greater load capacity for 55Cr3 helical coil springs as was indicated in Chapter 3. The sample before the preset process was of greater length than the desired free length; this allowed for the compressing of the spring beyond its elastic limit during scragging[2]. It is clear that residual stresses are induced during this process but from the results it is obvious that these stresses are not induced in or close to the surface. The effect of residual stresses during presetting can be better explained by considering the diagrams in Figure 5.15. Figure 5.15(a) shows the plastic deformation that

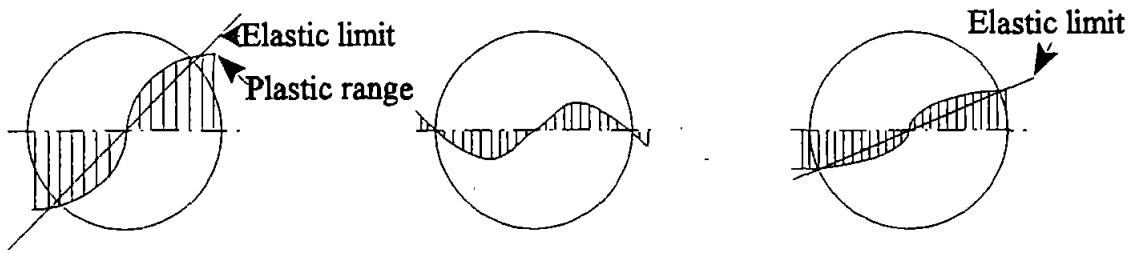

(a) During scrag (b) Residual stresses (c) Loaded after scrag

Figure 5.15: Schematic representation of residual stresses induced during scragging and the effect on re-loading after scragging.

takes place during presetting. The broken line indicates the elastic limit, while the solid line shows the maximum load stress distribution during preset loading. In (b) the residual stress pattern is revealed after the preset load has been removed. On reloading the spring to its normal working load the residual stresses will counteract load and the result is a more uniformed distributed field. This allows for the use of higher design stresses during loading. In the case of the cold scrag process it was evident that it had a major detrimental influence on the fatigue life of the component as was discussed in Chapter 3.

5.4.4 Shot peening

The fatigue strengthening effects of shot peening are well known and documented[16,41,42]. This was first discovered by General Motor Corporations, Buick Motor Division in 1929 when it was noted that the fatigue properties of valve springs greatly improved after being grit blasted to remove scale.

To obtain the full benefit of shot peening, several variables must be properly selected and controlled. This includes shot size, shape, velocity and duration of peening. The process itself is whereby small particles or steel shot are bombarded at a component surface at high velocity from a nozzle or wheel. It is a very versatile process being applicable to virtually all metals and shapes. Shot peening produces a lightly hammered surface which tends to reduce the diameter slightly at the same time increases the area of exposed skin due to the dimples.

Consider the results in Figure 5.16 of the residual stress distribution with depth for a shot peened surface of a 55Cr3 coil spring. Typical residual stresses from the shot peening process could be of the order of half the material yield strength, in the case of the 55Cr3 sample tested it varied from 34% to 53%. The maximum residual stresses due to shot peening always occur slightly sub-surface[16].

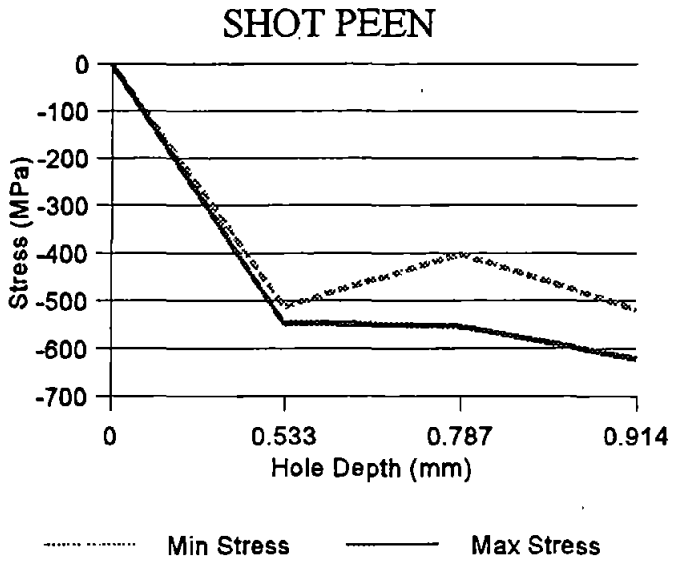

Figure 5.16:
Magnitude and nature of the residual stress distribution in a shot peened sample of 55Cr3 steel.

For material with a tensile strength between 25 MPa and 650 Mpa the maximum residual stress that can be induced due to shot peening can be estimated by the following equation:[16]

$$\sigma_m = 500 + (0.2 \times \text{tensile strength}).$$

For lower strength steels and alloys σ_m will initially reach the yield stress or 0,1% proof stress but will fade under cyclic loading.

The penetration of shot into the surface of material usually varies between hundreds of thousandths and a few thousandths of a millimetre. The smaller shot sizes are used to reach small radii, while the larger shot is used to produce relatively deep penetration of the residual compressive stress nature. It is important to realise that further fatigue strengthening can be obtained by removing just enough surface material to leave a smoother surface. One can also make use of "strain peening" which is the bombardment of the surface while applying external tensile loads. This will result in residual stresses approaching the full yield strength of the material and not only half as was the case earlier. Strain peening is advised only for

unidirectional loading, as the high residual stress is destroyed by relatively low applied compression stresses.

Shot peening is widely used in the manufacturing of springs, gears, shafts, structured tubing, connecting rods, etc. Machined parts made of very high strength of above 650 MPa or 400 Bhn (42 Rockwell C) stand to benefit the most from shot peening[4,41]. With shot peening, endurance strength increases with hardness. See Figure 5.20 for relation of micro-hardness values.

5.4.5 Painted

The painted samples revealed a compressive surface residual stress of similar magnitude as that of the shot peened sample as illustrated in Figure 5.17. The increase in fatigue life was of a very small magnitude and could be considered as a negligible.

There is no influence of this process on the surface residual stresses and are mainly done for protecting the shot peened component from corrosion. Corrosion can have major effects on

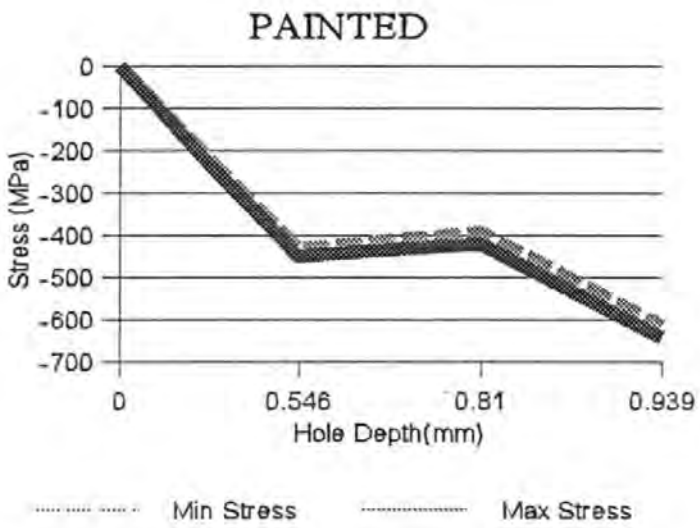

Figure 5.17:
Magnitude and nature of the residual stress distribution in a painted sample of 55Cr3 steel.

the fatigue performance of springs, it is well known that unprotected coil springs will only endure 10 to 25 per cent of the endurance limit of a corrosion protected spring[2]. On analysing and comparing the residual stresses in the painted sample to that of the shot peened sample, it reveals a slight increase. It was thought that this could be due to the painting process whereby the sample are baked at a temperature of 180°C and then moved in to the open air, which could be as low as 6°C, as these sample were manufactured during winter. This will cause a type of surface heat treatment effect with gradient which is known for inducing compressive residual stresses. After closer investigation it was decided that the change in residual stress was too small to substantiate the above theory and that it was very unlikely to take place with such a small temperature gradient.

5.4.6 Load tested

The load test procedure can be considered as a cold scrag process. These samples reveal on

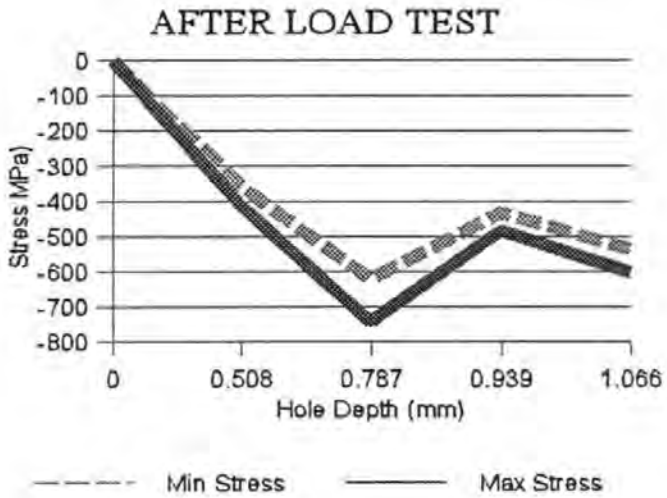

Figure 5.18:
Magnitude and nature of the residual stress distribution in a load tested sample of 55Cr3 steel.

average a very slight decrease in compressive residual stress but a substantial drop in fatigue resistance. This drop in fatigue resistance cannot be explained by the slight drop in residual stresses, but it is thought that the cold scrag set in a certain amount of plastic deformation

which adversely affects the fatigue life of the test sample. This is a phenomenon which needs further investigation. The same principle as in the case of the hot scragged samples is applicable to the load tested samples.

5.5 FADING OF RESIDUAL STRESSES IN 55Cr3 SPRING STEEL

Consider the following example which illustrates the existence of residual stresses in a component as long as heat or external loading does not remove them by yielding. This was cited by Almon and Black and published in their book "Residual Stress and Fatigue in Metals", 1963[11].

The Liberty Bell which was cast in 1753 had tensile residual stresses in the outer surface, the reason being that the casting must have cooled most rapidly from the inside surface. After 75 years in service the bell cracked, probably as a result of fatigue from the superimposed vibratory stresses present when the bell was rung; corrosion could also have played a roll. Interesting is the fact that the width of the original crack has subsequently increased further although the bell has not been in service. Alman and Black concluded[11]:

"The extension of the crack since its mutilation and without vibration is proof that residual stresses are still present in the bell."

The reduction of residual stresses in a component as a result of repeated stressing is known as fading of residual stresses[1,11]. This phenomenon can cause failure which then relates the failure directly to residual stresses. It can be said that a stressed grain of a metal has no way of distinguishing between loadings from its neighbouring grains due to residual stresses and/or due to external loads. Figure 5.19 shows a graph which compares the residual strain in 55Cr3 spring steel samples from before and after fatigue testing.

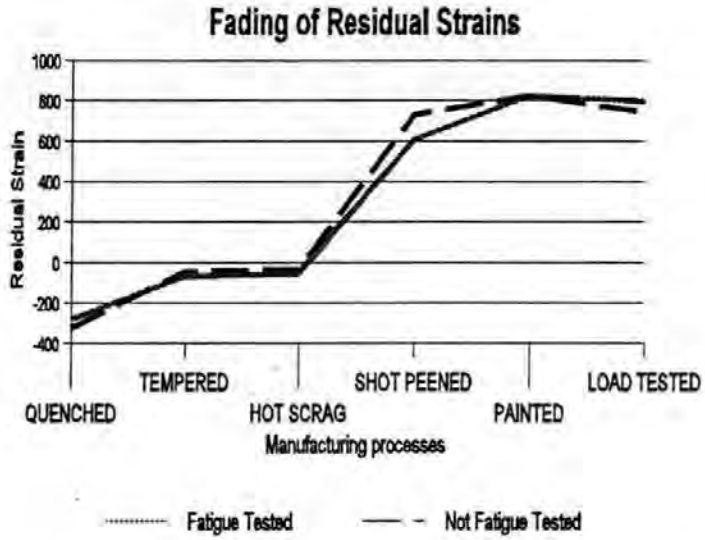

Figure 5.19:
Fading of residual strains at full depth(1 mm) in 55Cr3 processed samples due to fatigue cycling.

This reveals that in hard steels (e.g. 55Cr3) the residual stresses do not fade easily because of repeated cyclic loading. The reason for this must be because of their relatively high yield strength compared to their ultimate fatigue strengths. Very little influence is exercised by the fading of residual stresses in 55Cr3 spring steel on fatigue life or failures as the fading is negligible.

5.6 INFLUENCE OF RESIDUAL STRESSES ON FRACTURE PLANE OF 55Cr3 PROCESSED SAMPLES

The biaxial state of surface residual stresses, superimposed on stresses due to the external loads can alter the plane of fatigue fracture. With zero residual stresses the fracture plane will be more perpendicular to the specimen length, while in the presence of large tensile biaxial residual stress system, it will exhibit a more diagonal fracture when a bending load is applied[1,43]. This torsional type of fracture which was present in most of the quenched and tempered samples, can therefore, be attributed to a certain extent to surface-tangential residual stress in the samples.

A large number of failures is caused by residual stresses of which the following are the more common ones:

- Stress corrosion cracking can be directly related to residual stresses. This occurs in metals which are subjected to corrosive environments while stressed. The crack will initiate and appear in the surface layers.
- Residual stresses due to assembly is a source of potential failure where residual stresses in systems are induced by the assembly of components with an initial lack of fit. These failures could be caused by specifying shrinking or force fit of compound cylinders by the design without considering the influence of induced residual stresses on the assembly.
- In contact loading in gears and bearings, consideration should be given to the relationship between the distribution of residual stress with depth and the depth at which the peak alternate shear stress occurs under the contact load. If this is overlooked, the possibility of the peak residual stress overlapping with the peak shear stress exists which could cause crack initiation below the surface which will lead to the failure of the component.

However, when failure consists of ductile yielding, several questions may arise like:

- How much permanent distortion is associated with a given overload?
- How much yielding can a part experience before it is unsuitable for its intended service loads?
- If the part can still be used, what residual stresses are present?
- What will be the effect of influences of the residual stresses on the service performance of the part?
- What loads are needed to restore the part to its original shape?
- After the part has been restored, what residual stresses will remain, and what influence

will they have on the service performance of the part?

5.7 SUMMARY

As was explained in early chapters, we could see that in some cases residual stresses can be used to the advantage of the fatigue life of components. Process methods have major influences on the properties of 55Cr3 spring steel including the residual stresses and micro hardness values as illustrated in Figure 5.20. However no trend or pattern exists between residual stresses in the surface of the different samples and the micro hardness values. It would seem that very high hardness values associate themselves with high tensile surface residual stresses. Although the micro hardness and residual stress values for the shot peened, painted

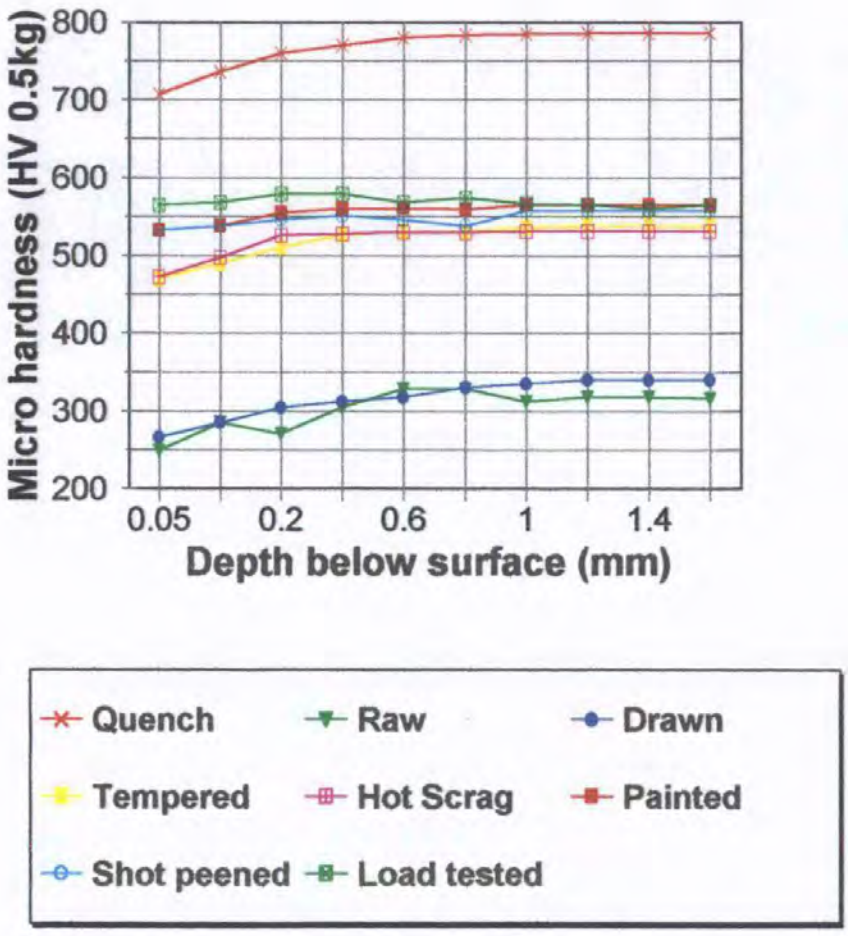

Figure 5.20:
Relation between micro hardness values and process effects on 55Cr3 spring steel.

and load tested sample were closely related, not much can be concluded as the hardness of the tempered and hot scragged samples were also in this range but their residual stresses were much smaller and of a different nature (tensile).

A very interesting relation was that of the residual stress and strain magnitudes as illustrated in Figure 5.21. Not important is the change of nature from a tensile strain to a compressive

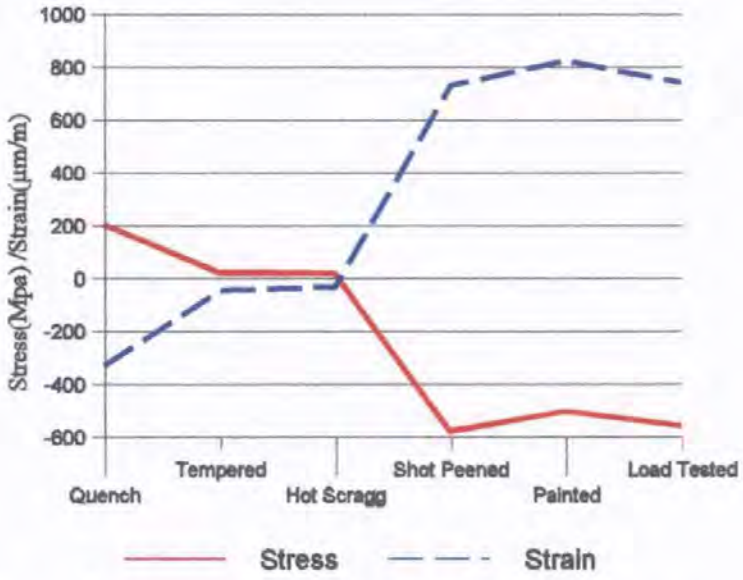

Figure 5.21:
The relation between residual stress and strain magnitudes for 55Cr3 spring steel samples withdrawn at different process stages.

stress and *vice versa* but the fact that the magnitudes were almost following a trend, the one just measured in micro strain and the other in mega pascal. On analysing this stress-strain trend it is discovered that in the first three processes a scale factor of -0.56 would produce the equivalent stress values from the strain data within a 12% error band which is well acceptable for residual values. The last three processes had a scale factor of 0.7 with an error band of 13%. This could lead to the conclusion that the residual stresses will be a mirror image of the strains values.

The air abrasive hole drilling method has proved to be an accurate method for determining surface residual stresses. The process has proved to be very effective on the very hard samples

for example the quench sample, which had a hardness of 61 Rockwell C. Typical problems encountered can be described as follows:

- Gauges had to be protected by a covering strip, as the abrasive nature of the over spray of aluminium oxide powder, could cause deterioration of the gauge which will influence strain reading.
- Alignment of the drilling device is critical and time consuming with the drilling of such small holes (0.9 mm to 1 mm in diameter).
- The strain amplifier must be well grounded or disconnected during drilling as a large build-up of static electricity can be experienced which could damage the amplifier cards during drilling. This-build up of static electricity is believed to be caused by the aluminium oxide moving with a high velocity.

Errors and uncertainties are always present to varying degrees in all measurement of physical variables. As a rule, their magnitudes are strongly dependent on the quality of the experimental techniques, as well as the equipment used. As was explained earlier in this chapter it is believed that the accuracy of residual stress values obtained during this research were in the range of ±20 MPa to ±30 MPa.

CHAPTER 6

PROCESS EFFECTS ON 55Cr3 SPRING STEEL TRANSFORMATIONS

INTRODUCTION

Micro structural analysis of metal can be divided into three categories, namely (i) crystal structure and distribution of phases, (ii) lattice defects and (iii) the relation between micro structural features and variation in chemical composition. The urge to understand the micro structure of metals and the structure sensitive properties has resulted in the development of more sophisticated metallographic techniques such as transmission microscopy.

Electron microscopes operate under high vacuum conditions. Preparation of samples for transmission electron microscope work requires extensive preparation to ensure a high image quality[44]. Imaging depends on a specimen that is thin enough for an electron beam to pass through as well as correct operation of specific image and magnifying lenses. Electron microscopy can be defined as the science and technology of using an electron beam to form magnified images of specimens. The principal advantage in using electrons is that they provide as much as a thousand fold increase in resolving power (detail to $\pm$ 0,2nm) compared optical microscopy. For this study it was attempted to examine interfaces, dislocations and diffraction patterns from the processed sample at a depth of 1mm below the surface.

6.1 INVESTIGATION INTO MICRO STRUCTURAL TRANSFORMATION OF 55Cr3 SPRING STEEL

6.1.1 Equipment (Transmission electron microscope)

The basic transmission electron microscope consists of an electron source and assembly of magnetic lenses arranged in a vertical column which is evacuated. The microscopist can control

a number of variables on the instrument to optimize the quality of the final image. At the top of the column is the electron source which consists of a filament assembly connected to a high voltage supply which range from 20 000 volts to 100 000 volts. The electron source produces a coherent parallel beam of electrons, which can be varied in diameter from about 1 mm to 50 mm at the specimen surface. This is done by means of the double condenser lens system.

The condenser lens system is used to control electron illumination on the specimen and viewing screen for such functions as viewing, focussing, and photography. The setting relation between the two condenser lenses affects the amount of illumination and image quality. The first condenser lens is a high power lens which can condense the 50 mm electron beam to as small as 1 mm, while the second condenser lens is a weaker variable lens controlling the beam size from 1 mm to 10 mm.

6.1.2 Sample preparation

6.1.2.1 Removal of specimen from bulk material

All samples for transmission electron microscopy require preparation of a high standard before analysis as the preparation can introduce microscopy features which can cause incorrect interpretations of the microstructure[45]. The first to consider is the final diameter and thickness of the sample that can be viewed. The standard support disk for a specimen is 3 mm in diameter and can take a specimen with thickness of approximately 0.2 mm.

The removal of the samples from the bulk material was done by using ECM/EDM (Spark Erosion) to machine a cylinder of 3 mm in diameter from a spring section as shown in Figure 6.1.

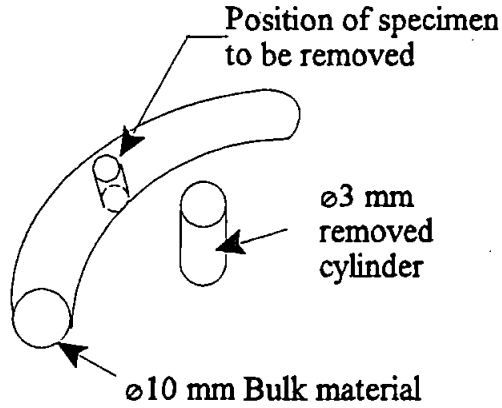

Figure 6.1: Removal of sample from bulk material.

The removed cylindrical sample is then sectioned perpendicular to its longitudinal axis into thin disks of 3 mm in diameter and ±0.5 mm thick. The parted-off disk can be thinned to the above requirement by grinding it on abrasive paper. The final finishing must be done on 1 000 grain paper. The parting off of the disks must be done carefully and they must not be too thin as the parting off could inflict damage on the specimen. If a diamond cutter is used, use the following suggested procedure:

1. Clamp a stop block 0.4 mm from the side of cut-off wheel.
2. Push the plain face of cylindrical sample against a stop block and clamp.
3. The metal between the stop block and disk can now be parted as a disk with a thickness of approximately 0.4 mm. The stop block also assists with the cooling of the disk and assures that the cut-off wheel is not bent.
4. The parted-off disk can now be ground down on abrasive paper to the desired thickness (<1 mm) and to a 1 000 grain size finish.
5. The specimen must be protected against oxidation or any fouling as it may cause the specimen not to be satisfactorily polished. The disk is now ready for final thinning and polishing.

6.1.2.2 Final thinning

This was done using a Tenupol-3 electrolytic thinning apparatus. The apparatus consists of a base plate with a polishing cell, a built-in infra-red detector system, a cooling coil and a pump system, all placed on top of a PVC reservoir for the electrolyte. The electrical parts are connected to a separate control and power supply unit through a single cable. It is used for electrolytic thinning of specimens for transmission electron microscopy and other methods of examination where the thickness of the specimen must correspond to or be smaller than the grain size of the material examined. Specimen of $\pm$ 0.3 mm thick was placed between two immersed jets. A pump system then pumps the electrolyte through the jets against the specimens. A direct current supply will establish an electric circuit through a cathode placed in the electrolyte and an anode connected to the specimen. When the circuit is closed, material is removed electrolytically from the specimen surface. This will result in forming a small hole in the centre part of the specimen of which the edge of the hole will have a v-shaped cross section. The hole is detected by an infra-red detector system, which automatically cuts off the process. By varying the photosensitivity the hole size can be changed.

As soon as the polishing is completed the sample holder is removed and opened in a small bath of ethanol. This batch must be kept ready as it has to be done immediately to neutralise the acid. It is not advisable to store specimens for long periods but this can be done under vacuum in a desiccator with silica gel.

If a sufficiently high quality polish is not obtained in electrolytic polishing, it will be necessary to alter the polishing conditions. There are four independent parameters, type of electrolyte, flow rate of electrolyte, temperature and electrical conditions. The type of electrolyte is highly important for the quality of the polishing. An unsuitable electrolyte will cause oxidized or

etched surfaces, pitting or one side polishing while the other side is black and oxidized. The proper flow rate to use is very difficult to determine as each material and electrolyte is different. If a current *versus* voltage curve is drawn the best polishing conditions will be found where the current is approximately constant with in a range of voltage.

For 55Cr3 spring steel, the following sample preparing variables were arrived at with acceptable final polishing results. This was done by trial and error changing variables selectively until the best results were achieved.

Electrolytic	:	5% Perchloric Acid 17% Glycerol 70% Ethanol 8% Butanol
Infrared setting	:	Just below maximum sensitivity. On the Tenupol-3 a setting of 8 was used.
Electrical supply	:	This was determined by plotting a graph of volts *versus* milliamps. Where the graph shows a flatter characteristic, it indicates the ideal electrical settings for achieving the best polishing of the specimen. For 55Cr3 samples, it showed that the best range was between 5 and 10 volts and 160 milliamps.
Flow rate	:	A low flow rate (2 on scale of 1-10) was used to try and prevent the jets from blowing a thin area off before cut off. This was arrived at after a number of specimens were finely polished but there was a lack of thin areas remaining to be looked at.
Time	:	The time from start to switch off varied but an average time for a small hole was approximately 18 seconds.

The above produced acceptable samples but is still a long way from ideal. More research will have to be done on the preparation of martensite samples to achieve the ideal polish parameters.

6.1.3 Image formation

Image formation using a magnetic material proved to be quite challenging. It seemed that the material was magnetised which caused the electron beam to be unstable and would move around causing fading or even in some cases total loss of the image. The image formation can shortly be described as follows:

The specimen fits in a holder that fits into the objective lens and enables the specimen to be tilted. The objective lens is the first magnified lens which makes it the most important and complex lens as any imperfections in this lens will be magnified further by the other lenses. The specimen is inserted into object plane of objective lens by means of a specimen rod through an air lock to preserve the high vacuum in the column. This operation can introduce contaminants from both specimen and specimen holder side which is reduced by allowing a copper braid to extend through the column to an external container of liquid nitrogen which keeps the metal cold to attract and hold contaminants.

Electrons pass through the thin specimen and interact with the specimen forming a number of signals which will generate the final image[46]. Various interactions occur between the primary electron beam and the atoms of the specimen to form the TEM image. The first image is from the electrons from the primary beam which pass through the specimen without any change. The second type is where these electrons interact with the nuclei of the atoms of the specimen and are elastically scattered. The third is where primary electrons interact with electrons from the atoms of the specimen and are inelastically scattered.

Electrons may also be absorbed into thick portions of the specimen or into areas of atoms with high atomic numbers. Very few electrons are prevented from passing through the specimen. Where too many electrons are absorbed into a small area it can result in distortion or even destruction of the sample due to heating[47]. Elastically scattered electrons contribute to both amplitude and diffraction contrast in an image whereas inelastic scattered electrons are more important in imaging of samples with low atomic numbers. They contribute to chromatic aberration because of energy loss and phase contrast.

The extent of electron scatter and interactions depend on mass thickness, the thickness, variation of thickness as well as the atomic number of various atoms making up the specimen[47]. This differential scattering between the transmitted and scattered electrons from a specific area of the sample results in the contrast necessary to form an image on the viewing screen. All these electrons are focussed in the back focal plane of the objective lens which acts as an electromagnetic converging lens which will form the diffraction patterns in this plane. An inverted image is formed in the first image plane then passed through the diffraction -, intermediate and projector lens which is responsible for either magnification of the image or diffraction pattern. If the diffraction lens is focussed on the back focal plane of the objective lens a diffraction pattern is magnified and displayed, whereas if the first image is imaged by the diffraction lens then a magnified image of the specimen is produced. Magnifications of 10^2 to 10^6 times can be produced.

6.1.4 Transformations in 55Cr3 spring steel

Martensitic transformation due to process effects in the surface 55Cr3 coil springs was done in an attempt to confirm the influence of the manufacturing processes on the deformation of the material and to relate this to the fatigue properties and the residual stresses in the material. All the samples were removed in an area of 1mm below the surface of the material. Only samples

from the quench, tempered, hot scrag and shot peened processes have been considered.

A microstructure transformation involves the changing of a crystalline structure for example from a face centre cubic structure to a body centre cubic structure[48]. It has been observed that ordered phases will transform into other ordered phases martensitically with a change in structure but with no evidence that diffusion had occurred in the martensitic transformations. The transformation in 55Cr3 steel, due to the process effect can also be viewed from a surface dislocation or slip approach. From the Burgers vectors of the dislocations, it can be determined whether the transformations in homogeneity is twinning[48]. The movement of dislocations due to process effects can result in simple shear deformations. This can account for the various habit planes and other crystallography features in the 55Cr3 processed samples. Consider the micrographs in Plates 6.1 to 6.4 for the influence of some of the manufacturing processes of 55Cr3 coil springs. Interpretation of these plates is very difficult and needs to be researched thoroughly. There is a definite change in the appearance of the diffraction patterns and microstructure of the different samples. In the quenched sample the structure appears to be a spread out mass with some indication of twinning or martensite lathes. The tempered samples reveal a change to more evenly distributed features. This is also evident in the hot scrag and shot peened sample with the exception that the structure appears more densely packed.

Each plate shows the diffraction pattern obtained using the selected area technique from a very thin portion of the 55Cr3 samples under consideration. The diffraction pattern consist of a series of well defined maxima where the most intense beam is the directly transmitted beam[46]. The other maxima are defining the direction in which strong diffracted rays left the crystal structure. It can be assumed that the planes giving rise to strong maxima are approximately parallel to the electron beam direction. Ultimately the appearance of the diffraction pattern depends on the crystal structure and the grain orientation to the electron beam. The diffraction

pattern can change from grain to grain.

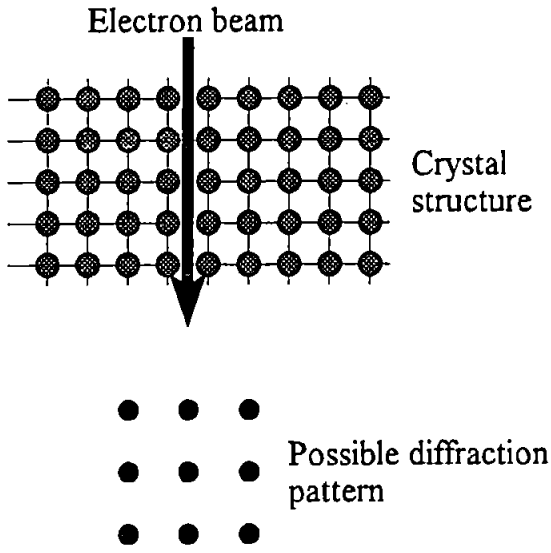

Figure 6.2: Diffraction pattern of a perfect crystal.

If the diffraction patterns are studied carefully it is clear that from the quench tempered samples more asterism is visible than in the quenched samples. This could be due to more lattice distortion. Considering a perfect undamaged crystal the electron beam will pass through forming

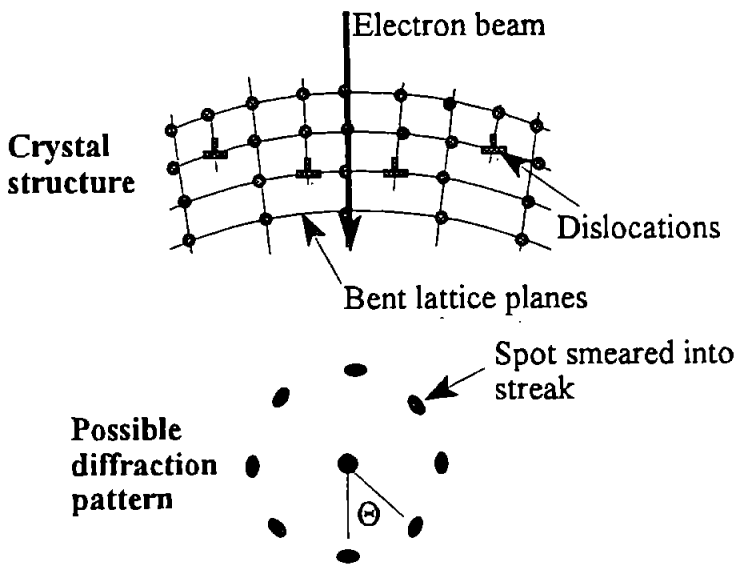

Figure 6.3: Diffraction pattern of damage crystal.

a more orderly pattern as shown in Figure 6.2.

If the crystal structure contains a certain amount of similar dislocations the lattice planes will be bent over to reverse automatic spacing. If an electron beam now passes through the crystal the spots are now smeared into streaks, as shown in Figure 6.3.

The amount of bending in the lattice planes are proportional to angle θ . Therefore this is an indication of the amount of internal stress and it could be said that the dislocation density is representative of these internal stresses.

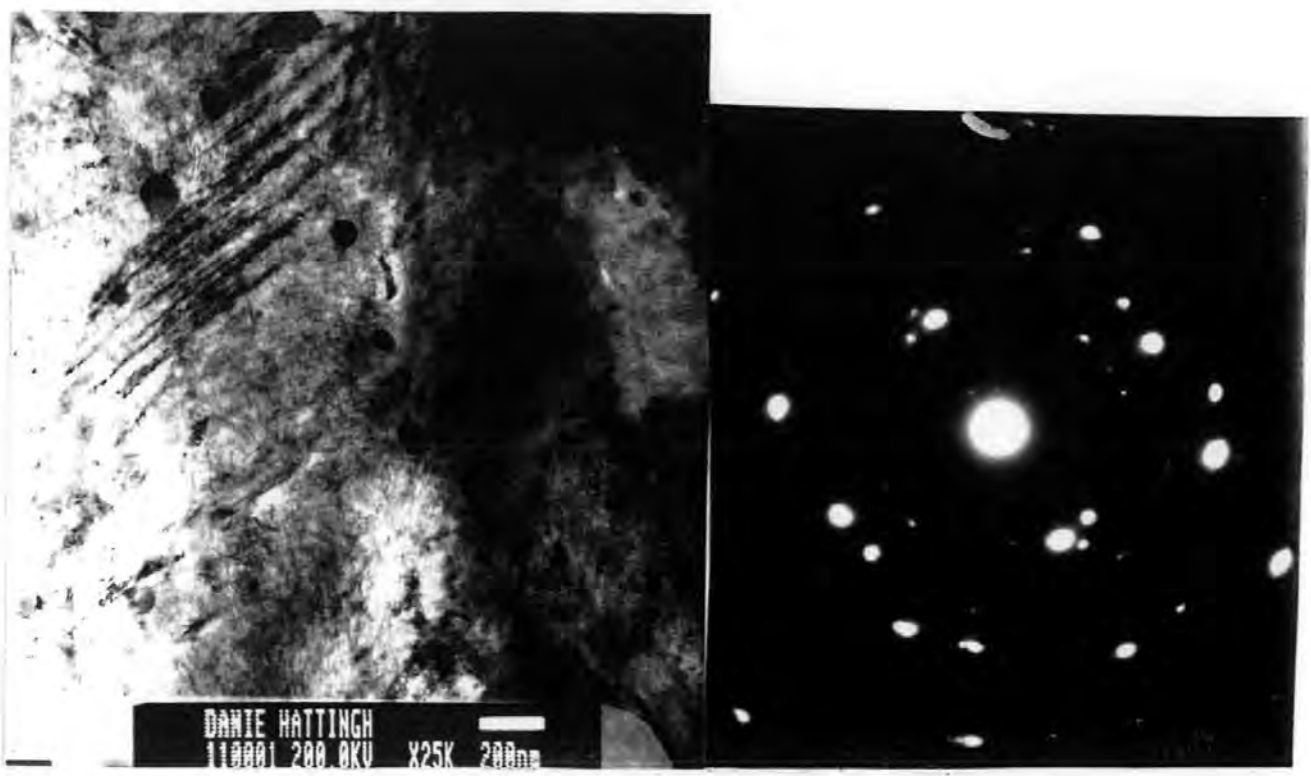

Plate 6.1:
Transmission electron micro graphs illustrating crystalline features and the diffraction patter quenched sample of 55Cr3 spring steel. (x25000-1mm below surface)

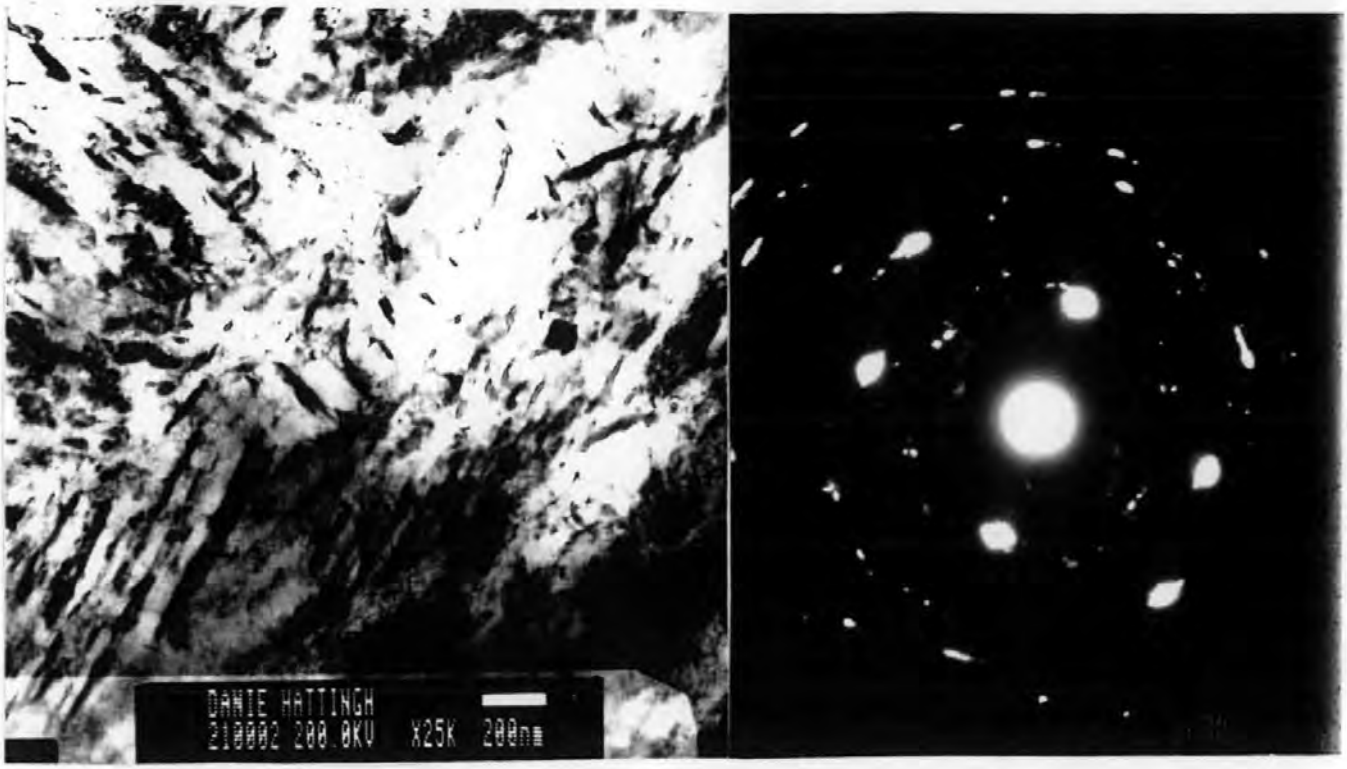

Plate 6.2:
Transmission electron micro graphs illustrating crystalline features and the diffraction patter quenched tempered sample of 55Cr3 spring steel. (x25000-1mm below surface)

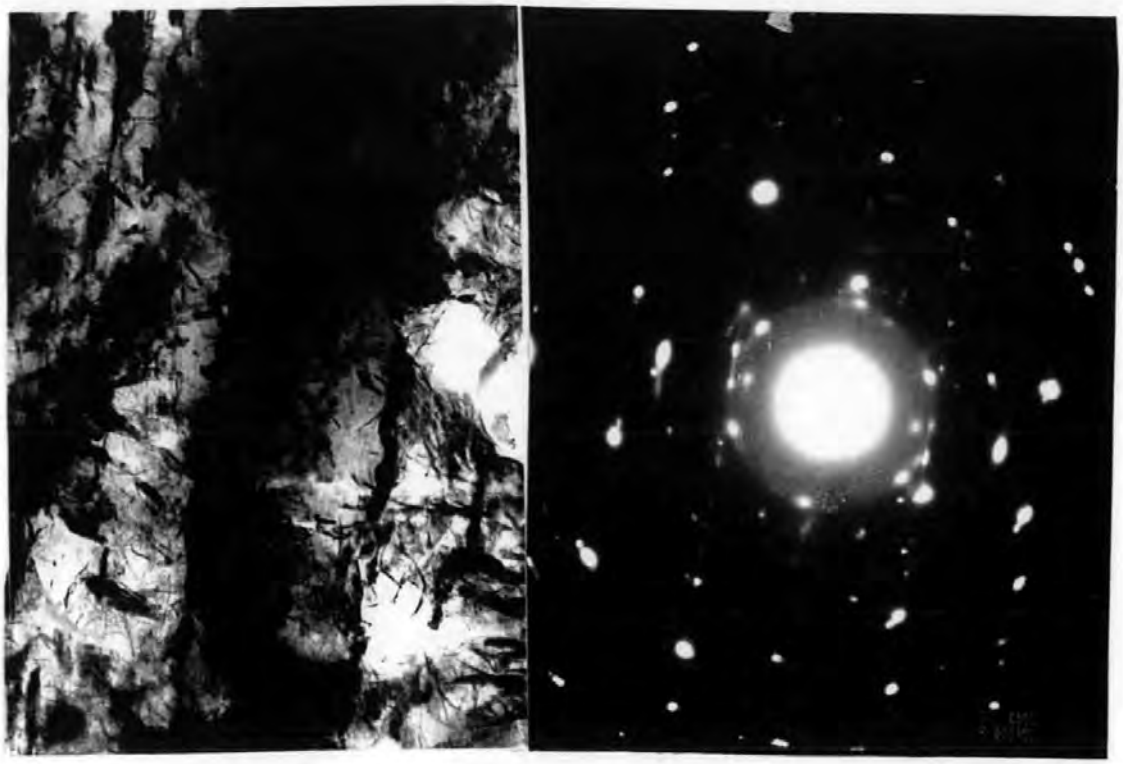

Plate 6.3:
Transmission electron micro graphs illustrating crystalline features and the diffraction pattern of scragged sample of 55Cr3 spring steel. (x25000-1mm below surface)

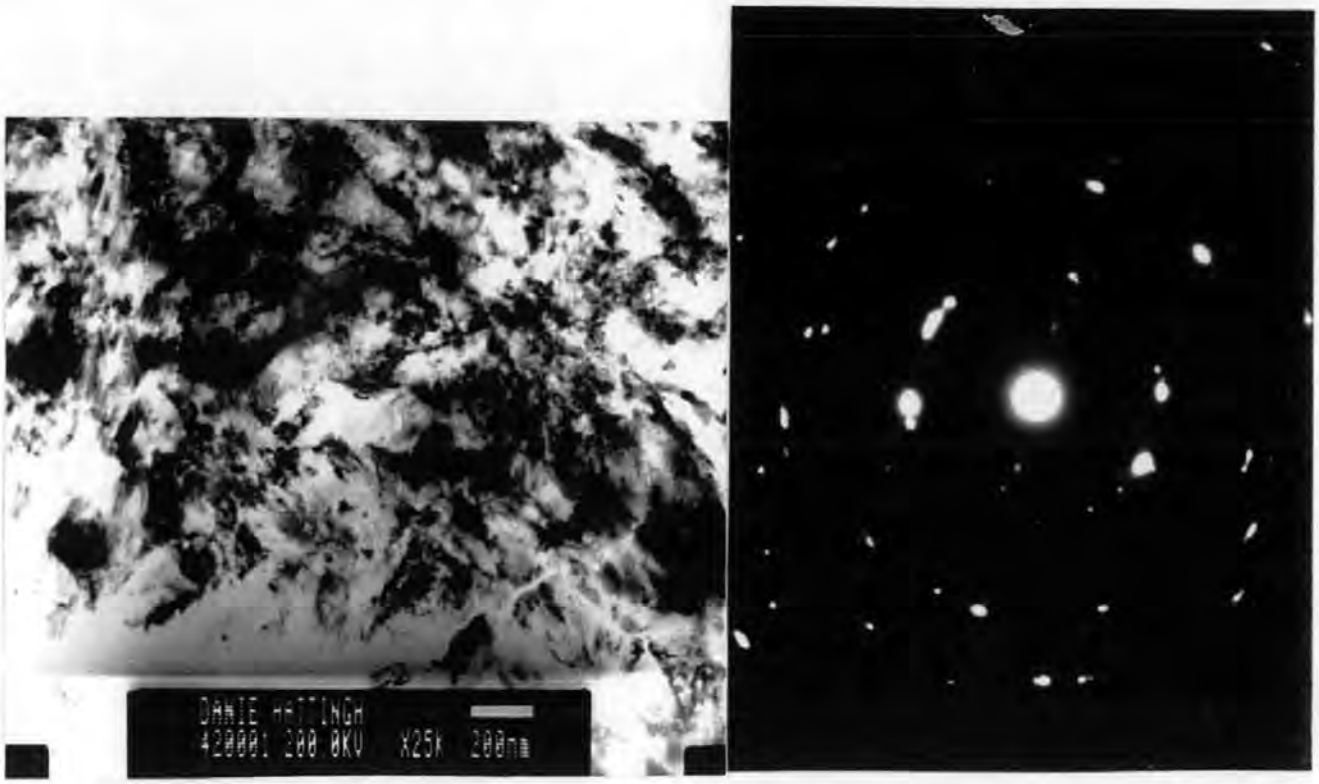

Plate 6.4:
Transmission electron micro graphs illustrating crystalline features and the diffraction pattern of a peened sample of 55Cr3 spring steel. (x25000-1mm below surface)

6.2 SUMMARY

This attempt at explaining the influence of the manufacturing process on the crystalline transformation in 55Cr3 spring steel cannot be considered successful. Valuable experience has been gained on the ability and possible scope for transmission electron microscopy work on materials This is a tool that can reveal the detailed microstructure within the grains of metals, such as dislocation density and distribution, twinning, martensitic shears, etc. The future for development of super material lies locked up in the crystalline structure of metals and will only really be solved when this can be interpreted and related to fatigue and other preparation of manufactured components. This study has definitely contributed to the better understanding of the preparation of and investigation of magnetic material samples used in transmission electron microscopy.

CHAPTER 7

FATIGUE ANALYSIS OF SPRING STEEL (DISCUSSION)

INTRODUCTION

World-wide trends in legislation and environmental considerations are demanding increasingly higher fuel economy from road vehicles. The manufacturing world is responding to this legislation through an overall reduction in component weight, thus requiring more efficient components that can operate under increased working stress.

The production of a suspension spring working at high stress levels yields a benefit in fuel economy since the component is not only lighter but can be more compact, thus aiding the reduction of vehicle frontal area and drag. There are two major properties of spring materials which govern the useful life of the spring component and which must be carefully assessed in the development of any new design or manufacturing process, these being sag (or relaxation) resistance and resistance to fatigue and their relation to residual stresses which play an important role in spring components.

The understanding of the relationship between fatigue life, residual stresses and process effects in spring steel components are of cardinal importance before the manufacturing process can be optimised to produce coil springs for enhanced performance operating at increased stress levels.

These mechanisms were investigated in 55Cr3 automotive suspension springs by subjecting coil springs withdrawn from different stages of the manufacturing process to a series of tests. In this manner it has been ensured that all possible sources of fatigue initiation in this material

batch have been identified, including those not dominant in the finished component. The results are indicative that decreasing defect levels in the material and better utilisation of beneficial residual stresses would represent a valid method for enhancing the fatigue response.

7.1 POSITION AND REASON FOR FAILURE

The location of the fatigue fractures was very process-specific as indicated by Table 7.1.

Manufacturing Process	Position of fracture		Fracture initiation		Cause of failure
	Bottom	Middle	Surface	Sub-surface	
Quench	✔✔✔✔		✔		Mechanical damage
Temper	✔✔✔✔		✔		Mechanical damage
Hot scrag	✔✔✔		✔		Mechanical damage
Shot peen		✔✔✔✔		✔	Inclusions related
Painted	✔	✔✔		✔	Inclusions related
Load tested	✔	✔✔✔		✔	Inclusions related

Table 7.1: Effects of manufacturing processes on position and cause of failure.

From the Table 7.1 it is clear that the majority of the samples broke within the first three turns of the spring. There is a definite move towards the centre of the sample after the shot peened process and the processes after this follow the same trend. This is also clearly illustrated by the graph in Figure 7.1. From the same graph it can be concluded the shot peened process is the turning point as far as position of failure and mechanical damage is concerned. The stress state in the first turn of coil spring design is complicated as the reduction in pitch has to be incorporated to give the component parallel ends. It would seem that this is only true for the first three manufacturing processes as the position of failure after the shot peened process is towards the middle part in the area of a more even helical pitch.

The most common type of failure was the helical type which occurred in all samples. The next

type was an axial/helical type fracture mainly present in samples withdrawn after the shot peened process, while the torsional slow type fracture occurred in only samples from the last three processes but was not process specific. Only one sample withdrawn from the hot scragging process failed by buckling. The microscopic analysis revealed three general causes of fatigue initiations, namely surface damage, non-metallic inclusions and an isolated case of hydrogen embrittlement which is also inclusion-related.

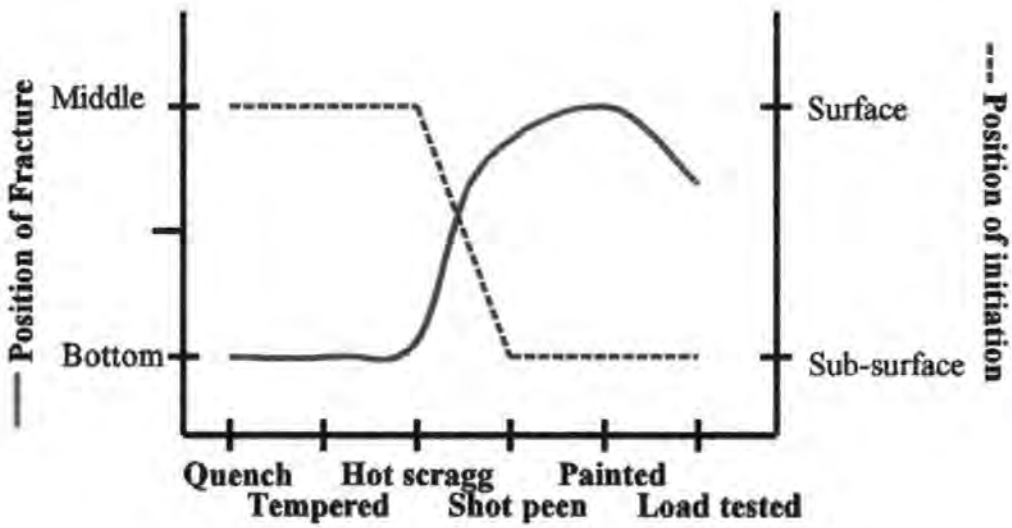

Figure 7.1: Influence of manufacturing processes of 55Cr3 spring steel on fracture position and initiation area.

The dominant failure of samples withdrawn before the shot peening process related to damage due to coil clash between the first turn and the coil end. The influence of coil clash on failure initiation seems to disappear after the shot peened process as was illustrated by Plate 3.37 in Chapter 3. This confirms that the shot peening process is largely responsible for reducing or eliminating the influence of surface damage responsible for fatigue initiations.

7.2 THE RELATION BETWEEN MECHANICAL AND FATIGUE PROPERTIES OF PROCESSED SAMPLES

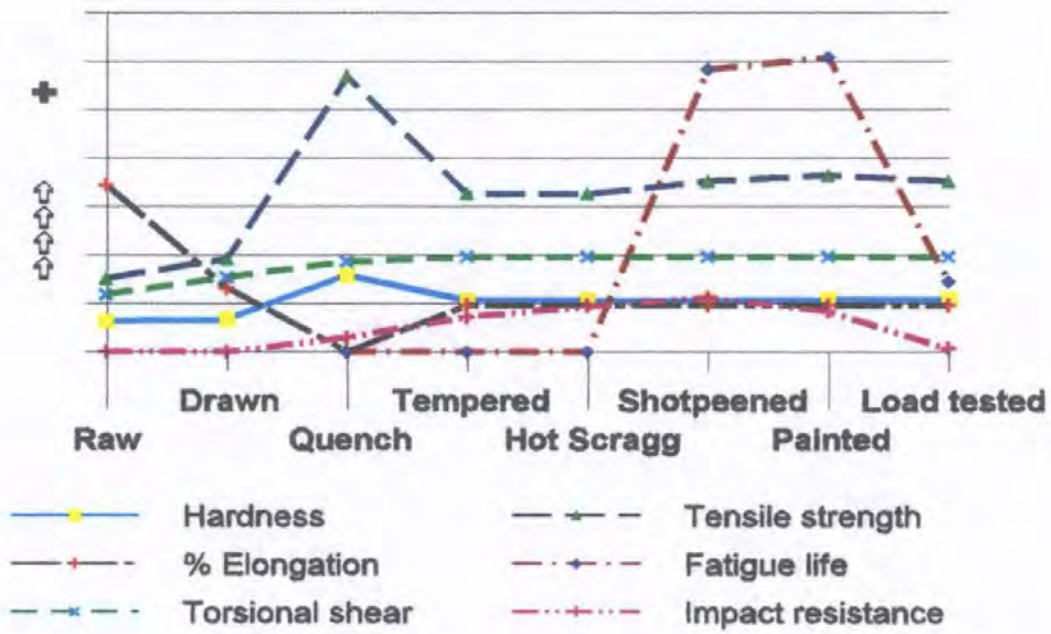

Figure 7.2: Relation between manufacturing processes and mechanical properties and fatigue.

From the graph in Figure 7.2 the following deductions could be made with relation to the mechanical properties and fatigue life of the samples. The tensile strength curve and that of full depth hardness values revealed very similar characteristics for the different process effects but yet no relation of this could be made with the trend in the fatigue life characteristic. The torsional shear resistance showed an increase until the tempered process, after which it stayed constant. This characteristic was very similar to that of the hardness properties except that the substantial increase in hardness due to the quench processes were not reflected by an increase in torsional shear resistance.

The only mechanical property that nearly reflected the trend in the fatigue life of spring steel was the impact resistance. Due to the use of non-standard size impact specimens the curve in Figure 7.2 reflects the percentage increase in impact resistance due to each process with

reference to the drawn and raw material. The only processes in which the impact resistance did not reflect this characteristic were in the tempering and hot scrag samples.

7.3 EFFECT OF PROCESS ON RESIDUAL STRESSES AND FATIGUE RESPONSE

Several sources of fatigue initiation have been identified in this thesis although not all dominant in the finished component, some interesting trends have emerged. Samples prior to the shot peening process failed mainly due to surface initiations and fracture occurred towards the end of the coil , while samples withdrawn from the shot peening process onwards mainly failed due to subsurface inclusions and fracture more to the middle of the coil. Despite a reduction in hardness during the tempering process, average fatigue life of tempered coils did slightly increase as expected. After subsequent processes the variation in measured hardness values proved insignificant. The hot scrag operation also affected the fatigue performance, resulting in an average increase in fatigue life of approximately 28% over the quenched tempered coils but this can be considered negligible compared to the ultimate fatigue life of the final components.

Figure 7.3: Fatigue life of processed samples.

The most significant process in terms of promotion of high fatigue life was that of shot peening,

producing a substantial increase of hundred thousand-fold compared to that of the previous process. A further increase in the fatigue performance was noted from the painted spring samples, although the increase was so small that it cannot be regarded as significant. The most interesting change in fatigue performance was observed in the final product(load tested), which resulted in a four-fold reduction in fatigue life. Considering the design formula for coil springs it would be expected that most coil failures should occur at the inside of the coil at the area of high stress, but instead it was found that approximately 70% of failures occurred at the top or bottom of the wire. The reasons for this could be that the bending element in this spring design is more significant than the design formulae suggest, thus creating a peak combined stress at the top/bottom of the wire or that the standard design theory assumes the ideal situation where the coil is loaded perfectly axially whereas in reality this is never achieved, resulting in the introduction of a bending element. The last possibility is that some damage to the top and bottom wire areas occurs during the manufacturing processes and that this is not well covered by the shot peening because the coverage is reduced in the inward surfaces of the component due to shielding of these areas.

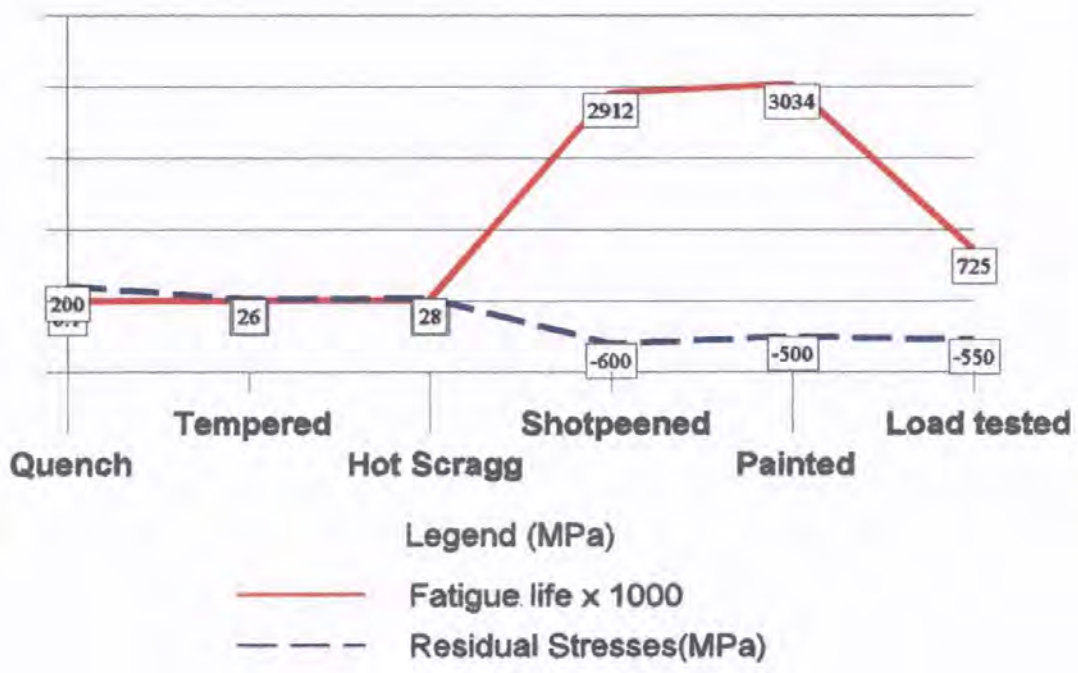

Figure 7.4: The relation between residual stresses and fatigue life.

Comparing fatigue results to the residual stress measurements clearly explains why variations in fatigue performances occur and, in particular, why coils from a given manufacturing stage are sensitive to specific defects. Figure 7.4 shows the results of the variation of the residual stress profile after each process and the relation to the corresponding fatigue life.

For quenched components it can be seen that a tensile residual stress was present which promoted fatigue initiation near the surface, thus making the material more notch sensitive and vulnerable to mechanical defects than non-metallic inclusions. The tempering operation leads to a reduction of the tensile quench stresses but the resultant is still of a tensile nature and the dominant failure mechanism remains to be mechanical damage.

The hot scragging process causes plastic deformation in the coil surface, thus creating a compressive residual stress to offset the existing tensile residual stress field. The resultant surface residual stresses after this operation are still of a tensile nature.

Further compressive residual stress, of significantly greater magnitude, is added by the shot peening process and is large enough to ensure that a wholly compressive residual stress state exists at the component surface. This significantly reduced effective peak stress area along with an altered stress profile in the surface which ensures that the surface is no longer the critical area in terms of defects, as was verified by the significant shift of failures to sub-surface defects. From Figure 7.4 it is clear that the introduction of compressive surface residual stresses have resulted in a substantial increase in fatigue life.

As was explained in early chapters, we could see that in some cases residual stresses can be used to the advantage of the fatigue life of components. Process methods have major

influences on the properties of 55Cr3 spring steel including the residual stresses and micro hardness values as illustrated in Chapter 5. However there does not exist a trend or pattern between residual stresses in the surface of the different samples and the micro hardness values. It would seem that very high hardness values associate themselves with high tensile surface residual stresses. Although the micro hardness and residual stress values for the shot peened, painted and load tested samples were closely related, not much can be concluded as the hardness of the tempered and hot scragged samples were also in this range but their residual stresses were much smaller and of a different nature (tensile).

7.4 SUMMARY

This chapter made a contribution towards the better understanding of the relationship between fatigue life, process effects and residual stresses. The manufacturing process which must be optimised for enhanced quality and product characteristics has been highlighted with the cold scragging process holding the most promise for contributing to this aim. Residual stresses in these samples due to the manufacturing processes proved to be either beneficial or detrimental to the fatigue properties. As soon as surface compressive residual stresses were introduced, it caused a substantial increase in the fatigue life of the samples although there was no change in the mechanical properties or microstructure structure of the material. This is clearly illustrated by the graph in Figure 7.5 which compare the characteristics of the different process influence on the material properties. It is felt that further investigation on a crystalline transformation level must be conducted into the mechanism that exists between fatigue properties and residual stresses and its relation to process.

The results revealed the nature and magnitude of the stresses induced, fatigue life and mechanical properties of each component from the different manufacturing process. This in the final analysis reveals the relation and impact of the manufacturing processes on fatigue

properties of 55Cr3 spring steel.

This research has attempted to make a contribution to solve the ubiquitous phenomenon of residual stresses and their relation to manufacturing processes of spring steel and to identify a model for this relation. Many opportunities for optimisation of design and manufacture leading to reduction of costs, are locked up inside the correct understanding of residual stresses.

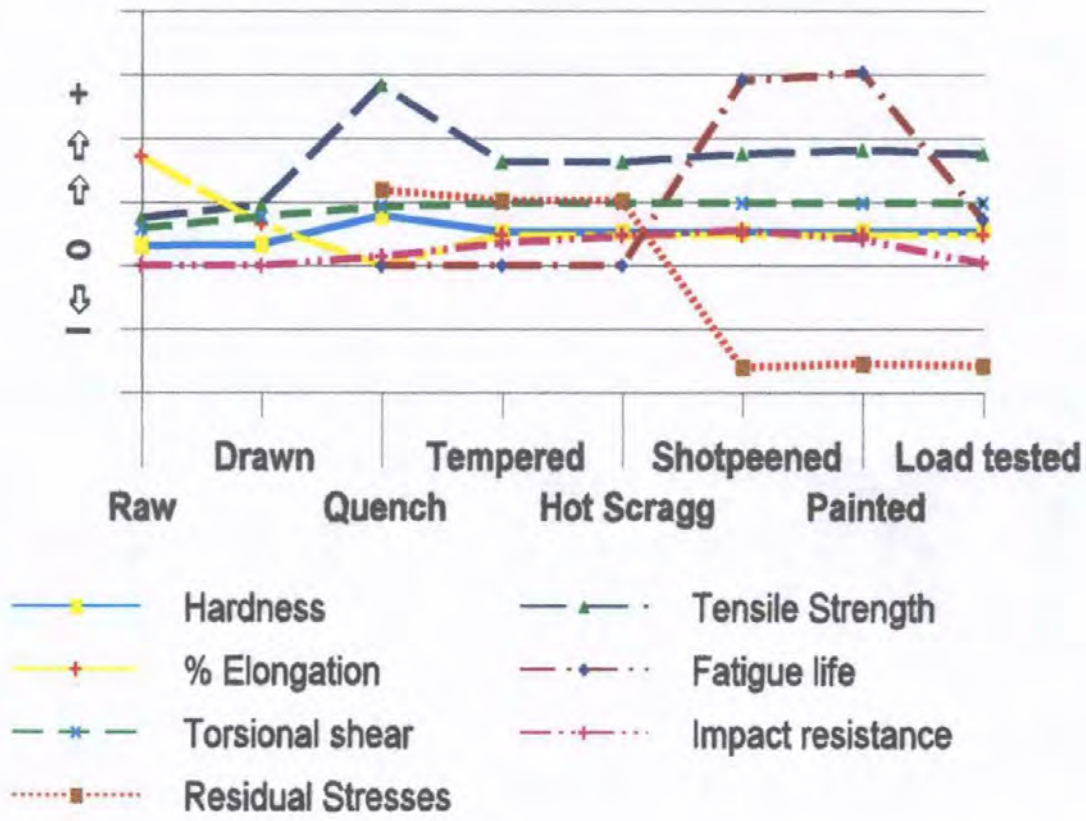

Figure 7.5: Model for the relation of process effects to 55Cr3 spring steel properties.

CONCLUSION

The stress state of coil springs during operation is considerably more complicated than what is suggested in most references. Current design formulae ignore the presence of any bending stresses as they revolves around the ideal conditions of loading the coil spring perfectly axially. The work done in Chapter 2 proved that this is not the reality and that although the bending component is quite a bit smaller than the torsional stresses it never should be disregarded. It was also verified that an isolated loop could be used as a replacement sample for fatigue tests. However great care should be taken as the load ratio could vary and that it is only valid with in a certain range of deflections.

The location of fatigue fractures were very process specific with the majority of samples fractured in the first three coils. The shot peening process proved to be the most significant as this resulted in a substantial increase in fatigue life and also resulted in failures to originate sub-surface and sample to fracture more toward the centre. However, failure analysis has revealed that more failures occurred at the top or bottom of the wire. This could be attributed to a number of reason eg. Bending element in coil springs are more significant than design formulae suggest or that some process damage to the top and bottom wire areas occurs during scragging or fatigue cycling. The work done has highlighted the relationship between fatigue failure and critical defect presence in automotive coil spring components.

The magnitude, presence and the nature of residual stress has been thoroughly investigated. The work revealed the relation between manufacturing processes and the residual stresses they induce and subsequently the influence of residual stresses on the fatigue life of spring steel. The most prominent manufacturing process in inducing residual stresses was shot peening which induced a large component of compressive residual stress into the surface which was very

advantageous to the fatigue life and caused a shift from surface fatigue initiations to sub-surface initiations.

This research has contributed towards the better understanding of the fatigue properties of spring steel. It revealed an important model around the relation of current manufacturing processes and the influence on fatigue behaviour of coil springs. All of this in turn was related to the presence of residual stresses and the relation to fatigue life of coil springs.

FUTURE RESEARCH

There is a number of possible areas that needs to be research more intensely to understand the operating conditions and manufacturing processes of automotive coil spring entirely.

Future research should concentrate on the following topics:

1. Investigation into the bending element present in automotive coil spring during normal operation. This must be done with the objective of developing new design formulas around combined twisting and bending.

2. The investigation of the mechanism of the cold scrag process. Better understand is needed of the mechanism causing the major decrease in fatigue life due to this process. This could be done by investigating crystalline transformations in the material due to the process.

3. The most significant research can be done in the field of the crystalline structure of spring steel. The research should concentrated on the presence of dislocation, twining, etc. and their relation to the manufacturing processes. This inturn can be relate to mechanical properties and the presence of residual stresses.

4. Some general research can be done on the measurement of residual stresses in spring steel by using another method like x-ray diffraction. It is always advice able to use different methods for measurement of residual stresses as it is such and abstract field. This could also be extended to different manufacturing procedures and materials.

REFERENCES

1 Hearn, E.J. Mechanics of Materials, 2nd Ed, Pergamon Press, Oxford, 1985. pp 502-750, pp299 -306.

2 Wahl, A.M. Mechanical Springs, 2nd Ed, McGraw Hill Book Company, New York, 1963. pp 229-312

3 Warnock, F.V. and Benham, P.P. Mechanics of Solids and Strengths of Materials, Pitman & Sons, 1965. Pp 168 - 253.

4 Anver, S.H. Introduction into Physical Metallurgy, 2nd Ed, McGraw Hill, Tokyo, 1974. pp 65-129, 147-155, 249-349, 633-666.

5 Almen, John O., and Paul H. Black. Residual Stresses and Fatigue in Metals, McGraw-Hill Book Company, New York, 1963.

5 Bob Ross. Investigation into Mechanical Failures, Chapman & Hall, Glasgow, 1995. pp 57-80, 257-282.

6 Jack. A. Collins. Failure of Materials in Mechanical Design, John Wiley & Sons, New York,1976. pp 8, 178-248, 255-314, 511-514

7 Kawakami, H. Effects of Chemical Composition on Sag Resistance of Suspension Springs, SAE. Technical Paper Series, International Congress and Exposition, Detroit, Michigan, 1982. 820128.

8 Furr, S.T. Development of a New Laboratory Test Method for Spring Steels, Trans, ASME. 71- MET - 7.

9 Ma Ming-Tu, A Study on Sag Resistance of New 35 SiMnB for suspension leaf springs, SAETechnical Paper Series, Seventh International Pacific Conference, Phoenix, Arizona. 1993. 931968.

10 Argon, A.S. Topics in Fracture and Fatigue, Springer Verslag, New York, 1991. pp309-331.

11 Metals Handbook, Fractography, Vol.10, American Society for Metals, Metal Park, Ohio, 1995. pp. 554-561

12 Budinski, K.G. Engineering Material, 5th Ed, Prentice Hall Inc, New Jersey, 1996. pp253-276, 301-320, 617-637.

14 Buchholtz, H. Residual Stresses in Structural Members, Welding Industry, v 3, 1935, pp 267-271, 337-339.

15 Parker, A.P. The Mechanics of Fracture and Fatigue, E.& F.N. Spon Ltd, New York, 1981. pp 138-163

16 Almen, J.O. Improving Fatigue Strength of Machine Parts. *Iron Age*, June 10, 1943,

pp 65-69, 125-131. Peened Surfaces Improve Endurance of Machine Parts, and related subjects in *Metal Progress*, Feb 1943, pp 209-215, 270; May 1943, pp 737-740; Aug 1943, pp 254-161; Sept 1943, pp 435-440, Shot Blasting to Increase Fatigue Resistance, *J Soc Automotive Engrs* (Trans), v 51, n 7, July 1943, pp 249-268.

17 Determining Residual Stresses by the Hole Drilling Strain Gage Method, ASTM Standard E837-92.

18 Duffy, J., and T. C. Lee Measurement of Surface Strain by Means of Bonded Birefringent Strips, SASA Proc., vol. 18, no. 2 (1961).

19 Hetényi, M. (ed.) Handbook of Experimental Stress Analysis, John Wiley & Sons, Inc., New York, 1950.
- a. Chap. 3, Mechanical Gages and Extensometers, by L. H. Donnell and W. T. Savage.
- b. Chap. 4, Optical Methods of Strain Measurement, by John L. Maulbetsch.
- c. Chap. 6, Electric-inductance Gages, by B. F. Langer.
- d. Chap. 7, Electric-capacitance Gages, by B. C. Carter, J. R. Forshaw, and J. F. Shannon.
- e. Chap. 11, Residual Stresses, by Oscar J. Horger.
- f. Chap. 18, X-ray Analysis, by Charles S. Barrett.

20 James, M.R. and J.B. Cohen. The Application of a Position-sensitive X-ray Detector to the Measurement of Residual Stresses, Adv. in X-ray Analysis, 19, 1976, pp 695-708.

21 Measurements of Residual Stresses by the Blind Hole Drilling Method. Tech. Data Bul, T-403, Photoelastic Div., Measurements Group Inc.

22 Murakami, M., A. Segmuller, K.N. Tu. X-ray Diffraction Analysis of Diffusion in Thin Films. In: Analytical Techniques for Thin Films. (K.N. Tu and R. Rosenberg, eds.) Academic Press, San Diego, 1988, p 201.

23 Winegar, J.E. Xray Measurement of Residual Stress in Metals at Chalk River Laboratories, Atomic Energy of Canada Limited Report, AECL-6961, 1980.

24 Bathgate, R.G. Measurements of Non-Uniform Bi-Axial Residual Stresses by the Hole Drilling Method. Strain, Vol. IV, No. 2, pp 20-29, 1968.

25 Bush, A.J. and F.J. Kromer. Simplification of the Hole-Drilling Method of Residual Stress Measurements. Trans., ISA 112, No. 3: 249-260, 1973.

26 Dally, J.W. and R.J. Sanford. Strain Gage Methods for Measuring the Opening Mode Stress Intensity Factor. Exp. Mech., vol. 27, no. 4, pp 381-388, 1987.

27 Dally, J.W. and J.R. Berger. Strain Gage Method for Determining K_I and K_{II} in a Mixed Mode Field. Proc. 1986 Spring Conf. SEM, June 1986.

28 Errors Due to Transverse Sensitivity in Strain Gages. Micro-Measurements publication TN-509, 1982.

29 Flaman, M.T., Manning, B.H. Determination of Residual Stress Variation with Depth by the Hole Drilling Method. Experimental Mechanics, Vol. 25, No. 9, pp 205-207, 1985.

30 Flaman, M.T., B.E. Mills, and J.M. Boag. Analysis of Stress-Variation-With-Depth Measurement Procedures for the Centre Hole Method of Residual Stress Measurements. Experimental Techniques 11 35-37, June 1987.

31 Measurement of Residual Stresses by the Hole Drilling Strain Gage Method. Measurements Group, Inc., TN-503-1, 1988.

32 Meier, J.H. On the Transverse-Strain Sensitivity of Foil Gages. Exp. Mech., vol. 1, no. 7, pp 39-40, 1961.

33 Schajer, G.S. Measurement of Non-Uniform Residual Stresses Using the Hole-Drilling Method. Part II - Practical Applications of the Integral Method. Journal of Engineering Materials and Technology, Vol. 110, No. 4, pp 344-349, 1988.

34 Nickola, W.E. Practical Subsurface Residual Stress Evaluation by the Hole-Drilling Method. Proc, 1986 SEM Spring Conference on Experimental Mechanics, Brookfield Center, Connecticut: Society for Experimental Mechanics, 1986.

35 Niku-Lari, A., Lu, J., Flavenot, J.F. Measurement of Residual Stress Distribution by the Incremental Hole Drilling Method. Experimental Mechanics, Vol. 25, No. 6, pp 175-185, 1985.

36 Kelly, A., and Groves, G.W., Crystallography and Crystal Defects, Longman, 1970.

37 Horger, Oscar J. (ed.). ASME Handbook: Metals Engineering-Design, 2d ed., McGraw-Hill Book Company, New York, 1965.
- a Part 2, sec. 7.5, Surface Finish, by B.C. Hanley and T.J. Dolan.
- b. Part 2, sec. 8.2, Shot Peening, by John C. Straub.
- c. Part 2, sec. 8.3, Cold Working, by Oscar J. Horger.
- d. Part 2, sec. 8.4, Decarburization, by Oscar J. Horger.
- e. Part 2, sec. 8.5, Case Carburizing, by R.L. Mattson and G.H. Robinson
- f. Part 2, sec. 8.6, Nitriding, by Carl F. Floe.
- g. Part 2, sec. 8.7, Metallic Coatings, by R.R. Moore
- h. Part 2, sec. 8.13, Flame Strengthening, by J.H. Zimmerman.

38 Wnuk, S.P. Residual Stress Measurements in the Field Using the Airbrasive Hole Drilling Method. Presented at the Technical Committee for Strain Gages, Spring Meeting of SESA, Dearborn, Michigan, June 1981.

39 ABAQUS Theory Manual, Ver.4.9, Hibbitt, Karlsson and Sorensen, Inc., Providence, Rhode Island, 1990.

40 Rendler, N.J., Vigness, I. Hole Drilling Strain Gauge Method of Measuring Residual Stresses. Experimental Mechanics, Vol. 6, No. 12, pp 577-586, 1966.

41 Almen J.O. Mattson R.L. and Fonda H.E. Effect of Shot Blasting on the Mechanical Properties of Steel, pt 1, 2 and 3, *Office Sci Research and Develop* Reports

3274, 4825, and 6647.

42 Frye, J.H. Shot Peening Applied to Ordnance Parts, Am Soc Metals Symposium on Shot Peening, Oct 1944.

43 Davenport, E.S. Austempering, Heat Treating and Forging, v 23, 1937, pp 170-173, 177.

44 Brandon, D.G. Modern Techniques in Metallography. Butterworths, London 1966.

45 Ancker C.J., (Jr) & Goodier J.N. Pitch and Curvature Corrections for Helical Spring.

46 Loretto, M.H., Smallman, R.E. Defect Analysis in Electron Microscopy, John Wiley & Sons In., New York.

47 Edington, J.W. Interpretation of Transmission Electron Micrographs, The MacmillanPress Ltd.

48 Christian, J.W., The Theory of Transformation in Metals and Alloys, Pergamon Press, New York, 1965.

49 Ryder, G.H. Strength of Materials, 3rd Ed, MacMillan Press Ltd., Hong Kong, 1982. pp 225-230.

50 Schajer, G.S. Measurement of Non-Uniform Residual Stresses Using the Hole-Drilling Method. Part I - Stress Calculation Procedures. Journal of Engineering Materials and Technology, Vol. 110, No. 4, pp 338-343, 1988.

Additional references:

51 Ades, C.S. Reduction of Strain Rosettes in the Plastic Range. Exp. Mech., vol 2, no. 11, pp 345-349, 1962.

52 A.S.M.E., Journal of Applied Mechanics, December 1958.

53 AL-Obaid, Y.F. A Rudimentary Analysis of Improving Fatigue Life of Metals by Shot-Peening. J. Appl. Mech., 57, 307-312, 1990.

54 Forrest, P.G. Fatigue of Metals, Pergamon Press, New York, 1962.

55 Zandman, F., and H. M. Maier. Six New Techniques for Photoelastic Coatings, *Product Engineering*, July 24, 1961.

56 Wu, C.T. Transverse Sensitivity of Bonded Strain Gages, Exp. Mech., vol. 2, no. 11, pp 338-344, 1962.

57 Amelinckx, S., Gevers, R., Remaut, G., and Van Landuyt, J. Modern Diffraction and Imaging Techniques in Material Science. Proceedings of the International Summer Course on Material Science, Antwerpen, Belgium, 28 July-8 August 1969, North-Holland Publishing Company, Amsterdam/London 1970.

58 Warren, B.E. X-ray Diffraction. Addison-Wesley, Reading, 1969.

59 Anderson, R.G. Improving Engine Parts by Direct Measurement of Strain, Trans Soc Automotive Engrs J, v 54, n 9, pp 466-475, 501-502.

60 Andrews, K.W. *et al.* Stress measurement by X-ray diffraction using film techniques, Strain, 10(3), pp 111-116, July 1974.

61 Segmuller, A. and Murakami, M. Characterisation of Thin Films by X-ray Diffraction. In Thin Films from Free Atoms and Particles. (K.J. Klabunde, ed.) Academic Press, p. 325, Orlando, 1985.

62 Sines, George, and J.L. Waisman (eds). Metal Fatigue, McGraw-Hill Book Company, New York, 1959.

63 Ascelrad D.R. 1966 Strength of Material for Engineers 1st edition. London. Pitman Publishers Limited.

64 Askeland, D.R.A. 1988. The Science of Engineering Materials, VNR International.

65 Bacon, G.E. Neutron Diffraction. Clarendon Press, 3rd ed. 1975.

66 Barrett, Charles S. Structure of Metals, McGraw Hill Book Co, New York, 1943.

67 Waisman, and Phillips. Simplified measurement of residual stresses, S.E.S.A., II(2), pp 29-44.

68 Becker, H., and G. Gerard. Photo elastic Model Engineering, *Mech. Engineering* (July, 1960).

69 Bedi D.S. 1984 Strength of Materials. 2nd edition. New Delhi S. Chand and Company Ltd.

70 Benham P.P. and Warnock F.V. 1979. Mechanics of Solids and Structures. London. Pitman Publishing Limited.

71 Bertea, O., Seagle, S.R. and Gross, J.R. Method of Imparting Corrosion Resistance to Zirconium-Based Alloys. U.S. Patent, 1,068,855, 1967.

72 Moore, M.G. and Evans, W.D. Mathematical correction for stress in removed layers in X-ray diffraction residual stress analysis, S.A.E. Trans., 66, pp 340-345, 1958.

73 Bowen, D.K. X-ray Topography of Surface Layers and Thin Films. In: Advances in X-ray Analysis. (C.S. Barrett, J.V. Gilfrich, R. Jenkins and P.K. Predicki, eds). Plenum, New York, 1990, vol. 33, p. 13.

74 Hardrath, Herbert G., and Lachlan Ohman. A Study of Elastic and Plastic Stress Concentration Factors Due to Notches and Fillets in Flat Plates, NACA Rept. 1117, 1953.

75 Bridgman, P. W. Studies in Large Plastic Flow and Fracture, McGraw-Hill Book

Company, New York, 1952.

76 Von Dreete, R.B. Reviews in Mineralogy. Volume 20 Modern Powder Diffraction, 333, 20, 1990.

77 Vaughn, Dale A. and Crites Nelson A. Measurement of Stress by X-ray Diffraction. Product Engineering, Sept 30, 1963.

78 Urbanic, V.F., Lesurf, J.E. and Johnson, A.B. Effect of Aging and Irradiation on the Corrosion of Zr-2.5Nb, Corrosion, 31, pp 15-20, 1975.

79 Carmichael Colin 1950 Kent's Mechanical Engineering Handbook. Design and Production Volume. 12th edition. New York. John Wiley and Sons, Inc.

80 Cernica John N. 1966 Strength of Materials. 1st edition. New York. Holt, Rinehard and Winston, Inc.

81 Cheadle, B.A. and Ells, C.E. The Effect of Heat Treatment on the Texture of Fabricated Zr-rich Alloys, J. Electrochem. Tech., 4, pp 329-335, 1966.

82 Toney, M.F. and S. Brennan. Structural Depth Profiling of Iron Oxide Thin Films using Grazing Incidence Asymmetric Bragg X-ray Diffraction. J. Appl. Phys. 65, 4763, 1989.

83 Crites Nelson A and Alvin R. Hunter., Experimental Stress Analysis by Photo elastic Techniques, *Product Engineering* (Sept. 3, 1962).

84 Crites, Nelson A. Which Type of Stress-analysis Method? Product Engineering (Oct. 16, 1961).

85 Crites, Nelson A., and Alvin R. Hunter Experimental Stress Analysis by Photoelastic Techniques, *Product Engineering* (Sept. 3, 1962).

86 Cullity, B.D. Elements of X-ray Diffraction, 2nd ed. Addison, Wesley, Reading, Mass. 1978, Ch. 16, pp 447-479.

87 Cullity, B.D. Elements of X-ray Diffraction. Addison-Wesley, New York, 2nd ed. 1978.

88 Dally, James W., and W. F. Riley Experimental Stress Analysis, McGraw-Hill Book Company, New York, 1965.

89 Timoshenko, Stephen P. Strength of Materials, 3d ed., part 2, D. Van Nostrand Company, Inc., Princeton, N. J., 1956.

90 Terranova, A., Vergani, L. Strength of Components in Low Cycle Fatigue with Different Surface Treatments. pp 1679-1684, FATIGUE '90, Proceedings of the IV the International Conference on Fatigue and Fatigue Thresholds, Honolulu, Hawaii, 1990. MCEP Ltd, Birmingham, 1990.

91 Teller, R.G., M.R. Antonio, A. Grau, M. Guegin and E. Kostiner. Details of the thermal decomposition of commercial slags. J. Solid State Chem. 1990.

92 Rees, D.W.A. 1990. The Mechanics of Solids and Structures, McGraw-Hill.

93 Matt Robert L. 1985 Machine Elements in Mechanical Design. 1st edition. Ohio. Charles E. Merrill Publishing Company.

94 Residual Stress for Designers and Metallurgists. Proceedings of a Conference held in Chicago, Illinois on 9-11 April 1980.

95 Redner, S. and C.C. Perry. Factors Affecting the Accuracy of Residual Stress Measurements Using the Blind-Hole Drilling Method. Proc., 7th International Conference on Experimental Stress Analysis. Haifa, Israel: Israel Institute of Technology, 1982.

96 Rhyne, J.J., R.W. Erwin, J. Borchers, M.B. Salamon, R. Du, and C.P. Flynn. Physica B. 159, 111, 1989.

97 Roark Raymond J. Formulas for Stress and Strain. 4th edition.McGraw-Hill Book Company New York. 1965.

99 Marin, Joseph. Mechanical Behaviour of Engineering Materials, Prentice-Hall, Inc., Englewood Cliffs, N. J., 1962.

100 Stowell, E. Z. Stress and Strain Concentration at a Circular Hole in an Infinite Plate, NACA Tech., Note 2073, 1950.

101 Dieter, E.G. 1988. Mechanical Metallurgy, McGraw-Hill.

102 Dobkin, H. Prestressing Rotating Disks. Steel, v 118, June 3, 1946, pp 104-106 and 150.

103 Dölle, H. Influence of Multiaxial Stress States, Stress Gradients and Elastic Anisotropy on the Evaluation of Stress by X-rays, J. Appl. Cryst., 12, 1979, pp 489-501.

104 Dölle, H. and J.B. Cohen. Residual Stresses in Ground Steels, Met. Trans. 11A, 1980, pp 159-164.

105 Stephens RC. 1970 Strength of Materials Theory and Examples. London. Edward Arnold (Publishers) Ltd

106 Durelli, A. J., and W. F. Riley Introduction to Photomechanics, Prentice-Hall, Inc., Englewood Cliffs, N. J., 1965.

107 Speriosu, V.S., M.A. Nicolet, J.L. Tandon, and Y.C.M. Yeh. Interfacial Strain in AlGaAs Layers on GaAs. J. Appl. Phys. 57, 1377, 1985.

108 Society of Materials Science, Japan Standard Method for X-ray Stress Measurement, Supplement VI (K. Hayashi), 1973.

109 Society of Automotive Engineers, SAE Handbook Supplement J784a Residual Stress Measurement by X-ray Diffraction, SAE, Inc. New York, 1971.

110 Singer Ferdinand L and Pytel Andrew. Strength of Materials. 3rd Edition. Harper and Row Publishers, New York 1980.

111 Procter, E. and E.M. Beaney. Recent Developments in Centre-hole Technique for Residual-stress Measurement. Experimental Techniques 6: 10-15, December 1982.

112 French, D.N. and Macdonald, B.A. Experimental methods of X-ray analysis, S.E.S.A., 26(2), 456-462.

113 Frocht, M ax M. Photoelasticity, John Wiley & Sons, Inc., New York, vol. 1, 1941; vol. 2, 1948.

114 Ramasubramanian, N. and Ling, V.C. Fourier Transform Infrared Reflection (FTIR) Spectroscopy of Corrosion Films on Irradiated Zirconium Alloys. J. Nucl. Mater., 175, pp 237-243, 1990.

115 Sandifer, J.P. and G.E. Bowie. Residual Stress by Blind-hole Method with Off-Center Hole. Experimental Mechanics 18: 173-179, May 1978.

116 Gadd C.W. Residual Stress Indications in Brittle Lacquer, Proc Soc Experimental Stress Analysis, v 4, n 1, 1946, pp 74-77.

117 Griffith, G. E. Experimental Investigation of Plastic Flow in Tensile Panels with Circular Holes, NACA Tech. Note 1705, 1948.

118 Grover, H.J., S.A. Gordon, and L.R. Jackson. Fatigue of Metals and Structures, Government Printing Office, Washington, D.C. 1960.

119 Guechichi, H. and Castex, L. Predicting Residual Stress Due to Shot-Peening. Proceedings of the Conference on Impact Surface Treatment, Bedford, England, Sept. 22-26, 1986.

120 Jorgensen, J.D. and J. Faber. ICANS-II, Proceedings of the Sixth International Collaboration on Advances in Neutron Sources. Argonne National Laboratory technical report ANL-82-80. 1983.

121 Harris, W.J. The Significance of Fatigue, Oxford University Press, 1976. pp 1-23

122 Kakudo, M. and N. Kasai. X-ray Diffraction by Polymers. Elsevier, Tokyo, 1972.

123 Heidenreich, R.D. Fundamentals of Transmission Electron Microscopy, Interscience, 1964.

124 Hetényi, M. The Fundamentals of Three-dimensional Photoelasticity, J. Appl. Mech., vol. 5 (1938).

125 Segmuller, A. and M. Murakami. X-ray Diffraction Analysis of Strains and Stresses in

Thin Films. In Analytical Techniques for Thin Films. (K.N. Tu and R. Rosenberg, eds). Academic, p. 143, San Diego, 1988.

126 Heywood, R. B. Designing by Photoelasticity, Chapman & Hall, Ltd., London, 1952.

127 Heywood, R.B. Designing against Fatigue, Chapman & Hall, Ltd., London, 1962.

128 Hibbitt, H.D. Contact and Friction Analysis with Abaqus. Proceedings of the III National Congress of Abaqus User Group, Milan, Italy, September 21-22, 1992.

129 Hoffman K. 1976 Theory of strain Gauge Techniques Germany. Hottinger Balwin Messtechnik.

130 Schwartz, L.H. and J.B. Cohen. Diffraction from Materials. Springer-Verlag, Berlin, 1987.

131 Horger, O.J. Mechanical and Metallurgical Advantages of Shot Peening, Iron Age, Mar 29 and Apr 5, 1945.

132 Iida, K. and Tosha, K. Behaviour of Surface Residual Stress Induced by Shot Peening(I). Int. Sympo. Calculation of Internal Stresses in Heat Treatment of Metallic Materials, Linkoping, Sweden, 1984.

133 Moore, H.F., Shot Peening, American Wheelabrator and Equipment Corp, Mishawaka, Ind., 1946.

134 James, M.R. and J.B. Cohen. Study of the Precision of X-ray Stress Analysis, Adv. in X-ray Analysis, 20, 1977, pp. 291-307.

135 James, M.R. and J.B. Cohen. PARS - A Portable X-ray Analyzer for Residual Stresses, J. Testing and Evaluation 6, 1978, pp 91-97.

136 Lee, G. H. An Introduction to Experimental Stress Analysis, John Wiley & Sons, Inc., New York, 1950.

137 Jones, R. and Wykes, C. Holographic and Speckle Interferometry, Cambridge Univ. Press, Sec. ed., 1989.

138 Jorgensen, J.D. and D.G. Hinks. Discussion of neutron diffraction studies of superconductors, Neutron News, 24, 1, 1990.

139 Lessells, John M. Strength and Resistance of Metals, John Wiley & Sons, Inc.

140 Lipson, Charles, and R.C. Juvinall. Handbook of Stress and Strength, The Macmillan Company, New York, 1963.

141 Kaufmann, A.R. and Magel, T.T. Physical Metallurgy of Zirconium and Its Alloys in the Metallurgy of Zirconium, (Eds. Lustman B. and Kerze Jr. F.), pp 348-431, McGraw-Hill Book Company, 1955.

142 Sachs, G. and Kent, R. Van Horn. Practical Metallurgy, American Society for Metals,

Cleveland, 1940.

143 Rosenthal, and Norton. A method of measuring tri-axial residual stresses in plates, Journal Welding Society,, 24, 295-307, Welding supplement, 1945.

144 Kelsey, R.A. Measuring Non-uniform Residual Stresses by the Hole-drilling Method. Proc., SESA XIV, No. 1:181-194, 1956.

145 Kirk, D. Theoretical aspects of residual stress measurement by X-ray diffractometry, Strain, 6(2), 1970.

146 Kirk, D. Experimental features of residual stress measurement by X-ray diffraction using film techniques, Strain, 10(3), July 1971.

147 Macherauch, E. and U. Wolfstieg. A Modified Diffractometer for X-ray Stress Measurements, Adv. in X-ray Analysis, 20. 1977 pp 369-377.

APPENDIX - A

Calculation of forces in a closed coil spring.

FORCES IN A CLOSED COIL SPRING UNDER AXIAL LOADING [1,2,49]

A helical spring is usually loaded by an axial force. For this study we will assume a circular cross section for the spring wire and the helix angle is very small. We will ignore small end effects, as when ends are unbent, or ground flat to provide a bearing plane. We will assume throughout this section that the wire diameter is considerably smaller than the helix radius (R) so that curved-beam considerations may be neglected.

1. Closed coiled spring

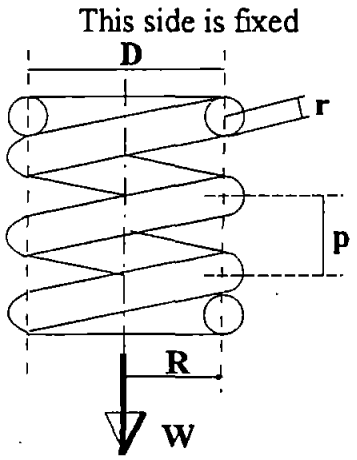

Figure 1: Closed coiled helical spring.

WHERE:

W = Axial load

D = Mean coil diameter

d = wire diameter

n = number of coils

R = Helix radius

If we work from the assumption that the angle of the helix is very small, the action on any cross section is approximately a pure torque (T = W.D/2).

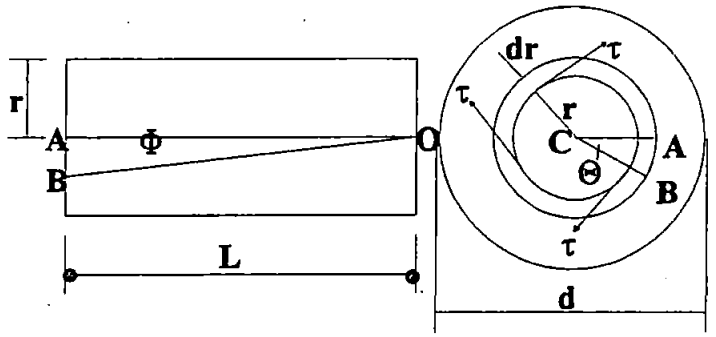

Figure 2: Schematic of torsion effect in a coil spring.

One can also assume that this pure torque is actively about the polar axis of the coil wire, therefore shear stresses (τ) will be set up in a direction perpendicular to the radius on all transverse sections. Consider the elementary strip with a thickness = dr in Figure 2. From the above we can see that a definite distortion of the filaments in the longitudinal planes was caused by the shear stress in this plane. Based on the assumption that points A and B are on the same radius after the wire had been twisted through an angle Θ over the length L. This justified by the correlation of symmetry of the cross-section before and after twisting.

On the left it shows the shear strain ϕ of the elements at a distance (r) from the axis, so that the line OA twists to OB, and < ACB = Θ (right hand sketch). $\sphericalangle$ ACB is therefore the relative angle of twist of cross sections at a distance L apart. Also we can deduce from this that the shear strain is constant for constant torque.

$\therefore$ Arc AB = $r\Theta = L\phi$ approx. 1

where (Θ = small angle)

But also the modulus of Rigidity (G) is the ratio of shear stress : shear strain

$$\therefore \quad G = \frac{\tau}{\Phi} \qquad \therefore \quad \Phi = \frac{\tau}{G}$$

By substitution and re-arranging equation 1.

$$\therefore \quad r\Theta = L\frac{\tau}{G}$$

$$\therefore \quad \frac{\tau}{r} = \frac{G\Theta}{L} \quad \text{.....(2)}$$

The total torque (T) will be the sum of the moments of the tangential stresses on the elements which has a cross-section area of $2\pi r\, dr$.

ie. $T = \int \tau(2\pi r dr)r$

Let us check this by dimensional analysis:

$N/m = \int N/m^2\ (m^2)\ m$

$\therefore\ N/m = N/m$

But $\tau = r\frac{G\Theta}{L}$ from equation 2.

$$T = \int r\frac{G\Theta}{L}(2\pi r dr)r$$

$$= \frac{G\Theta}{L}\int(2\pi r dr)r^2$$

$$= \frac{G\Theta}{L}\left[\frac{2\pi r^4}{4}\right]_0^{d/2}$$

$$= \frac{G\Theta}{L}\left[\frac{\pi d^4}{32}\right] \quad \text{when} \quad \frac{\pi d^4}{32} = \text{Polar Moment of Inertia}$$

$$T = \frac{G\Theta}{L}J \quad \text{.....(3)}$$

where J = Polar moment of inertia = $\frac{\pi d^4}{32}$ for round bar.

Combining equation (2) & (3)

$$\frac{T}{J} = \frac{G\Theta}{L} = \frac{\tau}{r} \quad \text{.....(4)}$$

Applying this formula for torsion of shaft and taking the approximate length (L) for the steel wire in the coil spring as:

$L = \pi Dn$

Then: $\frac{WD/2}{\pi d^4/32} = \frac{T}{J}$

Also maximum stress τ_{max} will occur at r = d/2

$\therefore \quad \tau_{max} = \frac{16T}{\pi d_3}$ from $\frac{T}{J} = \frac{\tau}{r}$

$\therefore \quad \frac{WD/2}{\pi d^4/32} = \frac{2\tau_{max}}{d} = \frac{G\Theta}{\pi Dn}$ .....(5)

Because the spring wire is twisted like a shaft through a total angle of Θ and deflected by distance x by a load W along the axis of the coils then:

$x=(D/2)\Theta$ approximately, therefore $\Theta=2x/D$

$\therefore \quad \frac{G\Theta}{\pi DN} = \frac{G.2x/D}{\pi DN}$

Re-writing eq.(5) (÷2)

$\frac{8WD}{\pi d^4} = \frac{\tau_{max}}{d} = \frac{Gx}{\pi D^2}$

The spring stiffness (k) of the helical spring will be the Axial Force divided by the deflection.

$\therefore \quad k = W/x = \frac{Gd^4}{8D^3n}$

The strain energy (U) caused by this pure torque is the work done by twisting.

$\therefore U = \frac{1}{2}T\Theta$ (only for gradually applied Torque) see Figure 3.

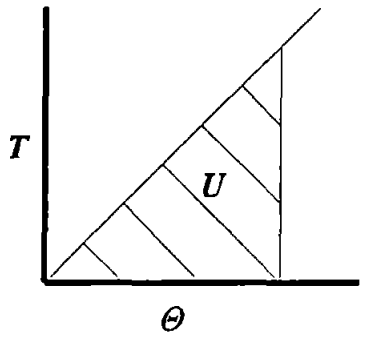

Figure 3: Total energy distribution.

where: U = area under graph

= ½ base × height

= ½ΘT

or U = ½Wx

2. Relation between stress and strain

The extreme fibre stress (τ), in the elastic range of a specimen, is related to the torque[3] (T) by the torsion formula for circular shafts by:

$$\tau = \frac{Tr}{J} \qquad \text{.....from equation 4}$$

From Figure 4 which shows a twisted shaft, and from the definitions of the modulus of rigidity $G = \frac{\tau}{\Phi}$,the angle of twist can be expressed as:

$$\Theta = \Phi\frac{L}{r} = \frac{LT}{rG}$$

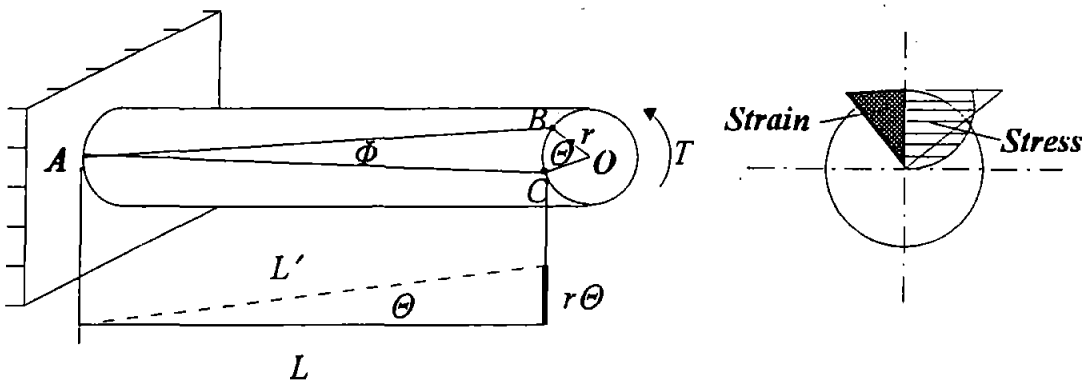

(a) (b)

Figure 4: Illustrating principal of twist in shafts.

Now consider the rod in Figure 4 with length (L) and radius (r) with a couple T applied to one end and the other end constrained. Line AB, on the surface of the rod, is parallel to the axis before any strain is exercised on the rod. When the rod is subjected to strain, line AB now forms a long helix, AC and the angle Θ, being the shear strain of the material at the surface. Since the ϕ can be considered a very small angle:

$$BC = L\phi$$

or $$\Phi = \frac{BC}{L}$$

But $\Phi = \frac{\tau}{G}$ where τ = shear stress in the material at the surface of the rod.

Also, ∠BOC is the angular movement of radius OB due to the applied strain in the length (L).

Therefore: $\tau = \phi G$

$$= \frac{r\Theta}{L}$$ (See also equation 4)

Now in the above formula Θ, L, and G will stay constant but r can be varied between 0 and r to find the shear stress at different points in the material.

Now let $k = \frac{\Theta}{L}G$ (constant)

$\therefore \tau = kr$

Hence if τ_1 is the shear stress at a radius r_1, we have $\frac{\tau_1}{r_1} = \frac{\tau}{r}$

with the above formula we can find the stress distribution from the centre to outside of the rod, and with the formula $\phi = \frac{\tau}{G}$ we can now also determine the strain distribution. Figure 4(b) shows a stress-strain variation within the proportional limit and a stress- strain variation above the proportional limit.

If a bar is subjected to torsional loading above the proportional limit the actual stress will not follow a straight line, but will follow the path of the solid line in Figure 4(b), but if proportionality between stress and stain was maintained up to the rupture point, the nominal stress distribution would be something like that shown by the dashed line. Ductility can also be determined by comparing the final fibre length L^l (Figure 4(a)) at rupture to the original length L. The value of L^l is computed knowing L and $r\phi$, the ductility is expressed as a percentage of elongation of the outer fibre and is equal to $[(L^l - L)/l] \times 100$. One can conclude by saying that the state of stress, at any point in the cross section of the rod, is one of pure shear and that the strain is such that one cross-section of the rod rotates relative to another.

APPENDIX - B

Results of strain gauge readings from isolated loop and complete coil spring.

Figure 1: Load versus strain graphs for all gauge positions.

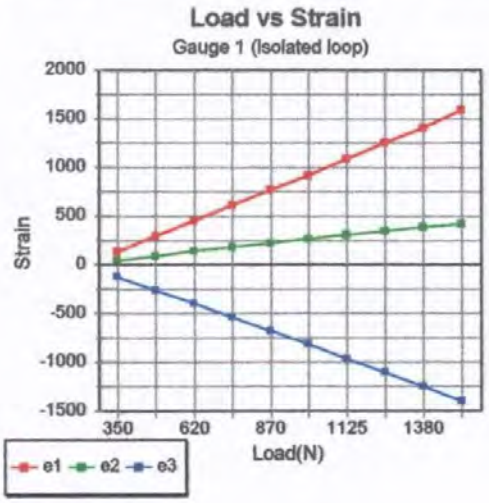

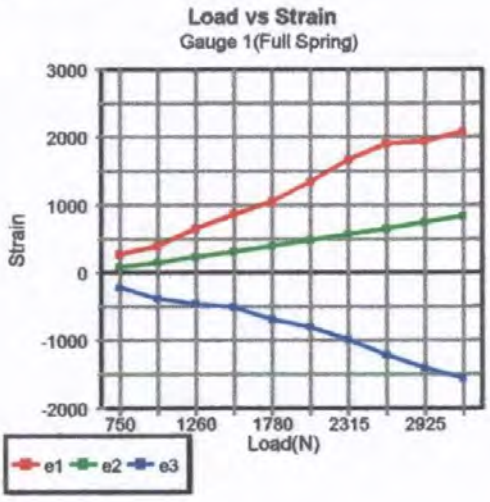

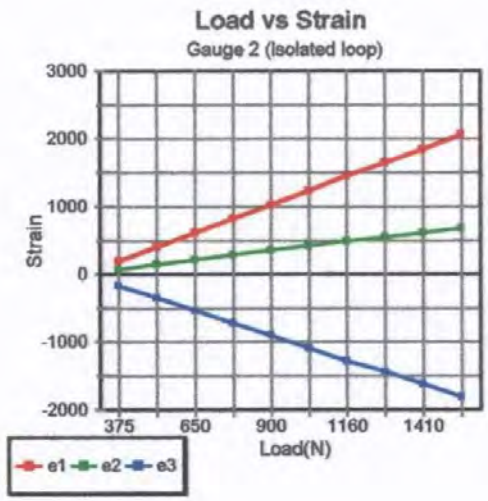

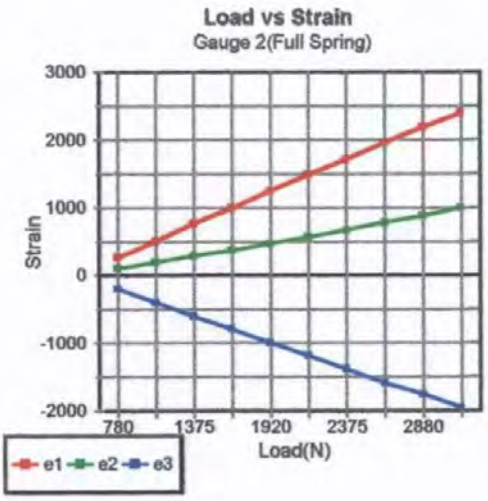

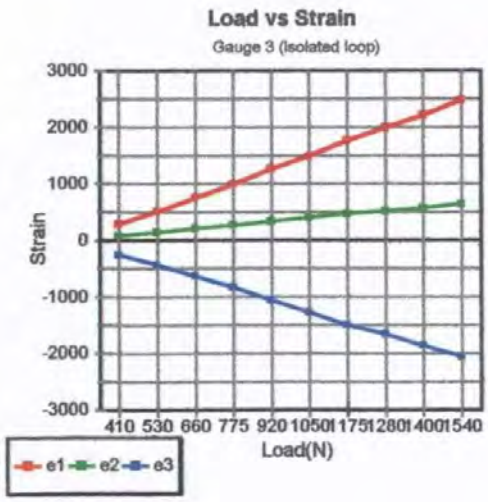

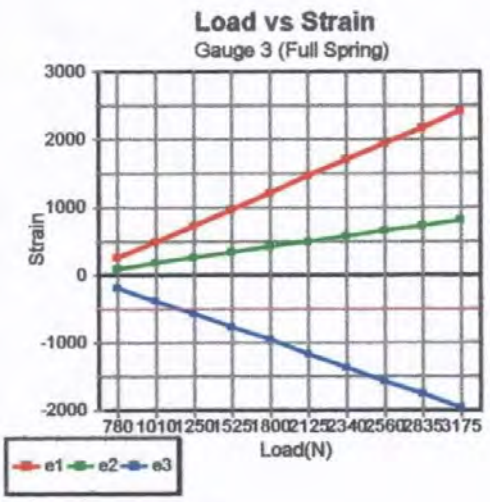

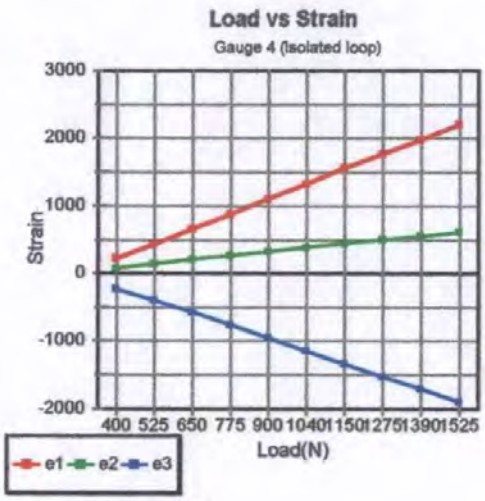
Load vs Strain
Gauge 4 (Isolated loop)
Strain
Load(N)
e1 e2 e3

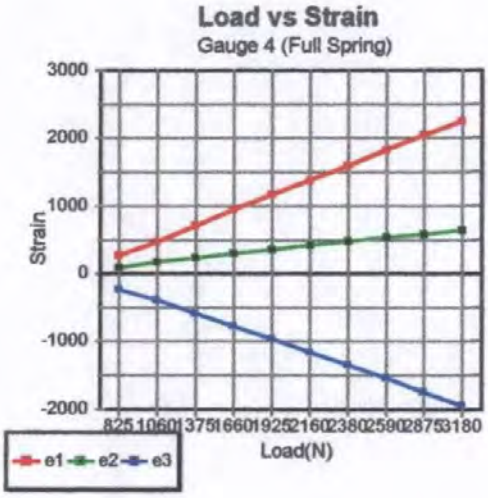
Load vs Strain
Gauge 4 (Full Spring)
Strain
Load(N)
e1 e2 e3

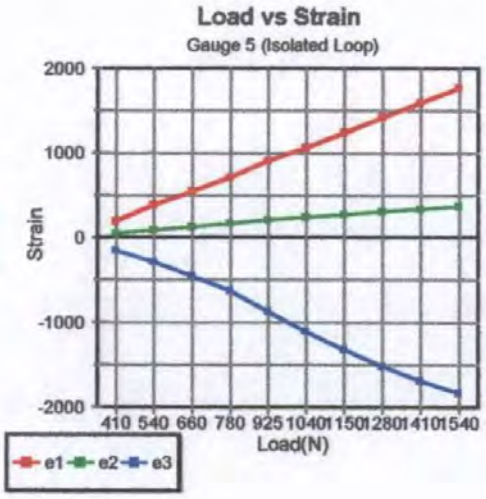
Load vs Strain
Gauge 5 (Isolated Loop)
Strain
Load(N)
e1 e2 e3

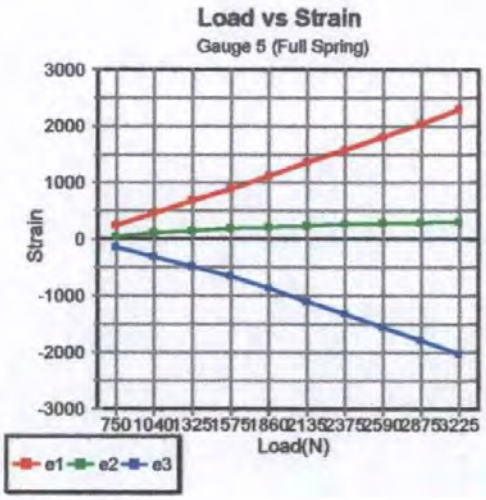
Load vs Strain
Gauge 5 (Full Spring)
Strain
Load(N)
e1 e2 e3

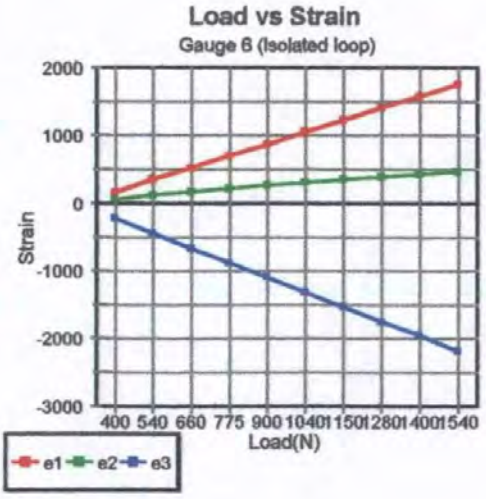
Load vs Strain
Gauge 6 (Isolated loop)
Strain
Load(N)
e1 e2 e3

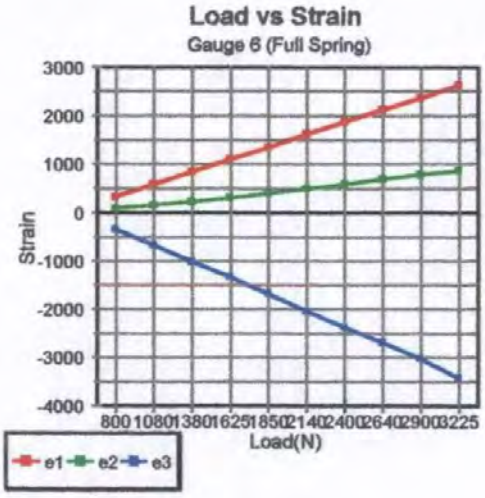
Load vs Strain
Gauge 6 (Full Spring)
Strain
Load(N)
e1 e2 e3

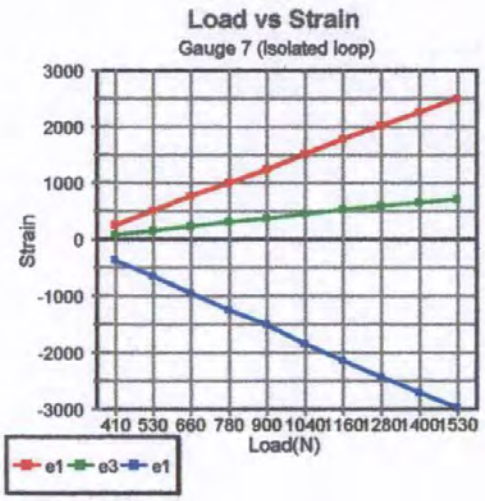
Load vs Strain
Gauge 7 (Isolated loop)
3000
2000
1000
0
-1000
-2000
-3000
Strain
410 530 660 780 900 1040 1160 1280 1400 1530
Load(N)
e1 e3 e1

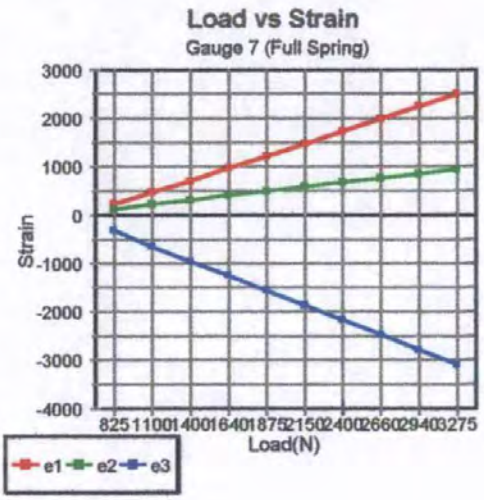
Load vs Strain
Gauge 7 (Full Spring)
3000
2000
1000
0
-1000
-2000
-3000
-4000
Strain
825 1100 1400 1640 1875 2150 2400 2660 2940 3275
Load(N)
e1 e2 e3

Figure 2: Principal stress versus deflection graphs for all gauge positions.

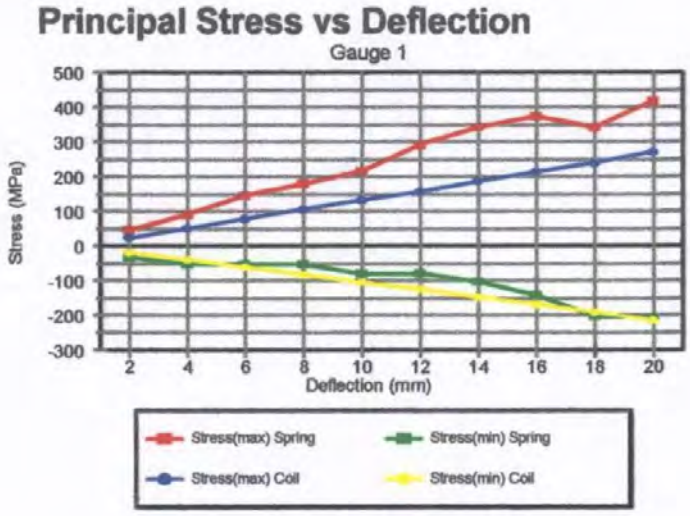

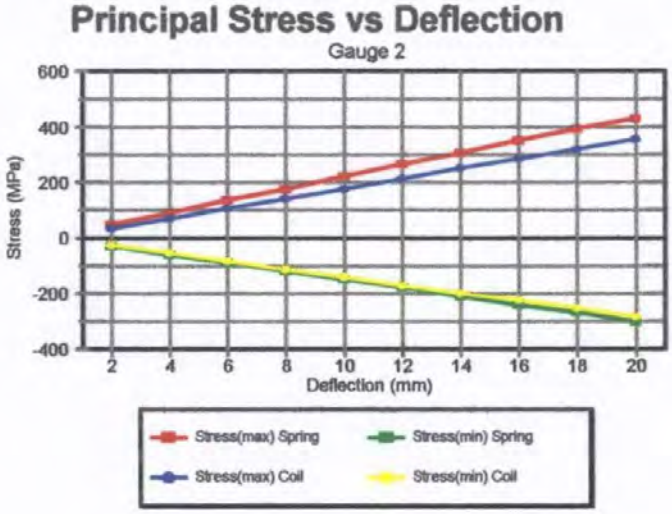

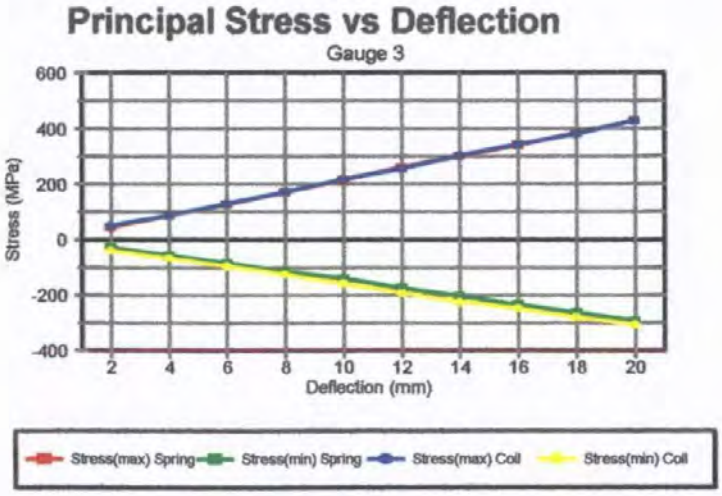

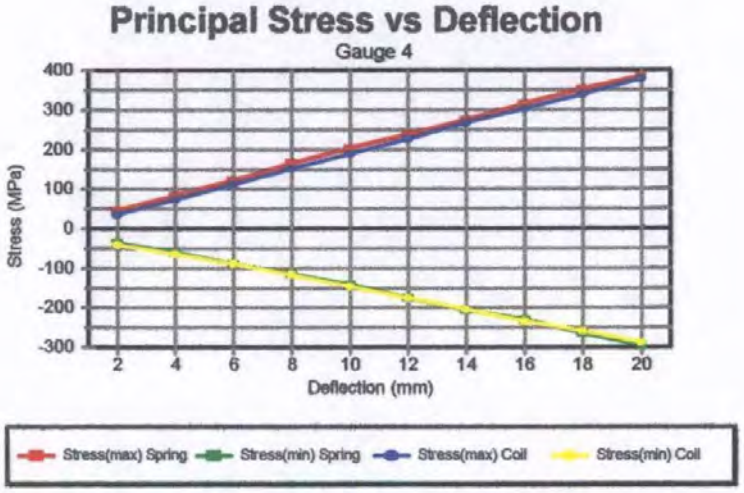
Principal Stress vs Deflection
Gauge 4
Stress (MPa)
400
300
200
100
0
-100
-200
-300
2
4
6
8
10
12
14
16
18
20
Deflection (mm)
Stress(max) Spring
Stress(min) Spring
Stress(max) Coil
Stress(min) Coil

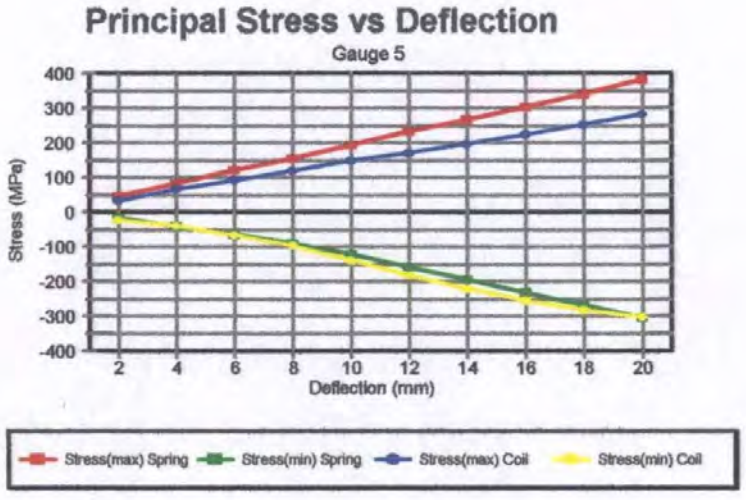
Principal Stress vs Deflection
Gauge 5
Stress (MPa)
400
300
200
100
0
-100
-200
-300
-400
2
4
6
8
10
12
14
16
18
20
Deflection (mm)
Stress(max) Spring
Stress(min) Spring
Stress(max) Coil
Stress(min) Coil

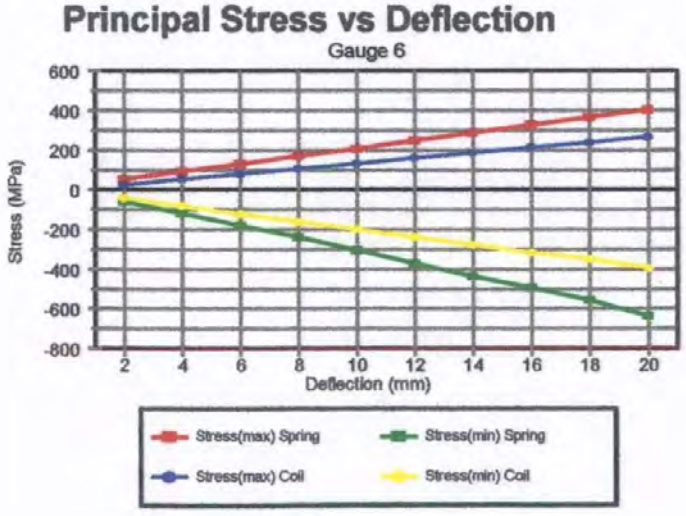
Principal Stress vs Deflection
Gauge 6
Stress (MPa)
600
400
200
0
-200
-400
-600
-800
2
4
6
8
10
12
14
16
18
20
Deflection (mm)
Stress(max) Spring
Stress(min) Spring
Stress(max) Coil
Stress(min) Coil

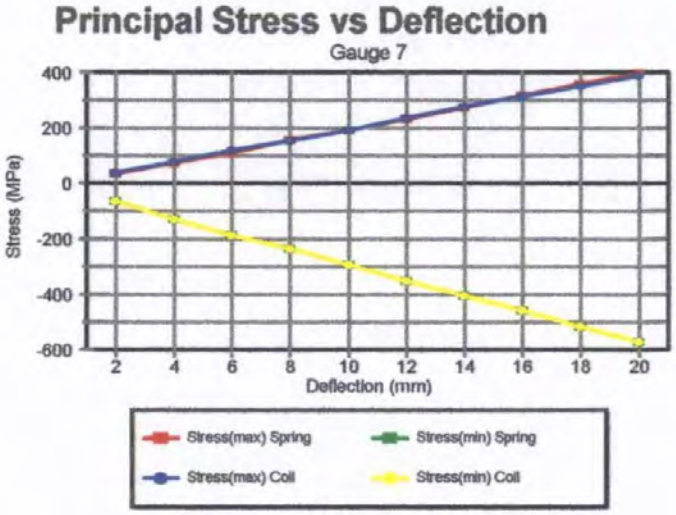
Principal Stress vs Deflection
Gauge 7
400
200
0
-200
-400
-600
Stress (MPa)
2
4
6
8
10
12
14
16
18
20
Deflection (mm)
Stress(max) Spring
Stress(min) Spring
Stress(max) Coil
Stress(min) Coil

APPENDIX - C

Calculation of residual stresses in a rectangular beam.

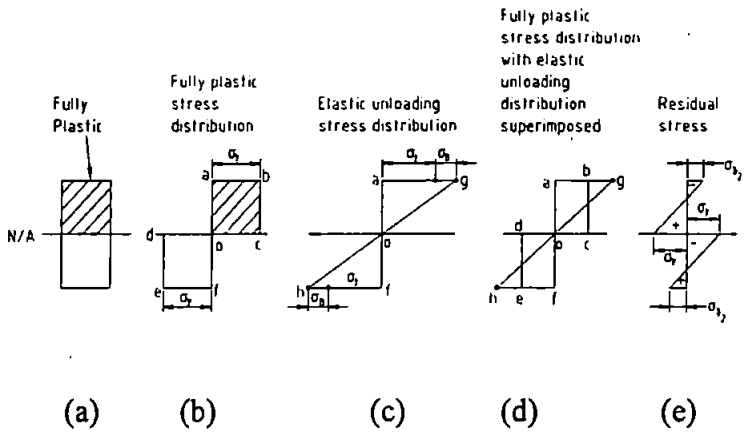

Figure 1: Stress distribution in a beam.

If the beam is loaded to a fully plastic state the stress distribution will be as represented by rectangles oabc and odef as illustrated in Figure 1(b). Because of permanent deformation when the beam is unloaded, bending stresses are set up, which are then superimposed during the unloading (Figure 1(c)). The bending stresses are of opposite signs and will therefore be given by the line goh. If the stress distributions are superimposed as shown in (d) and subtracted, it will then reveal the residual stresses present which remain after unloading the plastically deformed beam as revealed by (e). If we want to quantify the values of the residual stresses, the loading and unloading moments must be equal, therefore the rectangle distribution oabc about the neutral axis must equal the Moment of the force due to the triangular distribution oag.

Therefore:

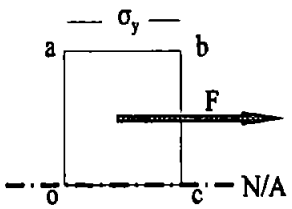

Moment of oabc = F × ½ oa

F = stress × area

Moment = stress × area × ½ oa

= ab × A × ½ oa.....1

(where A = area)

Moment of ▵oag:

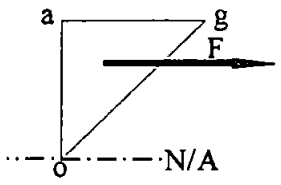

Moment = F × ⅔ oa

= Average stress × area × ⅔ oa

= ½ ag × A × ⅔ oa.....2

Now equating eq1 and eq2 :

ab × A × ½ oa = ½ ag × A × ⅔ oa

⅔ ab = ag

Now,

ab = σ_y (Yield stress)

Therefore,

ag = 1½σ_y

The residual stresses at outside surface (bg) = ½σ_y

and the residual stresses at the N/A (oc) = σ_y

In the case of partial plastic bending the maximum residual stress will not occur at the centre of the beam but may occur at either the outside or the inner boundary of the yielded portion, depending on the depth of plastic penetration.

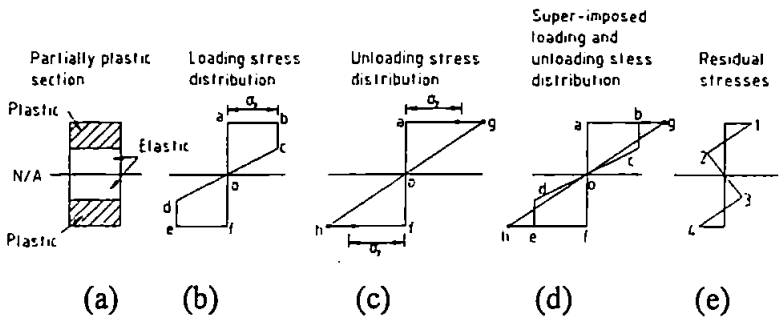

Figure 2: Stress distribution in a partial plastic beam.

There is no residual stresses at the centre of the beam. From Figure 2(e) we can see that the residual stress along the NA is zero, also that the residual stresses will be a maximum at the outside fibres at points (1) and (4) and at the inside fibres at points (2) and (3). The stress in the outside fibres ag is determined by considering the plastic moment M_{pp} applied to the beam, assuming it to be elastic; thus:

$$ag = \sigma = \frac{M_{yy}}{I} = \frac{M_{pp}}{I}\,\frac{D}{2}$$

Because of permanent deformation, beams which have been unloaded from plastic or partially plastic states, will be different from their original shapes. The moment needed at any section to return the beam to its original position, is that which is required to remove the residual stresses from the elastic core.

APPENDIX -D

Case study in applying the ASTM method for calculating residual stresses.

Case study

Consider the following example with respect to data reduction and data interpretation for a blind hole analysis.

Material: Cold rolled steel bar.

$E = 203$ MPa

$\upsilon = 0.29$

Drilled Hole ϕ: Do = 1.78 mm

Rosette ϕ: D = 5.13 mm

Ratio: $\frac{D}{Do} = 2.88$

Type rosette: TEA-06-062RK-120

Depth of drilled hole: z = 2.03 mm

After the gauge has been fixed and drilling equipment is aligned, we can follow the procedure as set out previously under determination of coefficient. After zeroing of the strain circuit the hole is drilled in increments and the following is recorded: Hole depth Z and strain values for ϵ_1, ϵ_2 and ϵ_3. See Table 1 for tabulation of results.

From the above data the percentage strain relieve can be calculated at each increment.

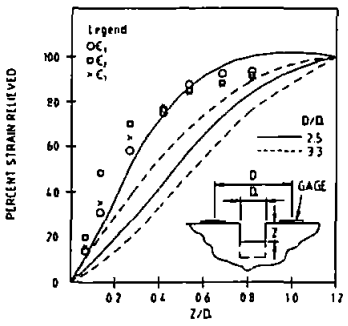

Figure 1: Normalised relieved strains compared to ASTM E837-94a.

(Illustration courtesy of the Micro Measurements division of Measurements Group Inc., Raleigh, NC, USA.)

Sample calculation

Take the full depth strain as representing 100% of strain relief (z = 2,03mm).

From this $\frac{Z}{Do} = \frac{2.03}{1.78} = 1.14$ (FULL DEPTH)

From Table 1 $\epsilon_1 = -152\ \mu\epsilon$

$\epsilon_2 = -42\ \mu\epsilon$

$\epsilon_3 = -85\ \mu\epsilon$ at $z = 2.03$ mm

The relieved strain at Z = 1.52 mm is calculated as follows:

$$\frac{Z}{Do} = \frac{1.52}{1.78} = 0.86$$

Relieved strain % $\epsilon_1 = \frac{\epsilon_1\ at\ Z = 1.52}{\epsilon_1\ at\ Z = 2.03} = \frac{-1.46}{-152} \times 100 = 96\%$

$$\epsilon_2 = \frac{\epsilon_2 \; at \; Z = 1.52}{\epsilon_2 \; at \; Z = 2.03} = \frac{-40}{-42} = 95\%$$

$$\epsilon_3 = \frac{\epsilon_3 \; at \; Z = 1.52}{\epsilon_3 \; at \; Z = 2.03} = \frac{-79}{-85} = 93\%$$

The above calculation procedure must be repeated for each set of readings recorded at each increment. The results for $\frac{Z}{Do}$ and for % relieved strains must then be tabulated as shown in Table 1.

In compliance with the recommendation in ASTM E837-94a the normalised strain is plotted versus $\frac{Z}{Do}$ on the graph shown in Figure 1. This is done to compare results to the published ASTM E837-94a scatter band.

From the graph it can be observed that the new data falls slightly outside of the scatter band. This indicate nonuniform residual stresses. For the purpose of this example lets ignore the scatter band comparison and assume a uniform stress distribution.

The coefficients $\bar{a}$ and $\bar{b}$ for this are determined with the aid of Table 2 in the ASTM 837-94a specifications.

For this case study: $\frac{Do}{D} = 0.347$

From ASTM E837 Table 2 for blind hole analysis the corresponding values for $\bar{a}$ and $\bar{b}$ for full depth of hole can be interpolated.

$$\bar{a} = O.155 \; at \; \frac{D_o}{D} = 0.347$$

$$\bar{b} = 0.370 \text{ at } \frac{D_o}{D} = 0.347$$

To find the $\bar{a}$ and $\bar{b}$ coefficients for the separate increments of hole depth one has to make use of the graphs as determined by Schajer by means of finite element-analysis as published Measurement Group TN-503-4 and also as in ASTM E837.

From these graphs determine the values for $\bar{a}$ and $\bar{b}$.

For $\frac{D}{Do}$ 2.88

$\frac{Z}{Do}$	$\bar{a}$	$\bar{b}$
0.07	0.016	0.031
0.43	0.109	0.215
0.86	#	#

Note: # Beyond the scope of the graph.

All values for $\bar{a}$ and $\bar{b}$ can be read off the graph and tabulated as shown by Table 1. Using these values for $\bar{a}$ and $\bar{b}$ and substituting it into equations (32) and (33) we can calculate the corresponding values of $\bar{A}$ and $\bar{B}$.

From equation (32) $\bar{a} = \frac{2E\bar{A}}{1 + \nu}$

$$\therefore \bar{A} = - \frac{1 + \nu}{2E} \times \bar{a}$$

From equation (33) $\bar{b} = 2E\bar{B}$

$$\therefore \quad \overline{B} = \frac{-\overline{b}}{2E}$$

[* Note: Coefficients $\overline{A}$ and $\overline{B}$ are always negative]

For $\quad \overline{a} = 0.155 \quad \overline{b} = 0.370 \quad E = 203\ GPa$

$\nu = 0.29$

$$\overline{A} = -\frac{1 + 0.29}{2 \times 203.55 \times 10^9} \times 0.155$$

$$= -4.91 \times 10^{-10}\ Pa^{-1}$$

$$\overline{B} = -\frac{1}{2 \times 203.55 \times 10^9} \times 0.37$$

$$= -9.09 \times 10^{-10}\ Pa^{-1}$$

Determine all coefficient $\overline{A}$ and $\overline{B}$ for the increments as well as $4\overline{A}$ and $4\overline{B}$ and write them into Table 1.

To find the maximum and minimum stress values we use equation (27) and (28)
e.g.

AT $\frac{Z}{Do} = 1.14 \quad \overline{A} = -4.91 \times 10^{-10} \quad 4\overline{A} = -19.64 \times 10^{-10} \quad \epsilon_1 = -152\mu\epsilon$

$\epsilon_2 = -42\mu\epsilon$

$\overline{B} = -9.09 \times 10^{-10} \quad 4\overline{B} = -36 \times 10^{-10} \quad \epsilon_3 = -85\ \mu\epsilon$

$$\sigma_{max/min} = \frac{\epsilon_1 + \epsilon_3}{4A} \pm \frac{\sqrt{2}}{4B}\sqrt{(\epsilon_1 - \epsilon_2)^2 + (\epsilon_2 - \epsilon_3)^2}$$

$$= +\ 166.609\ kPa$$

$$\therefore\ \sigma_{min} = +75{,}900\ kPa$$

Find α from equation (29): $\tan 2\alpha = \dfrac{\epsilon_1 - 2\epsilon_2 + \epsilon_3}{\epsilon_3 - \epsilon_1}$

$$\therefore \alpha = -33.18^\circ$$

Now from the general rules α refers to σ_{max}

since $\epsilon_3 > \epsilon_1$ [-85 >-152]

$\therefore \alpha_1 = -33^\circ$ from gauge (1) to σ_{max} .

By using this method the values for σ_{max}, σ_{min} and α can be determined for each increment.

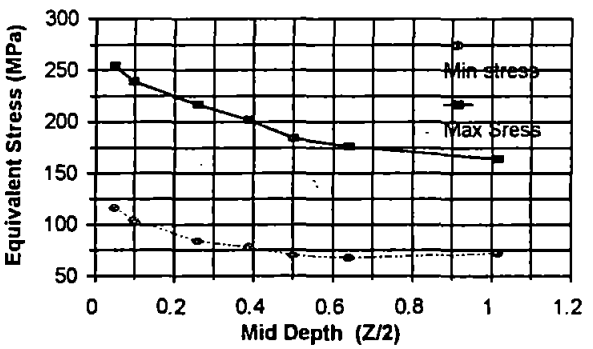

Figure 2: Equivalent stresses plotted at mid-depth.

At this point it is advisable to plot the maximum and minimum stresses (σ_{max},σ_{min}) for each increment *versus* the mid-depth of each increment (z/2) as shown in Figure 2.

From this graph it is quite obvious that the stress is not uniform but varies significantly with depth. For a uniform stress, two straight line graphs are expected.

From the data in Table 1 and the previous graph we can now attempt to calculate the "apparent" equivalent uniform stress for each increment.

If σ_n^1 = apparent equivalent uniform stress in the nth drilling increment

σ_n, $\sigma_n - 1$ = equivalent uniform stress from the surface depths z_n , $z_n - 1$ (σ_{max},σ_{min})

z_n , $z_n - 1$ = depths of drilling increments n and (n - 1).

$$\sigma_n = \frac{\sigma_n Z_n - \sigma_{n-1} Z_{n-1}}{Z_n - Z_{n-1}}$$

Sample calculation

	min	max
For n = 1	σ_n = 110 MPa	σ_n = 248 MPa
	σ_{n-1} = 0	σ_{n-1} = 0
	Z_n = 0.13 mm	Z_n = 0.13
	Z_{n-1} = 0	Z_{n-1} = 0
	$\therefore \sigma^1_{1min} = 1110\ MPa$	$\therefore \sigma^1_{1max} = 248\ MPa$
For n = 2	σ_n = 103 MPa	σ_n = 234 MPa
	σ_{n-1} = 110 MPa	σ_{n-1} = 248 MPa
	Z_n = 0.25 mm	Z_n = 0.25
	Z_{n-1} = 0.13	Z_{n-1} = 0.13
	$\sigma'_2 min = 95\ MPa$	$\sigma'_2 max = 219\ MPa$

The above calculation must be repeated for each point or increment; the data can be used to plot a graph of apparent stress *versus* depth increments.

The values for σ_{max} and σ_{min} as shown in Table 1 or as represented in the graph of equivalent uniform stress *versus* z/2 nor the data in the apparent stress graph represent the actual residual stress. This is only the case when the stress is uniformly distributed. However, the results are very useful in identifying the presences of non-uniform stresses and indicating the trend in stress distribution. If small increments were used and strain measurements done accurately, the data should yield a good estimate of the average stress in each increment.

TABLE 1

DEPTH		*MEASURED STRAIN* $\mu\epsilon$		*PERCENT* STRAIN RELIEVED	COEFFICIENTS Exponent of (10) $^{-10}$ with *A* and *B*				α	Equiv. Uniform Stress to Depth Z	
n) mm	Z/Do									σmin	σmax
0	0	ϵ_1	0	0	*a*	—	*b*	—	—	—	—
		ϵ_2	0	0	*A*	—	*B*	—			
		ϵ_3	0	0	4*A*	—	4*B*	—			
3 mm	0.07	ϵ_1	-23	15	*a*	0.016	*b*	0.031	-32°	110,320 +16	248,22 +36
		ϵ_2	-9	21	*A*	0,507 -0.035	*B*	-0.052			
		ϵ_3	-14	16	4*A*	-2,208 -0.140	4*B*	-0.210			
5 mm	0.14	ϵ_1	-49	32	*a*	0.037	*b*	0.067	-32°	103,425 + 15	234,43 +34
		ϵ_2	-21	50	*A*	-1,172 -0.081	*B*	-0.113			
		ϵ_3	-31	36	4*A*	-4,689 -0.324	4*B*	-0.453			
1 mm	0.29	ϵ_1	-90	59	*a*	0.077	*b*	0.147	-34°	82,74 +12	213,745 +31
		ϵ_2	-30	71	*A*	2,4399 -0.169	*B*	-0.248			
		ϵ_3	-55	65	4*A*	9,7597 -0.675	4*B*	-0.994			
6mm	0.43	ϵ_1	-118	78	*a*	0.109	*b*	0.215	-34°	75,845 +11	199,955 +29
		ϵ_2	-33	79	*A*	3,4539 -0.228	*B*	-0.363			
		ϵ_3	-68	80	4*A*	13,815 -0.911	4*B*	-1.453			
2 mm	0.57	ϵ_1	-136	89	*a*	0.131	*b*	0.27	-33°	68,950 +10	179,270 +26
		ϵ_2	-36	86	*A*	-4,151 -0.287	*B*	-0.458			
		ϵ_3	-73	86	4*A*	-16,604 -1.148	4*B*	-1.832			

7 mm	0.71	ϵ_1	-143	94 90	*a*	0.142	*b*	0.315	-32°	68,950 +10	172,375 +25
		ϵ_2	-38	89	*A*	-4,4996 -0.311	*B*	-7,7376 -0.532			
		ϵ_3	-76		4*A*	-17,9985 -1.244	4*B*	-3,095 -2.129			
2 mm	0.86	ϵ_1	-146	96	*a*	____	*b*	____	Beyond Range of graph		
		ϵ_2	-40	95	*A*	____	*B*	____			
		ϵ_3	-79	93	4*A*	____	4*B*	____			
3 mm	1.14	ϵ_1	-152	100	*a*	0.155	*b*	0.370	-33°	75,845 +11	165,480 +24
		ϵ_2	-42	100	*A*	-4.911	*B*	-9,0886 -0.625			
		ϵ_3	-85	100	4*A*	-19,6462 -1.356	4*B*	-36,354 -2.501	Coefficients *a* and *b* at full depth		
		ϵ_1			*a*		*b*				
		ϵ_2			*A*		*B*				
		ϵ_3			4*A*		4*B*				
	2	3		4	5		6		7	8	9

Data rounded for tabulation

e 1: Measured strain and calculated residual stress data

$D_o = 2$ mm; E = 203 MPa

$D/D_o = 2.88$; v = 0.29;

$$\frac{1+v}{2E} = 3{,}168 \times 10^{-9}$$

$$\frac{1}{2E} = 2{,}456 \times 10^{-9}$$

1Psi = 6,895 kN/m^2

Material: Cold rolled steel

APPENDIX - E

Principles of Photo-Elastic and X-Ray Diffraction

Techniques for the measurement of Residual Stresses.

INTRODUCTION

Residual stresses are difficult to measure since they are independent of the applied external load and they are imposed during the manufacturing or treatment processes. A wide range of methods have been used to measure residual stresses, with each method having a set of advantages or disadvantages for different applications.

The following are some of the methods that have been used in the past for measurement of residual stresses:

- Chemical etch
- Hardness studies
- Hole drilling
- Layer removal
- Magnetic method
- Modified layer removal
- Neutron diffraction
- Photo-elasticity
- Progressive turning
- Stress out brittle lacquer drilling
- Ultrasonic
- X-ray

The most frequently used techniques for the measurement of residual stresses are the hole-drilling and X-ray measurement techniques.

One of the biggest drawbacks of most of the methods mentioned is that they use destructive measuring techniques. Another problem is the mobility of equipment to do on-site measurements of residual stresses. The remainder of this paper will analyse the Photo-elastic

and X-Ray diffraction techniques.

1. PHOTO ELASTICITY

Photo elasticity stress analysis is a technique used for accurately measuring surface strains to determine the stresses in a part or structure during static or dynamic testing. It can be used to identify stress concentration, assembly stresses and residual stresses. Photo-stress coatings can be used on the surface of virtually any test part regardless of its shape, size or material composition. This technique has an established history of successful applications in virtually every field of manufacture.

1.1 Method of Application

The following is the sequence for application of this technique:

- A special strain sensitive plastic coating is first bonded to the test part.
- Service loads are applied to the part while the coating is illuminated by polarized light from a reflection polariscope.
- The part is viewed through a polariscope, the coating will display the strains in a colourful pattern that reveals the overall strain distribution.
- An optical transducer can be fitted to the polariscope for performing quantitative stress analysis.
- Video- or photo-recordings can be taken for permanent record of the overall strain distribution.

The operation of the technique can shortly be described as follows:

A light source emits waves containing vibrations in all perpendicular planes. The polarised filter will only allow one of the vibrations to be submitted. If V is the speed of light and C the airspeed, then the index of refraction will be equal to C/V. In a homogeneous body the index

is constant but in crystals the index depends on the orientation of the vibration with respect to the index axis. Certain materials e.g. plastic behaves isotopically when unstressed but become optically anisotropic when stressed. The change in index of refraction is a function of the resulting strain, analogous to the resistance change in a strain gauge.

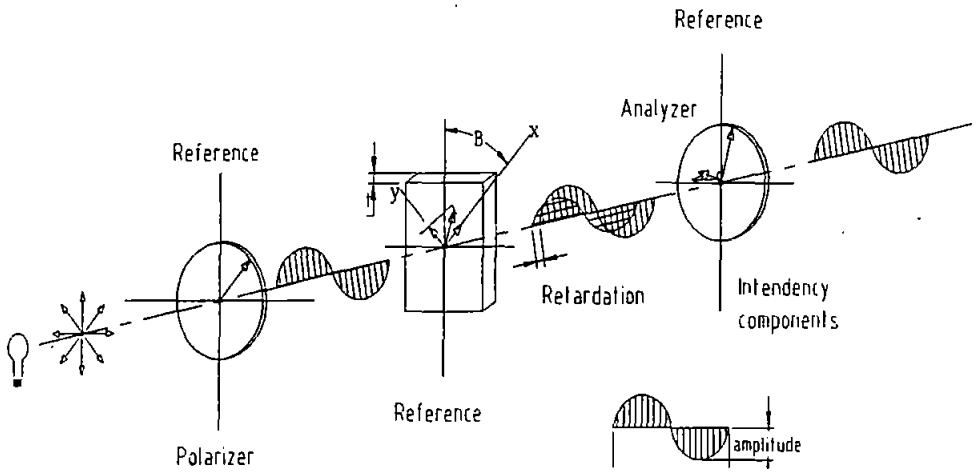

Figure 1: Schematic of the propagation of a polarised beam

With reference to Figure 1, when a polarised beam propagates through a transparent plastic of thickness t, where X and Y are the directions of principle strains at the point under consideration, the light vector splits and two polarised beams are propagated in planes X and Y.

Now if ϵ_x and ϵ_y is the strain intensity along X and Y and V_x and V_y the speed of light in these directions, the time taken to cross the transparent plate will be t/V and therefore the retardation between the two beams are:

$$\delta = C\left(\frac{t}{V_x} - \frac{t}{V_y}\right) = t\left(\frac{C}{V_x} - \frac{C}{V_y}\right) \quad \text{.....(1)}$$

and $\frac{C}{V}$ = Index of refraction (n)

$$\therefore \delta = t\,(n_x - n_y) \quad \text{.....(2)}$$

From Brewster's law: "The relative change in index of refraction is proportional to the difference of principal strains."

$$\therefore n_x - n_y = K(\epsilon_x - \epsilon_y) \quad \text{.....(3)}$$

K = Strain optical coefficient (similar to gauge factor of a strain gauge)

Substituting equation (3) into (2)

$$\therefore \delta = t\,[K(\epsilon_x - \epsilon_y)] \quad \text{.....(4)} \quad \text{for transmission.}$$

For reflection (light passes through plastic twice)

$$\delta = 2t\,[K(\epsilon_x - \epsilon_y)] \quad \text{.....(5)}$$

Therefor we can write the basic relation for strain measurement in Photo stress technique as:

$$(\epsilon_x - \epsilon_y) = \frac{\delta}{2tK} \quad \text{.....(6)}$$

Due to the relative retardation S, the two waves are no longer in phase when emerging from the plastic. The analyser will transmit only one component of each of these waves that will interfere and the resulting light intensity will be a function of retardation S, and of the angle between the analyser and direction of the principal strains $(\beta - \alpha)$.

The intensity of light emerging from a plane polariscope will therefore be:

$$I = a^2 \sin^2 2(\beta - \alpha) \sin^2 \frac{\pi\delta}{\lambda} \quad \text{.....(7)}$$

This intensity of the light becomes zero when $(\beta - \alpha) = 0$ or when the crossed polariser/analyser is parallel to the direction of principal strains. The plane polariscope is set to measure principal strain direction. If quarter-wave optical filters are added in the path of the light as shown in Figure 2, it will produce circularly polarized light and the image observed is not influenced by the direction of the principal strains.

Therefor: $I = a^2 \sin^2 \frac{\pi\delta}{\lambda}$

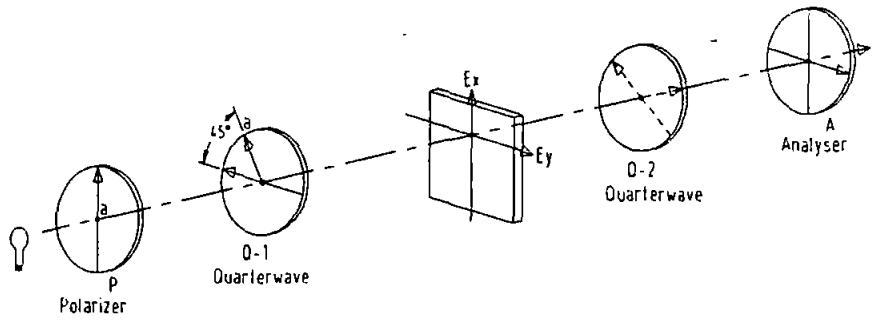

Figure 2: Circular Polariscope with quarter wave optical filters.

In the circular polariscope $I = O$ when $\delta = O$; $\delta = 1\lambda$, $\delta = 2\lambda$, ... , or $\delta = N\lambda$ N is the fringe order and it expresses the size of δ.

eg.: If for a selected wavelength $\lambda = 975\ mm$ and $N = 2$ then $\delta = 2\lambda = 1150$ mm

Once δ is calculated the difference in principal strains can be obtained by:

$$\epsilon_x - \epsilon_y = \frac{\delta}{2tK} = N\frac{\lambda}{2tK} = Nf$$

Where:f = fringe value (all constants)

N = result of measurement.

This is a very elementary description or explanation of polarized light principle used in photo elasticity, for a more comprehensive detail consult references listed.

1.2 INTERPRETATION OF STRAIN DISTRIBUTIONS

When an object coated with a photo-elastic coat is subjected to a load or loads the resulting strains are faithfully transmitted to the coatings. This will appear as iso-chromatic fringes when viewed with a reflection polariscope. At the start of applying a load to the part, fringes will first appear at the most highly stressed points and, as this load is increased, the fringes will be pushed to areas of low stress and new fringes will appear. Fringes are very ordered in the sense

that one continues and never cross or merge with another.

When observed with a reflection polariscope, the photo-elastic fringes appear as a series of different colour bands, responding to the underlying strain in the test part. Each of these colour fringes can be quantified as shown in Table 1:

Colour	Approximate Relative Retardation nm	Fringe Order N
Black	0	0
Grey	160	0.28
White	260	0.45
Pale Yellow	345	0.60
Orange	460	0.80
Dull Red	520	0.90
Purple (Tint of Passage)	575	1.00
Deep Blue	620	1.08
Blue-Green	700	1.22
Green-Yellow	800	1.39
Orange	935	1.63
Rose Red	1050	1.82
Purple (Tint of Passage)	1150	2.00
Green	1350	2.35
Green-Yellow	1440	2.50
Red	1520	2.65
Red/Green Transition	1730	3.00
Green	1800	3.10
Pink	2100	3.65
Pink/Green Transition	2300	4.00
Green	2400	4.15

Table 1: Quantification of colour fringes

Consider the following example of a cantilever form the Measurement Group Tech Note TN-702-1.

Figure 3 shows a beam coated on the one side with photo-elastic plastic and clamped to a table. A weight is hunged from the free end of the beam.

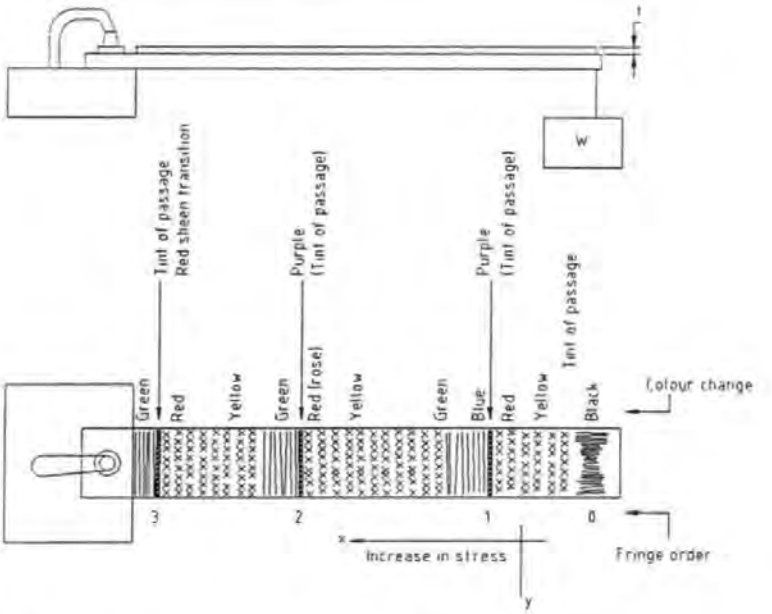

Figure 3: Beam subjected to photo elastic strain measurement.

Where: t = 2,54 mm

K = 0.15mm

λ = 575 mm for white light: $\therefore f = 754.6$ *μm/m/fringe*

FRINGE ORDER N	STRAIN (ϵ_x-ϵ_y = Nf) μm/m
0 BLACK	0
1 RED BLUE	754.3
2 RED GREEN	1509
3 RED GREEN	2271

When observed closely with the polariscope it can be seen that the retardation increases proportionally with strain.

The simple line relationship can be expressed as follows:

$$\epsilon_x - \epsilon_y = Nf$$

∴ In terms of shear strain τ_{xy}

$$\tau_{xy} = Nf$$

Where : τ_{xy} = maximum shear strain at any point

ϵ_x, ϵ_y = principal strains

N = fringe order

$$f = \frac{\lambda}{2tK}$$

λ = wave length (575 nm for white light)

t = thickness of coating

K = strain optical coefficient. of coating

The difference in principal strains, or the maximum shear strain in the surface of the test part, can be obtained by recognizing the fringe order and multiplying it by the fringe value of the coating. By Hooke's law the strain can be transformed to stress values in isotropic material by:

$$\sigma_x = \frac{E}{1 - \nu^2} (\epsilon_x + \nu\epsilon_y)$$

$$\sigma_y = \frac{E}{1 - \nu^2} (\epsilon_y + \nu\epsilon_x)$$

and $$\sigma_x - \sigma_y = \frac{E}{1 + \nu} (\epsilon_x - \epsilon_y)$$

$$\therefore \sigma_x - \sigma_y = \frac{E}{1 + \nu} Nf$$

Where: σ_x, σ_y = principal stresses in surface

E = elastic modulus of test part

ν = Poisson's Ratio of test part

Also $\tau_{max} = \frac{(\sigma_x - \sigma_y)}{2}$

$$\therefore \tau_{max} = \frac{1}{2}\left(\frac{E}{1+\nu}\right)Nf$$

The above is an introduction into strain and stress determination by the photo-elastic technique. It is a technique that has disappeared, but is slowly regaining its importance in stress distribution measurement. There are many new techniques and equipment available to the design engineer. The main disadvantage for measuring residual stresses are that it only considers surface stresses, but the method definitely holds promise for service or dynamic applications.

2. X-RAY DIFFRACTION

The principle of the x-ray methods for measuring residual stresses, one of the most highly developed non-destructive techniques available today will be reviewed in this part of the paper. Recent developments in this field have made field measurement possible, but it is still essentially a laboratory tool using high tech, expensive equipment. The technique of x-ray diffraction is mainly used for residual stress measurement in the surface that makes it essential that the thin layer under consideration reflects the true condition required for measurement.

The two main principles used in x-ray analysis are the diffractometer and the film approach. The x-ray technique has been in use for ± half a century and it is recognised as one of the standards to which other techniques must be compared. The characteristics of the method are that x-rays may be diffracted from metals under conditions which allow the use of distances between atoms as gauge lengths. From the measuring of the change in these interatomic distances the strain could be determined. The main difference between x-ray strain measurement and strain gauge measurement is that the x-ray only measures elastic while strain gauges measure elastic and plastic strains. The x-ray technique is one of a few methods that

can be used to measure residual stresses without cutting or drilling the specimen.

2.1 The principle of x-ray diffraction

The x-ray method measures the interatomic spacing of crystals which is in the order of 1 angstrom (1Å) or (1,57 x 10^{-10} mm). Taking into consideration that it is theoretically only possible to see objects larger than the wavelength of the light used for illumination, which is in the order of 2500Å. The wavelength of x-rays is ± the same as the atomic spacing in crystals.

To describe the mechanics of x-ray diffraction consider a hypothetical cubic crystal lattice fracture as shown in Figure 4 (edge view of a single lattice plane). The atoms is spaced in the lattice planes with an interatomic spacing *d* in the order of 1Å.

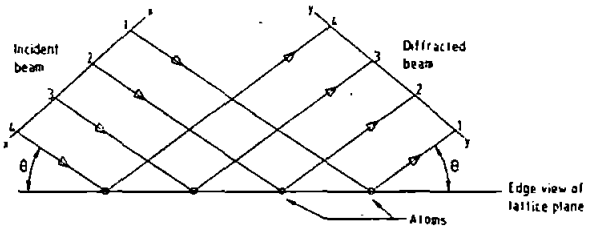

Figure 4: Schematic of a cubic crystal lattice fracture.
(Edge view)

It must be realised that most of the radiation from the incident beam will pass through the plane and only those beams which impinge on an atom will cause radiation of a small amount of diffracted x-ray energy. This diffracted energy or reflection of light produces the diffracted beam as illustrated in Figure 4. The length of the path of the beams from x - x to y - y is of the same magnitude. Now consider the case when diffracted beams from adjacent atomic planes are exactly in phase as illustrated in Figure 5.

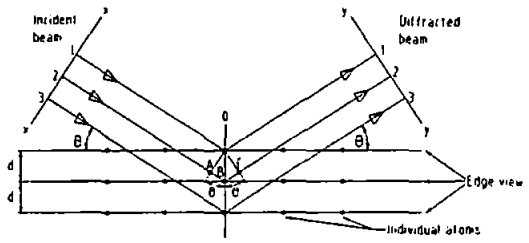

Figure 5: In-phase diffracted beams. (Edge view)

It can be observed in Figure 5 that in this condition where they are in phase the diffracted beams will reinforce each other. The length of e.g. path (2) between xx and yy exceeds the length of path (1) by distance AB +BC. Considering the right triangles AOB and BOC the difference in path length can be calculated as 2d sin ⊖.

$$\frac{AB}{d} = \sin\theta$$

$$\frac{BC}{d} = \sin\theta$$

$AB + BC = 2d\sin\theta$.

In order for path (1) and (2) to be in phase at yy, it is necessary that the lag of path (2) radiation correspond to some integral number (n) of wave lengths.

Therefore : $n\lambda = 2d\sin\theta$ .....(1)

Where: λ = wavelength of x-ray radiation

This equation (1) is known as the Bragg equation. From this it is clear that the radiation path (2) lags exactly $n\lambda$ behind path (1) and path (3) will lag by $2n\lambda$ behind (1).

For x-ray technique Bragg equation holds the key to stress determination. It can be explained

as follows: Any change to the value of *d* due to strain will cause sinθ to change correspondingly in order to keep n at its precise integral value needed for maximum strength of the diffracted beam. The x-ray diffraction wavelength used must be selected to put θ in the general range of close or about 90°. This will have the effect that any small change to sinθ will cause a relatively large change to θ. This is of utmost importance for experimental accuracy as the change in d for steel is very small. A change of 0,1% in steel subjected to 210 MPa uniaxial stress is common. To illustrate this point lets consider the graph in Figure 6.

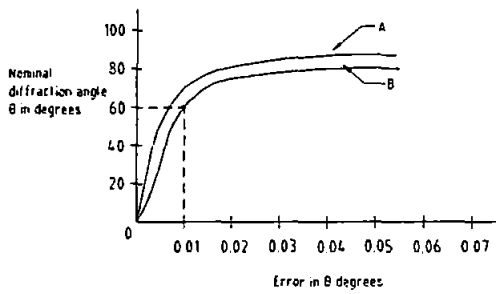

Figure 6: Effect of change in "d" on uniaxial stresses

A ⇒ 0,005% error in d ⇒ 10,59 MPa error in uniaxial stress

B ⇒ 0,01% error in d ⇒ 21,18 MPa error in uniaxial stress

The graph shows the relationship between θ, error in θ and the resulting error in the component value of d. It is also clear from the graph that best results will yield with a relative diffraction angle of above 80°.

Consider the following where surface residual stresses in a round shaft is determined assuming the surface residual stresses to be tangential. Ideally a direct measurement of lattice spacing would be made but this is impossible because of physical interference of the specimen with diffracted beam as shown in Figure 7.

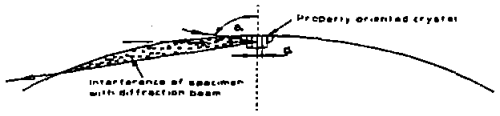

Figure 7: Required orientation of x-ray beams and lattice planes for direct measurement of dt for tangential strain.

The above problem can be solved by making two separate x-ray determination at two different angles $\theta\perp$ and $\theta\psi$. The two exposure x-ray diffraction involves the following: First a perpendicular exposure with ray bisector perpendicular to the surface giving a diffraction angle of $\theta\perp$ is made, this is followed by an angle exposure with ray bisector at angle ψ giving a diffraction angle of $\theta\psi$. This is shown in Figure 8. By determining the diffraction angles $\theta\perp$ and $\theta\psi$ the lattice spacing d_1 and d_4 can be determined using the principle of Bragg's equation.

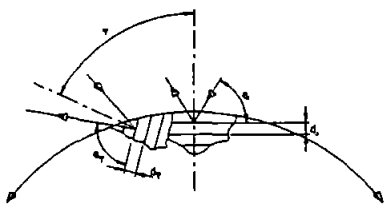

Figure 8: Two exposure x-ray diffraction method showing the relation for perpendicular exposure to angled exposure.

From the elastic theory the stresses parallel to the surface and in the plane of the paper can be calculated:

From: $$\sigma = \frac{E}{1+\nu} \cdot \frac{1}{\sin^2\psi} \cdot \frac{d\psi - d\perp}{d\perp}$$

Consider the following explanation for determining the stress components using the above stress equation and the polygon of strain in Figure 9.

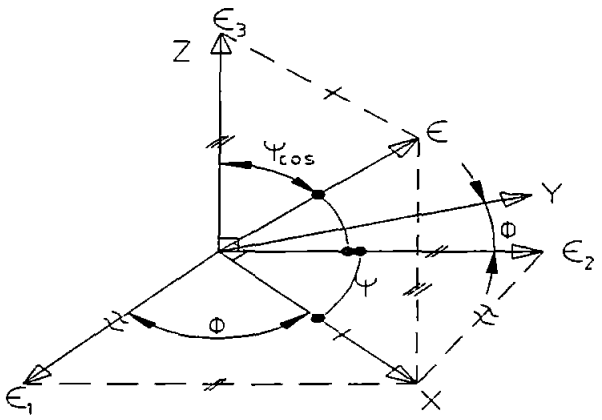

Figure 9: Polygon of strains.

If d_2 and d_0 are values for the spacing in a stressed and unstressed body the strain:

$$\epsilon = \frac{dz - do}{do}$$

This is the average strain in the direction midway between diffracted beams and the direction normal to the surface. If the diffracted beams are nearly perpendicular to the surface they approximate the strain normal to the surface, therefore the principal stresses:

$$\sigma_1 + \sigma_2 = \frac{-\epsilon E}{\nu}$$

Where E = Young's Modulus and ν = Poisson's ratio

For uniaxial stresses $\sigma_2 = 0$ and for biaxial stresses produced by torsion $\sigma_1 = -\sigma_2$.

The above method can be used to indicate generally the magnitude and distribution of biaxial stresses only. The stress in any direction in the plane of the surface, either in the direction of the principal stress, or otherwise, can be calculated from the following equation, derived from the approximate equation.

$$\epsilon = a_1^2\epsilon_1 + a_2^2\epsilon_2 + a_3^2\epsilon_3 \quad \ldots\ldots\ldots (2)$$

Where a_1 , a_2 and a_3 are the direction cosines of the measurement direction of ϵ with respect to ϵ_1 ,ϵ_2 and ϵ_3. In Figure 9 the notation is as follows:

$$a_1 = \sin\psi\cos\phi \quad \ldots\ldots\ldots (3)$$
$$a_2 = \sin\psi\sin\theta \quad \ldots\ldots\ldots (4)$$
$$a_3 = \cos\psi \quad \ldots\ldots\ldots (5)$$

Substitute equations (3), (4) and (5) into equation (2):

$$\epsilon = (\sin\psi\cos\phi)^2\epsilon_1 + (\sin\psi\sin\phi)^2\epsilon_2 + \cos^2\psi\epsilon_3$$

$$\epsilon = \sin^2\psi\ (\cos^2\phi\epsilon_1 + \sin^2\epsilon_2) + \cos^2\psi\epsilon_3 \quad \ldots\ldots\ldots (6)$$

ϵ_x is at an angle ϕ to principal strain ϵ_1

$$\therefore\ \epsilon_x = \epsilon_1\cos^2\phi + \epsilon_2\sin^2\theta \quad \ldots\ldots\ldots (7)$$

$\therefore$ Equation 6 now becomes:

$$\epsilon = \epsilon_x\sin^2\psi + \epsilon_3\cos^2\psi$$

$$\therefore\ \epsilon = \epsilon_x\sin^2\psi + \epsilon^3 - \epsilon_3\sin^2\psi \quad \ldots\ldots\ldots (8)$$

from $\cos^2\psi = 1 - \sin^2\psi$

NOW:

$\sigma_z = 0$ at surface of x-ray reflection

$$\therefore\ E(\epsilon - \epsilon_3) = [\sigma_x - \nu\sigma_y + \nu(\sigma_x + \sigma_y)]\sin^2\psi$$

$$= (1 + \nu)\ \sigma_x\sin^2\psi \quad \ldots\ldots\ldots (9)$$

Where:

$$\epsilon - \epsilon_3 = \frac{d\psi - do}{do} - \frac{dz - do}{do} = \frac{d\psi - dz}{do}$$

Now if the unstressed lattice spacing do is replaced by dz and it is considered to have negligible influence we can rewrite equation (9) as:

$$\sigma_x = \frac{E}{1 + \nu} \cdot \frac{1}{\sin^2\psi} \cdot \frac{d\psi - dz}{dz} \quad \ldots\ldots\ldots (10)$$

This is the stress component parallel to the surface, in the direction towards which the initial beam was tilted. It is not necessarily one of the principle stresses.

By adapting equation (10) to suit the original example of the round bar:

$$\sigma = \frac{E}{1 + \nu} \cdot \frac{1}{\sin^2\psi} \cdot \frac{d\psi - d_\perp}{d_\perp}$$

We can now also express the stress in terms of the diffraction angles:

$$\sigma = \frac{E}{1 + \nu} \cdot \frac{Cot\theta(\theta_\perp - \theta\psi)}{\sin^2\psi}$$

Where θ = nominal diffraction angle for unstrained material θ

$\theta_\perp - \theta\psi$ = change measured in radians

It must be noted that the above principle is based on the fact that the structure of the material is composed out of extremely small crystals of random orientation as shown in Figure 8. The interference of the specimen usually limits angle ψ to $\pm 60°$. This will cause some reduction in precision.

It should be noted that the stress can be computed by this equation without determining the lattice spacing in the unstressed condition. There is thus no need to cut or otherwise to reduce

the stress to zero in the specimen. The formula used for calculating the stress at an angle ϕ to the principal stress is:

$$\theta_{\phi} = \frac{E}{1 + \nu} \cdot \frac{1}{\sin^2\psi}$$

Consider the following explanation:

According to Bragg's Law $\lambda = 2d \sin\theta$ for an incident x-radiation of wave length λ which strikes a specimen at angle θ. The interplanar spacing *d* of the grains will cause diffraction at the same angle. Consider Figure 10 where the surface stress is in compression.

The only x-ray beams refracted onto the detector are those which impinge on grains with planes

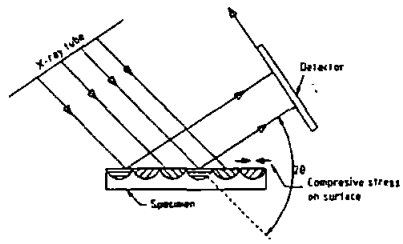

Figure 10: Schematic of diffractometer (compressive surface). Polygon of strains.

parallel to the sample surface and with atom spacing of "*d*" which then satisfy Bragg's law. It is important to realise that the planes are further apart in cases of compression than in a free state. The "d" space can as previously be obtained from the peak in intensity *versus* scatter angle (e.g. 2θ and Bragg's Law). Typical graph of intensity *versus* increase in scatter angle 2θ is shown in Figure 11.

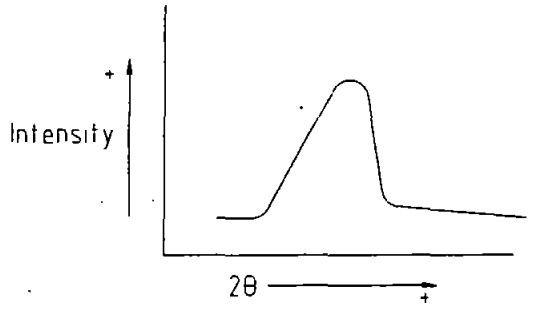

Figure 11: Intensity *versus* scatter angle.

The diffraction angle is a lot lower in the presence of surface stresses than without surface stresses because of Poison's effect on these planes. The sample or the x-ray can now be tilted as shown in figure 12, which will cause diffraction of the x-ray beams from different grains. This change in orientation will cause a change in d spacings and in θ.

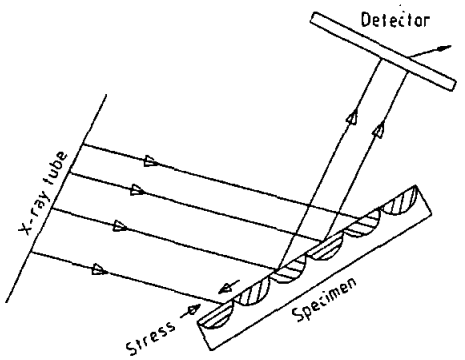

Figure 12: Effect of tilt of sample on x-ray beams.

Although diffraction occurs from other grains it is still from the same planes. These planes are now nearly perpendicular to the stress. Due to smaller influence of compressive surface stress on this orientation of planes, they are less separated causing the peak to occur at higher angles of 2θ.

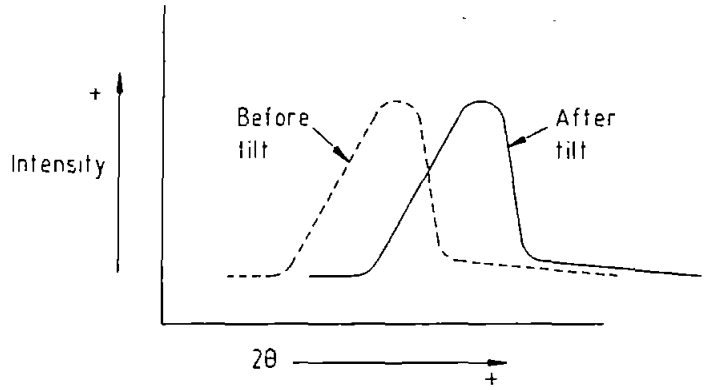

Figure 13: Effect of sample tilt on scatter angle.

The strain due to the residual stresses can now be measured from the angular shift due to the change in "d" spacings. It is only necessary to do measurements from different tilts and not necessary to determine the value of the "d" spacing in the unstressed material. If the measurement is only done on the surface so that stress components normal to the surface are zero and the material adheres to the isotropic elastic theory, the stress σ_ϕ at an angle ϕ to the principal stress can be calculated from:

$$0° = \left(\frac{1 + \nu}{E} \right) \sigma_\phi \sin^2\psi$$

Where E =Young's modulus

ν = Poisson's ratio

ψ = angle of tilt

This is based on the fact that the "*d*" spacing must be linear with sin2ψ and the stress is obtained from the slope. If this is verified for a specific case measurement at $\psi = 0°$, $\psi = 45°$, or $\psi = 60°$ must be made. It is now possible to combine the terms to write the stress in terms of the angular peak shift:

$$\sigma_\phi = K\Delta 2\theta \qquad When\ K = \left(\frac{E}{1+\nu}\right)$$

Peaks must be chosen at high values for θ because a given strain of $\Delta d/d$ causes the largest angular shift in such a region. Shift can easily be measured to $\pm 0.01°\theta$ and if $\psi = 45°$ for steel the uncertainty in peak shift relates to only ± 12 MPa stress uncertainty when a CrKα radiation is used with a 211 peak at $\theta = 78°$.

CONCLUSION:

Measurement of residual stresses with X-rays is a well established field. It is mainly applicable to crystalline materials having randomly oriented small grains. The specimen must be accessible to the x-ray beams that move in straight line, therefore deep notches or groves cannot be measured. The penetration of x-ray measurements is very shallow and therefore only suitable for surface stresses. The full principle, methods and the different techniques used in x-ray diffraction were beyond the scope of this document.

REFERENCES

Almen, John O., and Paul H. Black. "Residual Stresses and Fatigue in Metals. McGraw-Hill Book Company, New York, 1963.

Andrews, K.W. *et al.* "Stress measurement by X-ray diffraction using film techniques", Strain, 10(3), pp 111-116, July 1974.

Bowen, D.K. X-ray Topography of Surface Layers and Thin Films. In: Advances in X-ray Analysis. (C.S. Barrett, J.V. Gilfrich, R. Jenkins and P.K. Predicki, eds). Plenum, New York, 1990, vol. 33, p. 13.

Crites, Nelson A., and Alvin R. Hunter: Experimental Stress Analysis by Photo elastic Techniques, *Product Engineering* (Sept. 3, 1962).

Cullity, B.D. "Elements of X-ray Diffraction", 2nd ed. Addison, Wesley, Reading, Mass. 1978, Ch. 16, pp 447-479.

Dally, James W., and W. F. Riley: " Experimental Stress Analysis," McGraw-Hill Book

Company, New York, 1965.

Dölle, H. "Influence of Multiaxial Stress States, Stress Gradients and Elastic Anisotropy on the Evaluation of Stress by X-rays", J. Appl. Cryst., 12, 1979, pp 489-501.

Duffy, J., and T. C. Lee: Measurement of Surface Strain by Means of Bonded Birefringent Strips, SASA Proc., vol. 18, no. 2 (1961).

Durelli, A. J., and W. F. Riley: "Introduction to Photomechanics," Prentice-Hall, Inc., Englewood Cliffs, N. J., 1965.

French, D.N. and Macdonald, B.A. "Experimental methods of X-ray analysis", S.E.S.A., 26(2), 456-462.

Frocht, Max M.: "Photoelasticity," John Wiley & Sons, Inc., New York, vol. 1, 1941; vol. 2, 1948.

Hetényi, M.: The Fundamentals of Three-dimensional Photoelasticity, J. Appl. Mech., vol. 5 (1938).

Hetényi, M. (ed.): "Handbook of Experimental Stress Analysis," John Wiley & Sons, Inc., New York, 1950.

a Chap. 17-1, Fundamentals and Two-dimensional Applications [of Photoelasticity], by T. J. Dolan and W. M. Murray.

b Chap. 17-11, Three-dimensional Photoelasticity, by D. C. Drucker.

Hetényi, M. (ed.). "Handbook of Experimental Stress Analysis", John Wiley & Sons Inc., New York, 1950.

Heywood, R. B.: "Designing by Photoelasticity," Chapman & Hall, Ltd., London, 1952.

Horger, Oscar J. (ed.): "ASME Handbook: Metals Engineering-Design," 2d ed., McGraw-Hill Book Company, New York, 1965, part 5, sec. 3.4, Photoelasticity, by Max M. Frocht.

James, M.R. and J.B. Cohen. "Study of the Precision of X-ray Stress Analysis", Adv. in X-ray Analysis, 20, 1977, pp. 291-307.

James, M.R. and J.B. Cohen. "The Application of a Position-sensitive X-ray Detector to the Measurement of Residual Stresses", Adv. in X-ray Analysis, 19, 1976, pp 695-708.

James, M.R. and J.B. Cohen. "PARS - A Portable X-ray Analyzer for Residual Stresses", J. Testing and Evaluation 6, 1978, pp 91-97.

Kakudo, M. and N. Kasai. X-ray Diffraction by Polymers. Elsevier, Tokyo, 1972.

Kirk, D. "Experimental features of residual stress measurement by X-ray diffraction using film techniques", Strain, 10(3), July 1971.

Kirk, D. "Theoretical aspects of residual stress measurement by X-ray diffractometry", Strain, 6(2), 1970.

Lee, G. H.: "An Introduction to Experimental Stress Analysis," John Wiley & Sons, Inc., New York, 1950.

Macherauch, E. and U. Wolfstieg. "A Modified Diffractometer for X-ray Stress Measurements", Adv. in X-ray Analysis, 20. 1977 pp 369-377.

Moore, M.G. and Evans, W.D. "Mathematical correction for stress in removed layers in X-ray diffraction residual stress analysis", S.A.E. Trans., 66, pp 340-345, 1958.

Murakami, M.; A. Segmuller, K.N. Tu. X-ray Diffraction Analysis of Diffusion in Thin Films. In: Analytical Techniques for Thin Films. (K.N. Tu and R. Rosenberg, eds.) Academic Press, San Diego, 1988, p 201.

Rosenthal, and Norton. "A method of measuring tri-axial residual stresses in plates", Journal Welding Society, (Welding supplement, 1945), 24, 295-307.

Schwartz, L.H. and J.B. Cohen. Diffraction from Materials. Springer-Verlag, Berlin, 1987.

Segmuller, A. and M. Murakami. X-ray Diffraction Analysis of Strains and Stresses in Thin Films. In: Analytical Techniques for Thin Films. (K.N. Tu and R. Rosenberg, eds). Academic, San Diego, 1988, p. 143.

Segmuller, A. and Murakami, M. Characterisation of Thin Films by X-ray Diffraction. In: Thin Films from Free Atoms and Particles. (K.J. Klabunde, ed.) Academic Press, Orlando, 1985, p. 325.

Society of Materials Science, Japan "Standard Method for X-ray Stress Measurement", 1973. Supplement VI (K. Hayashi).

Society of Automotive Engineers, SAE Handbook Supplement J784a "Residual Stress Measurement by X-ray Diffraction", SAE, Inc. New York, 1971.

Speriosu, V.S., M.A. Nicolet, J.L. Tandon, and Y.C.M. Yeh. Interfacial Strain in AlGaAs Layers on GaAs. J. Appl. Phys. 57, 1377, 1985.

Toney, M.F. and S. Brennan. Structural Depth Profiling of Iron Oxide Thin Films using Grazing Incidence Asymmetric Bragg X-ray Diffraction. J. Appl. Phys. 65, 4763, 1989.

Vaughn, Dale A. and Nelson A. Crites: Measurement of Stress by X-ray Diffraction. Product Engineering, Sept 30, 1963.

Waisman, and Phillips. "Simplified measurement of residual stresses", S.E.S.A., II(2), 29-44.

Warren, B.E. X-ray Diffraction. Addison-Wesley, Reading, 1969.

Zandman, F., and H. M. Maier: Six New Techniques for Photo elastic Coatings, *Product Engineering* (July 24, 1961).

APPENDIX - F

PAPER 1

The analysis of process effects of 55Cr3 spring steel on residual stresses and the relation to fatigue properties.

The analysis of process effects of 55Cr3 spring steel on residual stresses and the relation to fatigue properties.

D.G. Hattingh and K.H. du Preez
Faculty of Mechanical Engineering, Port Elizabeth Technikon, Private Bag X6011, Port Elizabeth, South Africa
Email: danieh@ml.petech.ac.za
karl@ml.petech.ac.za

Abstract

The understanding of the relationship between fatigue life, process effects and residual stresses needs to be evaluated carefully before the manufacturing process can be optimised for enhanced quality and product characteristics. Residual stresses in manufactured components are those stresses that exist without prior application of service or external loads. Virtually all manufacturing and surface treatments will introduce residual stresses into a component which may either be beneficial or detrimental to the fatigue properties.

This paper investigates the mechanism that exists between fatigue properties and residual stresses and its relation to process effects by withdrawing samples from different stages of the manufacturing process. In order to measure the residual stresses present, the locked-in stresses must be relieved by removing material to enable a sensor to register the change in strain. These measurements were done by means of Centre Hole Drilling using an Air Abrasive Powder System and residual strain rosettes as sensors.

The results revealed the nature and magnitude of the stresses induced into each component by every manufacturing process and the relation these induced stresses have on the fatigue properties of the components. In the final analysis this research should reveal the relation and impact of the manufacturing processes on residual stresses and fatigue properties of 55Cr3 spring steel.

1. Introduction

Residual stresses are an ubiquitous phenomenon which has been given many names. Most processes will induce residual stresses[4,5,6] which include manufacturing processes and heat treatments. Residual stresses are receiving increased attention from the engineering research and design community because it is recognised that many opportunities for optimisation of design and manufacture leading to reduction of costs, are locked-up inside the correct understanding of residual stresses. Despite all the efforts, together with the

extremely large number of publications addressing residual stresses, it is still regarded as an area of uncertainty by most engineers.

There is therefore an urgent need for determining residual stress induced into manufacturing components together with the need for reliable non-destructive techniques for determining these stresses accurately. What makes the measuring techniques so important, is the fact that it is generally very difficult to determine residual stress by analytical and computational methods.

There are a number of techniques available for determining residual stress, each with its own set of advantages. Care should be exercised in selecting the technique to be used for measuring residual stresses for a specific application.

The test samples under consideration in this paper are 55Cr3 spring steel withdrawn at different stages of the manufacturing process. An important characteristic to consider when selecting a measuring technique is the hardness of the material. Due to this factor, most of the conventional methods for removing material was found to be unsuitable for spring steel. The air Abrasive Centre Hole drilling method (ACH) was selected to measure the residual stresses in the 55Cr3 spring steel samples specifically because of its ability to penetrate hard materials. It is believed that this method will induce negligible machinery stresses during the drilling process, because the inertia of the aluminium oxide power used is very low and cooling is effective when air is used as a transport medium from the abrasive powder[2].

The ACH method is a proven measuring technique which yields accurate and reliable results[2]. The above concept of the hole drilling method using strain gauges, was approved by ASTM and published in 1982 ASTM Book of Standards.

2. Nomenclature

D_o = hole diameter
D = gauge circle diameter
Z = depth of hole
E = Youngs' modulus
ā, b = data reduction coefficients
Ā, B = geometric constants
ACH = Abrasive Centre Hole Drilling
α = angle from first principle strain from first strain gauge
$\varepsilon_1, \varepsilon_2, \varepsilon_3$ = relieved strains
$\sigma_{max}, \sigma_{min}$ = maximum/minimum principal stresses
LT = Load Test
HS = Hot Scragg

3. Description of Equipment and Drilling Procedure

In order to measure residual stress, the locked-in stress must be relieved by means of the destructive removal of successive layers of material. The method

utilised as described in this document is the hole-drilling strain gauge method of stress relaxation, illustrated in the photograph in Figure 1.

Briefly summarised, the measurement procedure involves six basic steps:

1. A three element strain rosette is installed at the point where stresses are to be measured.
2. The three gauge grids are wired and connected to a static strain indicator.
3. A precision drilling guide is attached to the test component being tested and accurately centred over a drilling target on the rosette.
4. After zero balancing, a small hole is drilled through the centre of the rosette. The relieved strains are measured at three different depths, the final depth being 0.4D.
5. Readings are made of the relaxed strains, corresponding to the initial residual stress.

The foregoing procedure is relatively simple, and has been standardised in ASTM Standard Test Method E837.

Figure 1: Drilling of specimen

Introduction of the small hole into the test specimen is one of the most critical operations in the procedure. The hole should be concentric with the drilling target on the special strain gauge rosette. It should also have the prescribed shape in terms of cylintricity, flat bottom and sharp corner at the surface, as illustrated in the photograph in Figure 2 It is clear on the photograph that all the mentioned criteria were adhered to accepting the flat bottom of the hole. This characteristic is typical for small holes. An average depth was measured and used in calculation. This could result in variation of stress readings. Current

experimentation is underway in order to compare the current ACH results to a milling method utilising a Sint drilling device.

Figure 2: Hole cross section

4. Sample Preparation

Specimens were drawn from the standard spring manufacturing process line for 55Cr3 spring steel after the following stages :

1.	Hot coil and quench	2.	Tempering
3.	Hot scragg	4.	Shot peen
5.	Before load test (painted)	6.	Load test

5. Calculation of results

The following formulae were used:

$$A = \frac{1+\nu}{2E} \cdot a$$

$$B = \frac{1}{2E} \cdot b$$

$$\sigma_{max/min} = \frac{\varepsilon_1 + \varepsilon_3}{4A} \pm \frac{\sqrt{(\varepsilon_3 - \varepsilon_1)^2 + (\varepsilon_3 + \varepsilon_1 - 2\varepsilon_2)^2}}{4B}$$

$$\tan 2\alpha = \frac{\varepsilon_1 - 2\varepsilon_2 + \varepsilon_3}{\varepsilon_3 - \varepsilon_1}$$

Note: The constants a and b are determined according to ASTM E837-94a.

6. Results

6.1 Residual Strain Measurement and Stress Calculation

Manufacturing process : Quench									
Dia (mm)		**Depth**		**Measured Strain με**			α	**Uniform Sress (x10e6)**	
D_o	D_o/D	Z	Z/D	ϵ1	ϵ2	ϵ3		σ_1	σ_2
1.168	0.456	0.609	0.238	-331	-360	-344.5	-36.6	228	211
1.155	0.451	0.965	0.377	-286	-397	-346	-34.84	246	182
1.155	0.451	1.016	0.397	-330	-350	-343	-32.14	233	222
Manufacturing process : Before hot scragg (tempered)									
1.066	0.416	0.495	0.193	-21.5	-39.5	-36.5	-27.23	275	170
1.066	0.416	0.83	0.324	-27	-44	-43	-24.18	318	219
1.149	0.449	1.016	0.397	-42	-49	-47	-30.47	320	282
Manufacturing process : After hot scragg									
1.041	0.407	0.533	0.208	-25	-13	-36	-36.27	323	167
1.041	0.407	0.91	0.356	-35	-16	-32	-42.55	344	194
Manufacturing process : Shot peen									
1.023	0.340	0.533	0.208	611	665	647	-31.71	-511	-546
0.99	0.387	0.787	0.307	580	704	507	-38.59	-401	-553
1.02	0.397	0.914	0.357	679	796	676	-44.63	-517	-622
Manufacturing process : Before load test									
1.04	0.407	0.546	0.213	549	570	551	-43.56	-433	-450
1.04	0.407	0.81	0.316	539	507	474	-44.07	-393	-420
1.07	0.416	0.939	0.367	786	825	851	-5.65	-615	-642
Manufacturing process : After load test									
1.054	0.412	0.508	0.198	466	538	493	-38.50	-359	-410
1.016	0.397	0.787	0.307	684	766	940	9.88	-622	-743
1.079	0.422	0.939	0.367	565	649	627	-29.84	-432	-483
1.079	0.422	1.066	0.416	660	747	820	-2.50	-535	-601
(1+v) / (2E)		E (GPa)					v	D (mm)	
3.13e-12		206					0.29	2.56	

Table 1: Strain measurement and stress calculation

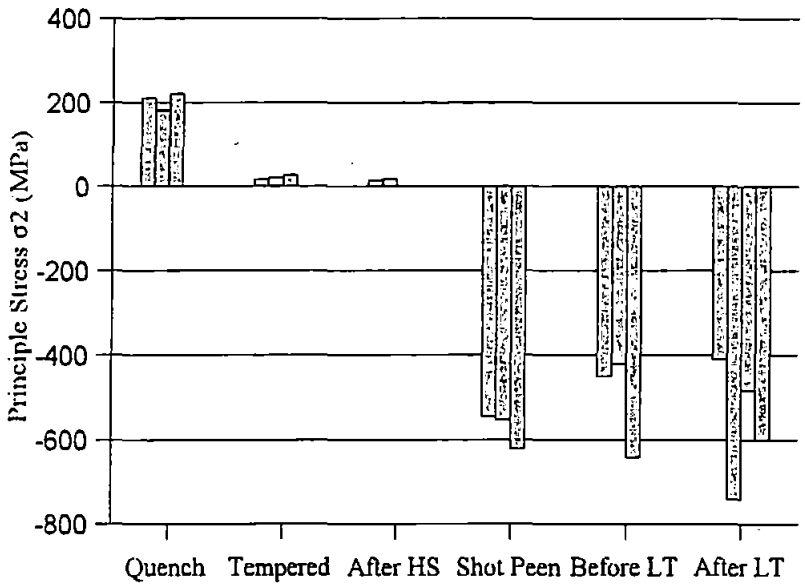

Figure 3: Process effects on principal stresses at different hole depths as indicated in table 2 (not fatigue tested)

	Quenched	Tempered	After HS	Shot Peened	Before LT	After LT
Hole Depths	0.609	0.495	0.533	0.533	0.546	0.508
	0.965	0.83	0.91	0.787	0.81	0.787
	1.016	1.016	-	0.914	0.939	0.939
	-	-	-	-	-	1.066

Table 2: Specific hole depths at different processes

6.2 Fatigue Test Results

From the graph shown in Figure 3 the following can be established:

1. Variation of residual stresses with depth of drilled hole for each process.
2. The change in the magnitude and type of residual stress.

The fatigue results and average hardness of the cross section of the sample are shown in Table 3.

Process stage	Cycles of failure (Avg)	Hardness (HRc)
Quench	737	61
Quench tempered	1 792	52
Hot scragged	2 315	51.6
Shot peen	2912710	52.7
Painted (Before LT)	3034650	52.7
Load tested	725480	52.2

Table 3: Relation between process effect, and fatigue cycles and hardness for 55Cr3 spring steel samples.

7. Discussion

7.1 Quenched Samples

It was evident from analysis done on failures of the above samples that all fatigue failures initiated near the surface[9] - thus indicating that mechanical defects played a more dominant role than non-metallic inclusions. From Figure 3 it can be seen that a tensile residual stress gradient was measured and it can be concluded that these tensile residual stresses in the surface promote fatigue initiations near the surfaces. Most of the residual stress was relieved before the hole depth reached 0.5 mm.

7.2 Quenched Tempered Samples

There was a slight increase in the fatigue resistance of the tempered samples but the fatigue initiation displayed the same phenomenon as the quenched sample. The tempering operation leads to a reduction of the tensile quench surface residual stresses but the result is still of a tensile nature and the dominant failure mechanism observed was a form of mechanical surface damage[9]. An important observation was that the decrease in magnitude of the tensile residual stresses lead to a slight increase in the fatigue resistance of these test samples. The variation of the tensile residual stress with a hole depth was very small and most of the stress was released before the hole depth reached 0.5 mm.

7.3 Hot Scragged Samples

The hot scragging process involves the compression of the component to solid length resulting in plastic work, thus creating residual stress that will resist sag of a coil spring. The resultant residual stresses after this, are still of a tensile nature but reveal very little change from the tempered samples. The fatigue life again increased slightly as indicated by Table 3 but overall was still very low. Variation of the residual stress with depth showed the same behaviour as the tempered

samples and the predominant cause of fatigue failure was still surface-related, although some failures revealed signs of a hydrogen blister[9].

7.4 Shot Peening

As illustrated by the graph in Figure 3, it is clear that the shot peening process induces significant compressive residual stress. This will ensure that a fully compressive residual stress state exists at the component surface and that any applied stress must now be superimposed on this compressive residual stress. This will result in an offsetting of the applied stress gradient and in effect will cause a more even tensile stress through the surface layer of the component. This is illustrated in Figure 4.

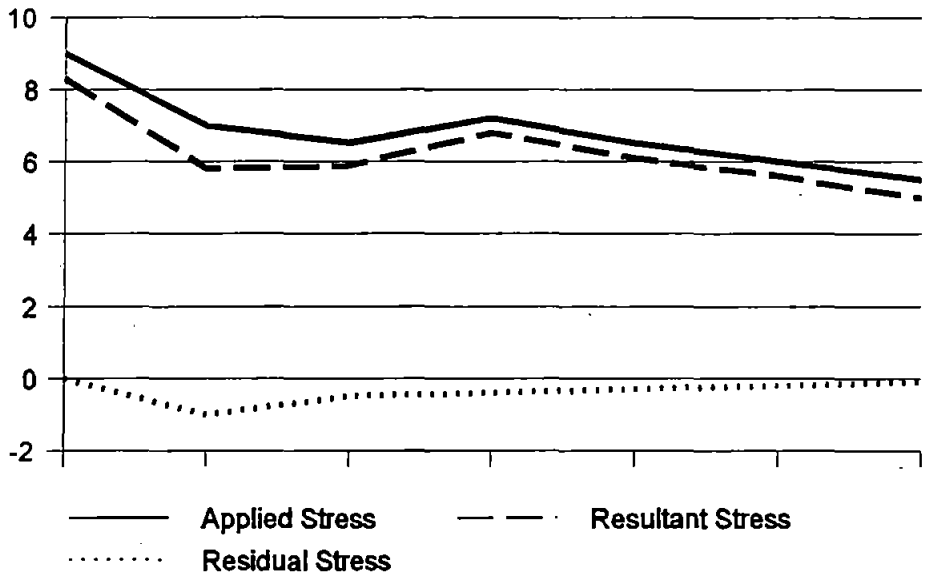

Figure 4: Effect of residual stresses on surface layer of component

By considering the fatigue results, it is clear that the shot peening process plays a major role in the increase of the fatigue life of the component. This increase in fatigue life coincides with the inducing of a significant large component of compressive residual stress in the surface. Failure analysis of the fatigue failures also reveals a shift away from surface initiates to sub-surface cause[9]. Initiations originated mainly from sub-surface inclusions. Most of the residual stress was released at 0.5 mm into the material.

7.5 Painted Samples

The painted samples revealed a compressive surface residual stress of similar magnitude as that of the shot peened sample. The increase in fatigue life was of a very small magnitude and could be considered as a negligible. The type of failure was very similar to that of the shot peened samples.

7.6 Load Tested Samples

The load test procedure can be considered as a cold scrag process. These samples reveal a very slight decrease in compressive residual stress but a substantial drop in fatigue resistance. This drop in fatigue resistance cannot be explained by the slight drop in residual stresses, but it is thought that the cold scrag set-in a certain amount of plastic deformation which adversely affects the fatigue life of the test sample. This is a phenomenon which needs further investigation. Failure analysis revealed that most failures occurred subsurface and a prominent characteristic of the fracture surfaces was the presence of axial growth[9].

In conclusion, the evidence is clear that compressive residual stresses near the surface are advantageous to the fatigue life of 55Cr3 spring steel. The shot peening process can be described as the most important process for inducing compressive residual stresses, which in turn contributes to a large increase in the fatigue life of the samples.

The mechanics of shot peening presents an exciting and challenging opportunity for research.

8. Conclusion

Process methods have major influences on the fatigue properties of 55Cr3 spring steel. It has also been revealed that there is a definite relation between the presence of compressive surface residual stresses and the improvement of fatigue results.

The air abrasive hole drilling method has proven to be an accurate method for determining surface residual stresses. The process has proved to be very effective on the very hard sample e.g. quench sample, which had a hardness of 61 HRC.

Typical problems encountered can be described as follows:

- Gauges had to be protected by a covering strip, as the abrasive nature of the over spray of aluminium oxide power, could cause deterioration of the gauge which will influence strain reading.
- Alignment of the drilling device was critical and time- consuming with the drilling of such small holes (0,9 mm to 1 mm in diameter).
- The strain amplifier must be well grounded or disconnected as a large build of static electricity can be experienced which could damage the amplifier cards during drilling.

Errors and uncertainties are always present to varying degrees in all measurement of physical variables. As a rule, their magnitudes are strongly dependant on the quality of the experimental techniques, as well as the equipment used.

9. Acknowledgements

1. Mr Mark Newby, ESKOM SA, for the use of equipment and expert assistance.

. Mr N Rafferty, VWSA, for the completion of the fatigue testing.

3. Federation for Research and Development and the Port Elizabeth Technikon for their financial assistance.

. Mr L Dockrey, National Springs, for the preparation of the samples.

10. References

1. Beany E.M. Accurate Measurements of Residual Stress on Any Steel Using the Centre Hole Method, *Strain*, 1976,12,99-106.

2. Bynum J.E. Modifications to the Hole-Drilling Technique of Measuring Residual Stresses for Improved Accuracy and Reliability, Experimental Mechanics, 1981, 21, 21-33.

3. Hattingh D.G. & Holman A.E.L. Observation of Fatigue Failures in 55Cr3 Automotive Coil Suspension Spring (Unpublished).

4. Perry C.C. Residual Stress ...the Nemises of the Liberty Bell, *Epsilonics*, 1983, 10-11.

5. Polakowski N.H. *Strength and Structure of Engineering Materials*, New Jersey, 1966, pp458-484.

6. Ragozin Y.I. & Polianin I.V. A New Express Method of Residual Stress Relief in Metals and Ceramics. Proceedings of the Fourth SEM International Conference on Residual Stresses, 1994, 23, 1300-1305.

7. Raleigh, N.C. *Measurement of Residual Stresses by the Hole-Drilling Strain Gauge Method*, Tech Note TN-503-4, Measurements Group, 1993.

8. Segal, A.M. & Tait R.B. *Residual Stress Evaluation Using the Air Abrasive Hole Drilling Technique*, R&D Journal, 1996, 12(2).

9. *Standard Test Method for Determining Residual Stresses by Hole Drilling Strain-Gauge Method*, E 837 - 94a, Annual Book of ASTM Standards, August 1994.

APPENDIX - G

PAPER 2

Observation of fatigue failures in 55Cr3 automotive coil suspension spring.

OBSERVATION OF FATIGUE FAILURES IN 55CR3 AUTOMOTIVE COIL SUSPENSION SPRING

Hattingh D.G.[1] Holman A.E.L[2]

Abstract

The understanding of the relationship between fatigue failure and process effects in spring steel components needs to be understood clearly before the manufacturing process can be optimised to produce coil springs for enhanced performance operating at increased stress levels.

The mechanisms responsible for component fatigue failure in a 55Cr3 automotive suspension spring steel have been investigated by subjecting coil springs, withdrawn from different stages of the manufacturing process, to fatigue tests. In this manner it has been ensured that all possible sources of fatigue initiation in this material batch have been identified, including those not dominant in the finished component. Fractographic analysis has revealed a number of sources of initiation, which are largely related to mechanical damage and inherent material defects.

The results indicate that decreasing defect levels in the material would represent a valid method for enhancing the fatigue response, specifically levels of non-metallic inclusions and surface mechanical damage.

1. Head of Mechanical Engineering, Faculty of Mechanical Engineering, PE Technikon, Port Elizabeth, South Africa

2. Researcher, School of Manufacturing, Materials and Mechanical Engineering, University of Plymouth, Devon, UK

Nomenclature

K = Wahl factor

D = Coil diameter (Mean)

d = Wire diameter

P = Spring load

τ = Induced stress

Introduction

World-wide government legislation and environmental considerations are demanding increasingly higher fuel economy from road vehicles. One way in which the motor industry is responding to this legislation is through an overall reduction in vehicle weight, thus requiring more efficient, lighter components, operating under increased working stress.

The production of a suspension spring working at increased stress levels yields a two fold benefit in fuel economy since the component is not only lighter but can be more compact thus aiding the reduction of vehicle frontal area and drag.

There are two major properties of spring materials which govern the useful life of the spring component and which must be carefully assessed in the development of any new design or manufacturing process, these being sag (or relaxation) resistance and resistance to fatigue.

This paper is concerned with the source of initiation of fatigue cracks in 55Cr3 spring steel components. To facilitate the initiation of fatigue cracks from a range of sources, fatigue tests were performed upon helical

coil springs drawn from several stages of the manufacturing process. In this way it has been possible to identify several sources of initiation, not all of which are dominant in the fatigue failure of finished components.

The steel spring manufacturing process

Incoming material is drawn to an area reduction of 15%. The drawn steel is then subjected to centre-less grind which reduces the diameter by 3%. This is done to reduce the decarburisation zone and to reduce surfaces damage inflicted during the steel manufacturing process.

The ground steel bar is austenised between 868°C and 880°C, hot coiled and then quenched in oil of which the temperature is maintained at 60 °C. After quenching, the component is tempered at 375°C for 90 minutes. The above process will produce coil springs with a grain size of 5 - 8 ASTM.

The component now goes through a process of hot-setting where by torsional residual stresses are induced. This is achieved by controlling the cooling after tempering, when the material temperature is between 180°C to 200°C it is scragged three times to its solid length. At this temperature the yield point of the material is lower so that during scragging the yield is exceeded. This results in a hysteresis effect which induces a torsional residual stress which will resist sagging of spring during service.

After scragging the component it is shot peened once only. This will induce a compressive residual stress on the surface that will offset any applied tensile stress, effectively increasing the fatigue life. The coil spring is now painted and finally it is subjected to a cold scragg and load test for rating purposes.

Stages of manufacture of fatigue samples:

Fatigue samples were withdrawn after the following stages of manufacture:

1. After Hot coil and quenching
2. After tempering
3. After Hot scrag
4. After shot peen
5. Before load test (painted)
6. After load test

For this work fatigue test samples were withdrawn on a random basis from the production line, five from each removal stage.

Fatigue test method

All fatigue tests were performed at Volkswagen SA quality assurance laboratory. The machine used was a "Coil Spring Fatigue Tester" Type: P137/1340/1-29 supplied by Rohloff, Germany, Figure 1.

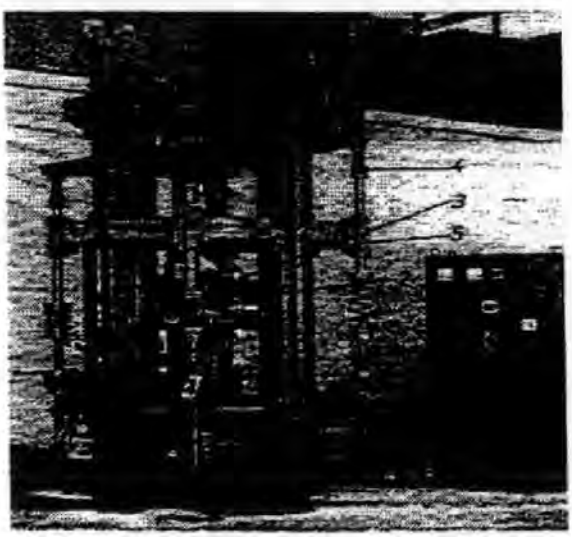

Figure 1 Fatigue test machine

The machine must be loaded with four springs simultaneously, uses an eccentric principle and is

Following process stage	Overall length* (mm)	Installed length** (mm)	Compressed length*** (mm)	Cycles to failure (N_f) (average)	Hardness (HRc)
Quench	396,5	376	176	737	61
Temper	396,5	376	176	1792	52
Hot scragg	346,5	326	126	2315	51.6
Shot peen	346,5	326	126	2912710	52.7
Paint	346,5	326	126	3034650	52.7
Load test	346,5	326	126	725480	52.2

*Overall length = Total length of coil spring
**Installed length = Length to ahead spring is compressed before fatigue test is command.
***Compressed length = Length to which spring is compressed during each fatigue cycle.

Table 1- Summary of spring dimensions following each processing stage

the machine automatically stops and a replacement sample must be installed to continue testing.

Test specification

Tests were performed according to the displacements given in Table 1.. The overall length of springs withdrawn after quenching and tempering was 50 mm longer than at later stages due to permanent deformation at the hot scrag stage.It was therefore necessary to adjust the test set-up for these samples in order to induce the correct stresses.

Springs where subject to a compressive stress range from 85.7MPa (min) to 951MPa (max.), calculated using standard theory[1,2,3] as follows:

$$K = \frac{4C - 1}{4C - K} + \frac{0,615}{C}$$

$$C = \frac{D}{d}$$

$$\tau = K\frac{8PC}{\pi d}$$

Analysis of fatigue failures

Seventeen of the twenty four fatigue failures were available for investigation and were analysed visually, optically and using a Phillips XL30 SEM. Some elemental analysis of particles was performed using a energy dispersive X-ray (EDAX) technique. Three of the eighteen inspected were damaged post fracture and were therefore beyond analysis. This post fracture damage can be attributed to the violent way the spring will leave the fatigue machine after fracture. Useful results were obtained using back-scatter image analyses, especially where prominent inclusions were present.

Position of failure in spring

The location of fatigue fracture were noted for each failure in turn of position on the complete spring. The majority of springs analysed, 12 out of 17, failed toward the ends of the component mainly within the first turn from the ends. In these areas the stress state is complicated due to a reduction in pitch designed to give the component parallel ends.

The remaining six failures occurred within the constant pitch section of the component and exclusively in components selected from after the shot peening process.

Macroscopic Observations

Three characteristic macroscopic fracture types were observed as illustrated in Figure 2

The dominant fracture was type I comprising of a fatigue crack site at approximately 45° to the wire axis and final fast fracture in a helical manner. Eleven of the eighteen failures analysed were of this type.

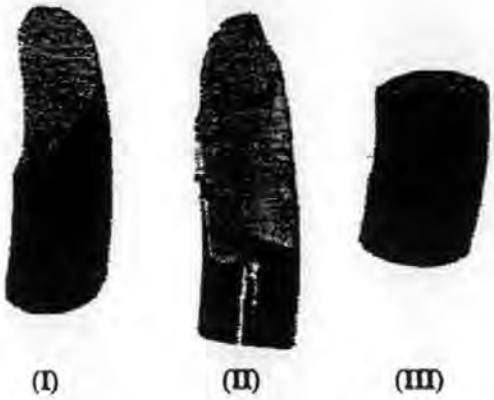

Figure 2. The three fracture types observed; (I) Helical, (II) Axial, (III) Torsional shear

A propensity towards, type II failure, essentially the same as type I with 45° fatigue crack and helical fast fracture, but with an intermediate axial crack growth was evident in four failures. Of these only one failure, number 17, exhibited an axial surface greater than 1 mm in length. In this case a significant seam was present in the material although the fatigue *initiation* did not occur at this feature. Three failures were of the torsional shear, type III, shape, characteristic of torsional shear.

Microscopic analysis

Three general causes of Fatigue initiation have been identified via optical and scanning electron microscopy, all being related to material and mechanical defects.

1) Failure from mechanical damage

Mechanical damage was the dominant cause of failure for coils drawn from before the shot peen process. Figure 3 shows an example of Fatigue initiation from mechanical damage in a quenched and tempered fatigue sample.

Only one case of fatigue initiation from surface damage in shot peened coils (or coils from later stages) was found. This case, in a shot peened sample, is illustrated in Figure 4. The indentation, Figure 4(a), is very large. Figure 4(b) also shows that a large particle has been driven into the coil surface. X-Ray analysis shows this particle to be composed essentially of Iron, but of markedly different composition to that of the matrix material

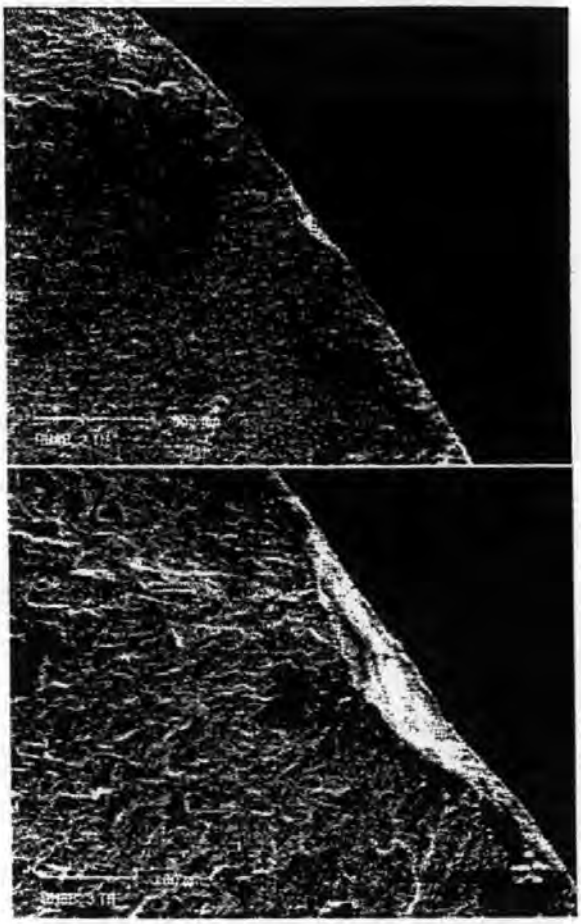

Figure 3. SEM micrographs - (a) Fatigue initiation at surface indentation in quenched and tempered sample.x50 (b) at x200.

Several coils failed from damage due to contact between the first coil and the coil end during fatigue testing. Figure 5 shows detail of the surface of coil 23 where this contact occurs. This example demonstrates the lack of sensitivity of post shot peened components to such damage since the test of this coil was suspended without failure at 6 million cycles.

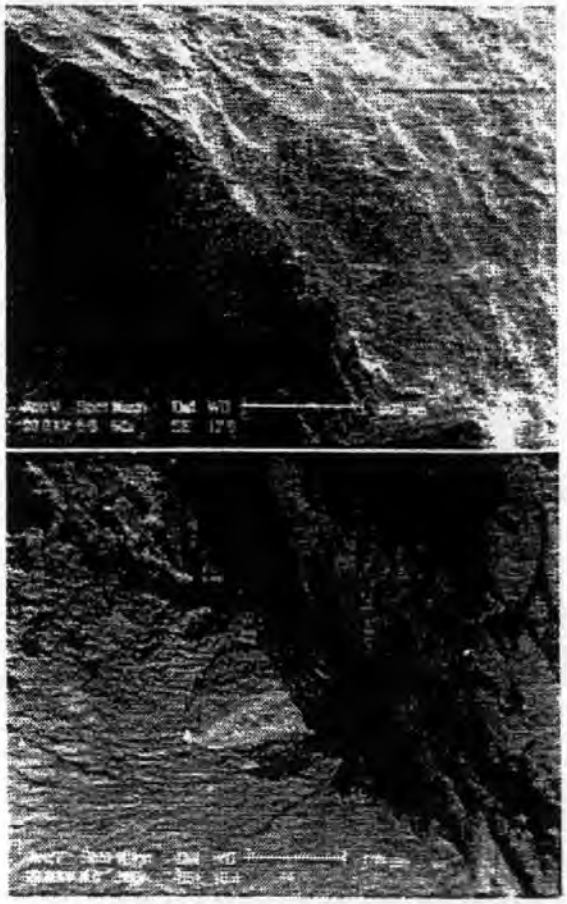

Figure 4. SEM micrographs - (a) Initiation at mechanical indent x50 and (b) Detail of particle x200

Figure5 Optical micrograph - Section - Mechanical damage due to clash of tail and first coil

2) Failure from non-metallic inclusions

In a previous analysis of fatigue failures of helical coil suspension springs [4] in a silicon manganese steel it was found that, in a batch of 28 fatigue tests, 61% of failures were inclusions related. One such failure is shown in Figure6.

Figure6. Fatigue initiation from a large non-metallic inclusion in a*silicon manganese*steel coil suspension spring

In the current tests 24% of failures have been analysed as originating at inclusions, therefore being significantly different. However it should be noted that the previous work was performed upon finished coils whilst the current work is concerned with coils drawn from various manufacturing stages. As an example, referring to Table 2, Appendix, it is seen that all failures in as quenched coils can be attributed to mechanical damage of the spring surface; only when the coils are tempered does the material become less sensitive to such damage and other failure types occur. In the current work 75% of failures of coils taken from after the shot peening process failed due to non-metallic inclusions. Thus it can be seen that the sole source of fatigue initiation in these coils springs has been mechanical defects and that in finished springs, presence of non-metallic inclusions becomes the dominant factor.

In the previous work it was noted that all failures were found to originate at or within approximately 20μm of the coil surface. This is to be expected since, for a bar in torsion, a stress gradient exists such that maximum stress exists at the surface, falling to nominally zero at the bar centre. However in this work two cases of fatigue failure from inclusions well within the material have been recorded, Figure 7(a),(b). In these two failures a large inclusion was

evident at the centre of a radial initiation at a depth of approximately 1mm.

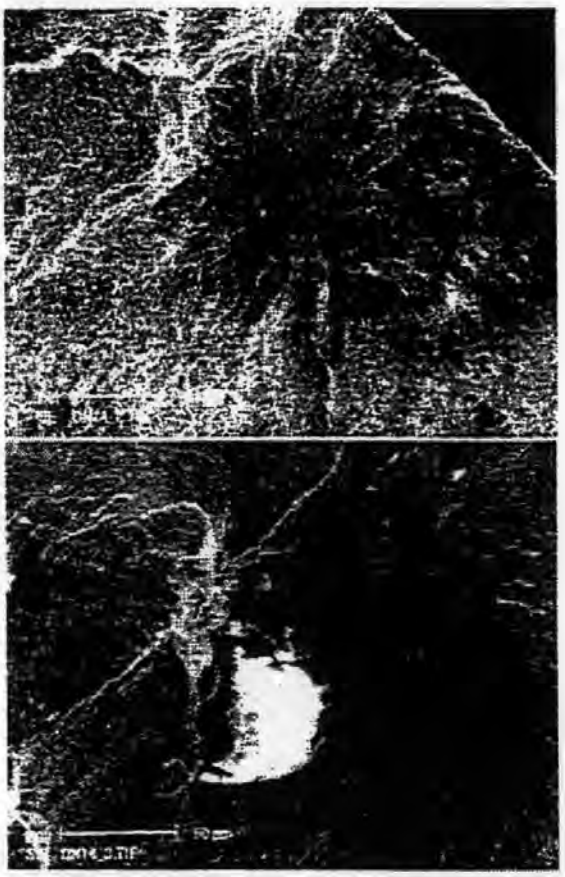

Figure 7 SEM Micrograph - Non-metallic inclusion at centre fo 'fish-eye' in shot peened sample. (a) x50 (b) x500

It would therefore seem possible that there is another mechanism evident which is related to that of non-metallic inclusion inclusions but, when present, is somewhat more insidious, namely hydrogen embrittlement.

3) Failure due to hydrogen embrittlement

Three of the twenty four failures analysed revealed evidence of Hydrogen embrittlement. This can clearly be seen from the "Fish eye" type initiation, shown in Figure 7(a) and (b), in a shot peened specimen. In addition Figure 8 shows a third fish eye fracture, found in a scragged coil failure, which shows no evidence of non-metallic inclusions.

All of these coils had been processed past the tempered stage, in the first case (No:12) was withdrawn after hot scragging, the second (No:14) after shot peening and the third (No:18) after painting.

Figure 8 Optical micrograph Fish-eye fracture with no inclusion evidence, x25

Hydrogen embrittlement[5,6,7] in this work, is the result of hydrogen absorbed throughout the metal at the molten stage. Sources of hydrogen are from moisture in the furnace atmosphere and additives to the melt. Insoluble hydrogen may be released around inclusions, precipitates and other discontinuities, perhaps forming local brittle ruptures, otherwise known as *blisters* or *flakes*.

Therefore the fish-eye fracture is often associated with an inclusion, as with the failures of test coils 14 and 18, see Table 2, Appendix. In failure 12 no evidence of an inclusion could be found, although the opposite fracture surface was not in suitable condition for analysis.

Discussion

A total of 24 fatigue tests were performed upon coil springs drawn from various stages of the manufacturing process. Of these coils, all fatigue test results were available but only 22 of the resulting failures were available for investigation. Only

seventeen of these were in suitable condition for successful analysis.

Effect of process upon fatigue response

Several sources of fatigue crack initiation have been identified in this experiment and, although not all are dominant in the finished component, some interesting trends have emerged. The sample size for each stage was four and this should therefore be considered before analysing the average fatigue performance figures presented in table 1.

In *as quenched* and *quenched and tempered* coils the cause of failure was found solely to be mechanical damage to the material surface. Despite a reduction in hardness during the tempering process, average fatigue life of tempered coils was significantly increased as expected. After subsequent processes the variation in measured hardness values proved insignificant.

The *hot scragg* operation is applied at the tempering temperature to coil springs manufactured from chromium steels in order to impart a degree of relaxation resistance to the finished component, however it is evident that the operation also has an effect in terms of fatigue performance, resulting in an average increase in fatigue life of approximately 28% over the quenched and tempered coils. In addition it was observed that subsurface fatigue initiation begins to occur only after this process; the effect of processing on the position of fatigue initiation is further discussed later.

The most significant process in terms of promotion of high fatigue life was that of *shot peening*, producing a massive increase in excess of one thousand-fold.

Coils withdrawn from after shot peening, or later stages, were found to fail predominantly from defects other than surface mechanical damage.

A further in fatigue performance was noted for *painted* springs although the increase can be regarded as insignificant due to the sample size..

The most surprising change in fatigue performance was observed for the final product, after *load testing*, resulting in a four-fold reduction in fatigue life. This stage consists of compressing each spring to solid height three times and is essential in order to ensure constant length of the finished components and for grading the final components into bands of equal stiffness. It is evident that a serious detrimental process is occurring at this stage and further investigation is in progress.

Position of failures

Of the 24 samples fatigue tested;

- One coil, drawn from the tempering stage, suffered a relaxation failure before fracture.
- Twelve were found to have fractured near to the end of the coil.
- One coil withstood six million cycles without failure.
- The remaining ten failures fractured in the main body of the component and were exclusively in components selected from after the shot peening process.

As discussed the stresses in a helical coil spring can be calculated using standard theory. For design purposes spring characteristics can be determined via standard formulae[1-3]. These formulae include a correction factor to accommodate the complex nature of stress in the helix which results in a higher stress on the inside of the coil, reducing towards the outside surface. There are two reasons for this

1. The torque moment results in a steeper twist angle for the short fibres at the inside

of the coil than for the long ones at the outside and thus produces a higher shear stress at the inside.

2. The axial load causes a direct shear stress which adds to the shear stress at the inside of the coil but is subtracted from the outside.

Considering this it would be expected that most coil failures should occur at the inside of the coil, whereas it was found that approximately 70% of failures occurred at the top or bottom of the wire.
Three reasons are suggested for this;

1. The bending element in this spring design is more significant than design formulae suggest, thus creating a peak combined stress at the top/bottom of the wire.
2. The standard design theory assumes the ideal situation where the coil is loaded perfectly axially. In reality this is never achieved, resulting in the introduction of a bending element.
3. Some damage to these (top and bottom) wire areas occurs during the scragging processes.

In addition it was noted that of the five failures from inside the coil, four occurred in shot peened coils. This would indicate that the shot peen coverage is reduced in the inward surfaces of the component due to shielding of these areas

Process, residual stress and fatigue

The fatigue and fractographic results presented can be compared to residual stress measurements made to the spring components from each manufacturing stage in order to clearly explain why variations in fatigue performances occur and, in particular, why coils from a given manufacturing stage are sensitive to specific defects. Figure 9 shows the results of preliminary work[8] to investigate the variation of residual stress profile after each process and the contribution of each stage to the composite residual stress, negative values representing a tensile residual stress and visa versa.

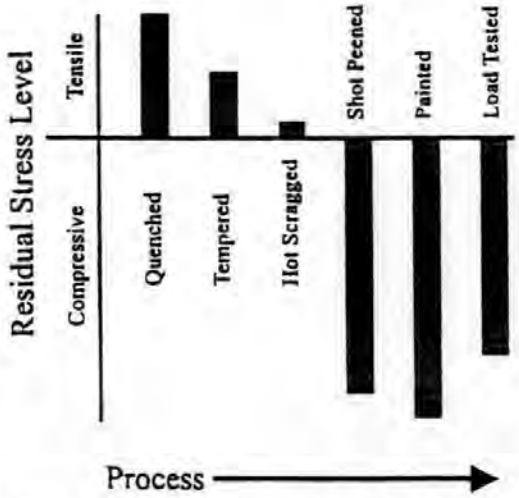

Figure 9 Schematic representation of residual stress levels after each manufacturing stage.

For quenched components it can be seen that a tensile residual stress gradient results and this promotes fatigue initiation near the surface - thus at mechanical defects which tend to be larger than non-metallic inclusions. The tempering operation leads to a reduction of the tensile quench stresses but the resultant is still of a tensile nature and the dominant failure mechanism remains to be from mechanical damage.

The hot scragging process consists of a compression of the component to solid length resulting in the coil surface undergoing plastic work, thus creating a compressive residual to offset the existing tensile residual stress field. The resultant residual stresses after this operation are still of a compressive nature but significantly reduced in magnitude. One subsurface fatigue initiation was observed in these coils, from three failures observed, this being from a significant hydrogen blister.

Further compressive residual stress, of significantly greater magnitude, is added by the shot peening process and is large enough to ensure that a wholly compressive residual stress state exists at the component surface, Figure 9 Any applied stress must now be superimposed upon the residual stress Figure 10, offsetting the applied stress gradient and resulting in a more even tensile stress through the surface layers of the component.

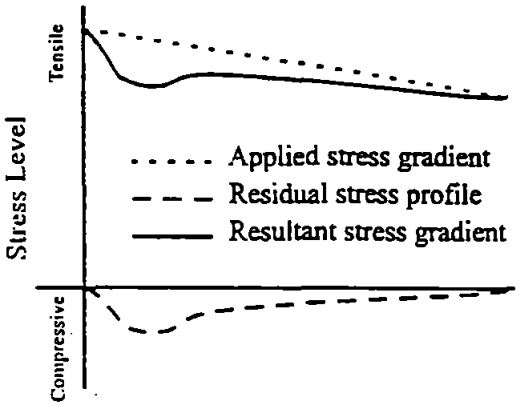

Figure 10 The superposition of compressive residual stress upon applied (tensile) stresses

This significantly reduced effective peak stress along with and altered stress profile means that the surface is no longer the critical area in terms of defects, as verified by the significant shift of failures to sub-surface defects. In addition the shot peening process serves to correct any stress raising surface damage, although this should be regarded as being of secondary importance.

Conclusions

The current work has highlighted some interesting relationships between fatigue failure and critical defect presence in automotive coil spring components. In addition it has been illustrated how the surface condition of the material, specifically with regard to the presence of residual stresses, alters the source of fatigue failure and the order of importance of defects in respect of detriment to fatigue performance.

It has been shown how, for components manufactured from the current material, the critical defects in *finished* components are subsurface non-metallic inclusions and hydrogen damage.

Finally it has become evident that the last stage in the manufacturing process, the cold scragg operation, actually leads to a reduction in the fatigue performance of the finished product. It is therefore clear that further work is required in this area in order to determine that nature of the process by which this detrimental effect occurs.

Acknowledgements

The authors would like to acknowledge the support of the following;

Mr Norman Rafferty, Q.A. Manager, Volkswagen S.A., Uitenhage.

Mr Len Dochray, Director, National Springs. Johannesburg.

Prof. J. Neethling, Dept. Of Physics, Uni. of Port Elizabeth.

REFERENCES

[1] SAE *Spring Design Manual* AE-11

[2] Carlsson, H. *Spring Designers Handbook*, ISBN: 0-8247-6623-7

[3] ASM *Metals Handbook* 8th edition. Volume 7, pp 5-54, 1972.

[4] Holman A.E.L. *Fractography of automotive suspension coil spring fatigue failures*, 1995, Unpublished

[5] Jones, D.A. *Principles and prevention of corrosion*, ISBN 0-02-361215-0

[6] Doi, s. *et al, Fatigue strength of austempered spheroidal graphite cast iron under temperature environment*, conf. Proc. 'Fatigue '96', 1996, pp245-250.

[7] Hertzberg, R.W. *Deformation and fracture mechanics of engineering materials*, Third edition 1989, pp 425-427.

APPENDIX

Specimen Number	Reason for Failure	Comments
1 : Quenched	From surface damage	Coil failed in bending manner - Probably due to bending element high in this (1st) coil
2 : Quenched	From surface damage	Helical initiation and fast fracture
3 : Quenched	From surface damage	Helical initiation and fast fracture
5b : Q & T	Initiation at surface indentation	Helical initiation - Quasi helical fast fracture
7 : Q & T	Initiation at clash from coil end	Helical brittle type
8 : Q & T	Initiation at clash from coil end	Helical brittle type
10 : Q,T, Scragged	Initiation from surface - damaged	Helical initiation, axial growth, helical fast fracture
11 : Q,T, Scragged	Initiation at clash from coil end	Helical brittle type
12 : Q,T, Scragged	Fisheye, depth ~4mm	Torsional overload perpendicular to wire axis
13 : Shot peened	Initiation from surface - damaged	Helical initiation at surface, some axial growth, mostly helical fast fracture
14 : Shot peened	Fisheye, depth ~ 1mm 60 μm inclusion	Helical brittle appearance Al, Mg, Ca, O inclusion
15 : Shot peened	Mechanical damage	Helical brittle type, V. minor axial
16 : Shot peened	Surface indentation particle embedded size 100 μm	Helical initiation -Shear failure perpendicular to wire axis
17 : Painted	25μm Inclusion at depth 10 μm	Helical initiation, Large axial growth along 2 seams, helical fast fracture
18 : Painted	Fisheye, depth ~ 1mm	Helical initiation at fisheye grew axially and perpendicularly. Helical fast fracture
20 : Post load test	Near surface initiation - damaged	Helical initiation near surface. Failure by torsional shear
22 : Post load test	10 μm inclusion at subsurface	Helical brittle

Table 2 Summary of fatigue investigation observations

Copyright statement